EOS: A Space-based Geoengineering Mission to Mitigate Climate Change

Final Report

AE3200: Design Synthesis Exercise

Group 14

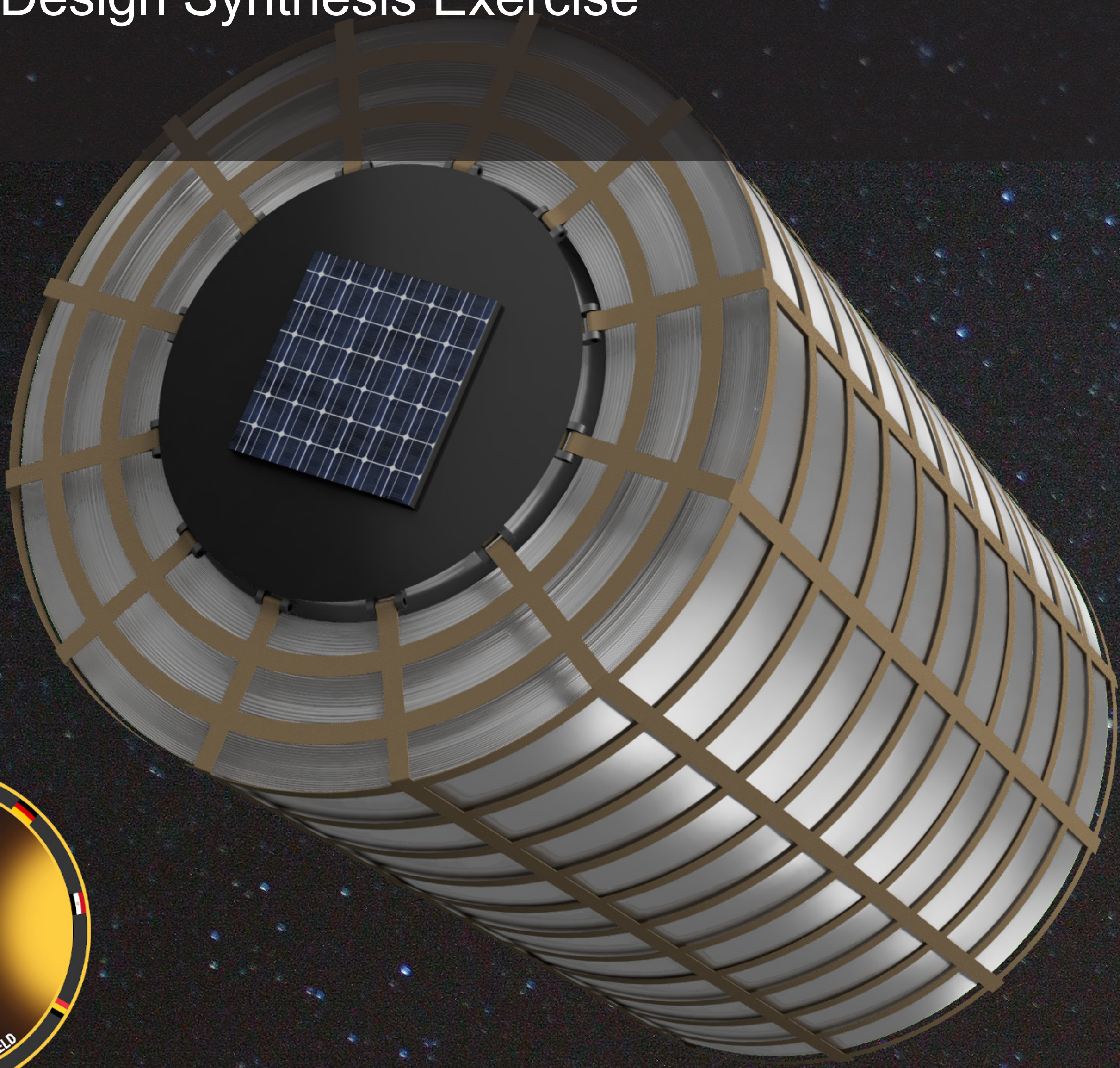

Delft University of Technology

EOS

EARTH OBSCURING SUNSHIELD

TU Delft

EOS: A Space-based Geoengineering Mission to Mitigate Climate Change

Final Report

by

Group 14

Student Name	Student Number
Aleksandrowicz, Filip	4809505
Crum, Stef	4787773
Dumitrescu, Andrei	4822684
Eichman Baquer, Nicholas	4532198
Golombek, Aron	4667751
van Ham, Torsten	4828046
Jodehl, Wim	4676874
Marquez Lopez,Sebastian	4678974
Rubbrecht, Niels	4876539
Yaakoub, Mohamed	4814185

Instructor:	Jeannette Heiligers
Coach:	Stefano Casini
Coach:	Hans Poulis
Teaching Assistant:	Carmen Immerzeel
Institution:	Delft University of Technology
Place:	Faculty of Aerospace Engineering, Delft
Project Duration:	April, 2021 - July, 2021
Version:	**2.0**

Contents

Nomenclature

Abbreviations

Abbreviation	Definition
ADCS	Attitude Determination and Control Subsystem
AHP	Analytical Hierarchy Process
CDHS	Command and Data Handling Subsystem
COPV	Composite Overwrapped Pressure Vessel
CR3BP	Circular Restricted Three Body Problem
DSE	Design Synthesis Exercise
EIRP	Effective Isotropic Radiated Power
EOS	Earth Obscuring Sunshield
EPS	Electrical Power Subsytem
GDP	Gross Domestic Product
HK	Housekeeping
IMU	Inertial Measurement Unit
I/O	In/Out
IPS	Instructions per Second
L_1	Sun-Earth Lagrange Point 1
LEO	Low Earth Orbit
MMH	Monomethylhydrazine
MON3	Mixed Oxides of Nitrogen 3
OBC	Onboard Computer
PD&D	Project Design and Development
RAM	Risk After Mitigation
RBM	Risk Before Mitigation
RCD	Reflectivity Control Device
RDR&E	Research, Development, Testing and Evaluation
R&D	Research and Development
SLOC	Source Line of Code
SNR	Signal to noise ratio
SSR	Solid State Recorder
TM/TC	Telemetry/Tele-command
TT&C	Telemetry, Tracking, and Command Subsystem
USD	United States Dollar

Symbols

Symbol	Definition	Unit
A	Area	[m^2]
$A_{x,y,z}$	Amplitude on the x, y, z plane CR3BP	[-]
$A_{effective}$	Effective shield area	[-]
A_{total}	Total shield area	[-]
a	Platform Outer Diameter	[m]
ab	Length Truss Member **AB**	[m]
A_{sub}	Subsystem Platform Area	[m^2]

Symbol	Definition	Unit
B	Bandwidth	[Hz]
b	Platform Inner Diameter	[m]
bc	Length Truss Member **BC**	[m]
C	Received signal power	[dB]
cd	Length Truss Member **CD**	[m]
d	Diameter	[m]
de	Length Truss Member **de**	[m]
d_{sc}	Spacecraft Bus Diameter	[m]
d_t	Propellant Tank Diameter	[m]
e	Antenna pointing error	[°]
E	E-modulus	[Pa]
$\frac{E_b}{N_0}$	Signal to noise ratio	[dB]
f	Carrier frequency	[Hz]
F_t	Compressive Load Propellant Tank	[N]
f_t	Throughput frequency	[Hz]
g_0	Standard Acceleration Due to Gravity	[m/s^2]
G_r	Receiver gain	[dB]
G_t	Transmitter gain	[dB]
h_C	Sandwich Panel Core Height	[m]
i	ith orbit used in the regression	[-]
I	Area Moment of Inertia	[m^4]
I_d	Inherent Degradation Factor	[-]
I_{sp}	Specific Impulse	[s]
I_T	Total Impulse	[N s]
J	Polar Area Moment of Inertia	[m^4]
k	Scaling Constant Platform Deflection	[-]
k_{eff}	Effective Stiffness of the Primary Structure	[N/m]
L	Length of Truss Member	[m]
L_a	Propagation loss	[dB]
L_d	Lifetime Degradation Factor	[-]
L_l	Line loss	[dB]
L_1	First Lagrange point	
L_θ	Pointing loss	[dB]
m	Mass	[kg]
$\dot{m}$	Mass Flow	[kg/s]
m_{prop}	Propellant Mass	[kg]
m_{ps}	Primary Structure Mass	[kg]
m_s	Margin of Safety	[-]
m_{ssh}	Sunshield Mass	[kg]
m_{sub}	Mass of All Subsystems Except Sunshield	[kg]
N_{SLOC}	Number of Source Lines of Code	[-]
m_1	Mass 1st body CR3BP	[kg]
m_2	Mass 2nd body CR3BP	[kg]
n_y	Load Factor in y-direction	[-]
n_z	Load Factor in z-direction	[-]
O/F	Propellant Mixture Ratio	[-]
P	Normal Load	[N]
P_f	Propellant Tank (Feed) Pressure	[Pa]
P_{sa}	Average satellite power required	[W]
P_t	Truss Member Normal Load	[N]
q	Platform Distributed Loading	[N/m^2]

Symbol	Definition	Unit
r_1	Distance to the 1st primary body CR3BP	[-]
r_2	Distance to the 2nd primary body CR3BP	[-]
R	Data rate	[bps]
S	Signal travel distance	[m]
S_{in}	Incoming solar power	[W/m^2]
t	Thickness	[m]
T	Torque on the Propellant Tank	[Nm]
t_f	Sandwich Panel Face Thickness	[m]
t_s	Truss Member Wall Thickness	[m]
T_s	System noise temperature	[K]
V_t	Propellant Tank Volume	[m^3]
U	Potential function CR3BP	[-]
$U_{x,y,z}$	Partial derivative with respect to x, y, z	[-]
α	Lay-up Angle COPV Fibers	[°]
ϵ	Constellation configuration efficiency	[-]
η	Solar Cell Efficiency	[-]
μ	Mass parameter CR3BP	[-]
ϕ	State Transition Matrix	[-]
ρ	Density	[kg/m^3]
ρ_c	Sandwich Panel Core Material Density	[kg/m^3]
ρ_f	Sandwich Panel Face Material Density	[kg/m^3]
λ	Eigenvalues CR3BP	[-]
σ	Stress	[Pa]
σ_{circ}	Pressure Vessel Circumferential Stress	[Pa]
σ_f	Pressure Vessel Fiber Stress	[Pa]
σ_{long}	Pressure Vessel Longitudinal Stress	[Pa]
σ_t	Tensile Stress	[Pa]
σ_{ult}	Ultimate Failure Stress	[Pa]
τ	Shear Stress	[Pa]
ω_n	Natural Frequency	[Hz]
ω_{xy}	Angular velocity in the xy plane CR3BP	[-]
ω_z	Angular velocity in the z plane CR3BP	[-]
J	Objective Function Trajectory Optimization	[$/kg]
$C_{launcher}$	Cost of a single launcher	[$]
$C_{launchers}$	Cost of the launchers required for one spacecraft	[$]
$C_{propellant}$	Cost of propellant used by one spacecraft, only used in trajectory optimization	[$]
M_{sc-pl}	Mass of the spacecraft payload, only used in the objective function	[kg]
$n_{refuelings}$	Number of launcher refuelings per spacecraft	[-]
t_{burn}	Burn time of the maneuver performed in the high-thrust scenario	[s]
θ_t	First thrust angle	[rad]
ϕ_t	Second thrust angle	[rad]
a_t	Propulsive acceleration	[m/s^2]
N	Number of parts for the low-thrust scenario design variables	[-]
p	Polynomial degree for the low-thrust scenario design variables	[-]

1
Executive Summary

Project Objectives

Following the mission scheme presented in the Project Plan [1], the Baseline Report [2] and the Midterm Report [3] the goal of this project has been summarized in the following Mission Need Statement:

> *"Provide a geoengineering solution to reduce solar radiation reaching Earth to limit the adverse effects of climate change on human life and living conditions on Earth."*

Then, in order to realize this mission within the scope of this project, the following Project Objective Statement has been derived:

> *"Design a space mission capable of blocking up to 2% of solar radiation reaching Earth with 10 students in 10 weeks, constrained by a theoretical design budget of 1 trillion USD."*

This is achieved by the EOS mission. This mission presents a constellation of $71\ 000$ sun shields in an orbit around the Sun-Earth L_1 point. Each spacecraft is equipped with a 91.4km^2 shield which employs centripetal force to create structural rigidity.

The key requirements for the EOS mission that have not yet been mentioned were that operation of the mission shall commence no later than 2031, and the operational lifetime of the mission shall be a minimum of 20 years.

Astrodynamics

The launch vehicle SpaceX Starship is selected due to significant advantages in terms of price and performance. Furthermore, it offers operational advantages, namely refueling capabilities which will be exploited. The final orbit constellation has been decided to be a constellation of 65 Lissajous orbits, each with a different inclination. These orbits have been chosen as they have the highest efficiency in regards to the shading pattern created on Earth. The final shading efficiency achieved is 93%. Lastly the optimal transfer trajectory to the L_1 point is found. This is done using the Differential Evolution method and results in a high thrust maneuver upon injection into the Lissajous orbit with a ΔV of 237.3 m/s and a flight time of 178.4 days.

Subsystems

The Command and Data Handling Subsystem (CDHS) will use the RAD6000 onboard computer linked to a SpaceWire data bus. The data bus has a double SpW-10X Radiation Tolerant Router architecture that allows for internal communication between instruments. The miniRv2 Solid-State Recorder will ensure onboard data storage. The CDHS has a total mass of 14 kg and a nominal power consumption of 44 W.

For the Telemetry, Tracking and Command (TT&C) of the EOS mission, the Deep Space Network is the selected ground station. The communications between the ground and the constellation will be performed through a relay spacecraft at L_1. Communications within the constellation are achieved through a shepherd and herd approach. The herd TT&C subsystem consists of two S-band patch antenna's and four transceivers from ISISpace. The total subsystem mass equals 1 kg and has a power consumption of 13 W.

The design of the Attitude Control and Determination Subsystem (ADCS) involved inspecting the disturbances, calculating the correction maneuvers, designing the attitude control and sensors configurations, and finally performing the sizing. It was concluded that the system configuration has four RCD panels, 16 thrusters, one reaction Wheel, 12 coarse sun sensors, two star trackers, and two IMUs. The total subsystem mass is 28.8 kg and consumes 289.4 W of power.

When it pertains to the Propulsion Subsystem, its main function is to provide the ΔV necessary for the L_1 transfer. Additionally, the propulsion subsystem supplies propellant to the reaction control thrusters for attitude control. A chemical bipropellant propulsion system utilizing the Aerojet Rocketdyne R-40B thruster was chosen for the mission. The thruster uses MMH and MON3 at an O/F ratio of 1.65. Pressure regulated propellant tank pressurization will be conducted using nitrogen stored at 250 bar. Combining the ΔV requirement for the transfer with the propellant requirement from the ADCS, and applying margins resulted in a propellant mass requirement of $12\ 048.15$ kg. The corresponding tank volumes are 5.32 m^3 for the fuel and 5.31 m^3 for the oxidizer. The pressurization subsystem would require 1.48 m^3, or 433.44 kg of nitrogen gas.

The Thermal Control for the spacecraft is analyzed with a nodal thermal mathematical model, and a passive thermal control methodology is used due to the large mass and low heat generation from each satellite. The spacecraft then maintains a balance within the operation limits of each subsystem, the values of which are found in Table 11.10. Kapton, due to it's low emissivity value (0.05), is chosen as a covering for the satellite's exposed surfaces.

The Power Subsystem employs 1.35 m^2 of AzurSpace TJ Assembly 3G30A Solar Cells to generate power. It generates over 437.8 W, this power is then distributed to the subsystems. This power transportation is also completed by the power subsystem. Additionally, the power system has the ability to store $10\ 516$ W of power using a 52.6 kg Lithium-Sulfur Dioxide battery. Using all of these components, the power system is able to generate and provide each subsystem with the power it requires.

The Structures Subsystem is made up from a truss structure, sandwich panel platforms, and a load carrying propellant tank. The mass of the resulting structure is $4\ 040$ kg and a natural frequency of 97 Hz. The truss structure is made from Titanium Ti6Al-4V, the sandwich panels are made from glass fiber with an aluminum core and the tank is a composite overwrapped pressure vessel or COPV.

The Payload consists of a 5.4 km radius Polyethylene Naphthalate shield with a thickness of 84.6 µm which will be stowed along the outside of the spacecraft using a net. The stowed radius of the spacecraft and shield will sum to 2.20 m and it will deploy using the spinning motion of the spacecraft. In order to stow such a large shield in such a way as to fit within the launch vehicle, origami folding is used. The Flasher model suits the needs of the spacecraft. Additionally, due to this material choice and deployment method, a maximum and minimum spin allowable before the shield either tears or deflects can be found. These are 0.102 rpm and 0.026 rpm respectively.

In conclusion, the EOS mission design has the ability block up to 2% of incoming solar radiation. The operational lifetime of the mission has the ability to exceed 20 years. Based on described assumptions, the lifecycle costs are less than 1 trillion USD, and the operation shall not commence later than 2031. This sows the mission design to be compliant to the requirements set at the start of the design process.

2
Introduction

Climate change is one of the biggest crises that humanity is currently facing[1]. Ongoing efforts to curb the greenhouse effect by reducing emissions are falling short. At the current rate of increase of global average temperatures, the effects may soon become irreversible, increasing the frequency and severity of cataclysms. Furthermore, the induced melting of polar ice caps is causing a rise in sea levels, putting entire nations at risk of getting submerged. Geoengineering is the concept of large-scale transformation of Earth's environment. Long a taboo, it could help delay the onset of climate change, giving humanity more time to resolve the underlying issues. Existing concepts include CO_2 removal methods and solar radiation reduction methods such as stratospheric aerosol injection, or a solar radiation reducing space shield.

The goal of this study is to investigate the feasibility of a large-scale space-based solution that would reduce the amount of solar radiation reaching Earth by 2%. Additionally, this study is to provide up with a detailed concept of such a scheme - in the form of the EOS mission. The mission need statement was formulated as follows:

The result is a complete start-to-end mission design that will go into deployment in 2031 and operate for 20 years. The budget of the EOS mission is 1 trillion USD.

For convenience of the reader, the report is split into two parts. In Part I, a summary of the delivered design is presented. First, a market analysis is performed in Chapter 3. Secondly, the description of the EOS mission layout is explained in Chapter 4. More detailed characteristics of the EOS mission and the spacecraft are elaborated upon in Chapter 5. Next, compliance with all the mission requirements is checked in Chapter 6. In Chapter 7, a sensitivity analysis for the EOS mission is performed. An overview of the mission logistics during the project lifetime can be found in Chapter 8. Lastly, in Chapter 9, the sustainable strategy regarding the EOS misson is presented.

Part II goes into the detailed design of the EOS mission and the process taken to reach the results. First, a complete analysis of the astrodynamic characteristics of the mission is given in Chapter 10. Secondly, a closer look will be taken at the specific subsystem designs of the EOS satellites in Chapter 11. This is followed by a risk assessment performed in Chapter 12. The reliability, availability, maintainability and safety regarding the EOS mission is investigated in Chapter 13. Next, the logistics regarding the different EOS mission phases are described in Chapter 14. A cost breakdown of the complete mission is performed in Chapter 15. The second part is concluded with the established verification and validation procedures given in Chapter 16.

[1]URL: `https://www.un.org/press/en/2021/sc14445.doc.htm` [cited 28 June 2021]

PART I

DESIGN SUMMARY

3 Market Analysis

This chapter aims to analyze both the geoengineering and economic landscape in which the mission will have to compete in.

3.1. Approach to Market Analysis

The approach to market analysis for this mission design project differs from a traditional market analysis due to the distinct characteristic of the mission objective not being to generate profit but to serve the common good through contributing to the mitigation of climate change. Because it is likely that public money will be used to finance the mission, it is imperative to challenge whether the chosen approach to mitigate the consequences of climate change is in fact the best choice. Thus, the method of using a Sunshield will be evaluated in comparison to other geoengineering methods with comparable objectives. This analysis will be conducted not only from a cost effectiveness point of view but will incorporate other factors which could have an influence on the common good such as the reversibility and possible side effects of the method in question. In addition to this approach, more conventional aspects of a market analysis, namely the evaluation of the economic landscape with the goal of identifying market trends and opportunities to attain funding will be conducted in order to gain an understanding of the likelihood that a mission with this economic scale will be able to commence in the near future.

3.2. Geoengineering Methods

Geoengineering can be defined as "the large-scale manipulation of a specific process central to controlling Earth's climate for the purpose of obtaining a specific benefit"[2]. Within the group of geoengineering methods aiming to mitigate the impacts of climate change, two distinct categories can be identified, namely Solar Radiative Heat Transfer Reduction Methods and CO_2 Reduction Methods. The methods within the respective categories will be introduced briefly as only an understanding of the fundamental idea, rather than the technical detail is necessary for the purpose of this section. Additionally, for some of the methods several variations exist, in this case only the most promising one has been considered for this comparison.

3.2.1. Solar Radiative Heat Transfer Methods

Solar Radiative Heat Transfer Reduction Methods aim to reduce the amount of solar radiation reaching or remaining within Earth's atmosphere.

[2]URL `https://www.britannica.com/science/geoengineering` [cited 11 June 2021]

Sunshield in Space
This method is what the detailed mission design described in this report is part of. It aims to deflect or reflect solar radiation before reaching Earth by launching elements for a Sunshield from Earth. Possible side effects of this are impacts on Earth's ecosystems, however a model estimating the severity of these effects with an appropriate level of accuracy is still to be developed[4]. Additionally, further possible impacts are explored in more detail in Chapter 9.

Stratospheric Aerosols
This method requires the injection of sulfate aerosols into the lower stratosphere. This has a cooling effect due to the scattering of shortwave as well as the absorption and emission of long-wave radiation. However, it causes a further depletion of the Ozone layer meaning that if the method is halted, climate change will continue at a faster rate than previously[4].

Increasing Cloud Albedo
This method refers to increasing marine cloud coverage and its reflectivity[3]. This is achieved by using wind energy to generate fine sea spray containing salt crystals on remotely controlled vessels. Similarly to the Sunshield, further research on the impact of the reduction of light availability on local ecosystems needs to be preformed[4].

Increasing Surface Albedo
This method increases the reflectivity of Earth's surfaces by covering deserts with reflective material. Deserts are convenient locations as they are often sparsely vegetated and relatively flat, however covering these areas will essentially destroy the extensive local ecosystems and due to the interrelation of Earth's processes affect adjacent ecosystems as well[4].

3.2.2. CO_2 Removal Methods
CO_2 Reduction Methods aim to actively remove CO_2 from Earth's atmosphere.

Land Carbon Sink
A carbon sink is a system which absorbs CO_2 from the atmosphere, the most simple example being trees. However implementing a land carbon sink would require drastic land use changes which is hard to implement and could lead to other side effects reversing the positive impact[4].

Ocean Carbon Sink
Most promising in this category is iron fertilization of the oceans. Experiments are being preformed on this topic rather than mere modeling of outcomes, however, the magnitude of the effect created by this method has not yet been determined accurately[4].

3.2.3. Comparison and Evaluation
The first point of differentiation between the two categories is that while treating the symptoms of climate change, Solar Radiative Heat Transfer Methods do not address the underlying issue of global warming, namely the pollution with greenhouse gases. CO_2 Removal Methods address the root of the problem and therefore also mitigate other consequences of climate change such as the acidification of Earth's oceans[4]. This concern in relation to the mission design is also addressed in Chapter 9.

Table 3.1 compares the individual methods based on 7 parameters. The effectiveness measured in radiative forcing per square meter, the main limiting factor of the method, the deployment time, the lifetime of the effect, the possibility to reverse the method after 1 year, main limitation and a preliminary cost estimate.

[3]URL `https://www.britannica.com/science/geoengineering` [cited 11 June 2021]
[4]URL `https://www.britannica.com/science/geoengineering` [cited 11 June 2021]

Geo-engineering Method	Radiative Forcing (Wm-2)	Limitation to Effect	Deployment Time	Lifetime of Effect	Switch off <1 yr	Limitation	Cost
Sunshield in space	-3.71	None	>20 yrs	~20 yrs	Yes	Control mechanism	>$1 T
Stratospheric aerosols	-3.71	Saturation	~10 yrs	~3 yrs	Yes	Particle residence time	$8 B/yr
Increasing cloud albedo	-3.71	Tropospheric pollution	~10 yrs	«1 yr	Yes	Contol mechanism	>$3 B
Increasing surface albedo	-2.12	Surface area	~10 yrs	<10 yrs	No	Surface replacement	n.a.
Land carbon sink	-2.5	Land area availability	~50 yrs	>1000 yrs	Yes	Eco-system changes	n.a.
Ocean carbon sink	-0.2	Limitation by other nutrients	~500 yrs	~500 yrs	Yes	Eco-system changes	n.a.

Table 3.1: Comparison of Geoengineering Methods [4, 5, 6, 7].

As seen in Table 3.1 the Sunshield is quite effective, however it not only has the highest price but also a relatively long deployment time. Nonetheless, while its potential effects on Earth's ecosystems need to be analyzed in greater detail, it could be one of the less invasive methods. Additionally, it is a solution which is easily adjustable and can quickly and effectively be varied over time. Because of these benefits it is worth investigating whether a Sunshield mission can be designed in such a way to drastically reduce the cost as well as the deployment time in order to make it competitive in regards to other methods. Furthermore, exploring the Sunshield method in detail will facilitate the decision making process as more conclusive statements will be possible than with the current level of knowledge.

As a concluding remark, it is essential to note that the aim of this analysis is not to find the one 'best' method which is then to be implemented. Rather it is expected that a systematic joint effort centered around coordination and cooperation between several methods will allow the most effective distribution of resources as well as the most balanced and efficient way to mitigate the impacts of climate change. This project aims to be a leader in regard to the implementation of this cooperation through aspects of the sustainability strategy discussed in Chapter 9.

3.3. Economic Landscape and Opportunities

This section of the market analysis will be approached in two ways. First the impact of climate change on economies will be explored broadly before looking at general market trends in regards to sustainable projects and enterprises in order to identify economic opportunities.

Climate change has an undeniable impact on current and future human life on Earth and while the debate around it remains to be characterized by the impact it can have on future generations, the impact it will over the near future is often neglected. This is demonstrated by the purely economic cost of climate change damages, which are estimated to be between 0.2-3.5% of the expected 2030 global GDP, and thus equivalent to USD 200-$2\ 000$ billion per year [8]. Furthermore, the shift to renewable energy is not only necessary but an economic opportunity that will lead to economic growth, especially when considering climate change damages [8][9]. Investing heavily in clean geoengineering solutions as well as the rapid transition to renewable energy sources may in fact be necessary to ensure economic growth and stability in the near future.

In order for this transition to take place, funding needs to be made available. While this is not happening at the pace that many say is required, changes are clearly visible. In the U.S. "the global Green Technology and Sustainability market size will grow from USD 11.2 billion in 2020 to USD 36.6 billion by 2025, at a Compound Annual Growth Rate (CAGR) of 26.6% during the forecast period "[10]. This also translates to Europe where the Paris Agreement designated funds of at least USD 13.5 trillion for the energy sector alone [5]. While this investment is carried mostly by the public sector, if the expected economic growth sets in, it is likely that private investors will join in, allowing more opportunity for funding to be acquired. Additionally, government policy incentivizing investment into sustainable projects could act as a catalyst for this process.

In conclusion it can be said that mitigating the impacts of climate change while concurrently investing into a more sustainable future is expected to result in significant economic growth. Furthermore, while these numbers do not refer specifically to the geoengineering sector, the trend of shifting investment to green and sustainable projects is expected to positively influence the availability of financial resources for geoengineering projects.

4 System Characteristics

As a manner of obstruction of incoming solar radiation, this report explores the possibility of a constellation of space-based solar Sunshields. The designed satellites in this report shall employ centripetal force to create the structural rigidity required to block incoming sunlight. In layman's terms, each satellite shall spin a very thin solar shield in order to keep it straight. Similar to how pizza-dough is kept flush while being spun in the air.

These satellites shall be transported into the unstable Lissajous orbit using SpaceX's 'Starships', where it can maintain the position relative to the Sun and Earth. The following sections will shed light on the design of the individual satellites and their cumulative functionality.

4.1. Satellite Design

To be able to compute a final design, the initial sizing of subsystems and their respective functionality was completed. This was done for the payload, structure, propulsion, CDHS and Telecommunication, ADCS, power subsystem and astrodynamics. Then, when these preliminary sizings and functionality estimates were completed, the next step could be taken towards a complete design.

In order to finalize the design, a convergence between the different functionalities and sizing of the subsystems had to be made. To complete this task, a circular design convergence methodology was established: with the limit of mass given by the chosen launcher, the astrodynamics becomes

[5] URL: `https://www.europeanbusinessreview.com/sustainability-a-12-trillion-a-year-market-by-2030/` [cited 28 April 2021]

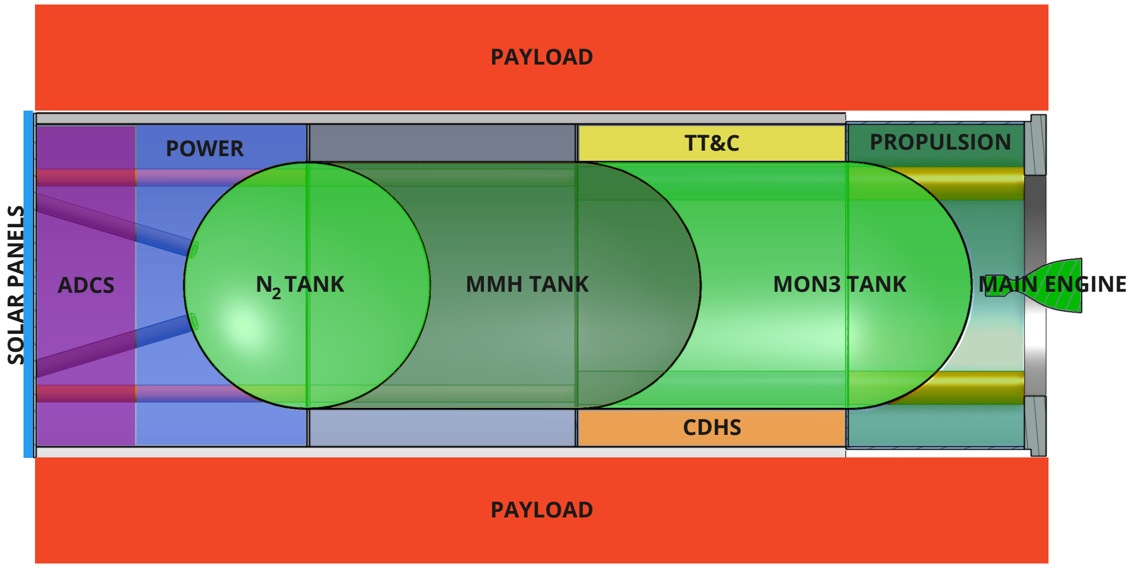

Figure 4.1: Subsystem layout of the satellite

the first point of design. Consequently, the propulsion subsystem can be designed. From there, an estimate is made of the payload mass, to be able to calculate both the structure and the ADCS subsystems. Then, telecommunications, CDHS are estimated, allowing finally the power subsystem to be calculated. The mass margin is then reviewed, and the payload mass adjusted for a new cycle of the design.

4.2. Constellation functionality

In order to block up to 2% of the incoming solar energy, a total of $6.0E6$ km^2 of sunshield is required, as per Chapter 10. As the area of a single satellite is described on Section 5.2.8, it can be computed that the minimum number of satellites is equal to $65\ 935$ satellites. Applying a redundancy factor of anticipating that every single production site described in Chapter 15 shall fail the production of at least one satellite, gives a redundancy factor of 7%. Applying this factor gives that with a constellation of $71E3$ satellites, in a Lissajous orbit at Earth-Sun L_1, the constellation will block up to 2% of incoming solar energy, and thus concur with the requirements described in Chapter 6.

5 Characteristics & Performance

In this chapter, the overall characteristics and performance of the system will be presented. This analysis will be a useful tool, when the compliance of the system and its subsystems with the requirements is analyzed. Ultimately, this analysis will verify whether the design is viable or if it needs to be improved upon. The performance analysis will be first done on the system level, before considering each subsystem individually.

5.1. System Level

Firstly, the system that was designed will be considered as a whole. This will include mass budgets, the power budget, the mission profile, the effectiveness of the sun blocking solution, and finally a

ΔV budget.

5.1.1. Mission Profile

Fig. 5.1 shows the mission/flight profile of a single spacecraft. After launch, the second stage of the launcher, Starship, will enter a low-earth parking orbit. In order to enable Starship to inject the payload into a trajectory to L_1, it has to be refueled in low-earth orbit by 2.6 refueler Starships. This means that it will have to be refueled by at least three other Starships before being able to transfer to L_1.

Following the refueling, the L_1 transfer burn is performed by Starship. After this, the payload separates from Starship and Starship will enter a trajectory back to earth. Once the payload spacecraft reaches L_1, a capture burn will be performed. Once the desired orbit is achieved, the spacecraft will be spun up and the Sunshield can be deployed. The spacecraft will then perform various station keeping maneuvers over the span of its lifetime. Finally, at the end of its lifetime, the spacecraft will be moved to a graveyard orbit, where it will then be decommissioned.

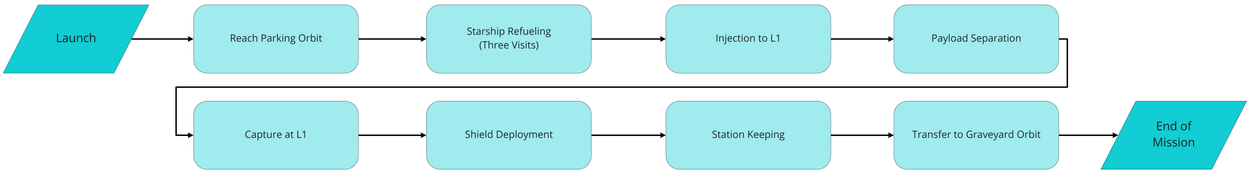

Figure 5.1: Mission profile from the perspective of a single spacecraft as part of the constellation

5.1.2. Mass Budget

Table 5.1 shows the mass budget of a single spacecraft, which will be part of a constellation of $71E3$ of these spacecraft. A margin of 5% was included in each mass estimation of the subsystems to account for any uncertainties within the respective mass estimations. Additionally, a margin of 1% was applied to final total mass estimation in order to account for any errors that were introduced within the final design convergence. The final spacecraft mass including all margins is within 100 kg of Starships payload mass limit.

Table 5.1: Mass budget of a single satellite in the constellation

Source	Mass [kg]
Starship Max. Payload Mass	125000
Propellant Mass	12050
Pressurant Mass	495
Thruster Mass	11.2
Primary Structure	4040
TT&C	0.968
CDHS	14.1
ADCS	30
Thermal Control	9.07
Power	60.1
Payload	107000
Subtotal	123710
Margin	1%
Total	124950

Table 5.2: Power budget of a single satellite in the constellation

Average Power	Power [W]
ADCS	289.4
Comms	13
C&DH	44
Payload	0
Thermal Control	0
Thrust Valves	0 - with impulses
Power Systems	34.64
Subtotal	381.0
Margin	15%
Total	437.75

5.1.3. Power Budget

Table 5.2 shows the power budget of the spacecraft after the design has been iterated as previously mentioned. Note that payload power is zero because the payload will be released by simply cutting a net, which secures the shield to the spacecraft during launch and transfer to L_1, using pyrotechnics. This will require very little power and also only for a fraction of second, and can therefore be neglected. Furthermore, the thermal control power is assumed to be zero as well, since a passive thermal control system will be used.

5.1.4. ΔV Budget

Table 5.3 shows the ΔV budget per individual spacecraft. The first contribution is the ΔV required to reach L_1. This only includes the capture burn for the targeted orbit at L_1, since the initial injection to L_1 is performed by the second stage of the launch vehicle. The process of determining this first part of the ΔV budget is outlined in detail in Chapter 10. Finally, a safety margin of 5% is applied to this value. The second part of the ΔV budget is used for station keeping, once the spacecraft is located at L_1. This value is based on a mission life span of 20 years. The approach used in determining this part of the budget is explained in Section 11.4.

Table 5.3: Required ΔV values

Phase	Required ΔV[m/s]	Margin	Final ΔV value [m/s]
Transfer	188.9	5%	198.35
Station-keeping	40.56	100%	81.12
		Sum	279.46

5.1.5. Volume Budget

Finally, a volume budget of the spacecraft will be presented. This gives a useful indication of how effectively the spacecraft utilizes the volume available in the starship payload bay. This budget can be found in Table 5.4.

Table 5.4: Volume budget of a single satellite in the constellation

Subsystem	**Volume [l]**
Starship Payload Bay	657000
Propellant	10970
Pressurant	1690
Thrusters	10
Structures	2700
TT&C	0.962
Payload	74000
CDHS	2.9
ADCS	30
Power	46.3
Subtotal	**89403**
Margin	5%
Total	**93873**

5.2. Subsystem Level

After analyzing the design on more system-level related aspects, the design will now be analyzed in terms of each individual physical subsystem. The order in which the subsystems are analyzed will be the same as laid out in Chapter 11. This is also where a detailed description of each of the subsystem design processes can be found. In order to fully understand the links between the subsystems, a hardware diagram is created. This diagram serves to portray the connection of the inputs and outputs of each subsystem among each other. Fig. 5.2 shows the hardware diagram. The connections shown are the inputs and outputs of data flow.

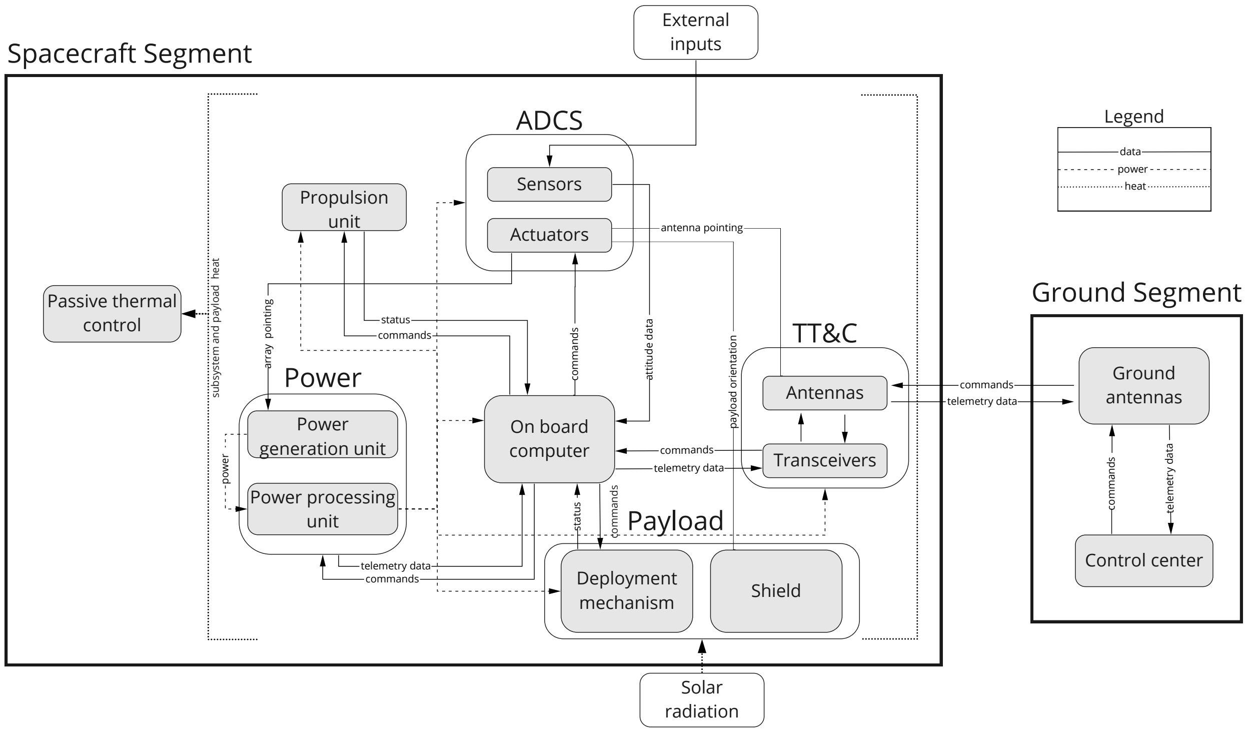

Figure 5.2: Hardware Flow Diagram

5.2.1. Command and Data Handling Subsystem (CDHS)

The CDHS forms the brain and nerves of the spacecraft as it controls all functions of the spacecraft. Fig. 5.3 shows a high level overview of the hardware used as a part of the CDHS. The RAD6000 onboard computer (OBC) [11] was selected for the EOS mission. The required amount of software and throughput capabilities of the OBC were determined using Table 5.5. An average data rate of 643.9 kilo bits per second (kbps) will be handled by the OBC while 2.7 Megabyte (MB) is occupied by the software. The Spacewire network [12] will be used as a data bus. The data bus facilitates communication links between the OBC and the individual subsystem instruments. The data bus has a double SpW-10X Radiation Tolerant Router architecture that allows for internal communication between instruments. The miniRv2 Solid-State Recorder [13] will ensure onboard data storage up to 64 GB. Each of the aforementioned instruments will be implemented twice to allow for redundancy. In total, the CDHS has a mass of 14 kg and a nominal power consumption of 44 W.

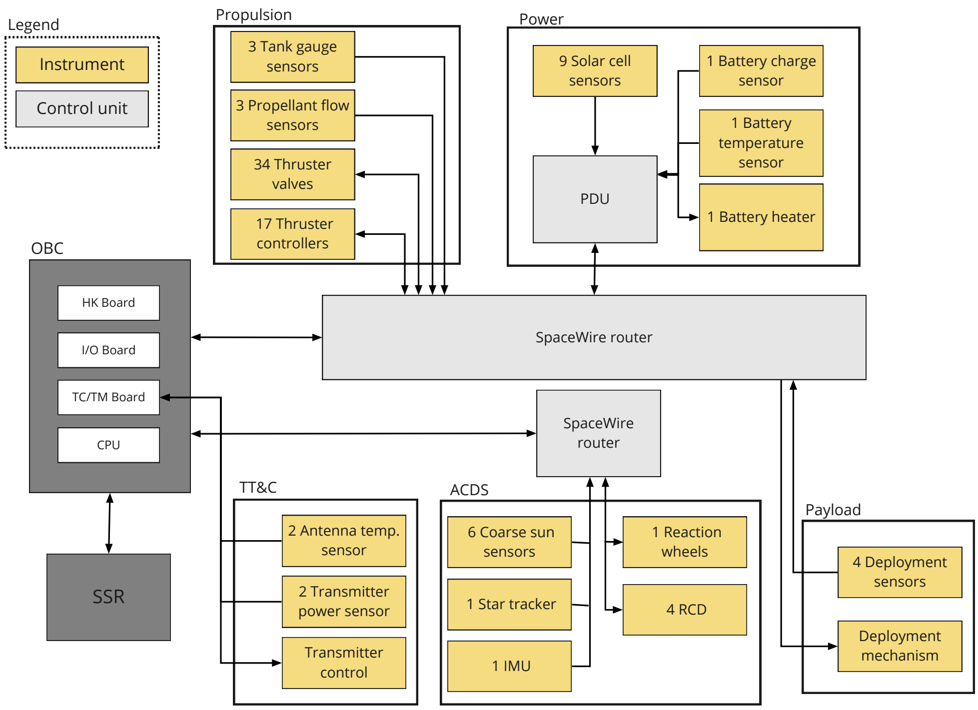

Figure 5.3: CDHS high level hardware diagram.

Table 5.5: Computer software components with the respective source lines of code (SLOC) and thousands of instructions per second (KIPS) for a typical satellite [14]

SW Category	SLOC	KIPS
Executive	1000	0
Communication	4500	10
Attitude/ orbit sensor processing	3300	12
Attitude determination and control	28 800	79
Attitude actuator processing	2700	26.2
Fault detection	11 500	41
Utilities	7250	0
Other functions	5000	88
Total	**64050**	**256.2**

5.2.2. Telemetry, Tracking, and Command Subsystem (TT&C)

The TT&C facilitates communication between the ground and the spacecraft by transmitting, receiving and handling data signals [3]. The 34 diameter reflector antenna from the Deep Space Network (DSN) was selected as the ground station for the EOS mission [15]. From the DSN, EOS will be monitored 4 times a day with contact periods of 2 hours each. The entire mission communication architecture will consist of 6 different links. As seen in Fig. 5.4 there exists an uplink between the ground station and a relay satellite system at L_1. A relay satellite is needed to avoid signal interference from the Solar Exclusion Zone (SEZ).

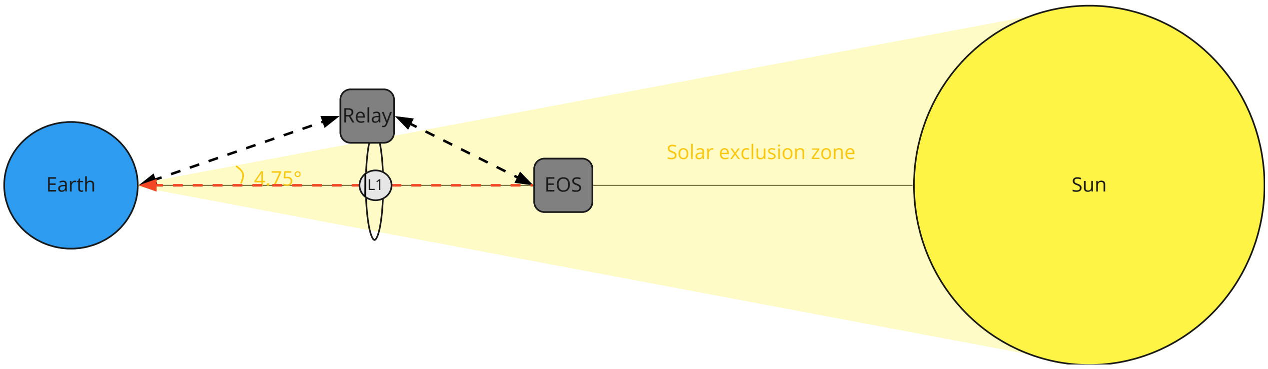

Figure 5.4: Solar exclusion zone as seen from Earth when receiving a signal from EOS.

Additional links exist within the EOS constellation itself. A hive communication with two types or levels of spacecraft was established. The relay satellites re-transmit the message to the level 1 satellites in the EOS constellation. These level 1 satellites are equipped with a high gain gimbal reflector antenna to point to the relay satellite. The level 1 satellite is able to broadcast the signal to 3600 individual level 2 satellites using two omni-directional antennas. The level 2 satellites are equipped with the same two omni-directional antennas and successively report back to level 1 satellite. Tables 5.6 and 5.7 show the downlink budgets within the EOS constellation and between the relay and level 1 satellites. The EOS constellation is divided into 20 sectors based on the total number of spacecraft. Two level 1 satellites will be in charge of the communication for each sector giving a total of 40 level 1 satellites within EOS. 20 Relay satellites will be used as each sector will have a link to a separate relay satellite.

Table 5.6: Downlink budget from level 2 to level 1 satellite.[14]

Parameter	Symbol	Value
Frequency [GHz]	f	2.2
Transmission distance [km]	S	500
Transmitter power [W]	P	2
Effective Radiated Power [dBm]	$EIRP$	33
Transmitter antenna gain [dBi]	G_t	1
Line loss [dB] [16]	L_l	-0.97
Space loss [dB]	L_s	-153.3
Pointing loss [dB]	L_θ	0
Data rate [kbps]	R	33.63
Occupied Bandwidth [kHz]	B	33.63
Receiver antenna gain [dBi]	G_r	1
Receiver system temperature [K]	T_s	85
Received signal power [dBm]	C	-120.2
Signal to noise ratio [dB]	$\frac{E_b}{N_0}$	14.8
Required signal to noise ratio [dB]	$\frac{E_b}{N_0}$	13.3
Link margin [dB]	-	1.5

Table 5.7: Downlink budget from level 1 to relay satellite.[14]

Parameter	Symbol	Value
Frequency [GHz]	f	8.5
Transmission distance [km]	S	7E5
Transmitter power [W]	P	12
Effective Radiated Power [dBm]	$EIRP$	71.79
Transmitter antenna gain [dBi]	G_t	31.97
Line loss [dB] [16]	L_l	-0.97
Space loss [dB]	L_s	-227.94
Pointing loss [dB]	L_θ	7.55
Data rate [kbps]	R	33.63
Occupied Bandwidth [kHz]	B	33.63
Receiver antenna gain [dBi]	G_r	50.21
Receiver system temperature [K]	T_s	253
Received signal power [dBm]	C	-163.71
Signal to noise ratio [dB]	$\frac{E_b}{N_0}$	15.8
Required signal to noise ratio [dB]	$\frac{E_b}{N_0}$	13.3
Link margin [dB]	-	2.5

The level 1 satellite contains four transceivers, two low gain patch antennas from ISISpace[67]. In addition, a 0.6 diameter reflector antenna will be used with a gimbal mount. This results in a total mass of 16.7 kg and a nominal power consumption of 39 W for the TT&C subsystem of the level 1 satellite. The level 2 satellite contains the same instruments except for the reflector antenna and gimbal mount. This gives the a mass of 1 kg and power consumption of 12 W for the level 2 satellite.

5.2.3. Attitude Determination and Control Subsystem (ADCS)

The ADCS is responsible for determining the attitude of the spacecraft and keeping it under control. It is vital for performing any type of controlled maneuver in space. Since the spacecraft will require some maneuvering in order to reach the L_1 point, the spacecraft needs to able to point itself into any direction needed for these maneuvers. Additionally, the payload will be deployed with the help of the ADCS. Finally, the ADCS is intended to resist all disturbances at L_1. Table 5.8 shows the chosen sensors and actuators was well as their masses, power requirements, and their quantity.

Table 5.8: ADCS Sensors and Actuators

Actuators & Sensors	Mass [kg]	Power [W]	Quantity
Thrusters	0.35	7	16
RCD	0.75	0.5	4
Reaction Wheel	13.5	135	1
Star Trackers[8]	0.3	0.2	2
IMU[9]	1.9	12	2
Coarse Sun Sensor[10]	0.215	Passive	12

[6]URL `https://www.isispace.nl/product/s-band-patch-antenna` [cited 19 June 2021]
[7]URL `https://www.isispace.nl/product/s-band-transceiver/` [cited 19 June 2021]
[28]URL `https://hyperiontechnologies.nl/wp-content/uploads/2015/07/HT_iADCS400_v2.1-flyer.pdf` [cited 19 May 2021]
[29]URL `https://satsearch.co/products/gnssmart-gs-imu3000ta-fiber-optic-gyroscopes-inertial-measurement-unit` [cited 19 May 2021]
[30]URL `https://static1.squarespace.com/static/603ed12be884730013401d7a/t/6054f5cb19b196477cd3f9cf/1616180685382/be_datasheet_css_2017jan.pdf` [cited 19 May 2021]

5.2.4. Propulsion Subsystem

The propulsion system uses MMH and MON3 at an O/F ratio of 1.65. Pressure regulated propellant tank pressurization will be conducted using nitrogen stored at 250 bar. Combining the ΔV requirement for the transfer with the propellant requirement from the ADCS, and applying margins resulted in a propellant mass requirement of $12\ 048.15$ kg. The corresponding tank volumes are 5.32 m^3 for the fuel and 5.31 m^3 for the oxidizer. The pressurization subsystem would require 1.48 m^3, or 433.44 kg of nitrogen gas.

After calculating the relevant volumetric flow rates, it was determined that the compressed gas regulator would need to have a flow coefficient (C_v) of at least 0.43. Additionally, the feedlines would need to have dimensions as listed in Table 5.9. The numbers of the feedlines are explained in Section 11.4.6.

Table 5.9: Feedline diameters

Line	1	2	3	4
d_i [mm]	2.71	7.82	5.52	13.0
d_o [mm]	4.48	8.26	5.84	13.8

5.2.5. Thermal Control Subsystem

The thermal control subsystem, due to the large size of the satellite, high thermal mass, and low internal energy generation, does not have any active components. An external layer of aluminized kapton is used to maintain the internal temperature balance between 280 to 310 K for the satellite, and 280 to 300 K for the propellant tank.

5.2.6. Power Subsystem

The power subsystem is responsible for the generation, storage, distribution and transport of the electrical power of the entire spacecraft. In order to compute how this system needs to be sized, it first has to be known how much power is used. Table 5.10 denotes the average power required per subsystem, and the corresponding total average power usage.

Table 5.10: Constellation Average Power Usage

Average Power	**Category 1**
ADCS [W]	289.4
Comms [W]	13
C&DH [W]	44
Payload [W]	0
Thermal Control [W]	0
Thrust Valves [W]	0 - with impulses
Power Systems [W]	34.64
Total [W]	381.0
Margin [-]	0.15
Nominal + Margin [W]	437.75

This satellite shall employ AzurSpace TJ Solar Cell Assembly 3G30A [17] solarcells to generate power. The required solar panel area was calculated to be equal to 1.35 m^2. As each respective solar cell has a total area of 30.18 cm^2, the total minimum amount of solar cells equals 448. The manner in which these solar cells are implemented onto the solar panel, and the accompanying stringing scheme have been detailed within Section 11.6.2.

The power generated and stored by the power subsystem needs to be relayed and connected to the proper systems. In order to complete that task, the power distribution system has been designed. Its layout is visible in Fig. 5.5. This system has the ability to transport, condition, distribute and store the power. The specific functioning of each part will be elaborated upon within Section 11.6.3.

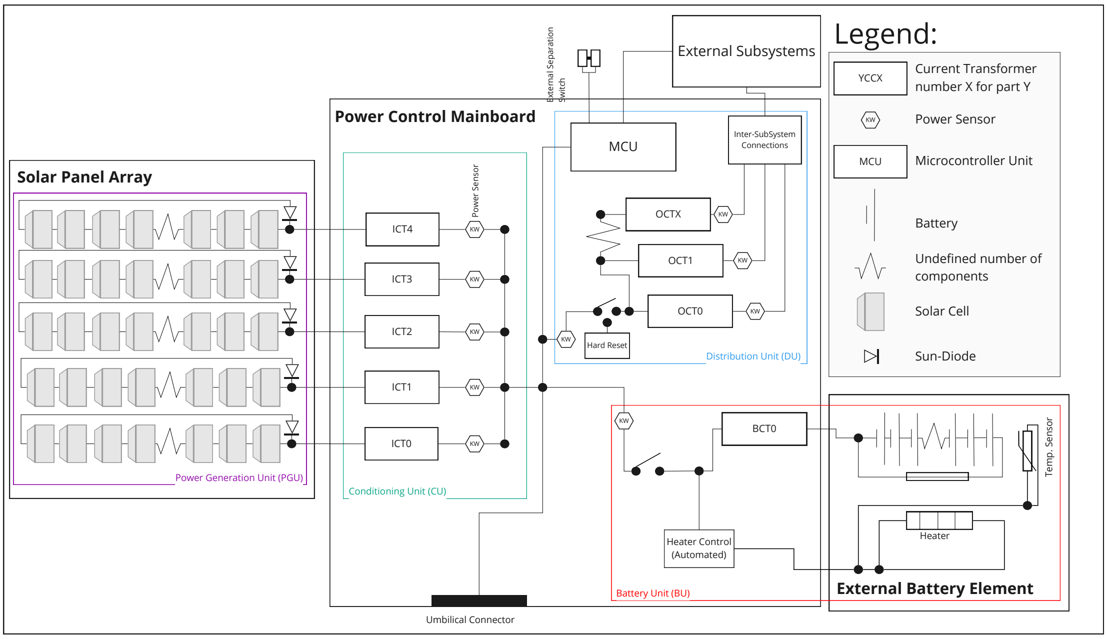

Figure 5.5: Power System Design

The power system of the EOS mission employs a Lithium-Sulfur Dioxide battery, within which it shall have the ability to contain 10516 Wh. Applying the material properties of said battery, it was computed that said subsystem has a mass of 52.6 kg and a volume of 0.0414 m^3. This part within the subsystem stores the energy to allow the system to maintain functionality.

5.2.7. Structures Subsystem

The design of the structures subsystem was based on a truss structure, with a central tank used as an additional structural member, and multiple sandwich panels forming platforms, on which other subsystems can be mounted. Initially, the outer dimensions like length, diameter and tank diameter were sized. The result was a spacecraft with a length of 7.30 m, a diameter of 2.38 m, and a tank diameter of 1.83 m. The structure was then simplified and modeled. A detailed description of this process can be found in Section 11.7. Fig. 5.6 displays the internal loading of the main structural truss and longitudinal load factor of 6 and a lateral load factor of 2.

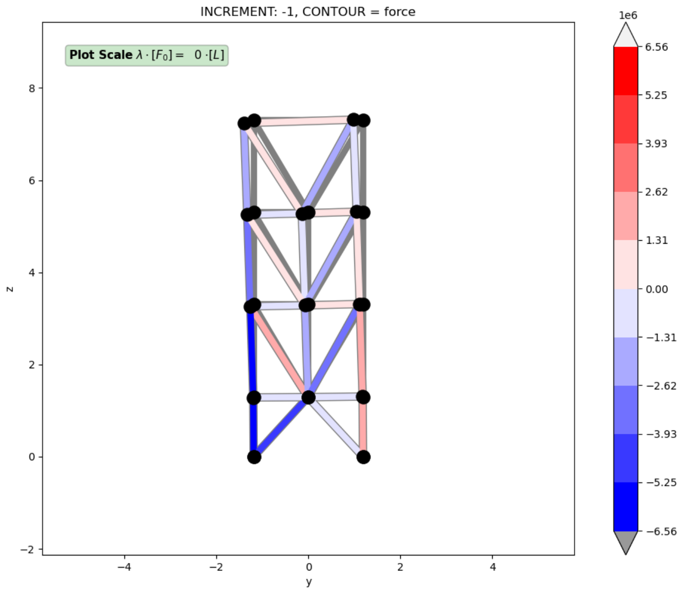

Figure 5.6: Internal loading of the modeled truss

These internal loads were subsequently used to size all of the structural elements. Different failure modes like buckling or tensile failure were taken into consideration, depending on the individual element and its expected loading. The tank thickness was sized, requiring a thickness of 5.71 mm. Furthermore, each truss element was sized to their maximum required load. Finally, the sandwich panels have been determined to require a face sheet thickness of at least 0.24 mm and a core thickness of at least 17.3 mm. Please note however, that especially the face sheet thickness will likely have to be increased in order to ensure the manufacturability of the design.

Afterward, the mass of the structure is determined by optimizing a lightweight solution. Table 5.11 shows the materials used for the individual structural elements. This then also allows for a mass estimation of the spacecraft primary structure. The primary structure will have a mass of $4.04E3$ kg, with the tank having a mass of 442.2 kg which is inluded in the overall primary structure mass.

Material	Use	Yield Strength [MPa]	Ultimate Strength [MPa]	Young's Modulus [GPa]	Density [kg/m^3]	Specific Cost [$\$$/kg]
Titanium Ti6Al-4V	Truss Structure	910	980	119	4450	26.8
HT Carbon fibers	Tank over-wrap	N/A	4400	225	1840	33.6
E-Glass fibers in epoxy	Sandwich panel face	N/A	304	21.8	1970	37.1
Aluminum 5056 honeycomb	Sandwich panel core	0.222	0.253	0.017	150	36.5
Aluminum 6061-T6	Tank liner, debris shield	241	289	67	2710	2.79
Basalt Fiber	Debris shield	N/A	2800	85	2800	37.1 (similar to E-Glass)
Polyethylene Naphthalate	Payload Shield	N/A	175	5.5	1360	5

Table 5.11: Characteristics of the materials used in the primary structure[11] [18]

Additionally, the natural frequency was estimated using a simple single degree of freedom, undamped model. This estimation resulted in the spacecraft having a natural frequency of 97.8 Hz, which is far above the 35 Hz lower limit defined by the launch provider. Finally, the separation mechanism and the debris shielding have been also designed, with the debris shield being taken into account for the mass estimation.

5.2.8. Payload

The final design of the shield is based on the remaining mass and volume available after the bus was completed. It was determined that mass was the critical of the two conditions and therefore the mass was maximized in order to have the largest payload possible. The radius of the shield is, in the end, found to be approximately 5.4 km which will successfully deploy if spun with an angular velocity between the lower limit of $26E-3$ rpm and the upper limit of $102E-3$ rpm. The material used is Polyethylene Naphthalate which is used for solar sail membranes in solar sail missions. Its thickness of 84.6 μm is smaller than previous missions due to an assumed value for areal density that is smaller than has so far been achieved. The form of the shield itself will be origami-like using the Flasher model for the folding pattern. This, along with the extremely thin material used, will allow the entire shield to be compacted such that it fits within the launch vehicle itself. In order to deploy, the satellite spins. As such, the deployment mechanism is a simple net which breaks into two pieces to free the shield at the L_1 point.

[11] URL `https://www.ansys.com/products/materials/granta-edupack` [cited 22 June 2021]

6
Requirements and Compliance

Requirements are the key drivers of any mission design. Table 6.1 lists all the requirements that were imposed on the EOS mission throughout the design. Additionally, requirement compliance is denoted by color, where green means that a requirement is met, yellow that it is to be met at later stages of the design, and red means that the mission does not comply to the requirement. Additionally, for met requirements the section discussing the relevant part of the design is referenced.

Table 6.1: User Requirements

Requirement	Compliance
User Requirements	
DSE14-USR-PER-01 The Sunshield shall block up to 2% of the incoming solar radiation	Section 10.2
DSE14-USR-PER-02 The operational lifetime of the mission shall be a minimum of 20 years	Chapter 8
DSE14-USR-PER-03 The Sunshield shall be located in the vicinity of the Sun-Earth L_1 point; the exact location is to be determined and optimized in light of other mission requirements	Section 10.2
DSE14-USR-PER-04 The Sunshield communication concept with a ground system on Earth shall be defined	
DSE14-USR-PER-05 Operation of the Sunshield shall commence no later than the year 2031	Chapter 8
DSE14-USR-SR-01 The use of toxic and radioactive materials should be avoided	Except propellant (agreed with client) Section 11.4
DSE14-USR-SR-02 The Sunshield shall be able to withstand all launch, mission, and deployment loads	Section 11.7
DSE14-USR-SR-03 Orbit and attitude control of the Sunshield shall be ensured both during the operational mission and the End-of-Life strategy	Section 11.3
DSE14-USR-SR-04 The Sunshield shall not pose a collision risk or other form of interference to other spacecraft	
DSE14-USR-SUS-01 An End-of-Life strategy in compliance with international guidelines shall be specified	Chapter 8
DSE14-USR-EB-01 The spacecraft design of the Sunshield shall be compatible with existing launch systems or launch systems under development (e.g., Starship and New Glenn)	Section 10.1
DSE14-USR-CST-01 The overall lifecycle cost shall be less than 1 trillion USD	Chapter 15
DSE14-USR-OTH-01 The (in-situ) manufacturing, deployment, and maintenance of the Sunshield shall be included in the concept trade-off with proper engineering calculations/justifications	

Continued on next page

Table 6.1 – continued from previous page

Requirement	Compliance
DSE14-USR-OTH-02 The cost and performance of the space-based Sunshield shall be put in perspective to Earth-based geoengineering concepts (market analysis)	Chapter 3
Key Stakeholder Requirements	
DSE14-KSH-OTH-01 The project shall meet the requirements as specified by OHB Systems **DSE14-KSH-OTH-02** The project organization and schedule shall be structured according to the project manual. **DSE14-KSH-OTH-03** The project deliverables shall meet the requirements as set by the OSSA/OSCC, supervisor and coaches.	
DSE14-KSH-PER-01 The satellite shall not cause damage to the launch vehicle or any other payload on-board the launch vehicle.	
DSE14-KSH-SR-01 The mission shall not pose a risk to other missions. **DSE14-KSH-SR-03** The mission shall not affect the power generation of other Earth-orbiting satellites. **DSE14-KSH-SR-04** The mission shall minimize the amount of space debris created. **DSE14-KSH-SR-05** The mission shall not physically block other possible missions.	Section 11.8.5
DSE14-KSH-OTH-04 The mission shall collaborate with other geoengineering projects during execution.	
Stakeholder Requirements	
DSE14-SH-SUS-01 The mission shall not pose a threat to all life on Earth **DSE14-SH-SUS-02** The mission shall adhere to ISO, ILO, SSR, Fair Trade, and Diversity Abroad standards. **DSE14-SH-SUS-03** The mission shall not invade and/or disturb sacred and national parks at any point of the mission. **DSE14-SH-SUS-04** The mission shall have a dedicated space for political, social, and religious discourse. **DSE14-SH-SUS-05** The mission shall not advantage any single or group of countries over others. **DSE14-SH-SUS-06** The mission shall only be performed if it has widespread international support. **DSE14-SH-SUS-07** The mission shall infringe upon the minimal possible number of religious beliefs. **DSE14-SH-SUS-07** At EOL, the Sunshield shall be retracted at the rate that will not cause excessive warming up on Earth.	
DSE14-SH-CST-01 The financial sponsors shall be represented on the final product in some capacity **DSE14-SH-CST-02** The financial budget shall be transparent such as to show the use of the funding	
DSE14-SH-OTH-01 The manufacturing of the mission shall be realistic in terms of size, techniques and materials used	Chapter 8

Continued on next page

Table 6.1 – continued from previous page

Requirement	Compliance
DSE14-SH-OTH-02 Material availability shall be a trade off criteria	
DSE14-SH-OTH-03 The mission objective and effects shall be communicated with full transparency.	
Technical Requirements	
DSE14-TECH-GEN-01 The materials in the Sunshield shall be non-toxic and non-radioactive.	Sections 11.7.7 and 11.8
DSE14-TECH-GEN-02 The mission shall have a reliability of <TBD> %	Chapter 13
DSE14-TECH-GEN-03 Each subsystem shall have a reliability of <TBD> %	Chapter 13
DSE14-TECH-AST-01 The Sunshield's orbit and transfer orbit shall not interfere with other spacecraft.	Chapter 10
DSE14-TECH-AST-02 The Sunshield's orbit shall be optimized such that the required total mission delta-V is the smallest.	Chapter 10
DSE14-TECH-AST-03 The Sun-shield's orbit's orbit amplitude shall be less than 2.6 earth radii.	Chapter 10
DSE14-TECH-AST-04 The distance between shields shall be at least 2 shields between end-to-end of neighbor shields.	Chapter 10
DSE14-TECH-PRP-01-1 The propellant shall be able to be stored for the duration of the mission	Sections 5.2.4 and 11.4
DSE14-TECH-PRP-02-1 The propellants shall be non-toxic and non-radioactive, unless their risks are well understood and the propellants are actively used in industry with proper mitigation strategies.	Sections 5.2.4 and 11.4
DSE14-TECH-PRP-03-1 The propulsion system shall be able to deliver a total ΔV of 249.17 m/s.	Sections 5.2.4 and 11.4
DSE14-TECH-PRP-04-1 The propulsion system shall be able to provide sufficient total impulse for the required ΔV	Sections 5.2.4 and 11.4
DSE14-TECH-ADC-01 The ADCS subsystem components shall be 1 level redundant.	Section 11.3 and Chapter 13
DSE14-TECH-ADC-02-1 The ADCS subsystem components shall have a pointing knowledge accuracy of 18 arcsec.	Sections 5.2.3 and 11.3
DSE14-TECH-ADC-03-1 The spacecraft shall have a pointing accuracy of 360 arcsec.	Sections 5.2.3 and 11.3
DSE14-TECH-ADC-04-1 The spacecraft shall have a slew rate of 0.03 deg/s	Sections 5.2.3 and 11.3
DSE14-TECH-ADC-05 The ADCS subsystem shall compensate for all disturbances experienced during the mission.	Sections 5.2.3 and 11.3
DSE14-TECH-PWR-01-1 The power subsystem shall generate 438.2 W.	Sections 5.2.6 and 11.6
DSE14-TECH-PWR-02 The power subsystem shall have the ability to distribute power to all necessary subsystems.	Sections 5.2.6 and 11.6
DSE14-TECH-PWR-03-1 The battery shall have a maximum battery degradation of 0.02 1/y.	Sections 5.2.6 and 11.6
DSE14-TECH-PWR-04-1 The power subsystem shall have a maximum degradation of 2 % per year.	Sections 5.2.6 and 11.6
DSE14-TECH-PWR-05-1 The battery shall have a capacity of $10\,516$ Wh.	Sections 5.2.6 and 11.6

Continued on next page

Table 6.1 – continued from previous page

Requirement	Compliance
DSE14-TECH-PWR-06-1 The power subsystem shall be able to dissipate 200 W in case of energy excess.	Sections 5.2.6 and 11.6
DSE14-TECH-STR-01 The primary structure shall have a natural frequency higher than 35 Hz	Section 5.2.7
DSE14-TECH-STR-03 The primary structure shall sustain a longitudinal acceleration higher/lower than 6g/-2g	Sections 5.2.7 and 11.7.4
DSE14-TECH-STR-04 The primary structure shall sustain a lateral acceleration higher/lower than $\pm$ 2g	Sections 5.2.7 and 11.7.4
DSE14-TECH-STR-05 The primary structure shall be designed with a safety factor of at least 1.4	Sections 5.2.7 and 11.7.4
DSE14-TECH-STR-06 The primary structure shall protect the other subsystems from the radiation	Section 11.7.6
DSE14-TECH-STR-07 The primary structure shall protect the other subsystems from debris	Section 11.7.6
DSE14-TECH-STR-08 The primary structure shall provide mounting to all other subsystems	Section 5.2.7
DSE14-TECH-STR-09 The primary structure shall provide mounting a separable connection between the spacecraft and launcher	Section 11.7.5
DSE14-TECH-THM-01 The thermal control subsystem shall maintain the spacecraft at a temperature range of 270-310 K	Section 11.5.4
DSE14-TECH-TDH-01-1 The Telecommunication and Data Handling Subsystem shall store data at a rate of 34 kbps	Section 11.1.3
DSE14-TECH-TDH-02-1 The Telecommunication and Data Handling Subsystem shall handle data at a rate of 675 kbps	Section 11.1.3
DSE14-TECH-TDH-03-1 The Telecommunication and Data Handling Subsystem shall Monitor subsystems and payload	Section 11.1.1
DSE14-TECH-TDH-04-1 The Telecommunication and Data Handling Subsystem shall receive data from ground station at a rate of 2 kbps	Section 11.2.3
DSE14-TECH-TDH-05-1 The Telecommunication and Data Handling Subsystem shall send data to ground station at a rate of 34 kbps	Section 11.2.3
DSE14-TECH-TDH-06 The Telecommunication and Data Handling Subsystem shall be able to perform self-diagnostics	Section 11.1.3
DSE14-TECH-TDH-07 The Telecommunication and Data Handling ground segment shall be repairable and replaceable in case of failure	Section 11.2.1
Sustainability Requirements	
DSE14-SUS-SOC-01 An R&D department for sustainable development shall be crated.	
DSE14-SUS-SOC-02 The mission shall join or organize a geoengineering consortium.	
DSE14-SUS-SOC-03 The mission shall have a dedicated space for political, social and religious discourse.	
DSE14-SUS-SOC-04 The mission shall not be affiliated with any one government, political group or religious groups.	
DSE14-SUS-ENV-01 The mission shall systematically attempt to minimize greenhouse emissions in all mission phases.	
DSE14-SUS-ENV-02 The launch vehicle shall be fully reusable.	Section 10.1

Continued on next page

Table 6.1 – continued from previous page

Requirement	Compliance
DSE14-SUS-ENV-03 The net CO_2 emission of the mission, including for example manufacturing, transport and launch shall not exceed 155 million tonnes.	
DSE14-SUS-ECON-01 Lean manufacturing philosophy shall be implemented in all manufacturing processes.	
DSE14-SUS-ECON-02 Mission design shall accommodate synergies with market.	Chapter 3
Risk Mitigation Requirements	
DSE14-RK-RLA-1 A launch provider with a reliable track record according to set launch standards shall be employed.	Section 10.1
DSE14-RK-RLA-4 A set time buffer shall be created to allow for launch delays, as well as contractual incentives to comply with the established schedule.	Outline defined in Section 8.1
DSE14-RK-REX-2 A detailed agreement on the continuation of the mission shall be established with governments and clients before the start of the next mission phase.	
DSE14-RK-REX-4 Protective measures to prevent attacks on the Sunshield shall be investigated and created before the start of the operational phase of the mission.	
DSE14-RK-REI-1 A marine biosphere analysis and consequence prediction shall be performed before the start of the next mission phase.	
DSE14-RK-REI-2 An analysis and consequence prediction of the ramifications on global rainfall shall be performed before the start of the next mission phase.	
DSE14-RK-REI-3 The orbit selection for the Sunshield shall be done in order to optimize the shading pattern in light of an even climate temperature decrease on Earth.	Section 10.2.4
DSE14-RK-REI-4 Research and development of methods to support ecosystems during the operational phase of the mission shall be performed before the next mission phase.	
DSE14-RK-REI-5 An analysis of the mission's synergies with other supplementary bioengineering and geoengineering strategies shall be performed before the next mission phase to reduce the total environmental impact.	
DSE14-RK-REI-6 An end-of-life strategy shall be established in order to minimize global warming effects created by the removal of the Sunshield.	Section 8.4
DSE14-RK-ROR-1 A closed budget shall be established before the initial launch of the project.	Chapter 15, to be updated
DSE14-RK-ROR-2 Materials for spacecraft construction shall be analyzed and selected based on a RAMS analysis.	Section 11.7.7 and Chapter 13
DSE14-RK-ROR-3 Verification and validation procedures shall be integrated in the production plan.	Section 16.2, to be updated
DSE14-RK-ROR-4 Buffers shall be implemented taking into account delays throughout the entire production process to maintain target timelines up until launch.	Section 8.2, to be updated

Continued on next page

Table 6.1 – continued from previous page

Requirement	Compliance
DSE14-RK-ROR-5 A cost analysis with implemented contingencies shall be performed and frequently updated along the design process.	Chapter 15, to be updated
DSE14-RK-RSY-PRP-TECH-1 Flight proven and reliable engines shall be used.	Section 11.4.2
DSE14-RK-RSY-PRP-TECH-2 The tanks shall have protection against overpressure.	Section 11.4.7
DSE14-RK-RSY-PRP-TECH-3 There shall be means of shutting on/off the flow of pressurant.	Section 11.4.7
DSE14-RK-RSY-PRP-TECH-4 The thrusters shall be able to be cut off.	Section 11.4.7
DSE14-RK-RSY-TT-TECH-1 The transceiver system shall be redundant to achieve a minimum reliability of 0.95 over the mission operational lifetime	Section 11.2.3
DSE14-RK-RSY-TT-TECH-2,3 There shall be no single points of failure in the sectoral control of the level 1 satellites.	Section 11.2.2
DSE14-RK-RSY-CD-TECH-1 The OBC shall be able to receive software uploads.	Section 11.1.3
DSE14-RK-RSY-CD-TECH-2,3,4 The CDHS instruments shall be able to handle a total radiation dose of 7E5 rad [19].	Section 11.1.3
DSE14-RK-RSY-ST-TECH-1,2,3 Sufficient safety factors shall be used in the design of the structural elements.	Section 11.7
DSE14-RK-RSY-ST-TECH-1,2,3,5 Design reviews with experts shall be held regularly in the design process.	Section 11.7
DSE14-RK-RSY-ST-TECH-4 Sufficient debris shielding shall be implemented on the spacecraft.	Section 11.7
DSE14-RK-RSY-ST-TECH-5 Vibration tests shall be part of the acceptance/qualification tests	
DSE14-RK-RSY-ST-TECH-6 The separation mechanism shall be thoroughly tested before launch	
DSE14-RK-RSY-PW-TECH-1 A minimum power generation margin of 20% shall be employed in the sizing of the power system.	Section 11.6
DSE14-RK-RSY-PW-TECH-2 Failure of any solar cell shall not reduce the functionality of any other solar cell.	Section 11.6
DSE14-RK-RSY-PW-TECH-3 Each Hardware Connection shall be tested.	
DSE14-RK-RSY-PW-TECH-4 The functionalities of the software shall be verified and validated.	
DSE14-RK-RSY-AD-TECH-1,2 All the ADCS components shall be implemented with redundancies.	Section 11.3

7
Sensitivity Analysis

The sensitivity analysis will be used to assess how strongly the overall design reacts to changes in the inputs of the design or to particular design choices. This will help uncover sensitivities of the design, which could be an indication of a non-optimal design or faulty modeling. The sensitivity analysis will be done be in two steps. First, the sensitivity of the design will be analyzed qualitatively by considering design choices that were made during the design process and assessing how a different choice would have affected the design outcome. After this, the sensitivity within those design option choices will be analyzed quantitatively by applying variations to the numerical design inputs.

7.1. Qualitative Analysis

The qualitative analysis will be performed by considering the different design choices made within each subsystem's design and analyzing how these design changes affected the overall outcome of the design process.

7.1.1. Command and Data Handling Subsystem (CDHS)

For the CDHS system, some of the main parameters that it has to be sized by are the data rates it has to be able to provide. These data rates are set out by the technical requirements in Chapter 6. The most drastic change with in increase of data rates would be an increase of required power. This is because the onboard computer would require more electrical power to perform the additional actions and computations in the same amount of time, increasing the data rate. The biggest implication of this would be the need to increase the size of the solar panel as well as the battery storage. Furthermore, an increase in data rate would also warrant an increase in mass for the CDHS. While this would cause a mass of the power subsystem increase, this change would be negligibly small on the scale of an EOS spacecraft. Even if the mass of the power subsystem would have to increase by a factor of 10, this would still make less than 1% of the overall spacecraft mass. Similarly, a mass increase in the CDHS itself will have next to no impact on the overall design. Even a volume increase would not pose a large problem as there is still large amounts of volume left in the launcher, which could be used for a volume increase for any of the subsystems.

7.1.2. Telemetry, Tracking, and Command Subsystem (TT&C)

The most driving design parameter for the TT&C is the frequency with the which the subsystem sends status updates to ground station as well as how large these updates are. Changing these parameters would mostly affect the power subsystem as well as the CDHS because of the increased need for data storage and processing. Furthermore, this may require larger TT&C hardware to be mounted on the spacecraft. Similarly to the CDHS, while these changes would require an increase in mass of the Power subsystem, since more power would be required for using a higher frequency, the mass increase caused by this would be significant on the scale of the spaceraft itself. However, at some point, the required TT&C hardware would become to large to safely mounted on the outside of the bus. This is enhance by the TT&C hardware having to be placed outside the bus and behind the sunshield, in order to not be able to communicate with the relay spacecraft/ground station.

7.1.3. Attitude Determination and Control Subsystem (ADCS)

For the ADCS, a combination of RCDs, thrusters and a reaction wheel were chosen. If for example only thrusters were to be chosen, than this would greatly drive up the propellant requirement, especially if propellant mass for the propulsion system would be comparatively low. Equivalently, if only reaction wheels were to be used, the ADCS would require a large amount of power. This would either affect the propulsion system of the power subsystem, or both, depending on the propulsion system type. In both cases, this would also affect the bus geometry since the structrure would either have to accommodate either a larger power subsystem or a larger propellant tanks.

7.1.4. Propulsion Subsystem

The main design choices here were the choice of whether to use high thrust or low thrust propulsion as well as the choice between chemical and electrical propulsion systems. The former has a large impact on the ΔV requirement whereas the latter has a large impact on the thruster choice and the propellant volume requirement. The current design uses chemical propulsion, but if this were to be changed to electrical propulsion, this would have major implications on multiple subsystems. With an electrical propulsion system, the required electrical would drastically raise up, potentially into the mega watt range. This would result in a drastic increase the required battery mass and volume as well solar panel size, most likely to the point that it will start majorly driving the bus geometry sizing. At the same time, however, the use highly efficient electrical propulsion would also drastically reduce the required tank volume for the spacecraft, which could counter act the increase battery mass. Finally, large reconsiderations would have to be put towards the design of trajectory. The low thrust would mean that most maneuvers could not be treated as impulsive shots anymore and would have to extensively reevaluated.

7.1.5. Thermal Control Subsystem

The biggest design choice in the thermal control subsystem was to make use of passive thermal control techniques. This means that no electrical is needed to actively regulate the temperature environment onboard the spacecraft. If the thermal control system were to require active thermal control, this would mostly affect the power subsystem once again. Active thermal control would most likely require larger amounts of power than the total current power budget. This would increase size and mass of the power subsystem, and the bus geometry would also be affected by this change.

7.1.6. Power Subsystem

The main design choice in this subsystem was the choice of power generation method. In the end, solar panels were chosen as the preferred option, however RTGs were also considered. If RTGs would have been chosen this would have greatly affected the volume budget of the spacecraft. An RTG would be much more difficult to mount to outside of the spacecraft because of the sunshield mounting during launch. Hence, it would have to be mounted on the inside of the spacecraft. Since RTG's produce waste heat, this would have to be managed and an active thermal control system would have to be implemented, which itself would require more power. Furthermore, RTGs are very expensive with ones producing only a few dozens watts already being in the millions of dollars price range [20].

7.1.7. Structures Subsystem

For the structures, the main driving design factor is the size, and thus mass, of the sunshield. It is by far the largest load on the structure and hence will dominate the sizing of the main structural members. If the payload were to become much lighter than it currently is, other structural designs like a sandwich structure cylinder or a shear panel design may become more effective. This would greatly affect the positioning of subsystem as well as the possible tank sizes and geometries.

7.1.8. Payload

Finally, the main design choice for the payload was the type of deployment. This heavily influences the maximum possible size of the shield. This comes both from a volume limitation within the launcher payload bay as well as from the feasibility for the maximum size. A reduced maximum shield size would also drastically increase the number of launches requried to achieve the same amount of sun blocking performance, which would drive up both the cost and the environmental impact of the mission. Furthermore, the payload may then also require more complex deployment mechanisms, which may be more prone to failure.

7.2. Quantitative Analysis

The quantitative analysis will be performed by varying design parameters and observing the impact on the overall design of the spacecraft. The models of the different subsystems have been integrated into one model used in this analysis. It links the different subsystems inputs and output to each other and is hence able to analyze the impact that changes within one subsystem have on the other subsystems. This will be done for parameters for mass, power, and geometry.

7.2.1. Payload Mass Variation

Firstly, variations in different mass components will be used to determine, how the system reacts to the design input changes. Finally, the sensitivity of the payload will be assessed. The main driving input for the sizing of the payload are the masses of the other subsystems. The wet mass of the spacecraft will always be close to $125E3$ kg, since this the maximum payload mass for the chosen launcher. The shield mass will always be close to difference between the maximum allowable payload mass and the wet mass of the spacecraft bus (i.e. without the payload), since this will minimize the number of required launches. This means that every mass saving on the spacecraft bus can directly translated to an increase in payload mass. By extension, this allows the Sunshield area to be increased, which will reduce the number of required spacecraft.

Since the driving parameter in the shield design is the mass, the reaction of the shield area, deployed diameter and stowed diameter shall be analyzed for a range of masses. Figure 7.1 shows the payload area in relation to the payload mass. A clear linear relation can be seen between these two parameters. This is to be expected as the shield has a uniform mass per unit area, and thus with increasing mass, the area should increase at the same rate. This can be extended to the deployed area and its relation to the payload can be seen in Fig. 7.2. Since the payload mass and area are related linearly, the diameter should have a square-root relation to the payload mass. When considering Fig. 7.2, this is exactly what is observed. A similar square-root relation can be observed for the relation of payload mass to its stowed diameter in Fig. 7.3, however in this case, the diameter starts from an initial value, since the minimum diameter here must be the spacecraft bus diameter.

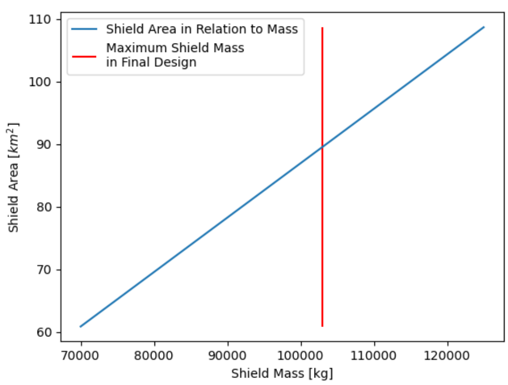

Figure 7.1: Payload area as a function of payload mass

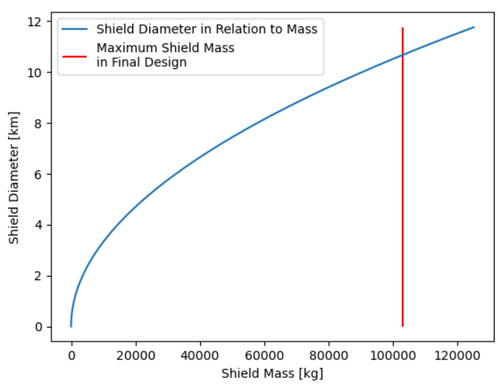

Figure 7.2: Payload diameter as a function of payload mass

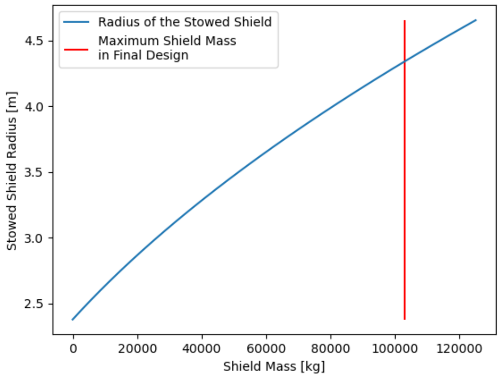

Figure 7.3: Stowed payload diameter as a function of payload mass

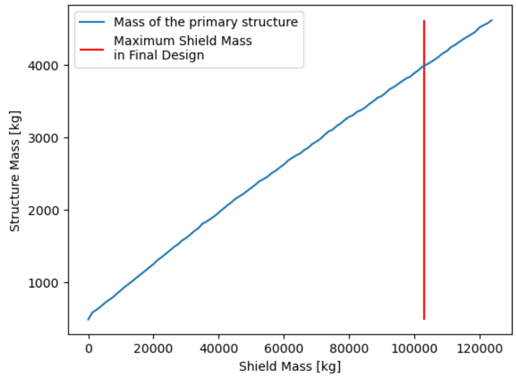

Figure 7.4: Structure mass as a function of payload mass

Among the other subsystem, the strongest affected subsystem by the change in payload mass are the propulsion system and the structures subsystem. The propulsion subsystem is affected by the changing mass influencing the required propellant mass in order to fulfill the ΔV requirement. Since the wet mass is computed using the payload mass multiplied by a set of constants, this relation will be linear. The structure is affected twice by a change in payload mass. Firstly, the primary structure mass will increase, since the structure needs to be stronger for to support more payload mass during launch. On top of this, the change in propellant mass from the propulsion system will also change the required tank size and thus its mass. This means that structure subsystem will increase both from the increased loads from the payload and the increased propellant mass. However, it should be noted that the increase due the increased payload mass will be far stronger than the increase of the tank, since the loads carried are orders of magnitude different to each other. Fig. 7.4 shows the reaction of the structure mass to changes in the mass of the payload.

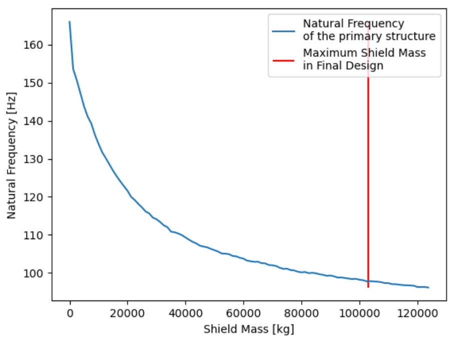

Figure 7.5: Primary structure natural frequency as a function of payload mass

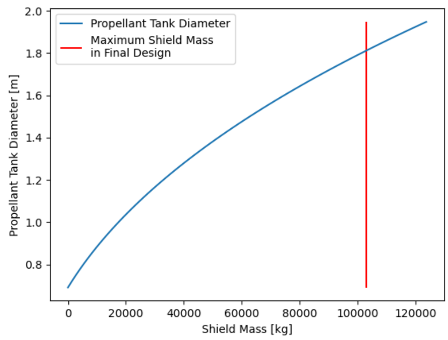

Figure 7.6: Propellant tank diameter as a function of payload mass

Figure 7.5 shows the behavior of the natural frequency. As can be seen, the reduces with increasing mass in an inverse-square-root relationship. This makes sense as the natural frequency is dependent of the square-root of the ratio of stiffness to mass. Stiffness does not greatly increase, as the structure is always sized to the loads it is supposed to carry, whereas mass clearly increases with increasing payload mass, as it has to sustain larger loads. In Fig. 7.6, it can be seen that the propellant diameter increases with increasing payload mass. This is to be expected, since a larger payload mass will require more propellant mass to provide the same amount of ΔV. The graph in Fig. 7.7 representing the spacecraft diameter in relation to the payload mass has a very similar shape to the one in Fig. 7.6. This is to be expected, since the spacecraft diameter is directly dependent on the propellant tank diameter. The spacecraft diameter is sized by considering the volume required by the subsystems housed within the primary structure, and choosing the spacecraft diameter in such a way, that the difference between the volume of the primary structure and the tank is large enough to provide enough room for these subsystems.

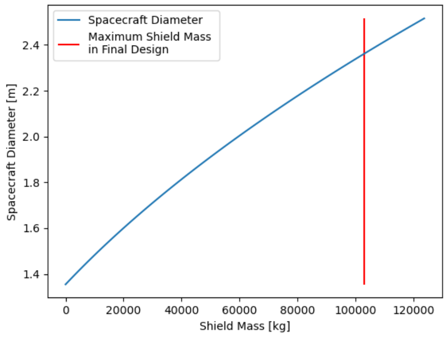

Figure 7.7: Spacecraft diameter as a function of payload mass

Finally, the change in payload mass also indirectly influences the mass moments of inertia of the bus. This is caused by the bus diameter changing based on the changing propellant tank volume. Figures 7.8 and 7.9 show the reaction of the mass moments of inertia about the spacecraft z-axis (longitudinal) and y-axis (lateral) respectively. However, these variations would have little effect on the moment of inertia of the entire spacecraft since the dominating contribution in the mass moment of inertia is the payload itself, since it forms the biggest mass fraction. Naturally, an increase in payload mass would also increase the mass moment of inertia contribution of the payload, however this is not considered here.

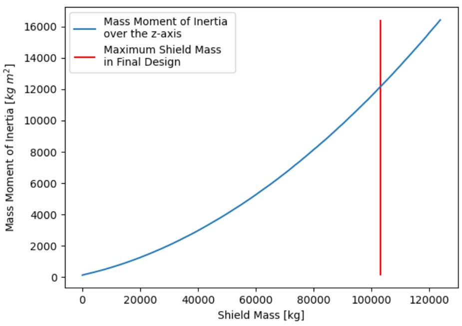

Figure 7.8: Bus mass moment of inertia (z-axis) as a function of payload mass

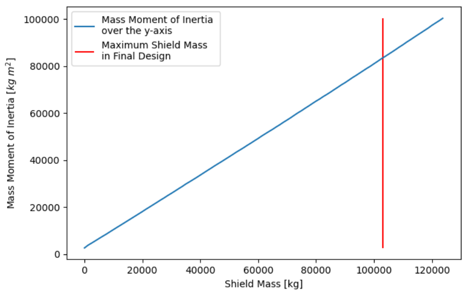

Figure 7.9: Bus mass moment of inertia (y-axis) as a function of payload mass

The other subsystems will either not be affected by these variations, or they will be affected so negligibly that they may be considered not affected.

7.2.2. Outer Geometry Variation

Another set of major design parameters that can be varied are those related to the outer spacecraft geometry. More specifically, the lengths ab, bc, cd, and de from the simplified truss structure in Fig. 11.19 are varied in 100 steps between their 50% and 150% of their original value. Varying these parameters will mainly have an impact on the structures and propulsion system. Fig. 7.10 shows the variation in structure mass for given variation in each of the four lengths in the truss structure. Overall, an increase in mass for increase in length can be observed, which is to be expected. In Fig. 7.10a, the strongest variation in mass can be observed. This is to be expected since the members in this part of the structure carry largest loads, hence increasing their length will affect the overall mass the most. Similarly, Fig. 7.10d has the smallest mass variation, since this section of the truss carries the smallest overall load. Note however, that the mass variations in Fig. 7.10b to 7.10d are relatively close to each other since the load carried in sections bc, cd, and de are equally similar.

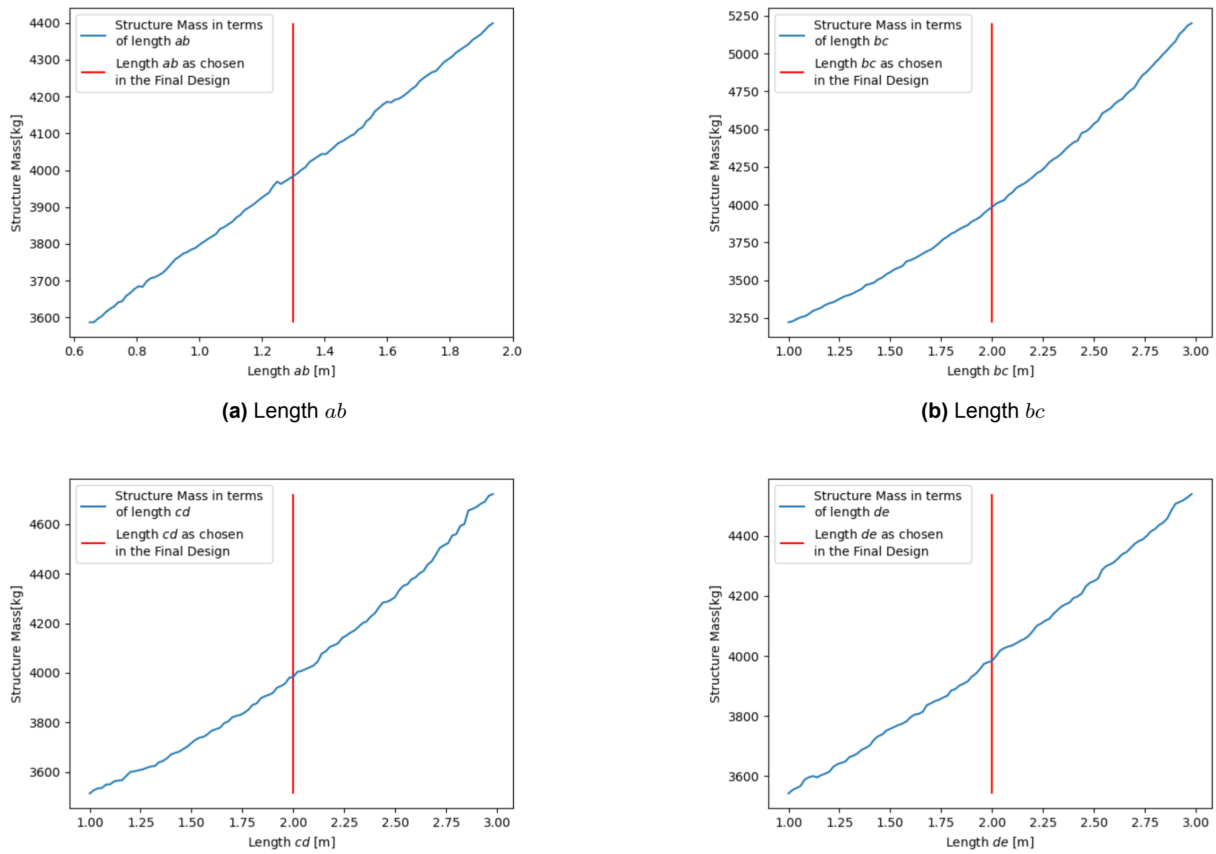

(a) Length ab

(b) Length bc

(c) Length cd

(d) Length de

Figure 7.10: Primary structure mass response to variation in lengths ab, bc, cd, and de

In Fig. 7.11, the variation of the primary structures natural frequency caused by a variation in length can be seen. Overall, the natural frequency tends to decrease with increasing lengths. This meets the expectation that structures with an increased length will have a lower frequency, since their effective stiffness will be reduced. This effect is also enhanced by the fact that an increase in length will also imply a reduction in diameter since the tank has become longer and hence needs less diameter to achieve the same internal volume. Note however, that this is only the case for the lengths represented in Fig. 7.11b and 7.11c since these two lengths influence the tank lengths. The lengths shown in Fig. 7.11a and 7.11d will not affect the propellant tank sizing.

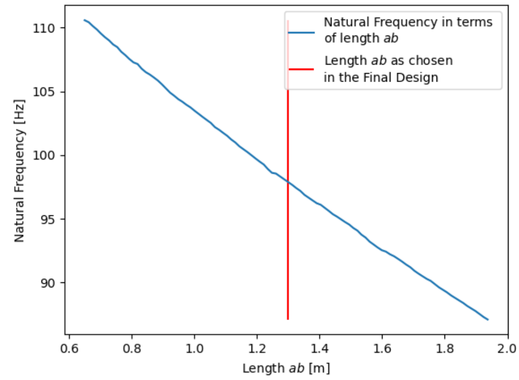

(a) Length ab

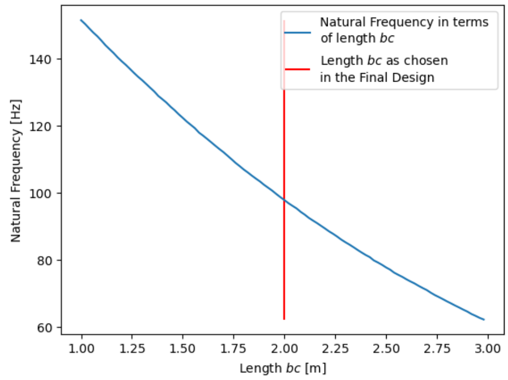

(b) Length bc

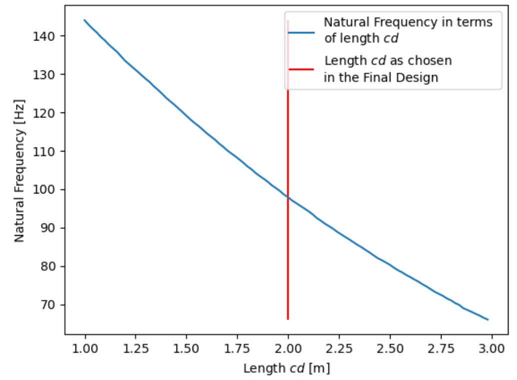

(c) Length cd

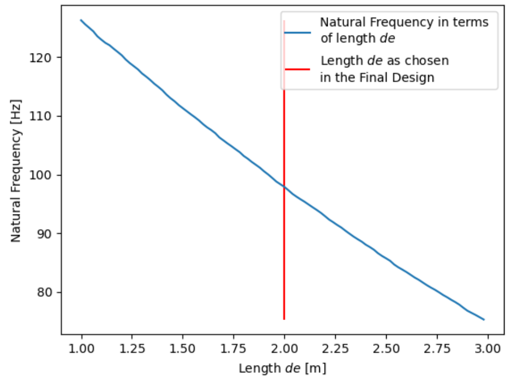

(d) Length de

Figure 7.11: Primary structure natural frequency response to variation in lengths ab, bc, cd, and de

The previously mentioned effects on the tank geometry are confirmed by the reactions of the propellant tank diameters in Fig. 7.12. Figures 7.12a and 7.12d show no variation since these lengths do not affect the tank sizing. The opposite is true for the reactions in Fig. 7.12b and 7.12c, where a clear reaction to the change in lengths can be observed.

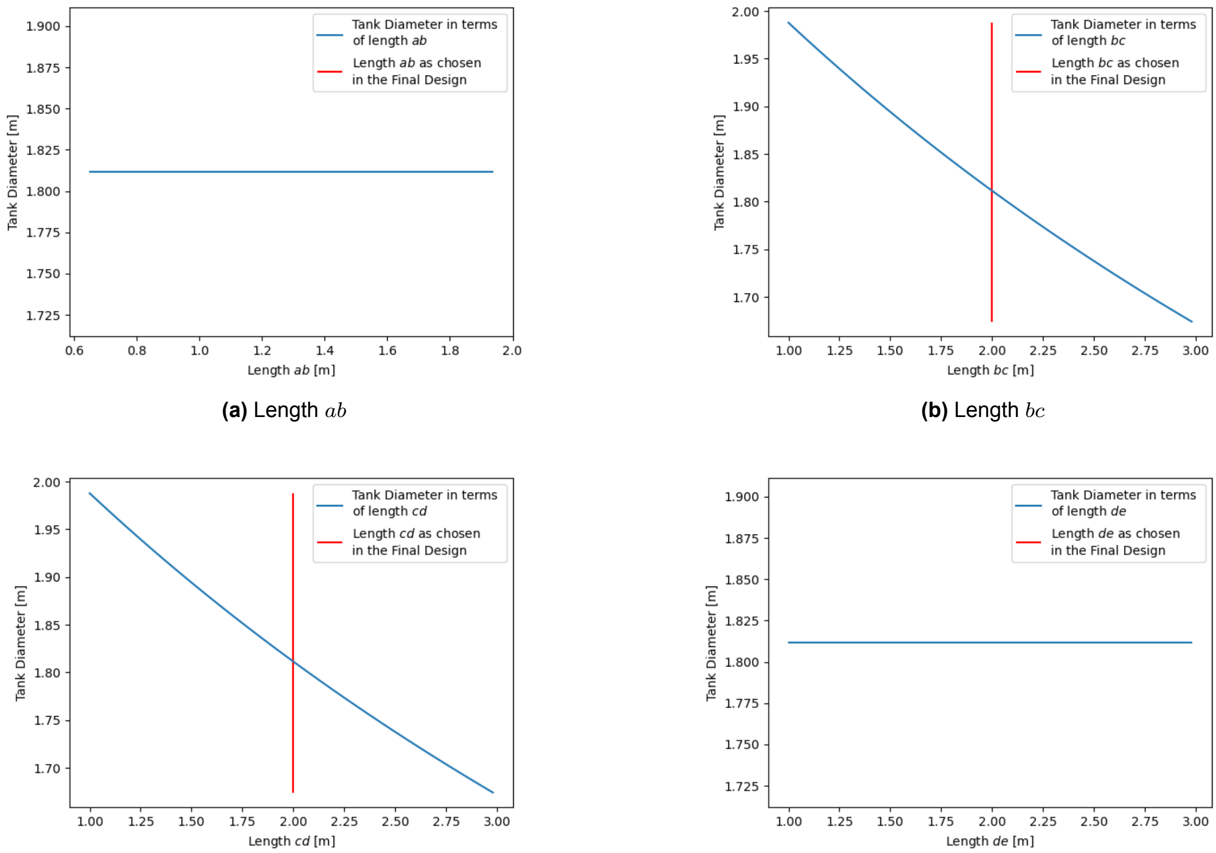

(a) Length ab **(b)** Length bc

(c) Length cd **(d)** Length de

Figure 7.12: Primary structure natural frequency response to variation in lengths ab, bc, cd, and de

Furthermore, these changes will also have an impact on the mass moments of inertia of the spacecraft. However, similarly to the previous section, the largest contribution to the mass moment of inertia will be the payload mass, which remains unaffected in this variation. Therefore, the impact on this subsystem is negligible

7.2.3. Subsystem Power Variation

Finally, a variation in power required by the different subsystems will be considered. These values can vary quite easily, if the choice of components is changed. Therefore it is beneficial to perform the analysis for this parameter as well, such that potential changes can be anticipated. Similarly to the previous section, the combined power requirements of the subsystems will be varied between 50% and 150% of their original values. Furthermore, parameters like battery degradation and solar panel efficiency will be varied as well. The reaction in battery mass, solar panel area, battery volume, and total power subsystem mass to a subsystem power variation can be seen in Fig. 7.13. A clear linear relation can be seen in each of these plots. Note that Fig. 7.13a and 7.13d are nearly identical. This an indications that the battery mass is by far the largest contribution to the entire EPS mass.

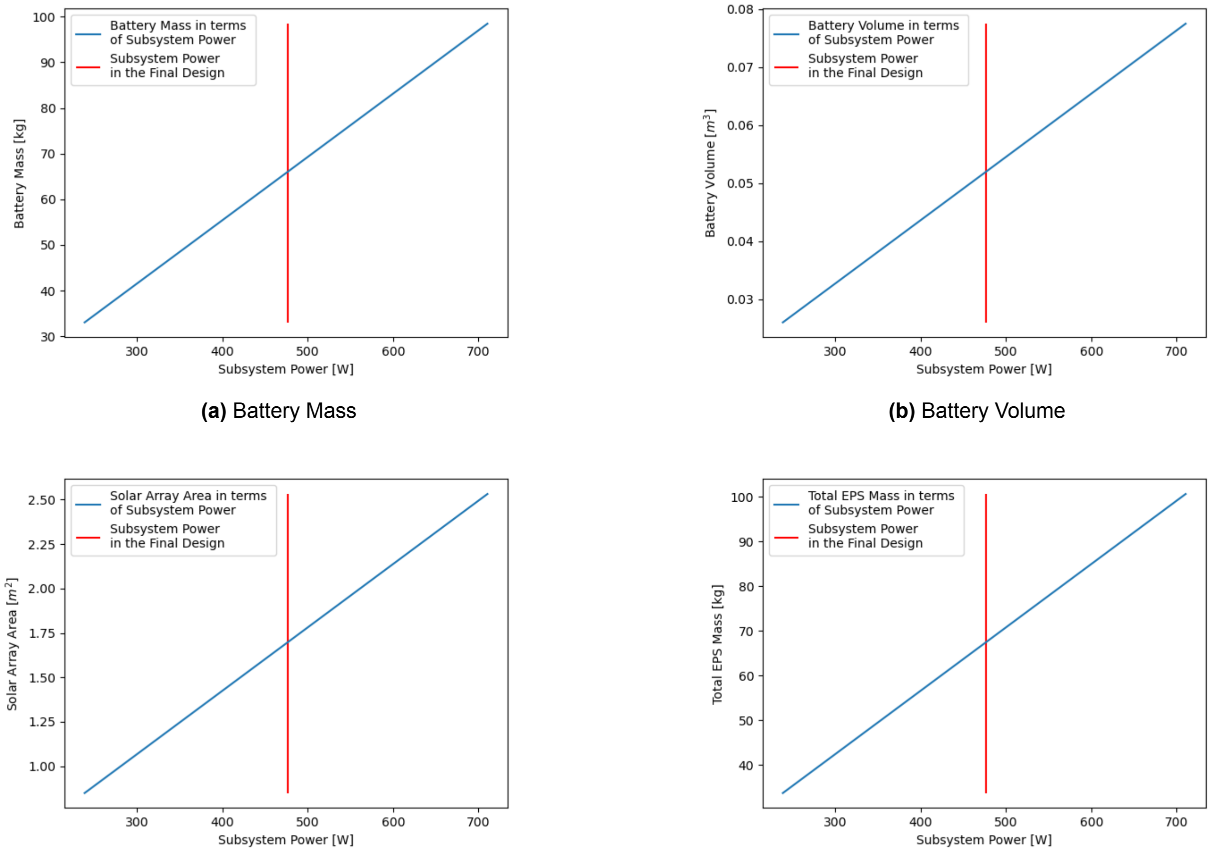

(a) Battery Mass

(b) Battery Volume

(c) Solar Array Area

(d) Total EPS Mass

Figure 7.13: Variation in EPS characteristics as response to a variation in required subsystem power

8 Project Lifetime

In this chapter, the steps for the execution of the mission that come after the DSE are indicated. This chapter documents all of the steps that need to be completed in order to operate the EOS mission within Section 8.1. Additionally, the production plan of an individual satellite is denoted in Section 8.2. Finally, Section 8.3 describes the functioning of each satellite and Section 8.4 documents the end of life strategy.

8.1. Project Design and Development Logic

The Project Design & Development (PD&D) logic shows the logical order of activities to be executed in the post-DSE phases of the project. Within Fig. 8.1 the blocks connected by arrows contain a description of the activities necessary to complete this mission.

When this DSE finishes, the next step in the EOS mission would be to complete the design into detail, such that the production can start. In order to do this, there are some other details that need to be taken care of. Specifically, the folding method needs to be optimized and the payload material needs to be finalized.

Additionally, funding needs to be found in order to complete the design. Note, throughout every stage of design, it will be documented that funding needs to be obtained in order to complete said step. This is documented like this because the manner in which funding will be obtained is unknown, and therefore it has to be accounted for that funding needs to be obtained in every stage of design.

Another factor that needs to be completed after the DSE finishes is research and analysis into the consequences to the marine biosphere, as well as other biological equilibrium'. Other equilibrium's whose ramifications must be investigated are; global rainfall, optimized shading patterns.

Then, a test model may be developed in several steps, throughout this process, funding must also be obtained for the test model. Then a subsequent demonstrator model must be developed to demonstrate the feasibility and functionality of the technology.

The next step is the creation of the logistical network that may be responsible for the development of an unprecedented amount of satellites. Followed by the production and launch of the those satellites.

Then, comes the maintenance of the EOS constellation in orbit. This is then followed by the decommissioning of the constellation, which is the last step that ends the EOS mission.

Additionally, the activities were collected in a Gantt chart which can be found in Fig. 8.3.

8.2. Production Plan

In order to create the satellites which will be used to form the shield, a production plan is required to outline the stages of a satellite's construction. This plan, shown in Fig. 8.2, dictates the steps from the initiation of the satellite production to the final product for a single satellite. The procedure is equivalent for all other satellites in the constellation.

The satellites make use of mainly off the shelf components and existing technology for the majority of the components due to the high production quantity requirements and facility development costs. There are, however, certain key parts which must be designed specifically for the mission. The sheer quantity in which these are needed requires some form of automation in order to be viable, although elements such as the payload cannot be fully automated. Fig. 8.2 is split into unique stages. The main stages are manufacturing, assembly and launch vehicle integration. Each of these stages has some form of production process and testing processes.

The manufacturing stage is where most of the custom and new components must be designed and created. Within this stage there are three key sub-stages: preparation, manufacturing and quality control. The procedures with which the components will be made along with the ordering of materials is done in the preparation sub-stage. After this, the sub-components such as the parts of the shield and the basic parts of the structure enter in the manufacturing sub-stage where they are manufactured. Following this, testing is conducted on the parts. Mainly non-destructive testing would be applied as otherwise new replacements would be necessary, however, where possible, the material or component batches would have samples tested destructively to ensure the batch quality.

The next stage is the assembly. Again, multiple sub-stages exist for the preparation of the assembly, assembly itself and then testing. Important to note is that there are two assembly sub-stages. The first assembles the main three final components of the spacecraft, the bus, shield sheets and deployment mechanism, and the second puts them all together. The preparation for assembly consists of ordering all the off the shelf components and constructing procedures along with jigs to use for satellite construction. Testing too is done in two sets. The first set of testing is done on the sub-assemblies while the second occurs once the complete assembly is finished. Unfortunately, due to the size of a single shield, a deployment test is unrealistic especially for each satellite. A space test above Earth cannot be done as the satellite cannot be returned to Earth to be folded again nor can the payload be stowed for the transfer to L_1 and testing on ground is not possible as it would involve spinning the entire satellite while under the influence of far larger gravitational forces. A demonstrator model, as appears in Fig. 8.1, will be created such that it can be determined if the satellites will function as intended to the best degree possible.

Finally, the launch integration occurs. In terms of tasks, this stage encompasses the fewest individual things to do. Here the satellite is simply integrated into the launch vehicle and final testing is done.

Since the quantity of spacecraft is unprecedented, it becomes extremely important to create each satellite as efficiently as possible. This includes the automation discussed before, but also the fundamental mentality behind the process. The 'just-in-time' manufacturing mentality and method is the best option for such a mission. This is due to a couple of reasons. Firstly, satellites of this scale require entire facilities to be constructed and having multiple satellites in storage would be expensive and inefficient. Furthermore, the satellites can only be launched one at a time, this means that for the highest efficiency each spacecraft should be launched as soon as it is finished such that the next spacecraft has both space to be constructed in and can take the next launch.

8.3. Satellite function

In Fig. 8.4 and Fig. 8.5, the functional behavior of the satellite is included. In those diagrams, the different stages of the mission is included starting from the pre-launch phase to the end-of-life strategy phase. Several functions within each phase is expanded on to provide a better overview of the stages.

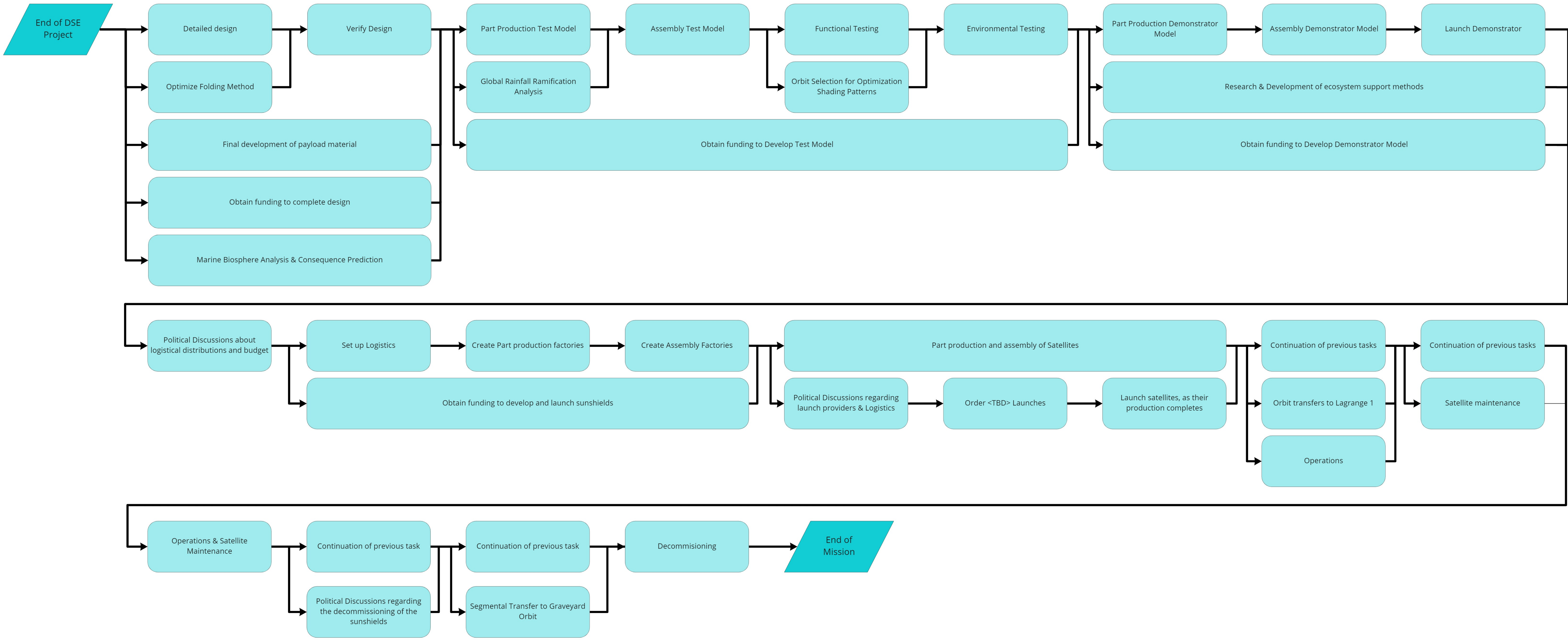

Figure 8.1: Project Design & Development Logic

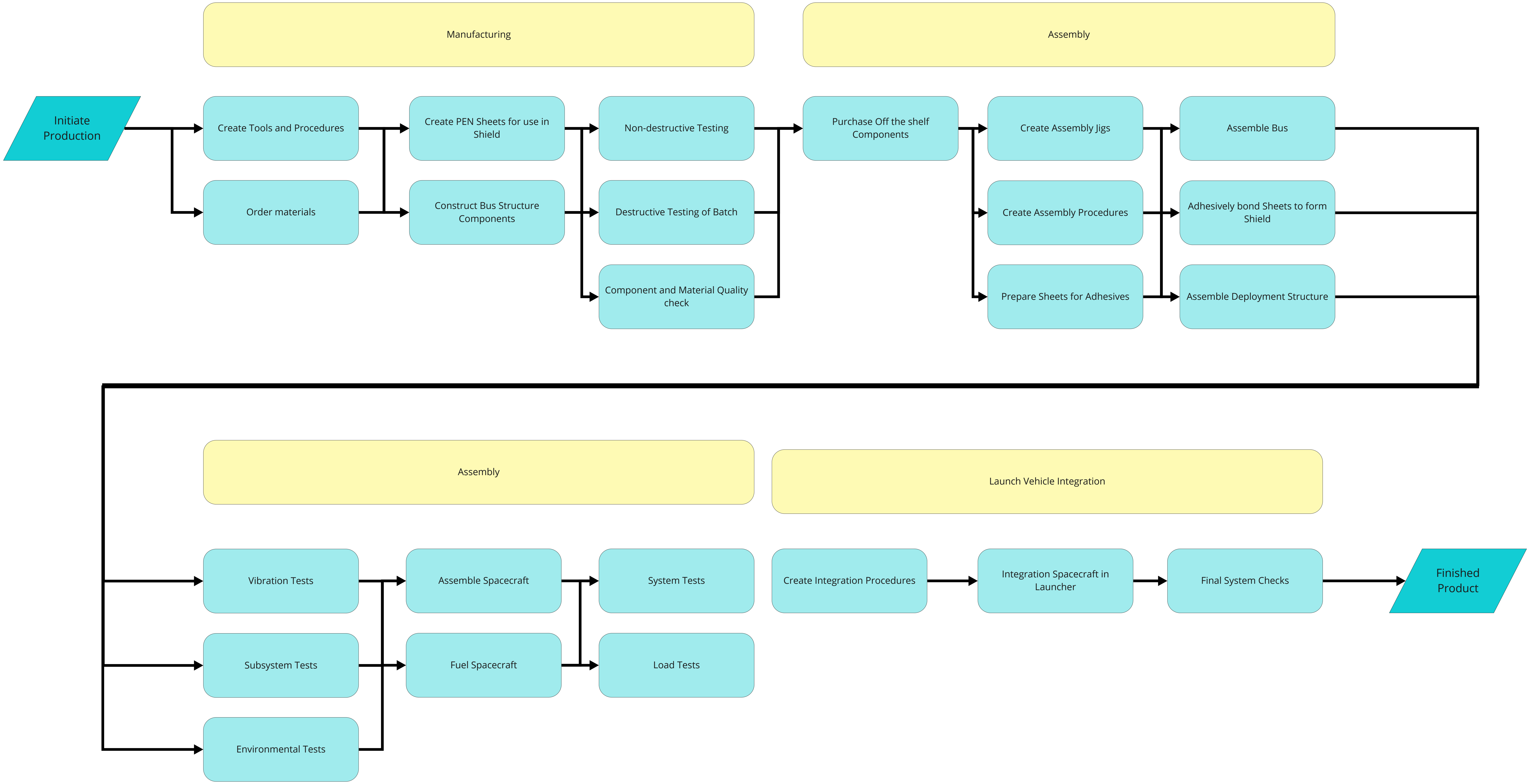

Figure 8.2: Production Plan

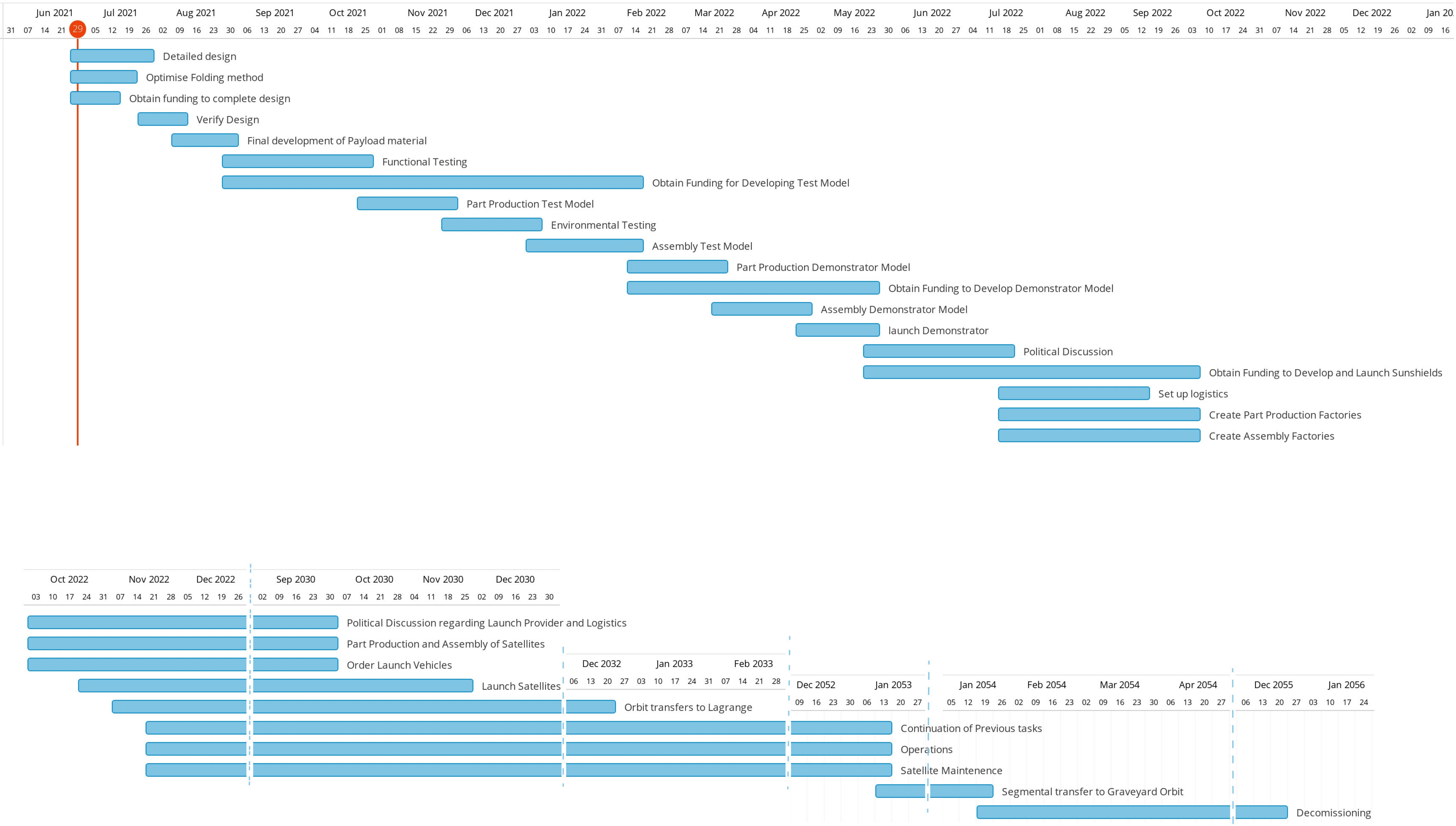

Figure 8.3: Project Execution Gantt Chart

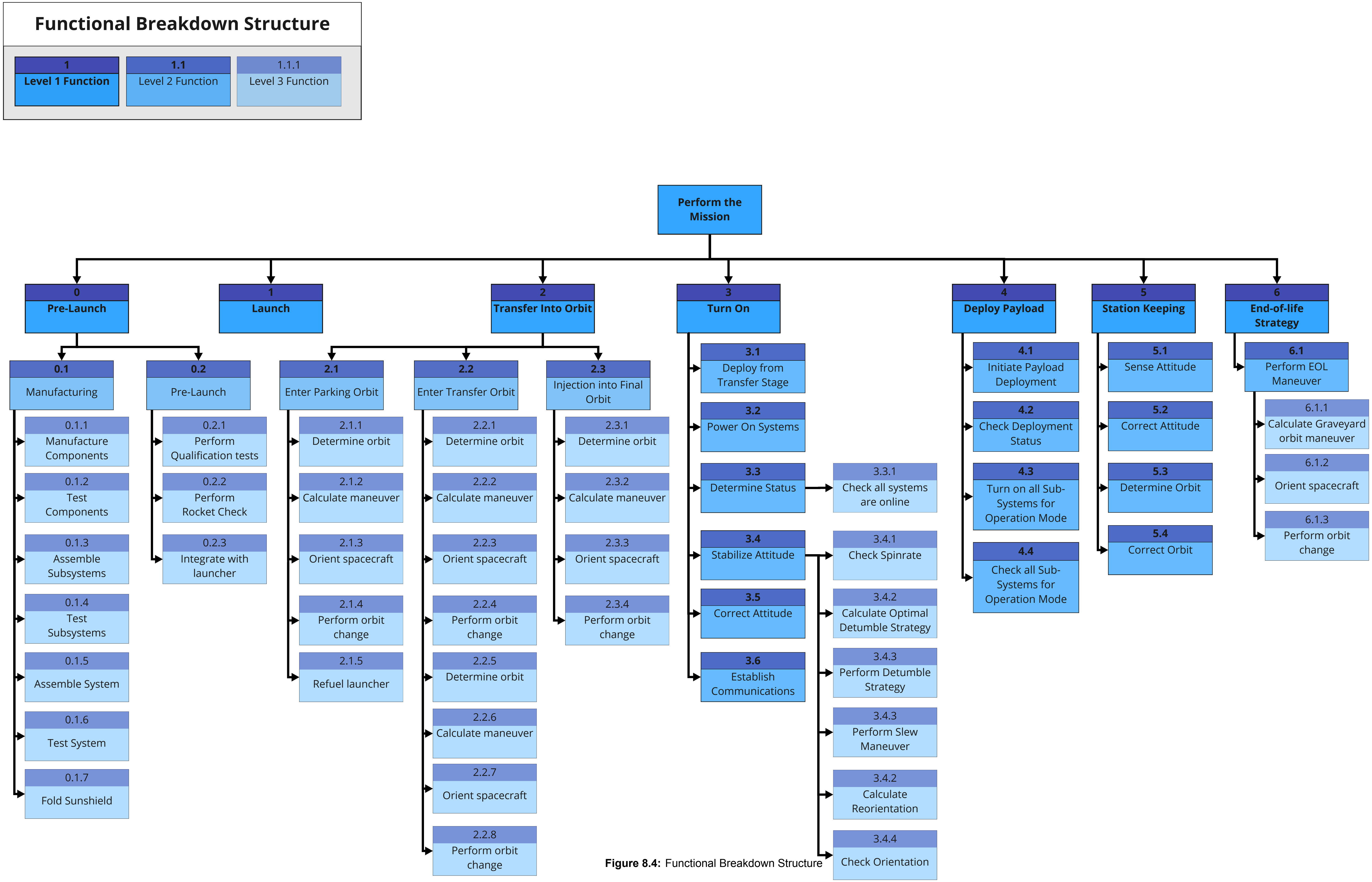

Figure 8.4: Functional Breakdown Structure

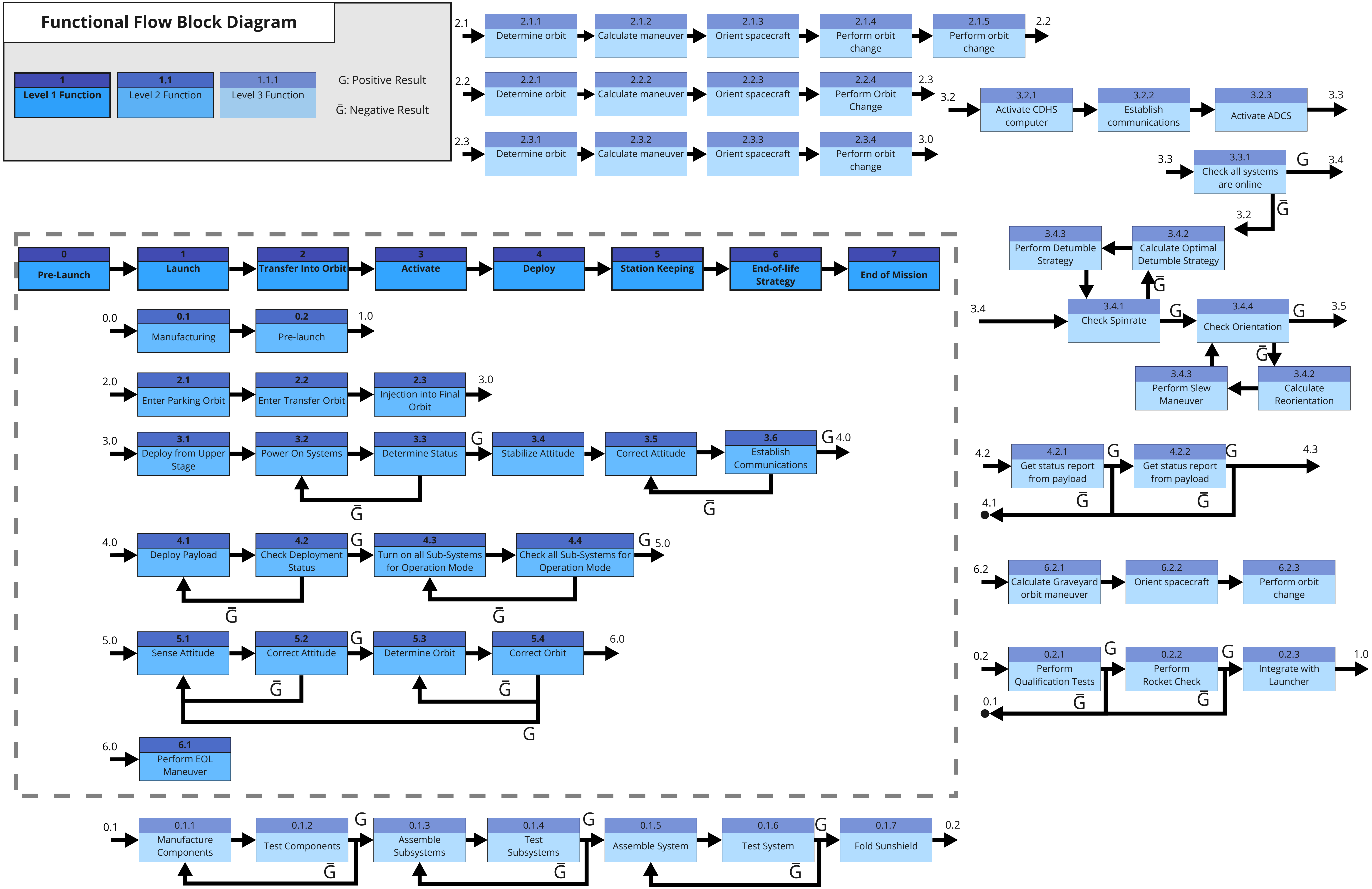

Figure 8.5: Functional Flow Block Diagram

8.4. EOS End-of-Life Strategy

For the End-Of-Life strategy, multiple options are considered, though these are not fully investigated due to time constraints. The two main options which were determined to be worth looking into were a Solar Disposal Orbit where, using the instability of the L_1 point, the Sunshields are pushed into the Sun's gravitational influence and maneuvered to collide with the Sun in the long term future. The alternative would be to use the instability to instead shift the orbit towards Earth and end with the Satellites entering a disposal orbit around Earth.

The Earth disposal orbit poses the problem of having $71E3$ extremely large satellites enter said orbit in order to be disposed of. In order to prevent collisions and potential issues in a near-Earth setting, the disposal would have to occur in a step by step process where the satellites are sent to Earth in sets. This would mean, for example, sending back a level 1 satellite with its corresponding level 2 satellites at any one time and, once these have entered a disposal orbit with no issue, the following set would be sent for disposal. No issues are expected to occur during reentry even with the shield deployed as it is extremely thin and can be expected to deteriorate during reentry with little issue. By instead choosing the solar disposal option, the need for the stratified disposal is negated as there is no threat posed by accidents occurring when already under the significant influence of the sun. The main concerns are arriving at the necessary orbit without intersecting other space bodies such as other planets before the necessary trajectory is established. This is, however, unlikely to occur in the first place and simply requires an adjustment of the trajectory to avoid the orbits of said bodies.

9 Sustainability

This chapter will summarize the sustainable development strategy developed iteratively throughout this project, the final mission design will be evaluated in terms of sustainability, and lastly further ethical consideration are discussed.

9.1. Strategy Summary

The mission is intrinsically tied to sustainability as the mission objective is to mitigate the consequences of climate change. However, a conscious effort needs to be made to develop a holistic strategy, ensuring that sustainability goals are clearly defined and met throughout all phases and in all aspects of the project.

The first step taken in the project was to create an awareness and protocols for sustainability in a context of internal project processes, this was documented in the project plan[1].

Subsequently, the focus was shifted to sustainability of the mission itself. The mission is expected to have a net positive impact on sustainability, it is nonetheless imperative to analyze whether the mission could have unanticipated impacts on different aspects of sustainability. This analysis was preformed from a environmental, economic and social perspective. The central positive impact is anticipated to be a reduction in the rise of Earth's temperatures, leading to a reduction of the associated problems such as large scale climate induced migration as well as a reduction of climate change damages discussed in Section 3.3. Furthermore, it increases the time margin for a transition to fully sustainable resources to occur before consequences become irreversible. However, also negative impacts are possible. Problems associated to climate change other than rising temperatures such as the acidification of Earth's oceans could be neglected and Earth's ecosystems could suffer under the reduced availability of light as discussed in Section 3.2. Furthermore mitigating the impacts of climate change may lead to a decreased sense of urgency in transitioning to sustainable resources, thus being detrimental in the long term.

In order to ensure that sustainability remains a priority throughout the mission design and execution, a strategy was developed in the framework of the previously mentioned pillars of sustainability, namely environmental, economic and social. First, individual strategies enabling the project to reach a higher sustainability standard were identified and grouped in relation to the three pillars as shown in Fig. 9.1.

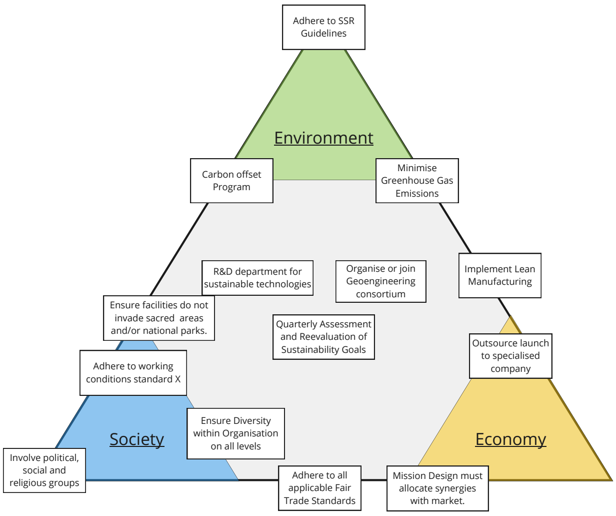

Figure 9.1: Sustainability Pillars

Subsequently, these strategies were translated into specific requirements. These requirements have been expanded throughout the project with increasing level of detail and the results are documented in Chapter 6. The key strategy from an environmental perspective revolves around minimizing greenhouse gas emissions as manufacturing, transport and launching will have to be preformed extensively during project execution. A limit for this was set based on the emissions of an environmentally conscious country with a similar GDP as the mission budget, namely the Netherlands. From an economic perspective it will be imperative to work in cooperation with other geoengineering projects, rather than in competition, allowing efficient distribution of financial resources and thus leading to maximum net impact. Furthermore the social strategy in centered around ensuring public support for the project is maintained by involving political, social and religious groups in the process and informing them thoroughly.

9.2. Concept Analysis

Sustainability was also considered during the trade-off stage, where several concepts possibly capable of completing the mission were considered. These concepts are not discussed in this report but are extensively covered in the midterm report[3]. These concepts were compared using specific trade-off criteria, namely risk, cost, square meters per unit mass, timeliness, simplicity, end of life[3]. In order to measure the sustainability of the distinct concepts the impact of the trade-off criteria on sustainability was investigated. The impact and conclusions drawn from this are displayed here as they allow insight into the strengths and weaknesses of the chosen concept in terms of sustainability.

Environmental While all concepts are expected to have the same impact due to the blocking of solar radiation, the net impact may vary. The criteria chosen to evaluate this aspect are mass per area, end of life strategy and risk. Mass per area has been chosen as more mass means that more transportation and launches will be necessary, resulting in higher greenhouse gas emissions. The end of life strategy is important to prevent space debris, especially due to the scope of the project. Finally the risk is an essential criteria for the environmental aspect as a failed mission could have potentially catastrophic consequences if long term strategies were defined with the expectation of the shield being functional.

Economic From an economic standpoint the central trade-off criteria is the cost. This is key due to the limited availability of financial resources for geoengineering projects. If one method absorbs too much financial capital, this has an effect on other projects leading to a decreased net impact. Additionally, the timeliness criteria is used as a faster implementation would result in a faster reduction of the financial climate change damages, potentially freeing up financial resources for other sustainability related projects.

Social The simplicity criteria is used to judge the social sustainability aspect. The reasoning for this is that it is deemed likely that the public will perceive more simplistic concepts as more feasible. Whether or not these opinions are based on robust knowledge, they will have an impact on the level of support for the project coming from the population.

A trade off in terms of sustainability of the different concepts was preformed in a previous report [3]. The average scoring was of all concepts used in the final trade off was 3.97, with the chosen concept receiving a score of 8.16 and the second highest score being 7.74. Thus, the chosen concept was indeed the correct choice from a sustainability standpoint.

Furthermore, this analysis was used to determine which aspects of sustainability may require stricter sustainability requirements. The chosen concept received the by far highest score for social sustainability. It received the second highest score for environmental sustainability, being 3.8% lower than the best concept. The economic sustainability scoring was also second highest, being 11.9% lower than the best concept in this category. Thus, a focus should be placed on further improving the environmental and economic sustainability strategies without neglecting social sustainability. It was not deemed necessary to generate additional requirements for economic sustainability as it is expected that both cost and timeliness will have be minimized naturally due to the user requirements DSE14-USR-PER-05 and DSE14-USR-CST-01 stated in Chapter 6. In order to ensure a higher level of environmental sustainability of the final mission, two additional requirements where introduced. These are stated below.

- **DSE14-SUS-ENV-02 -** The launch vehicle shall be fully reusable.
- **DSE14-SUS-ENV-03 -** The net CO_2 emission of the mission, including for example manufacturing, transport and launch shall not exceed 155 million tonnes.

The latter requirement was generated by researching the yearly CO_2 emissions of an environmentally conscious country with a GDP similar to the mission budget[12]. The country chosen for this purpose is the Netherlands with a GDP of $907 Billion [13] and yearly CO_2 emissions of 155 million tonnes[14].

9.3. Ethical Considerations

This section discusses and highlights some additional ethical consideration, which have not been directly addressed by the sustainable development strategy defined above. Keeping these issues in mind and finding appropriate solutions is absolutely crucial for a geoengineering mission of this scope.

Not Addressing The Underlying Issue Although having an operational sunshield will mitigate the impacts of climate change, it does not address the root cause of the problem, the large amount of

[12] URL `https://earth.org/global_sustain/netherlands-ranked-13th-in-the-global-sustainability-index/#:~:text=Netherlands%20%E2%80%93%20Ranked%2013th%20in%20the%20Global%20Sustainability%20Index` [cited 28 May 2021]
[13] URL `https://data.worldbank.org/indicator/NY.GDP.MKTP.CD?locations=NL` [cited 28 May 2021]
[14] URL `https://ourworldindata.org/co2/country/netherlands` [cited 28 May 2021]

CO_2 in Earth's atmosphere. This means that implementing a sunshield is essentially a way of buying time to transition to more renewable resources and methods of energy generation. If this does not occur, or is delayed due to a delayed sense of urgency, the sunshield will not be able to have a net positive impact. Furthermore, the solution mitigates only one of the impacts of climate change, Earth's rising temperatures, but fails to mitigate other consequences such as the acidification of Earth's oceans[15]. Different approaches to geoengineering are able to address the problems related to climate change in a more holistic manner, an evaluation the sunshield method in relation to these methods is thus required and preformed in Section 3.2.

Cooperation with the Oil Industry Due to the extensive use of polymers in the design as well as the use of methane as fuel for the launcher, cooperation with the oil industry will be inevitable. The oil industry has not only heavily contributed to the issue of global warming itself but has additionally been exceptionally active in pushing propaganda denying the existence of climate change as well as in political lobbying to slow the sustainability transition[16]. This raises the question of whether the industry should profit from the project both from a financial and a possible marketing point of view.

Removing Vast Quantities of Material from Earth Lastly the sheer quantity of materials, which will have to be sent into space and are unlikely to fully return, needs to be questioned. The amount of materials required for this mission will far exceed the material sent into space up to this point. As for all other resources required for this project, these materials could be used for other, possibly more efficient, geoengineering methods or sustainability projects.

[15]URL `https://www.britannica.com/science/geoengineering` [cited 11 June 2021]

[16]URL `https://www.forbes.com/sites/niallmccarthy/2019/03/25/oil-and-gas-giants-spend-millions-lobbying-to-block-` [cited 29 June 2021]

PART II

DETAILED DESIGN

10 Astrodynamics

This mission, being of unprecedented scope, presents a tough challenge from an astrodynamics perspective. Tens of thousand of spacecraft will need to be launched, transferred and maintained in a close constellation at or around the Sun-Earth L_1 point. An efficient strategy for this is imperative as even slight improvements have the possibility to create major impact due to a positive snowball effect. For example, reducing the ΔV required for transfer means that less fuel mass is required, possibly resulting in more spacecraft payload being carried to L_1 and thus ultimately less total launches will be necessary. Therefore this chapter aims to maximize the efficiency of the astrodynamic aspects of the EOS mission. The objective for the astrodynamic part of the mission is to optimize the shading efficiency of the constellation and minimize the cost for sending the spacecraft to L_1. In order to achieve this, the problem has been broken down into three sub-problems. These are the launch, transfer and orbit constellation. The objective of Section 10.1 is to select the most efficient launch vehicle. Section 10.2 aims to determine the most efficient orbit constellation. Finally Section 10.3 will introduce the astrodynamic model used in Section 10.4 for the purpose of optimizing the transfer to the previously selected orbit. Section 10.5 will show the results and conclusion of this optimization process. Recommendations for further research will be shortly discussed in Section 10.6.

10.1. Launcher Selection

A launch vehicle is required to take each satellite from Earth to its parking orbit. Because of the large amount of launches required for this mission, in combination with the mission's strive for holistic sustainability, only a fully reusable launch vehicle was considered a feasible option. Three spacecraft, namely SpaceX Starship, SpaceX Falcon Heavy, and SpaceX Falcon 9 where compared in terms of launcher payload mass and volume with SpaceX Starship outperforming the other options clearly in both categories [3]. Furthermore, this launch vehicle is expected to reduce launch costs by an order of magnitude which, given the scope and cost requirement on the mission will be critical for mission success[17]. Moreover, the mission will exploit the refueling capabilities of the SpaceX Starship in order to increase the launcher payload capability to L_1, which decreases launch costs. The calculation of the launch costs is explained in more detail in Section 10.4.2. Having discussed the benefits of using SpaceX Starship, it is also critical to mention that this launcher is not yet operational, thus introducing a high level of risk as it is uncertain whether the mission will be able to meet its time requirement. However, because the development of the launcher is relatively advanced and is expected to become available for commercial use within the next couple of years, combined with

[17]URL `https://www.cnbc.com/2021/02/19/spacex-valuation-driven-by-elon-musks-starship-and-starlink-/ /projects.html` [cited 27 May 2021]

the fact that it is realistically the only viable option given the mission constraints, SpaceX Starship has been selected as the launch vehicle for this mission.

Starship will be capable of bringing $125E3$ kg to a LEO parking orbit of 550 km [21], these values are used for the further analysis in this chapter.

10.2. Orbit Constellation Selection

An orbit constellation of this size has never been attempted. It will be extremely complex as many spacecraft will have to fly in a close formation. A constellation which is both safe and efficient needs to be found. This section will discuss the orbital options, introduce the central criteria, analyze distinguishing factors of the option in more detail and finally preform a trade-off based on this analysis.

10.2.1. Trade off Criteria

Initially 5 different options for keeping the spacecraft at or close to L_1 were considered. These were a static position at L_1, halo orbits, horizontal Lyapunov orbits, vertical Lyapunov orbits and Lissajous orbits. These are described in more detail in Section 10.2.2. In order to preform an informed and thorough trade-off, a proper choice and definition of criteria is essential. The criteria considered necessary to include all relevant aspects associated with finding the ideal orbit constellation are listed and explained below.

Orbital Amplitude - The orbital amplitude is important as the shield shall remain between the Sun and the Earth at all times. The maximum orbital amplitude for this requirement to be met is 2.6 Earth radii as calculated in Section 10.2.4.

Transfer ΔV required - The ΔV required to transfer the spacecraft to its final orbit is expected to have a significant effect on the overall mass of the spacecraft as more fuel is required for a higher ΔV. Thus minimizing the required ΔV is favorable.

Time of Flight - Due to the the time requirement of the mission, it is favorable to minimize the time of flight.

Effective Shield Area - Due to the large number of spacecraft in the constellation it is expected that some spacecraft will at certain points be on the same line between the Sun and the Earth, thus reducing the effective efficiency of the shield. Certain orbits constellations are expected to produce more efficient shading patterns than others.

Collision Risk - Minimizing the collision risk reduces the risk of the mission itself. Because the spacecraft are likely to be extremely close to each other, a single crash could create a snowball effect, eventually causing mission failure and large amounts of uncontrollable space debris.

Communication Risk - Crossing the Sun-Earth line can lead to disturbances in communication as explored in Section 11.2.1. Some of the considered orbits frequently cross the Sun-Earth line meaning that significant communication issues could arise.

Stability - Higher stability not only means lower risk but also results in less ΔV being required for orbital station keeping.

10.2.2. Preliminary Trade off

In order to prevent wasting resources it is imperative to preform a preliminary suitability analysis of the individual orbital options in regards to the mission. The distinct options are explained and evaluated in an elemental fashion in terms of the trade-off criteria.

At L_1 point - Instead of an orbit around L_1 it was considered to have the spacecraft at a static position at or close to L_1. While a position at the L_1 point itself is unstable as demonstrated in Section 10.2.3, the orbits around it are also inherently unstable making this a realistic option. However due to the final shield design being a constellation of approximately $71E3$ spacecraft, this is not a viable option.

Horizontal Lyapunov Orbits - These types of orbits have no minimum amplitude and are entirely in the ecliptic plane. Infinitely many of these orbits exist meaning that a family of orbits with different amplitudes can be found which is highly relevant considering the amount of spacecraft which will have to be placed in a constellation. This is visualized in Fig. 10.1. Due to its favorable characteristics, this type of orbit will be considered a viable option and further analyses on it will be preformed.

Vertical Lyapunov Orbits - In the same fashion as horizontal Lyapunov Orbits, these orbits have no minimum amplitude and infinitely many orbits exist. They are curved, three dimensional, figure eight shaped orbits with the intersection on the Sun-Earth line as seen in Fig. 10.1. Due to this intersection and the large number of spacecraft which will be need, this option is neglected due to a significant increase in collision risk.

Halo Orbits - While these 3 dimensional orbits also displayed some favorable characteristics, they where neglected quickly as their minimum amplitude exceeds the requirement of maximum amplitude set in Section 10.2.1 [22].

Lissajous Orbits - Lissajous Orbits are not periodic orbits but open trajectories. They are three dimensional orbits with the motion in z direction being uncoupled from the motion in the $x - y$ plane. Shown in Fig. 10.1, these orbits are also considered for further analysis as infinitely many of them exist and their out of plane component may be able to increase the efficiency of the shading pattern.

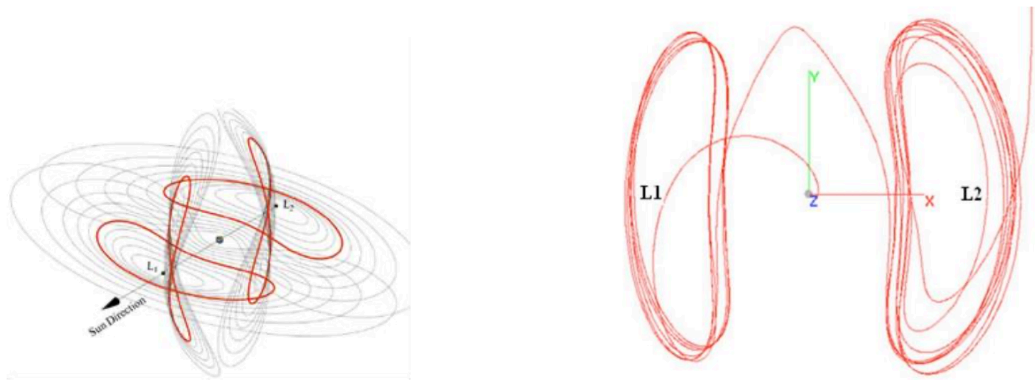

(a) Horizontal and Vertical Lyapunov Orbits [22]

(b) Lissajous Orbits [22]

Figure 10.1: Orbits around L_1

In summary, horizontal Lyapunov Orbits and Lissajous Orbits will be considered for further analysis. In order to devote as much time as possible to analyzing the central distinguishing aspects in greater amount of detail, the following simplifying assumptions have been made.

- **The transfer ΔV required to reach both orbits is the equal.** This assumption is made as both orbits are around the same point with extremely similar amplitudes.
- **The time of flight to reach both orbits is equal.** The reasoning for the assumption above applies here as well. Furthermore, the choice of propulsion discussed in Section 11.4 is considered more critical than orbit choice for this aspect.
- **The communication disturbances effect both orbit constellations to the same degree.** This assumption is made as both orbit types will face difficulty in communication due to the time spend in the solar exclusion zone. Strategies to ensure communication nonetheless are described in Section 11.2.1.

Thus, the remaining criteria which need to be analyzed are the stability, the effective shield area, and the collision risk.

10.2.3. Mathematical Method

In order to analyze the respective orbits accurately, they need to be found mathematically. The first step to achieve this was to implement a simulation of the circular restricted three body problem

(CR3BP). The CR3BP assumes two primary bodies with masses m_1 and m_2. In this case these bodies are the Sun and Earth, respectively. A third body, in this case a satellite, is introduced, the motion of which is described. Next the following assumptions are made [23].

- The third body is assumed to have negligible mass and thus a negligible gravitational pull on the primary masses.
- The primary masses orbit the system's center of mass in circular orbits.

The frame used corresponds to $x-y-z$ frame displayed in Fig. 10.2 and will be described shortly. The origin is placed at the center of mass. The $x-y$ plane is the ecliptic plane in which m_1 and m_2 rotate. The z-axis is perpendicular to the $x-y$ plane. The frame rotates around the z-axis with a constant angular velocity ω, equal to the angular velocity of the primary bodies around the center of mass. The problem is made dimensionless by setting the total mass $m_1+m_2=1$. The mass parameter μ is defined as $\mu = m_2/(m_1+m_2)$. Thus, the masses of bodies m_1 and m_2 are $1-\mu$ and μ respectively. Furthermore, the distance between the two primary bodies is set equal to one. This, combined with the rotational frame results in the masses m_1 and m_2 having a fixed position within the frame at $[-\mu, 0, 0]^T$ and $[1-\mu, 0, 0]^T$ respectively. Finally the unit time is defined by setting the orbit of the primary bodies around the center of mass equal to 2π time unit, resulting in one time unit being equal to $1/\omega$[23].

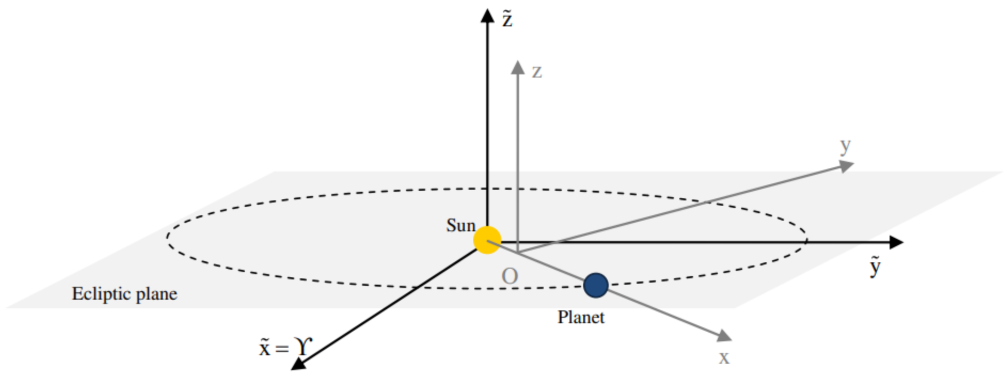

Figure 10.2: Reference frame CR3BP [24]

The equations of motions used are displayed in Eq. (10.1) with U_p representing the partial derivative of the potential with respect to a variable p. Due to the dimensionless nature of the analysis, the gravitational constant is equal to one resulting in the equation for potential given in Eq. (10.2) with r_1 and r_2 being the distance from the body to the Sun and Earth, respectively[23].

$$\ddot{x} = 2\dot{y} + U_x, \quad \ddot{y} = -2\dot{x} + U_y, \quad \ddot{z} = U_z \tag{10.1}$$

$$U = \left(\frac{1-\mu}{r_1} + \frac{\mu}{r_2}\right) - \frac{1}{2}\left(x^2+y^2\right) \tag{10.2}$$

$$r_1 = \sqrt{(x+\mu)^2 + y^2 + z^2}, \quad r_2 = \sqrt{(x-(1-\mu))^2 + y^2 + z^2} \tag{10.3}$$

The numerical method used for the forward integration of the problem was a Runge-Kutta fourth-order method (RK4). The verification of the correct implementation of the CR3BP as well as the integrator was done as described in Section 10.3.3.

Sun-Earth L_1 Point

To accurately calculate the position of the L_1 point the value used for the mass parameter of the Sun-Earth system was $\mu = 3.0043E - 6$[25]. The L_1 point can only be found numerically by finding the point where U_x is equal to zero[23]. The recursive bisection method was used. The range of x values the algorithm searched for a solution within was set from 0.970 to 0.999. This was obtained by looking at standard values for the L_1 point in a dimensionless system. The tolerance level was set to $1e - 15$ and the algorithm converged to the following location $[0.9900256894818678, 0, 0]^T$. This is the location of the Sun-Earth L_1 point used in all subsequent calculations presented in this section. At this point it is essential to state that although the effective L_1 point is shifted due to the solar radiation pressure acting on the spacecraft as demonstrated in Section 10.2.4, this will be neglected for the analysis conducted in this section as the effect of the solar radiation pressure has not been implemented as part of the CR3BP.

The eigenvalues and eigenvectors of the L_1 point can be found by analyzing the motion in close vicinity to the L_1 point in response to a small linear perturbation, using the linearized equations of motion in a local coordinate system. This analysis yields that the out-of-plane motion is not only uncoupled from the in-plane motion but that it is stable. In order to analyze the in-plane motion ($x - y$ plane) it is convenient to rewrite the equations of motion associated with the in-plane motion, expressed in the local coordinate system, into vector form with **x** being the state vector and A being the Jacobian derived from the Equations of Motion in the local coordinate system [23].

$$\dot{\mathbf{x}} = A\mathbf{x} \tag{10.4}$$

$$A = \begin{bmatrix} 0 & 0 & 1 & 0 \\ 0 & 0 & 0 & 1 \\ -U_{xx} & -U_{xy} & 0 & 2 \\ -U_{xy} & -U_{yy} & -2 & 0 \end{bmatrix} \tag{10.5}$$

The stability of a linearized system is given by the eigenvalues of its Jacobian matrix. Therefore the stability of the L_1 point can be evaluated by finding the eigenvalues of the matrix shown in Eq. (10.5), evaluated at the equilibrium point, in other words at the L_1 point [23]. The 4 eigenvalues obtained given the mass parameter and the location of L_1 stated above are displayed below.

$$\lambda = 2.53256148, -2.53256148, 2.08639393i, -2.08639393i$$

The eigenvalues are conjugate pairs with the expected form of 2 purely real and 2 purely imaginary eigenvalues[23]. As can be seen the system is unstable as there is one real positive eigenvalue. The correctness of these eigenvalues has been verified by comparing the output of the algorithm for several systems with distinct mass parameters and initial conditions to the eigenvalues found in literature [26]. Furthermore, this showed that the implementation of the Jacobian Matrix in our program and thus the partial derivatives within it where correct. This is important for the content discussed in Section 10.2.3, which builds on the content discussed in this section.

Horizontal Lyapunov Orbits

As mentioned in Section 10.2.2, Horizontal Lyapunov Orbits are entirely in the ecliptic plane, the $x-y$ plane, thus the analysis can be preformed in two dimensions. The method described in this section is employed to find initial conditions for any number of periodic orbits around the L_1 point. This is achieved through the exploitation of symmetry of periodic orbits through the use of a differential corrector.

The first step is too find a single orbit. To achieve this, an initial guess is generated by exiting the eigenvector ξ corresponding to one of the imaginary and therefore periodic eigenvalues shown in Section 10.2.3 multiplied with a magnitude of $E - 6$. This is shown in Eq. (10.6), with $\mathbf{x}_{L_1}$ being the equilibrium position at L_1. Given that the state vector is of the form $[x, y, \dot{x}, \dot{y}]^T$, this results in an initial guess $\mathbf{x}_0$[23].

$$\mathbf{x}_0 = \mathbf{x}_{L_1} \pm \xi E - 5 \tag{10.6}$$

Due to the symmetry of the desired orbit about the x-axis, it is required for this guess to be of the form $[x_0, 0, 0, \dot{y}_0]^T$. Furthermore, the velocity after half an orbit should also be perpendicular to the axis of symmetry, meaning that $\mathbf{x}_{1/2}$ is of the same form. This is visualized in Fig. 10.3[23].

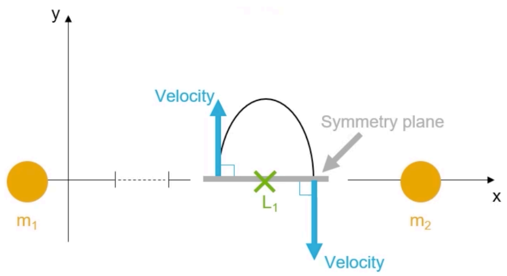

Figure 10.3: Orbital Symmetry [23]

Having obtained the guess for the initial conditions from the eigenvector, it is forward integrated in time, however the requirement of the velocity being perpendicular to the x axis after half an orbit is not met i.e. $\mathbf{x}_{1/2} = [x_{1/2}, 0, \dot{x}_{1/2}, \dot{y}_{1/2}]^T$. Therefore the initial guess needs to be modified, this occurs using a differential corrector which iterativlely improves this guess. This method makes use of the so called State Transition Matrix (STM), which estimates how a small deviation in the state variables propagates along the trajectory. Thus at time t_0 the STM, represented by ϕ is given by a 4x4 Identity Matrix. The STM is integrated simultaneously with the CR3BP equations of motion using the RK4 and the differential equation shown in Eq. (10.7), with A being the Jacobian Matrix stated in Eq. (10.5) [23].

$$\dot{\phi} = A\phi \tag{10.7}$$

Because the STM estimates the change in states at an arbitrary time t due to a change in state at t_0, it can be used at time $t_{1/2}$ to adjust the initial conditions in order to achieve a periodic orbit. This is done by adjusting only one of the initial conditions while keeping the other the same. The method employed here adjusts $\dot{y}_0$ while keeping x_0 the same. The change in $\dot{y}_0$ necessary to improve the initial guess is then given by Eq. (10.8) with $\dot{x}_{1/2} \mid_{Guess}$ being the velocity in x direction after half an orbit which essentially needs to be removed [23].

$$\delta \dot{y}_{t_0} = -\left(\phi_{34} \mid_{t=t_{1/2}} - \frac{\ddot{x}_{1/2}}{\dot{y}_{1/2}} \phi_{24} \mid_{t=t_{1/2}} \right)^{-1} \dot{x}_{1/2} \mid_{Guess} \tag{10.8}$$

This process was repeated until $\dot{x}_{1/2} \mid_{Guess}$ was smaller than $E-8$ and thus a symmetric and periodic orbit had been obtained. The process resulted in the initial conditions,

$$\mathbf{x}_0 = [0.989985929700, 0, 0, 0.000268825774]^T$$

Having found the first orbit, an infinite amount of Horizontal Lyapunov Orbits can be found. This is achieved by simply shifting the x coordinate of the initial condition by a small amount, applying the initial velocity of the previous orbit and subsequently applying the differential correction method until the error reduces to below the previously mentioned threshold. This method was applied to all Lyapunov Orbits discussed in the following chapters, with the algorithm converging to the solution in four or less iterations.

Furthermore, the stability of these orbits can be analyzed by finding the eigenvalues of the STM after a complete orbit [23]. This was done but could not be used in the stability comparison as explained in Section 10.2.5. However, the form of the eigenvalues followed the one expected i.e. $\lambda_{1,2} = 1, \quad \lambda_4 = 1/\lambda_3$ and could thus be used as a means of verification that the process had been implemented correctly [23].

Lissajous Orbits

Finding Lissajous Orbits was achieved using the same method detailed in Section 10.2.3. However due to the Lissajous Orbits being three dimensional the equations of motion in z direction can no longer be neglected resulting in a new state vector $[x, y, z, \dot{x}, \dot{y}, \dot{z}]^T$ and a new Jacobian Matrix shown in Eq. (10.9) [27].

$$\begin{bmatrix} 0 & 0 & 0 & 1 & 0 & 0 \\ 0 & 0 & 0 & 0 & 1 & 0 \\ 0 & 0 & 0 & 0 & 0 & 1 \\ -U_{xx} & -U_{xy} & -U_{xz} & 0 & 2 & 0 \\ -U_{xy} & -U_{yy} & -U_{yz} & -2 & 0 & 0 \\ -U_{xz} & -U_{yz} & -U_{zz} & 0 & 0 & 0 \end{bmatrix} \tag{10.9}$$

Furthermore, an initial velocity in z direction is present. However because the motion in z is uncoupled from the motion in the $x-y$ plane, the differential correction method remains the same as only the initial velocity, $\dot{y}_0$ needs to be corrected[23].

10.2.4. Pattern Optimization

At any given moment during the orbit, some shields will obscure other shields. The pattern must be optimized such that the overlap of shields is minimized. To optimize the shading pattern, all of the shields must be modeled such that the degree of overlap can be quantified.

Modeling Orbits

Integrating the trajectory of an orbit in the CR3BP is relatively computationally expensive. The number of shields will be in the order of $70E3$. Therefore, $70E3$ orbits would have to be integrated in parallel to model the orbits using the CR3BP. Since the computational resources are limited, a different approach must be taken.

The orbits are modeled by using the linear approximation of the equations of motion near the L_1 point Eq. (10.1). The linear approximation has periodic solutions of the form:

$$x = -A_x cos(\omega_{xy} t), \quad y = A_y sin(\omega_{xy} t), \quad z = A_z sin(\omega_z t) \tag{10.10}$$

The amplitudes and periods (A and ω) of the orbits were solved accordingly. This was done using the differential corrector and continuation method described in Section 10.2.3. The periods and amplitudes of 900 orbits were solved for with a starting maximum amplitude of three and a minimum of one Earth radii. The 900 orbits were selected such that the entire solution space was filled while having a minimum distance between orbits to ensure no collisions. In Fig. 10.4a and Fig. 10.4b the solution space for which the orbits were solved for is shown. Then, A and ω were extracted from this analysis and used to model the orbits via Eq. (10.10). The Lissajous orbits shown in Fig. 10.4b were solved such that the inclination increases as the amplitude decreases, such that the orbits are as spread out as possible.

Using the data of the 900 orbits, a regression model was built such that the configuration of orbits can be quickly adjusted for the optimization process. The following relationships were found for the Lyapunov and Lissajous orbits. It can be seen from the R^2 value in Table 10.1, that the regression model accurately represents the CR3BP orbits. The regression is valid for $i = 0, 1, 2, ..., 450$. $i = 0$ represents the starting orbit (three Earth radii) and $i = 450$ represents the smallest orbit (1 Earth radii).

Table 10.1: Regression orbit amplitudes and angular velocities

	Lyapunov		Lissajous	
Variable	Regression	R^2	Regression	R^2
A_x [-]	$8.0215E-8i-3.9759E-5$	0.9999999	$8.0215E-08i-3.9760E-5$	0.9999999
A_y [-]	$-2.6038E-7i+1.2892E-4$	0.9999998	$-2.6038E-7i+1.2892E-4$	0.9999987
A_z [-]	N.a	N.a	$-7.7772E-11i+1.3405E-5$	0.9999988
ω_z [-]	N.a	N.a	$7.1231E-11i+2.0116E-5$	0.9999294

Lastly, the validity of modeling the orbits using Eq. (10.10) must be verified. This was done by comparing an orbit produced by the CR3BP with one that uses Eq. (10.10) and Table 10.1. In Fig. 10.4c, it can be seen that the linearized solutions model the orbits very well. The similarity is such that careful attention is necessary to notice the difference between the orbits.

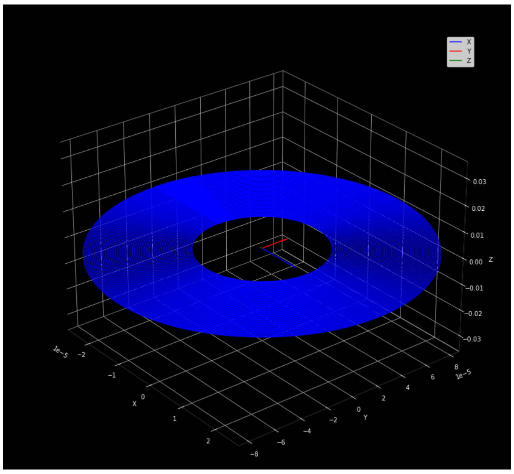

(a) Lyapunov Solution Space

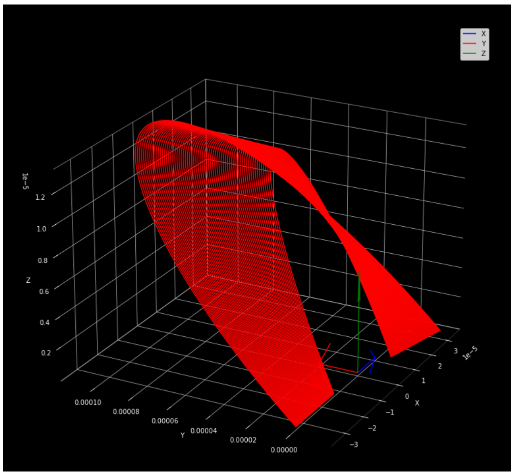

(b) Lissajous Solution Space

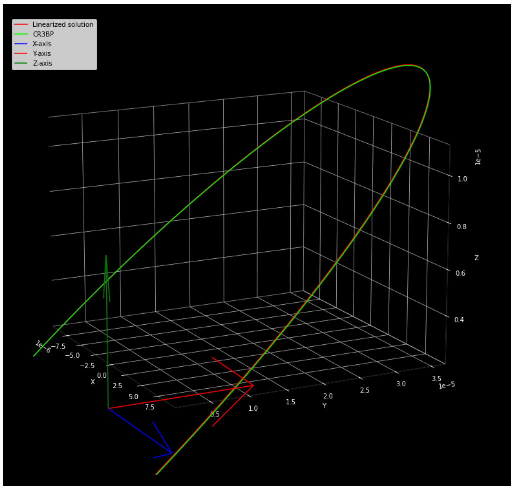

(c) Comparison between CR3BP and liner solution Lissajous Orbits

Figure 10.4: Modelling Orbits

Fitness Function

In order to assess the fitness of the constellation configuration, the constellation efficiency was defined as $\epsilon = A_{effective}/A_{total}$. A_{total} is the sum of the area of the shield and $A_{effective}$ is the sum of the projected area of the shields in the target area such that the overlap of shields is accounted for. The value of ϵ gives an indication of how much overlap there is between the shields. Therefore, a value as close to 1 is desired since this would mean fewer spacecraft are required.

Pixel Model

In order to model the overlap of the shields, the target area was discretized such that 1 unit area equals the area of one shield 91km^2. This assumption will undoubtedly result on deviations since the circular area of the shields is modeled as a squared one as seen in Fig. 10.5a. Nevertheless, due to the large solution space and number of spacecraft, it is expected that this model represents the problem accurately enough. In Fig. 10.5b, Lissajous's orbits are shown in the pixel model with the shields represented as pixels.

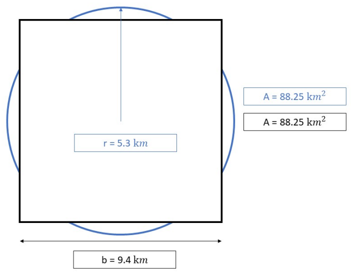

(a) Area representation

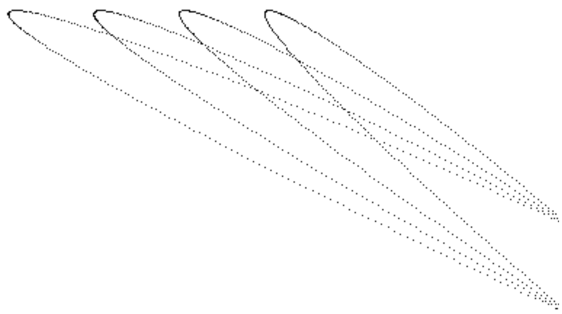

(b) Lissajous Orbits with constellation of shields

Figure 10.5: Pixel model

Monte Carlo Simulation

The effectiveness of any given constellation will fluctuate as a function of time since the overall constellation does not have a period. This means that the configuration at $t = 0$ will never be reached again. Therefore the only way to estimate the average value ϵ of a constellation configuration is through a Monte Carlo simulation. In Fig. 10.6b, it can be seen that the value ϵ is indeed not constant and is in fact described by a minimum extreme distribution.

In order to calculated the distribution shown in Fig. 10.6b, the value ϵ for a set of random points is calculated such that all of the possible values from Eq. (10.10) can be tested. The average estimated efficiency of a constellation configuration can be then found by taking the average of these test points.

In order to ensure that the Monte Carlo simulation converges, the relationship between the average ϵ and the number of Monte Carlo points was investigated in Fig. 10.6a. From this, it can be seen that the average does indeed fluctuate and converges around a center value.

The distribution of the efficiencies for a given constellation was also investigated in Fig. 10.6b. From this, it can be seen that most of the efficiencies are centered around a central value. Moreover, it can be seen that the distribution follows a minimum extreme type. Minimum extreme distribution has more variance towards the lower values of the distribution.

From this analysis, it can be concluded that any given constellation will have fluctuating efficiency. This is described by a minimum extreme distribution. Therefore, the amount of solar radiation obstructed will fluctuate around a central value.

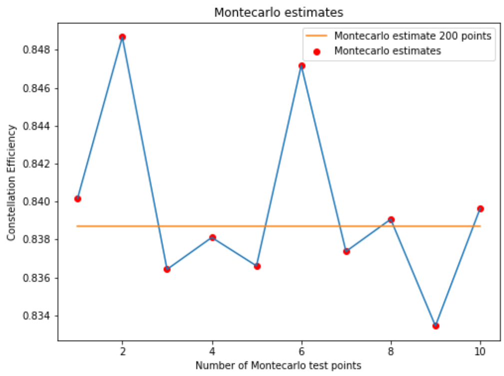

(a) Monte Carlo Convergence

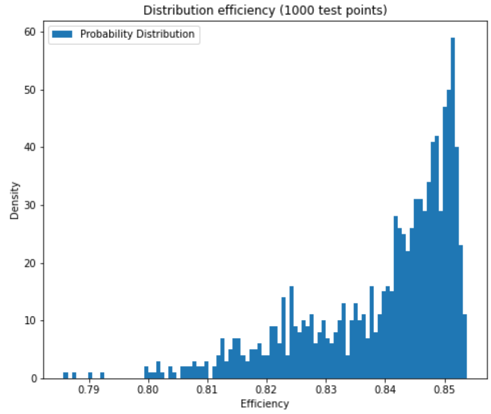

(b) Distribution efficiencies

Figure 10.6: Monte Carlo ϵ estimation for a given orbit configuration

Optimization setup and Constraints

In order to optimize the constellation, some constraints must be imposed. The following section explains the reasoning behind these constraints.

Maximum orbital amplitude

Due to the solar pressure, the position of the L_1 is shifted. The choice of reflectivity and area density of the shield will have an influence on this position and therefore the required mass and area to reduce the solar radiation by 1.8 %. The maximum amplitude that the orbits can have is a direct result of the position of the L_1 point. The closer to the Sun, the more area is needed.

The optimal position in terms of total mass occurs at $2.2E6$km from the Earth with a density of 1.15 g/m^2 and a reflectivity of 3.2%. The final area density of the design was aimed to satisfied this value. Moreover, the required reflectivity of the shield is believed to be possible, but further research will have to be conducted in order to confirm this. In Fig. 10.7b it can be seen that indeed the total required mass of the shield is minimized when the L_1 point is at $2.2E6$ km from Earth.

Finally, the target area can be calculated by assuming solid angles between the Sun and the Earth as shown in Fig. 10.7a. The maximum amplitude of an orbit shall be less than or equal to 2.6 Earth radii in order to always be in between the Sun and Earth.

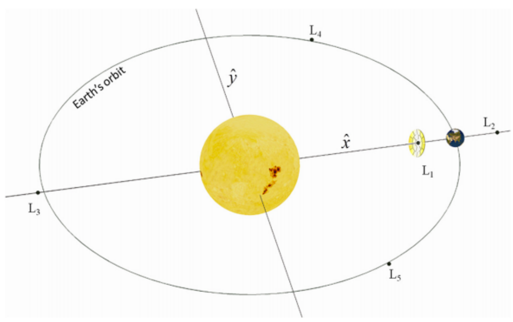

(a) Geometrical description of the problem [28]

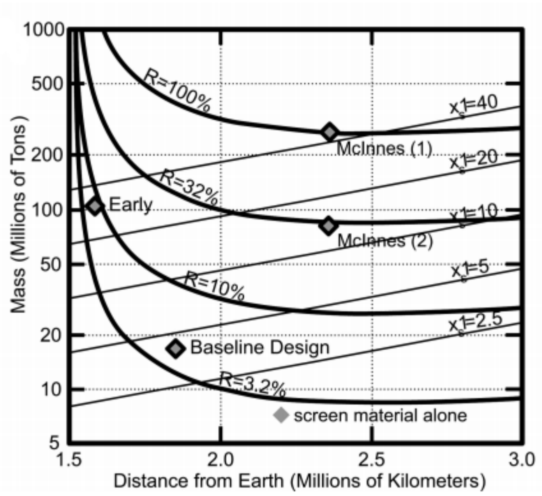

(b) Total shield mass as function of L_1 distance [29]

Figure 10.7: Analysis Location of L_1

Maximum number of Spacecraft per orbit

The maximum number of spacecraft per orbit must not exceed 1026. This number was found by calculating how many spacecraft fit in the smallest orbit possible while maintaining a spacing of two shields between end to end of the shields. The circumference of the smallest Lyapunov orbit is equal to 4.62 Earth radii, therefore a maximum of 1026 fit inside this circumference.

Minimum number of spacecraft

The minimum number of total spacecraft is $65\ 935$ as this number of shields required to cover the target area of $6E6$ km^2 with a shield of 91 km^2.

Minimum spacing between orbits

The radius of the shield is equal to 5.3 km, Therefore a minimum distance of 10.6 km must be maintained such that neighboring orbits do not collide. A safety margin was imposed, therefore the minimum distance between orbits is 12 km.

Minimum orbital amplitude

The minimum orbital amplitude was arbitrarily set at 1 Earth radii since the stability characteristics quickly worsen for smaller orbits. Further analysis must be done to determine what are the stability limits to determine the exact minimum amplitude.

Pattern Optimization Results

In Fig. 10.8, the results of the optimization can be seen. From this, it can be concluded that Lissajous offer much better ϵ values. The best configuration found is composed of 65 Lissajous orbits. These orbits are said to be "oscillating" since the biggest orbit has a positive A_z, the second biggest has a negative A_z, and so on. Therefore, the constellation has creates this oscillating effect since half of the orbits have negative amplitudes and half positive amplitudes. In contrast, Fig. 10.5b shows a constellation of Lissajous with all the orbits having a positive A_z value.

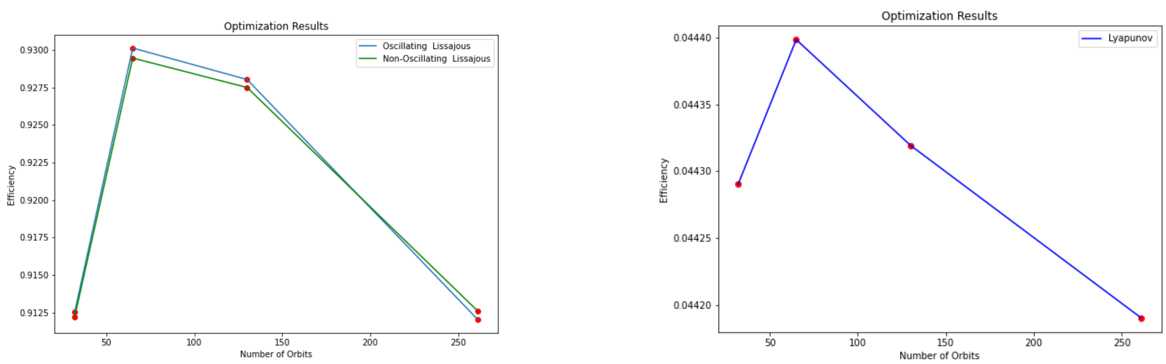

(a) Lissajous Results

(b) Lyapunov Results

Figure 10.8: Optimization Results

10.2.5. Final Trade Off

Effective Shield Area

From the results of Section 10.2.4, it is clear that the best option is Lissajous orbits shown in Fig. 10.9a. Not only is it the most efficient configuration, but it also shades the Earth more uniformly than the other options. A uniform shading pattern will cause a more gradual change in solar radiation which would cause the least disruption environment.

Collision Risk

The collision risk is expected to be marginally higher for Lissajous's orbits since it has a more complex motion. Nevertheless, at this stage of the analysis it is not certain if other issues might arise to a specific configuration.

Stability

All of the orbits around L_1 are unstable. Because Lissajous's orbits are not technically periodic orbits but rather open trajectories, the stability of Lissajous could not be assessed in the same way as Horizontal Lyapunov Orbits. Regardless of not knowing the exact stability properties of Lissajous's at this moment, it is known from the literature that it is possible to maintain a spacecraft in a Lissajous orbit around a Sun-Earth collinear Liberation point without excessive amounts of ΔV being required [18].

Although the collision risk may be slightly higher and the precise stability characteristics are unknown, Lissajous Orbits have been selected due to the efficiency being two orders of magnitude larger compared to Lyapunov orbits. The final orbit constellation consists of 65 orbits and around $1\ 076$ shields per orbit with an average efficiency ϵ of 0.93. Therefore, for this configuration, a minimum of $70\ 898$ shields would be necessary to cover the target area at all times. In Fig. 10.8, a part of the final orbit configuration is shown. Additionally, the projection of the orbits in the $x-y$ planes is presented to demonstrate the orbits do not collide at any point. For the rest of the report, the total number of spacecraft will be rounded to $71\ 000$

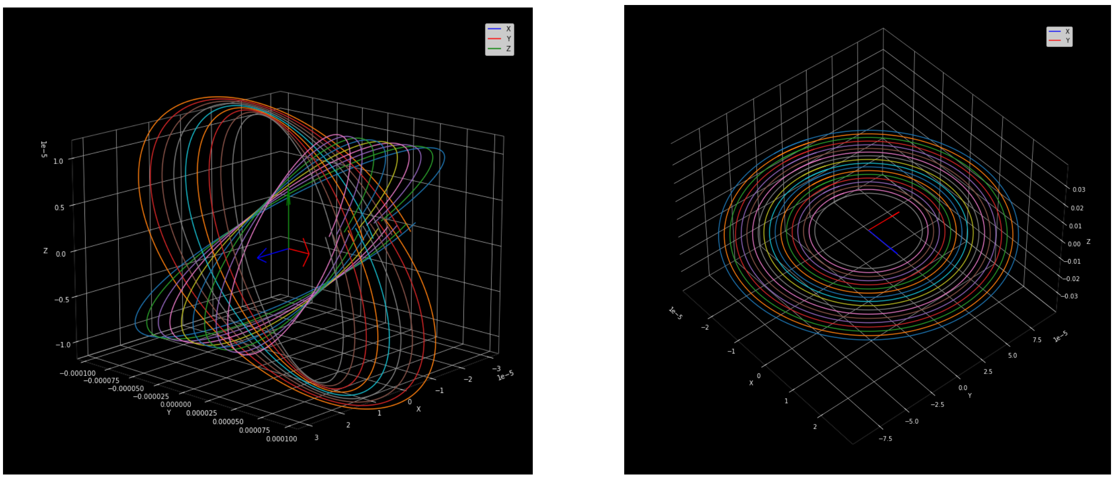

(a) 3D orbits

(b) Projection in the $x-y$ plane

Figure 10.9: Final constellation (only a third of the orbits shown for visual purposes)

10.3. Dynamical Model

This section describes the dynamical model used for the trajectory analysis and optimization. The information shown in this section was mostly already published in [3], with only small changes made in this report.

Section 10.3.1 will elaborate on the chosen tool for making the dynamical model. Section 10.3.2 describes how the model was set up. Finally, Section 10.3.3 will show the verification of the model.

10.3.1. Software Choice

The complexity of simulating the n-body problem comes from ensuring accuracy and efficient computation. An efficient algorithm can significantly speed up the simulation and reduce the truncation error. However, designing such an algorithm and simulation environment is time-consuming. Therefore existing mission design tools will be used. There are several trajectory analysis tools available. The Delft University of Technology's own 'TU Delft Astrodynamics Toolbox' (Tudat) was selected [19].

[18]URL `https://sci.esa.int/web/planck/-/34728-orbit-navigation` [cited 22 June 2021]

[19]URL `https://tudat-space.readthedocs.io/en/latest/` [cited 19 May 2021]

Other tools were considered, like for instance the General Mission Analysis Tool (GMAT) from NASA. However, the free version of GMAT is quite limited and it uses a non-standard scripting method. The tudatpy library on the other hand, uses Python, a beginner friendly programming language, and offers much more flexibility.

10.3.2. Model Setup

This subsection elaborates on the model setup, specifically, the reference frame, integrator and acceleration models.

Reference Frame

The spacecraft is propagated in an Earth-centered inertial (ECI) frame defined by the J2000 standard epoch. The start epoch is defined as the amount of seconds after J2000. J2000 is a widely used standard that can be used to define a celestial reference frame.

Integrator

For the integrator method, there are several options available in the Tudat library. The options are: Euler, Runge-Kutta 4, Runge-Kutta-Fehlberg, Runge-Kutta Dormand-Prince, Bulirsch-Stoer, and Adams-Bashforth-Moulton

The Euler method can be immediately discarded as the documentation of the Tudat library discourages its use due to its inaccuracy.[19].

The Runge-Kutta 4 integrator is discarded since its fixed time step size does not allow for an efficient allocation of computational resources. Variable step size methods decrease the time step in the solution space where greater accuracy is needed and increase it where it is not. The appropriate step size is determined by the integrator, which bases the step size on the allowed relative and absolute error. These errors were set to $1E-9$, since this was similar to what was used in the documentation for Tudat[19].

The Runge-Kutta-Fehlberg was chosen since it was well described and used in the Tudat documentation[19].

Acceleration Models

The acceleration models are defined separately for each body. The default acceleration models in the Tudat documentation example are used[19].

For the gravitational acceleration models, the Sun, Moon, Mars and Venus are all modeled as point masses. This assumption can be considered a valid one because these celestial bodies are far away from the spacecraft during the entire mission. One exception might be the Moon, in case a lunar gravity assist is used. However, the optimal trajectory does not use a lunar gravity assist. Earth's gravity will be modeled as a spherical harmonic field of degree and order 5. The spacecraft is often quite close to Earth, making the point mass assumption invalid for Earth. Earth's atmosphere is also included through a simple aerodynamic acceleration model. The parking orbit might be high enough to not be affected much by the atmosphere, since the spacecraft is not in this orbit for very long. However, including Earth's atmosphere does prevent the optimization process from considering trajectories going through the lower part of Earth's atmosphere as viable. Finally, the solar radiation pressure is also included in the acceleration model, as this can have a considerable effect on the spacecraft during this mission.

10.3.3. Verification

In order for the results obtained by the model described in Section 10.3 to carry gravity, the model needs to be verified first. The verification methods have been described in detail previously [3] and will be shortly repeated here.

[19]See page 56

Code verification

Before the verification of the models was performed, several other verification methods were applied to eliminate trivial errors in the code. For the trajectory design, a few methods proved to be particularly useful. Firstly, preliminary sub-optimal trajectories were plotted to quickly confirm the correct implementation of not only the model, but also the optimization strategies. Secondly, numerous small tests that check only a specific part of the code were set up and successfully completed. For instance, the implementation of the maneuvers in the trajectory design was checked by comparing the velocity at the start and end of the maneuver and comparing that difference with the expected ΔV of the maneuver.

Verification Model

The Circular Restricted Three Body Problem (CR3BP), in combination with a Runge-Kutta fourth-order method (RK4) as an integrator, was used as the verification model. The precise implementation of this has already been described in Section 10.2.3 and will not be repeated here.

Lyapunov Orbits on the CR3BP

In order to ensure that the CR3BP was implemented correctly, a Lyapunov Orbit with initial conditions known from literature and displayed in Table 10.2 was successfully recreated. The mass parameter used was $\mu = 0.012155092$.

Table 10.2: Initial Conditions Lyapunov Orbit [25]

Orbit	x_0	y_0	z_0	$\dot{x}$	$\dot{y}$	$\dot{z}$
A	0.804226	0	0	0	0.325927	0

The comparison of the reference orbit and the orbit generated by our algorithm can be seen in Fig. 10.10.

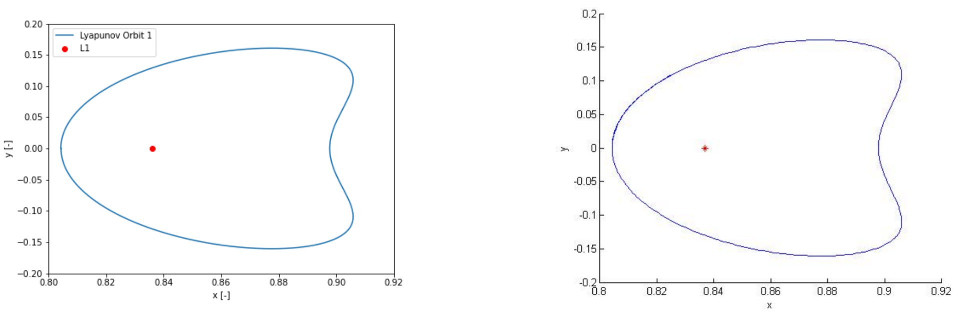

(a) Lyapunov Orbit CR3BP

(b) Reference Lyapunov Orbit [25]

Figure 10.10: Orbit A

Comparison Between CR3BP and Tudat Model

This section will offer a detailed comparison between the Tudat Model described in Section 10.3 and the verification model, namely the CR3BP. Both the solar pressure and aerodynamic forces are neglected, thus only the gravitational accelerations were included. Table 10.3 provides and overview of the two models and the configurations used for the comparison.

Table 10.3: Model Comparison Overview

Description	**Tudat**	**CR3BP**
Central Bodies	Sun, Earth,Mars,Venus Moon	Sun, Earth
Gravity model	Sun, Mars,Venus Moon = point mass Earth = spherical harmonic	Sun, Earth = point mass
Dynamics Bodies	System of differential equations with a J200 initial condition.	Sun and Earth circular orbits
Integration	Runge-Kutta 4th order	Runge-Kutta 4th order
Step size	1000 seconds	1000 seconds
Dynamics Vehicle	System of differential equations for all Central Bodies.	CR3BP
Initial condition Vehicle $[x, y, z, \dot{x}, \dot{y}, \dot{z}]^T$	$[1.08E11, 0, 0, 0, 0, 0]^T$	$[1.08E11, 0, 0, 0, 0, 0]^T$

The final comparison was preformed in the ecliptic J2000 inertial frame with the Sun as the origin. The comparison itself consists of the orbital elements of the orbits produced by the respective models, this is displayed in Table 10.4. Furthermore, a visual comparison can be found in Fig. 10.11.

Table 10.4: Orbital Elements Comparison

	Earth		Vehicle	
Elements	**Tudat**	**CR3BP**	**Tudat**	**CR3BP**
Eccentricity [-]	0.017	0.0	0.62	0.61
Semimajor axis [Au]	1.0	0.98	0.44	0.45
Period [Days]	365.3	365.0	108	113

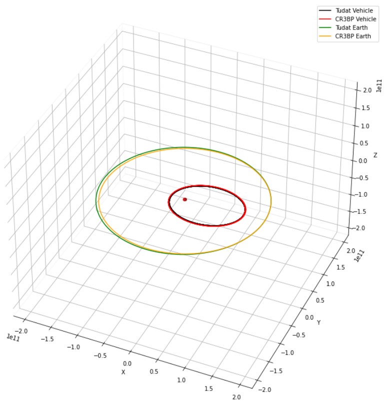

Figure 10.11: Verification Tudat model with the CR3BP

As can be seen in Table 10.4, the orbital elements of the two orbits are within 4% of each other. These differences can be traced back to the slight differences in configurations as well as differences is assumptions, such as the circularity of the orbit of the primary bodies. Thus it can be concluded that the Tudat model has been implemented correctly.

10.4. Trajectory Optimization

For the transfer subproblem defined in the chapter introduction, the goal is to minimize the cost per kg to L_1. First, the mission assumptions are stated in Section 10.4.1. In order to find this minimum cost per kg to L_1, an optimization problem is defined in Section 10.4.2. In order to solve this optimization problem, an optimization algorithm is needed, which will be found in Section 10.4.3. Finally, the setup of the optimization algorithm is documented in Section 10.4.4.

The results and conclusion of the trajectory optimization process will be shown in the next section, Section 10.5.

10.4.1. Mission Assumptions

In order to ease the design of the trajectory to L_1, the following assumptions were made.

- The propulsive acceleration of the spacecraft is equal to the propulsive acceleration at the start of the trajectory and will remain constant for the rest of the transfer.
- The spacecraft is able to perform maneuvers with 100% accuracy.
- The launcher's maneuvers are impulsive.
- The start epoch was set to zero seconds after J2000 for all the simulations.

10.4.2. Optimization Problem

In order to find an optimal solution faster, the spacecraft was propagated backwards in time from the L_1 point instead of forwards from the Earth parking orbit. This makes the optimization process faster, because at the parking orbit there are more valid final state vectors compared to L_1. There are many valid final state vectors at Earth because the launcher performs a transfer from the final state to the parking orbit, which results in a more flexible boundary condition than the one for the L_1 point. This makes it easier to target Earth when compared to targeting L_1.

Although the spacecraft is propagated backwards in time starting from L_1, the parking orbit state and L_1 state are still referred to as start and end of the simulation, respectively. This way the time at the end of the simulation is always larger than the time at the start.

After the spacecraft performs all its maneuvers (considered backwards in time), the launcher provides the ΔV necessary to change the velocity and altitude at the spacecraft's closest approach to Earth to the velocity and altitude of the spacecraft at the parking orbit. The launcher achieves this with two Hohmann maneuvers to bring itself to a circular orbit at the closest approach altitude and another maneuver to raise the velocity at this circular orbit to the velocity at closest approach. The launcher trajectory is not designed, instead it is assumed that the launcher's maneuvers are impulsive. These assumptions reduce the problem down to only the design of the maneuvers performed by the spacecraft itself.

The goal is to minimize the cost per kg to L_1, where the cost includes only the propellant and launcher costs, therefore the objective function is given by:

$$J = \frac{C_{launchers} + C_{propellant}}{M_{sc-pl}} \tag{10.11}$$

Where $C_{launchers}$ is the cost of the launchers required for one spacecraft, $C_{propellant}$ is the cost of the propellant and M_{sc-pl} is the mass of the spacecraft payload delivered to L_1. For the spacecraft payload mass, only the spacecraft propellant mass is deducted from the launcher payload mass brought to the parking orbit.

All costs are in 2020 USD unless stated otherwise.

Costs

The cost of the launchers required for one spacecraft ($C_{launchers}$) is equal to $C_{launcher} \cdot (1+n_{refuelings})$, where $C_{launcher}$ is the cost of a single launcher and $n_{refuelings}$ is the number of refuelings utilized. The number of refuelings is equal to the propellant mass required for Starship to put the spacecraft on the escape trajectory, which is calculated with the Tsiolkovsky rocket equation, divided by the launcher payload mass Starship will bring to LEO, which is equal to $125E3$ kg (Section 10.1). Since the maximum propellant mass Starship can store is $1\ 200E3$ kg, the maximum number of refuelings is equal to 9.6.

The cost of the propellant is simply calculated by multiplying the mass of the propellant used by the spacecraft by the cost per kg of the used propellant. The amount of propellant used by the spacecraft is calculated with the Tsiolkovsky rocket equation, where the initial mass is $125E3$ kg. It was found that the total cost is minimized if the initial mass of the spacecraft is equal to $125E3$ kg, the maximum launcher payload Starship is capable of putting into the parking orbit. The cost per kg of the propellant is discussed further in Section 11.4.

Propulsive acceleration ranges Another objective, which is not included in Eq. (10.11), is to minimize the propulsive acceleration required, as this puts less strain on the propulsion subsystem. However, since the propulsion subsystem is not designed in the astrodynamic analysis, the propulsive acceleration or the effect it has on the cost cannot be included in Eq. (10.11). Instead, the optimization process is performed for multiple propulsive acceleration magnitudes. The results that follow can then be used to design the propulsion subsystem.

The range of propulsive accelerations that will be tested depend on the available thrusters and the mass of the launcher payload that is put into the transfer trajectory. The propulsive acceleration ranges are split into the low-thrust propulsion scenario and the high-thrust propulsion scenario, which allows for fine-tuning of the optimization process for these scenarios. The propulsive acceleration range for the low-thrust scenario is $1E-6$ to $1E-4$ m/s^2. The propulsive acceleration range for the high-thrust scenario is $7E-3$ to $2E-1$ m/s^2. These propulsive acceleration ranges are based on the thrusters described in Section 11.4.2 and the initial mass to LEO of $125E3$ kg.

Solar sailing was dismissed as a propulsion method, since the effect it has on the other subsystems could not be analyzed. In the solar sailing scenario, the shield would be used as the solar sail.

10.4.3. Choice of Software

The Python Parallel Global Multiobjective Optimizer (PyGMO) library was chosen because the Tudat documentation encourages and facilitates the use of this library. The PyGMO library is developed by ESA and offers optimization algorithms that can be applied to a trajectory optimization problem [3].

Choice of Optimization Algorithm

Low-thrust scenario For the optimization of the low-thrust scenario, a custom algorithm was built after no algorithm from the PyGMO library provided a sufficient convergence rate. This custom algorithm used simple iterative methods similar to Newton's method to converge to a near-optimal solution within a reasonable amount of time.

High-thrust scenario For the optimization of the high-thrust scenario, several algorithms available in PyGMO were considered, from which Differential Evolution was chosen after internal testing showed that this algorithm converges the fastest to a near-optimal solution for the problem that is considered for the analysis in this section. Differential evolution (DE) is a method that optimizes a problem by iteratively trying to improve a candidate solution with regard to a given measure of quality [30].

10.4.4. Optimization Setup

With the optimization problem definition and the selected optimization algorithm, the optimization algorithm can be set up to accurately and quickly find a near-optimal solution for the problem. Firstly, the design variables are discussed. Afterwards,the approach to generate a fitness value for a given solution is explained. Finally, the optimization algorithm settings and termination settings are discussed.

Design Variables

To make optimal use of computational resources, the low- and high-thrust scenarios will have different design variables. Both of them will generate thrust timings and thrust direction functions. The thrust timings are saved as start and end times of the maneuvers. The thrust direction functions are retrieved using the following method, which was described before in [3].

The thrust vector for each maneuver is defined by a thrust magnitude and a unit vector. The unit vector $[x, y, z]^T$ can be retrieved by $x = cos(\phi_t)sin(\theta_t)$; $y = sin(\phi_t)sin(\theta_t)$; $z = cos(\theta_t)$, where θ_t and ϕ_t are the thrust angles for a maneuver, and x, y, z are coordinates in the reference frame described in Section 10.3.2. This unit vector is then multiplied with the propulsive acceleration magnitude to get the thrust vector.

Low-thrust scenario In order to make full use of the capabilities of the low-thrust propulsion method, the spacecraft needs to be able to activate its engines at any moment in time and aim the thrust vector in any direction during the transfer. To achieve this with a reasonable amount of design variables, polynomials are used to determine the thrust timings and the direction of the thrust vector. Before using the polynomials, the transfer is divided into N equal sized parts. For each part, three Chebyshev polynomials of degree p are used, one for the thrust timing and two for the thrust angles θ_t and ϕ_t, which are used to retrieve the thrust vector.

The design variables are then the coefficients for these polynomials, giving a total of $N \cdot p \cdot 3$ design variables. For the initial analysis, N and p were both set to 4, and for the final analysis, they are set to 20 and 4 respectively. Before the polynomials are evaluated, the time since the start of the part is transformed to the interval $[-1, 1]$, as on this interval the Chebyshev polynomials are most useful, as each one ranges from $[-1, 1]$ for a coefficient of 1.

The upper and lower bounds of the polynomial coefficients were set to 1 and -1 respectively, as [31] determined that Chebyshev polynomials provide small errors for small coefficients. The coefficient bounds $[-1, 1]$ encompass the values of the coefficients used in [31].

The thrust is activated when the polynomial for the thrust timing evaluates to a positive value.

High-thrust scenario The propulsive acceleration range considered for the high-thrust scenario was first analyzed with the design variables considered in the low-thrust scenario. This analysis resulted in a solution where there was only one maneuver, the L_1 capture maneuver. In order to find a better solution with the given computational resources, the amount of design variables is reduced for the high-thrust propulsive acceleration range. In fact, only three design variables were deemed necessary, namely the burn time and the two constant thrust angles. The end time of the burn was set to the end time of the simulation, which is when the spacecraft is at L_1. The bounds for t_{burn}, θ_t and ϕ_t were set to $[-450/a_t, -150/a_t]$, $[0, \pi]$ and $[0, 2\pi]$ respectively, where t_{burn} is the burn time, θ_t and ϕ_t are the thrust angles used to construct the thrust vector and a_t is the propulsive acceleration of the spacecraft.

Fitness

The fitness of a solution is equal to the value of Eq. (10.11) with the addition of a penalty, which steers the optimization algorithm towards the optimal solution. This penalty is applied when the spacecraft's closest approach to Earth is too far away for the Hohmann maneuvers performed by the launcher to this closest approach to be accurate. This prevents the use of Hohmann maneuvers directly to L_1 for instance. Another goal of this penalty is to steer the algorithm towards the right solution: having the final state vector at the parking orbit. The threshold for the use of this penalty was set to a distance of one Earth radius to the parking orbit, with a penalty of 10 m/s applied for every Earth radius after that.

Optimization Algorithm Settings

For the DE algorithm, most settings were kept at their default values. The seed was set to 123456, the population number to 50 and the number of generations to $1E3$. An algorithm that depends on random numbers should be run for multiple seed values to confirm that the algorithm converges to the global optimal solution. However, due to the time constraint, the decision was made run the algorithm for only one seed value. The population number was based on the population size used in [3]. The number of generations was based on the rate of convergence of the DE algorithm, it was terminated after no meaningful improvement was made in a considerable time span.

Termination Settings

The termination settings were previously shown in [3]. They are used to make sure the spacecraft does not collide with either the Moon or Earth. Only the end time of the simulation is changed, which was increased to 500 days, to provide more time for the low-thrust scenario, while also making sure that the transfer is completed well within the total mission time of 10 years.

10.5. Trajectory Optimization Results and Conclusion

The results and conclusions drawn are shown in this section. This section is once again divided into the low and high-thrust scenarios, with a trade-off between the two discussed at the end of the section.

10.5.1. Low-thrust scenario

An initial analysis of the range of propulsive accelerations for the low-thrust scenario provided two insights. Firstly, lower propulsive accelerations can provide more optimal trajectories. Higher propulsive accelerations use ΔV more quickly, thus decreasing the total thrust time for a given amount of ΔV. The optimization algorithm cannot precisely time when to thrust due to the low polynomial degree of the thrust timing function. Therefore more thrust time results in more stable control over the trajectory, since small inaccuracies will not quickly lead to an undesirable trajectory. Secondly, below a certain propulsive acceleration magnitude, the optimization algorithm is not able to find a valid trajectory.

This initial analysis gave an optimal propulsive acceleration of $1.6681E-5$ m/s^2. This propulsive acceleration requires 9 Aerojet Rocketdyne NEXT-C engines (Section 11.4.2), which can provide $1.692E-5$ m/s^2. The optimization algorithm was then run until it converged to a near-optimal solution for this propulsive acceleration. The information on this near-optimal solution are shown in Table 10.5 and Fig. 10.12a.

10.5.2. High-thrust scenario

From the initial analysis of the range of propulsive accelerations given in Section 10.4.2, it became clear that the spacecraft did not benefit from an propulsive acceleration higher than the minimum in this range. Therefore, for the final analysis, only the minimum propulsive acceleration of $7E-3$ m/s^2 was optimized for. At this propulsive acceleration, the Aerojet Rocketdyne R-42 thruster can be used (Section 11.4.2). However, this engine did not conform to the requirements set for the propulsion subsystem, because the burn time was too long. Therefore the stronger Aerojet Rocketdyne R-40B was chosen for the high-thrust scenario. This engine choice is detailed further in Section 11.4.2. Since this engine is able to deliver $4\ 000$ N of thrust, the propulsive acceleration considered for the final analysis for the high-thrust scenario is $3.2E-2$ m/s^2.

The results for the final optimization process are shown in Table 10.6 and Fig. 10.12b. The flight time of 178.4 days is quite a bit longer than an actual mission that went to L_1, the LISA pathfinder, which took about 50 days to get from Earth to an orbit around L_1[20]. The total ΔV of $3\ 437.8$ m/s is close to the ΔV of $3\ 370$ m/s estimated in [22].

Table 10.5: Results low-thrust scenario

Propulsive acceleration	$1.692E-5$ m/s^2
ΔV spacecraft	202.6 m/s
ΔV launcher	3142.1 m/s
Propellant mass spacecraft	628.3 kg
Spacecraft payload mass to L_1	$124\ 371.1$ kg
Number of refuelings	2.68
Flight time	293.6 days
Eclipse time	-
Cost per kg to L_1	84.1 $

Table 10.6: Results high-thrust scenario

Propulsive acceleration	$3.2E-2$ m/s^2
ΔV spacecraft	188.9 m/s
ΔV launcher	3249.0 m/s
Propellant mass spacecraft	$7\ 951$ kg
Spacecraft payload mass to L_1	$117\ 049$ kg
Number of refuelings	2.82
Flight time	182.5 days
Eclipse time	163.4 s
Cost per kg to L_1	96.0 $

10.5.3. Trade-off low and high-thrust scenarios

From Tables 10.5 and 10.6 it can be seen that the low-thrust method of propulsion offers a lower cost per kg to L_1 (84.1 $) than the high-thrust method (96.0 $). However, this cost estimate only

[20] URL `https://sci.esa.int/web/lisa-pathfinder` [cited 22 June 2021]

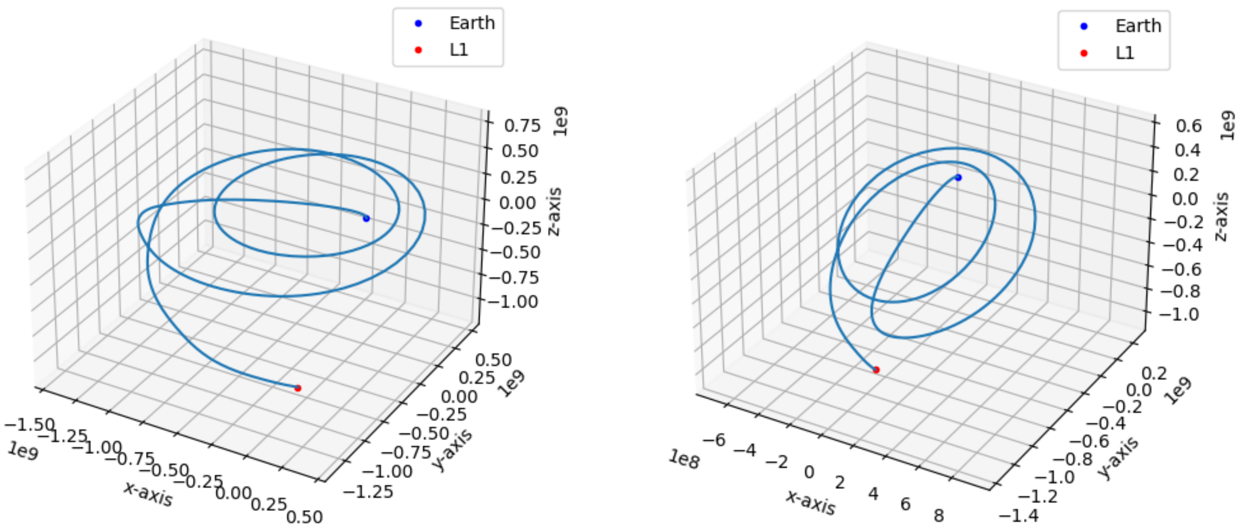

(a) Optimal trajectory low-thrust scenario

(b) Optimal trajectory high-thrust scenario

Figure 10.12: Optimal Trajectories

includes the launcher and propellant costs. The cost of the engines, power subsystem and the Technological Readiness Factor (TRL) are all not included, but still very significant. These elements combined should cost less than $1.49E6\ USD$ per spacecraft more for the low-thrust scenario than the high-thrust scenario in order for the low-thrust scenario to be cheaper.

As mentioned before, for the low-thrust scenario, nine Aerojet Rocketdyne NEXT-C engines are used, which have a TRL of 8 and require 6.9 kW each (Section 11.4.2). The high-thrust scenario uses a single Aerojet Rocketdyne R-42 thruster, which has a TRL of 9 and requires only small amounts of power for valve switching (Section 11.4.2).

Although no good estimate for the cost of both engines was found, the cost of the 9 electrical engines would likely exceed the cost of the single chemical engine by a large margin. The cost of the solar arrays necessary to produce the power for the electrical propulsion is also significant. The cost per Watt of the production of a solar cell that is usable for space applications can be reduced from about $50\ \$/$kg [32] to about $2\ \$/$kg 'in the relatively short term' [33], by scaling up manufacturing. This would require significant R&D, but the solar cells necessary for the nine ion engines would only cost $124E3\ USD$ after this reduction in costs. This cost is solely for the solar cells, so for instance the cost of the integration of the solar cells into the rest of the spacecraft is not included. The 62.1 kW solar panel would also require a significant structure, lowering the available spacecraft payload mass.

Although there is still a chance that the low-thrust scenario can still be more cost effective even with all these extra costs, it is unclear whether this is reachable within the mission operational deadline of ten years. Significant R&D into the electrical engines themselves but also the solar cells is needed. Although the costs for R&D can be shared by the tremendous amount of units that will be required, the time required for R&D cannot. The combination of the extra time required for R&D and uncertainty about the potential performance of low-thrust propulsion resulted in high-thrust propulsion being chosen for this mission.

10.6. Recommendations

This section discusses the recommendations that pertain to the astrodynamics section that should be considered at more detailed stages of the EOS mission design.

10.6.1. Orbit selection

While the most central criteria for orbit selection have been explored, more detailed analysis into other criteria will need to be preformed until a mission can commence. Below are a list of recommendations for further investigations to be conducted:

- Define a strategy concerning in which manner and order the orbits shall be filled.
- Preform a detailed study on the stability of Lissajous Orbits of this size in order to estimate risks and required ΔV for orbital maintenance.
- Further Investigate the collision risk in Lissajous Orbits and define a strategy for instances of spacecraft malfunctions.
- Investigate possibility of combining orbit types to further increase efficiency.
- Investigate how orbit constellation can be altered to shade specific areas on Earth.

10.6.2. Trajectory design

There are several improvements that can be made to the design of the trajectory to L_1. Several assumptions were made in Section 10.4.1. For the analysis presented in this chapter, there was not enough time available to analyze these assumptions, but it is recommended to do so in further research. The main recommendations, including the analysis of some of these assumptions, are listed below.

- The implementation of variable propulsive acceleration can improve the performance of the spacecraft, while including the imperfect execution of maneuvers can require some extra correction maneuvers.
- Unfortunately both low-thrust electrical propulsion and solar sailing had to be dismissed because of the uncertainty they bring. Both of these propulsive methods have the potential to be more cost effective than chemical propulsion if more research into them is conducted.
- It is recommended to change the start epoch in further research to represent the flight conditions more accurately.
- Investigation into the use of different acceleration models than the ones described in Section 10.3.2.
- Find the precise ΔV required to transfer to each of the orbits.

11 Subsystems Design

In this chapter, the design process for each of the subsystems will be laid out in detail. The results of these design processes can also be found in a more condensed version in the performance analysis in Chapter 5. The subsystems treated in this chapter will be the command and data handling subsystem (CDHS), the telemetry, tracking, and command subsystem (TT&C), the attitude determination and control subsystem (ADCS), the propulsion subsystem, the thermal control subsystem, the power subsystem, the structures subsystem, and finally, the payload.

11.1. Command and Data Handling Subsystem (CDHS)

The CDHS or Command and Data Handling Subsystem forms the brain and nerves of the spacecraft. The CDHS functions are: to handle and transfer status data from the subsystems, command actions to be performed by the subsystems, store necessary data, and autonomously computed commands. [34] [3]. In Section 11.1.1 the general architecture of the CDHS will be discussed. Next, a more detailed size, mass and volume estimate for the different CDHS components will be presented in Section 11.1.3.

11.1.1. CDHS Architecture

In Fig. 11.1 the lay-out of the CDHS hardware is shown. The onboard computer (OBC) can be divided in to four different parts. Firstly, the Central Processing Unit or CPU executes the implemented software. This software is stored in a primary memory unit included in the CPU. Secondly, a housekeeping board receives the housekeeping data of the various instruments in order to check the status and well-being of the spacecraft. Next, an In/Out (I/O) board is included to command the different instruments for example turning them off or changing the settings. Lastly, the TM/TC telemetry/tele-command (TM/TC) board handles the data that is to be sent to the ground as well as the commands from the ground to the spacecraft instruments. The OBC is connected to a solid state recorder or SSR. This instrument stores the gathered data before it can be send to the ground.[34]

The Spacewire network [12] will be used as a data bus. The data bus facilitates communication links between the OBC and the individual subsystem instruments. Spacewire routers will be implemented in between the OBC and the instruments which will be explained in more detail in Section 11.1.3. These routers select and handle packets of information to send it to the desired destination. [34]

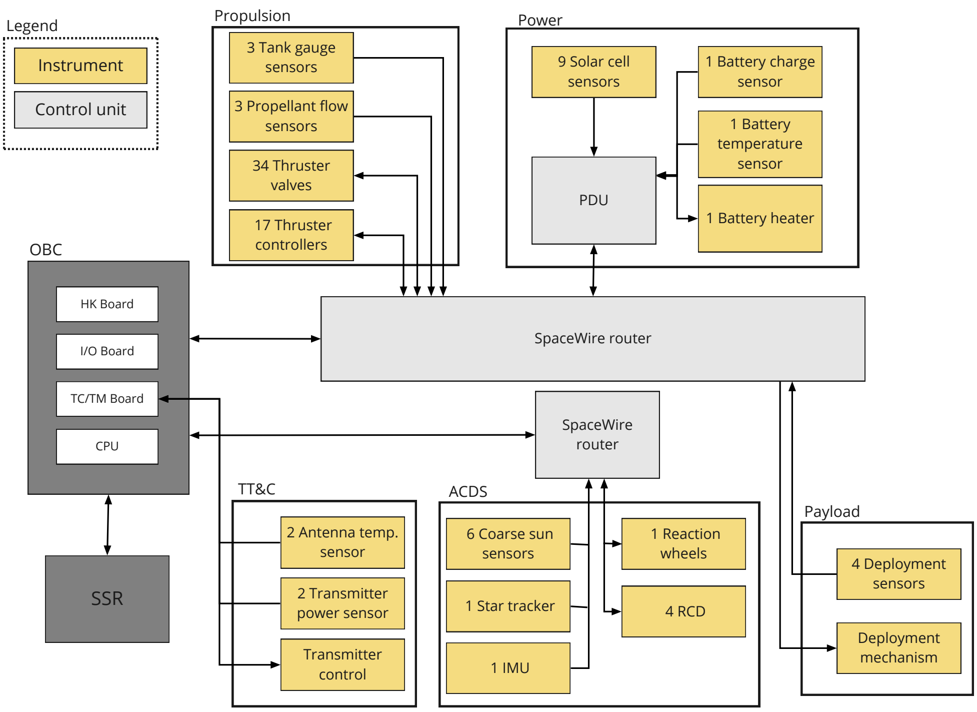

Figure 11.1: CDHS high level hardware diagram.

11.1.2. Housekeeping and Command Data Rates

The OBC monitors the health of the satellite instruments by receiving data from various sensors, control units and switches within the subsystems. This gathered data is also called housekeeping data. A detailed breakdown of the generated housekeeping data can be seen in Table 11.1. This data was derived from the ESA sentinel satellites[21] and adapted to this specific mission. Redundant instruments were not taken into account as these are only activated when the primary instrument fails. This results in a total housekeeping data rate of $3\,363.2$ bps entering the OBC. The data rates

[21] URL `https://sentinel.esa.int/web/sentinel/home` [cited 20 June 2021]

that come out of the OBC orginate from commands which are either received from the ground or generated by the OBC itself. These command data rates will be further discussed in Section 11.1.3.

11.1.3. CDHS Sizing

In this subsection the sizing of each of the instruments included in the CDHS will be performed based on off-the-shelf components. These instruments are: the OBC , the SpaceWire data bus and the SSR. Each instrument will be implemented twice to avoid single points of failure.

On Board Computer

The OBC can be sized by estimating the amount of onboard software that is needed as well as the required processing speed in order to handle all the subsystems. The amount of software can be quantified by source lines of code or SLOC. The SLOCs required to perform typical satellite functions was estimated from [14] and can be seen in Table 11.2. Here, the executive category includes the implementation of states to make the software compatible with the mission. The fault detection is linked to the autonomy of the OBC which is the ability to solve problems and generate commands based on satellite input. Utilities include packages for mathematics and conversions for time, management and coordinates. Lastly, some other functions like power and momentum management require additional SLOCs. For these functions the throughput or processing speed was determined with Eq. (11.1) [34] based on typical throughput frequencies [14] where N_{LOC} is the number of SLOCs, $\frac{\text{I}}{\text{SLOC}}$ the instructions per SLOC and f_t the throughput frequency. The throughput is calculated in instructions per second or IPS (KIPS = thousand IPS, MIPS = million IPS).

$$\text{Throughput} = N_{\text{SLOC}} * \frac{\text{I}}{\text{SLOC}} * f_t \tag{11.1}$$

From [34], on average, 1 KIPS results in 2.5 kbps which sums up to a total of 640.5 kbps of commands being processed by the on board computer. From [14], using the "C" software development environment there are seven instructions per SLOC. In addition, it is estimated that the onboard software takes up 42 B/SLOC [14] resulting in 2.69 MB of memory that is occupied by the software.

The Lockheed Martin RAD6000 processor [11] was chosen for the on board computer for this mission. The configuration of this specific board will be similar to that of the Gravity Probe B mission with a mass of 1 kg, an average power consumption of 3 W and a volume of 0.158 L. The processor meets the required processing speed with speeds up to 18 MIPS and has a primary memory of 4 MB allowing for additional software uploads to meet requirement **DSE14-RK-RSY-CD-TECH-1**. This chip is compatible with the "C" software environment and has sufficient radiation hardening, therefore meeting the radiation survivability requirement **DSE14-RK-RSY-CD-TECH-2,3,4**.

Data Bus

The SpaceWire data bus consists of two main elements: the wires that connect the instruments and the data routers. The data router allows the different instruments to send or receive data from another instrument. The data can be transmitted via the router to the OBC for processing. This versatile architecture is especially beneficial because of the large size of the satellite structure. The otherwise very long cables can now be connected to a nearby router. The router can then have a single connection with the OBC which reduces the total cabling mass. A disadvantage of the router architecture is the blockage of data. This occurs when two instruments send data simultaneously through a single link in the router. One message will be put on hold till the other message has passed through. From Table 11.1 it can be seen that the largest data rates with high sampling frequencies come from the ADCS and CDHS-TT&C links. Therefore, the ADCS will be connected with a separate router and the TT&C will be directly connected to the OBC to avoid blockage.

The SpW-10X Radiation Tolerant Router [36] was selected with a power consumption of 4 W with all interfaces running at 200 Mbps. For nominal operations a power consumption of 2 W was assumed. The mass and volume of the routers can be neglected with respect to the total satellite dry mass.

Table 11.1: Housekeeping data gathered per satellite subsystem.

System	**Telemetry Type**	**Quantity**	**Sampling Rate [Hz]**	**Word Size [bits]**	**Data rate [bps]**
CDHS					
CPU power level sensor	Voltage	1	1	8	8
Fault detection watchdog	ON/OFF	1	5	1	5
Fault status	ON/OFF	1	5	1	5
TM out (in TT&C)	Serial	1	100	8	800
TC in (from TT&C)	Serial	1	100	8	800
Propulsion					
Tank gauge sensor	Voltage	3	10	8	80
Propellant flow sensor	Voltage	3	2	8	16
Thruster valve status	ON/OFF	34	5	1	5
Thruster control	Voltage	17	1	8	8
TT&C					
Transmit Power	Voltage	1	1	8	8
Power					
Solar cell voltage DU sensor	Voltage	5	1	8	8
Solar cell voltage CU sensor	Voltage	4	1	8	8
Battery charge sensor	Voltage	1	1	8	8
Battery status	ON/OFF	1	1	1	1
Battery temperature sensor	Voltage	1	1	8	8
Battery heater	ON/OFF	1	1	1	1
External separation switch	ON/OFF	1	1	1	1
Power management	ON/OFF	2	1	1	1
ADCS					
Coarse sun sensor	Voltage	6	10	8	80
Star tracker [35]	Voltage	1	60	8	480
Inertial measurement unit	Voltage	1	10	8	80
Payload					
Deployment sensors	Voltage	4	0.1	8	0.8
Total					**3363.2**

Table 11.2: Computer software components with the respective source lines of code (SLOC) and throughput for a typical satellite [14]

SW Category	SLOC	KIPS
Executive	1000	0
Communication	4500	10
Attitude/ orbit sensor processing	3300	12
Attitude determination and control	28 800	79
Attitude actuator processing	2700	26.2
Fault detection	11 500	41
Utilities	7250	0
Other functions	5000	88
Total	**64050**	**256.2**

The SpaceWire cables have a mass density of 87 g/m [12]. A rough wiring length estimate based on the satellite architecture gave a total wire length of 112 m which results in a mass of 9.74 kg.

Solid State Recorder

The selection of the solid state recorder was based on the amount of data that must be stored and a sustainable data rate for the transmission. The required memory volume can be computed with Eq. (11.2) where $R_{produced}$ is the housekeeping data rate and $t_{\text{monitoring}}$ the monitoring time. From Section 11.2.2 this results in a total of 34.03 kb of housekeeping data that needs to be stored on the SSR. Commands from the ground must also be stored as these cannot be directly transmitted to the instruments. Yet, this value cannot be immediately estimated. The miniRv2 Solid-State Recorder [13] from AMPEX with a 64 GB capacity was chosen to allow for enough data storage. This large margin is possible since modern SSRs can easily store data in the magnitude of Gigabytes while requiring low mass and power. This SSR has an average power consumption of 15 W, a mass of 1.19 kg and a volume of 1.3 L.

$$V_{\text{produced}} = R_{\text{produced}} \cdot t_{\text{monitoring}} \tag{11.2}$$

11.2. Telemetry, Tracking, and Command Subsystem (TT&C)

The telemetry, tracking, and command subsystem or TT&C ensures communication between the ground and the spacecraft by transmitting, receiving and handling data signals. TT&C gathers the housekeeping data from the CDHS and sends it to the ground station so that the status of the spacecraft can be monitored and controlled. On the opposite end, commands from the mission control center can be sent to the spacecraft to perform certain functions [3]. In Section 11.2.1 an overview will be given of the overall TT&C communication links. Next, in Section 11.2.2 a technical approach to size the links and the final budgets will be shown. Lastly, in Section 11.2.3 the specific components included in the TT&C will be chosen.

11.2.1. TT&C Overview

The communication links for the constellation mission will differ from most standard mission links. The links will be discussed starting from the ground station and ending at the EOS constellation. An overview of the complete communication flow between the ground station and EOS is presented in Fig. 11.2 [37]. The mission communications are split in two segments, a ground segment and the space segment. The ground segment consists of a mission operations and control center from which commands are generated and incoming data is analyzed. The ground station antenna forms the link between both segments, it allows for the commands to be sent to EOS as well as receive the data from the constellation. Before the signal from EOS can reach the ground station it will be passed by a relay satellite. In addition, EOS will have cross-links within the constellation itself also called hive communication. The ground station, relay and hive communication links will be discussed in more detail in this section.

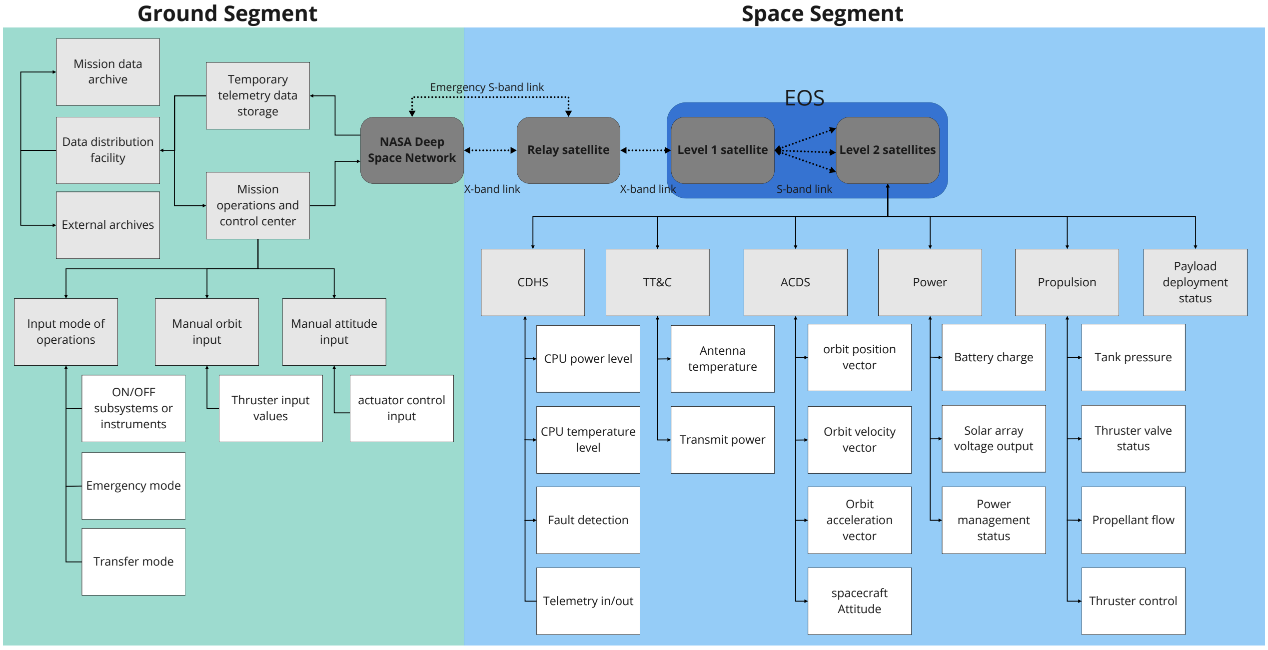

Figure 11.2: Mission communication flow diagram

Ground Station

The selection of the ground station was based on reliability, performance, availability and similarity to other missions at L_1. The NASA Deep Space Network (DSN) was selected as the optimal ground station network for the EOS mission, more specifically the 34 m diameter beam waveguide (BWG) antennas. These antennas were used by L_1 missions like SOHO [37], ACE[22] and provided frequent and reliable monitoring for other deep space missions (category B, >$2E6$ km from Earth). The 70 m antennas were not considered as these suffer from severe availability constraints. The DSN has three ground station locations around the world allowing for omni-coverage, the technical details of the 34 m BWG antenna in Canberra, Australia can be found in Table 11.3 [15]. These parameters will be used and further discussed in Section 11.2.2.

Table 11.3: Capabilities of the DSN 34 BWG Antenna

Parameter	S-band	X-band
Uplink frequency [MHz]	2025-2120	7145-7235
Downlink frequency [MHz]	2200-2300	8400-8500
Transmitter power [W]	20 000	20 000
EIRP [dBW]	78.7-98.7	89.5-109.5
Gain [dBi]	56.7	68.2
G/T [dB/K]	40.5	53.9

Relay Satellite

It important to note that the communications around L_1 can be obstructed by crossing the solar disk. A large amount of solar noise is introduced to the downlink signal if the sun is positioned directly behind the satellite resulting in an unreadable distorted signal. The region where the disturbed communication occurs is called the solar exclusion zone [38]. This zone can be approximated as a $4.75°$ cone[22] starting from the ground station on Earth to the Sun. The constellation will remain in

[22]URL `http://www.srl.caltech.edu/ACE/ace_mission.html` [cited 19 June 2021]

the exclusion zone as it needs to block the incoming solar radiation on Earth. Therefore, no direct communication link between EOS and Earth is possible.

A solution for this problem is that a relay satellite provides an undisturbed link between the ground and the constellation by redirecting the signal as seen in Fig. 11.3. The disturbed direct link is shown in red while the undisturbed links are shown in black. It was determined that positioning the relay satellite in an orbit around the L_1 point is the best option. This position successfully mitigates the solar noise from the exclusion zone while reducing the link distances. This smaller distance results in a lower signal space loss and therefore requires less power and mass from the TT&C subsystem onboard EOS and relay satellites. For subsequent calculations, it is assumed that the orbit is circular with a radius of $0.125E6$ km to avoid the solar exclusion zone at L_1. An infinite number of orbits is possible depending on the number of relays that need to be deployed, the desired link downtimes and orbit types. The exact orbit determination for the relay satellite is therefore left to be investigated in further research. Communications through the relay will be performed in the X-band frequency range through high gain antennas. An emergency S-band omnidirectional antenna system will be included to restore communications when the pointing attitude is disturbed.

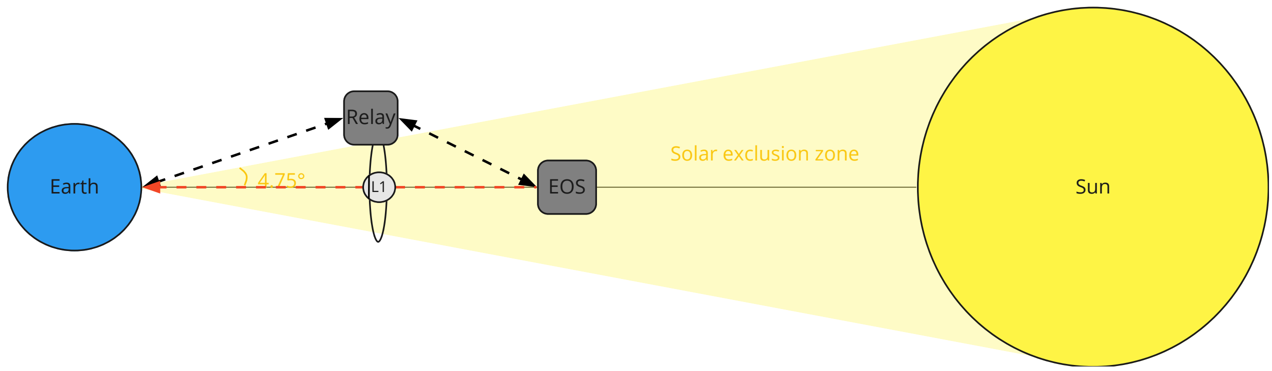

Figure 11.3: Solar exclusion zone as seen from Earth when receiving a signal from EOS.

Hive Communication

Now that the communication between the ground and EOS is discussed, the communication links within the constellation itself can be investigated. From a previous study [3] it was estimated that a hive-like communication is more efficient in terms of average mass and power consumption across the satellites in the constellation. The hive communication principle is best explained with Fig. 11.4. Commands from the ground station are passed by the relay satellite and sent to a level 1 satellite equipped with a high gain parabolic antenna. The level 1 satellite then broadcasts an isotropic signal using a low gain antenna to the surrounding level 2 satellites in its sphere of influence. The individual level 2 satellites each report their data back to the level 1 spacecraft which can send the gathered data to the relay satellite. The level 1 satellite essentially acts like a shepherd for the herd of level 2 satellites. This method efficiently mitigates the need for high gain reflector antennas on each satellite in the constellation which require more power and mass. Instead each level 2 satellite can be equipped with a light and power efficient low gain antenna which only needs to send data over small distances and with low pointing accuracy.

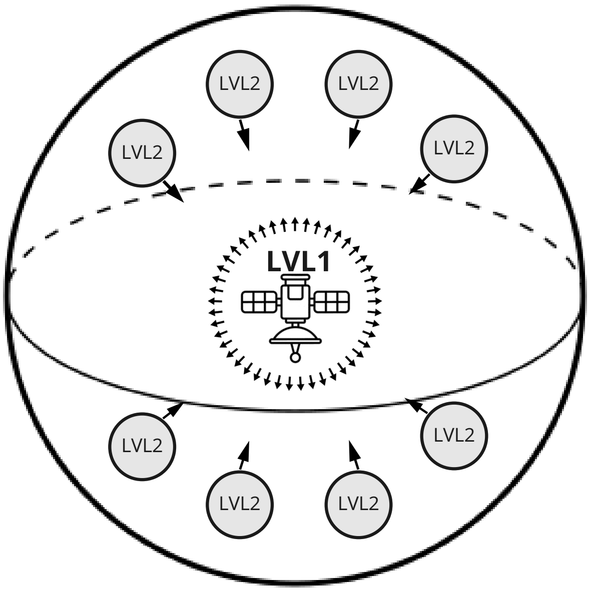

Figure 11.4: Hive communication between level 1 and level 2 satellites within the constellation.

11.2.2. Link Budget

Downlink and uplink budgets where established for each of the aforementioned links in Section 11.2.1 starting from the ground station and moving up to the level 2 satellites. First, a general introduction of the equations used to create the budgets will be given. Next, the link budget tables for the hive and relay communication links will be presented.

Link Equations

The gain factor of an antenna is the property to focus the radiated signal in a desired direction and is given by Eq. (11.3). A fully isotropic antenna will have a gain equal to 1, for high gain deflector antennas the gain increases with the diameter of the reflector. [34]

$$G_t = \frac{\text{Surface area of sphere}}{\text{Surface area of antenna beam}} \tag{11.3}$$

With the obtained gain factor, the effective (isotropic) radiated power can be computed through Eq. (11.4) where P is the transmitter output power of the antenna and L_l the line loss between the transmitter and the antenna. All parameters are expressed in Decibels.[14]

$$EIRP = P + L_l + G_t \tag{11.4}$$

The link can be sized by means of the link budget equation given in Eq. (11.5). This equation forms a relation between the EIRP, propagation losses (L_a), the gain G_r and system noise temperature T_s of the receiver and the data rate (R). The signal to noise ratio ($\frac{E_b}{N_o}$) also called SNR gives the received energy per bit to the noise density. [14]

$$\frac{E_b}{N_o} = EIRP + L_a + G_r + 228.6 - 10\log T_s - 10\log R \tag{11.5}$$

The propagation losses consist of variable losses that reduce the signal's strength. The most prominent loss is the space loss L_s given in Eq. (11.6). This loss increases with the distance that the signal has to travel (S) and depends on the carrier frequency (f). The pointing loss L_θ in Eq. (11.7) can be significant for narrow beam widths. It originates from the pointing error (e) which is the offset angle from the center of the receiver with respect to the received beam; θ is the half power beamwidth.[14]

$$L_s = 147.55 - 20\log S - 20\log f \tag{11.6}$$

$$L_\theta = -12\left(\frac{e}{\theta}\right)^2 \tag{11.7}$$

The receiver gain is an input based on the geometry of the chosen antenna. The system noise temperatures were obtained from existing systems like DSN [15] and TDRSS [39] or calculated based on estimations from [14]. The uplink data rate is set equal to 2 kbps as a conservative estimate, which is the maximum command data rate from the DSN 34m antenna [14]. This uplink data rate is assumed to be equal for every uplink. The downlink data rates originate from the telemetry data determined in Table 11.1.

The message has to be modulated on a radio frequency carrier in order to send it successfully. Modulation alters certain properties of the carrier wave to encode the message. Similarly, the signal must be demodulated at the receiver to read the message. Reliable demodulation requires a minimum signal to noise ratio depending on the type of modulation. More errors are introduced to the message if the signal to noise ratio is lower. The probability of receiving a faulty bit is called the bit error rate (BER). A BER of $10E-6$ results in one faulty bit per $100E3$ bits received and is seen as sufficient to establish a reliable link. With the chosen differential phase shift keying (DPSK) modulation type this results in a required SNR of 10.3 dB. A maximum margin of 3 dB must be added to this theoretical value to account for filtering, timing and frequency errors [14]. Finally, the required transmitter power and antenna gain were determined based on the required SNR for each link.

Link Budget Table

The downlink budget from the level 2 satellite to the level 1 satellite is shown in Table 11.4. These type of tables were created for all uplink and downlinks. For this budget the data rate is determined by using a certain monitoring frequency. Once every hour the level 2 satellite records its telemetry data for 10 s. Afterwards, it is sent to the level 1 spacecraft. It is assumed that the level 1 satellite can receive only one signal at a time. Therefore, each level 2 spacecraft has to send the data one after the other. Assuming a continuous transmission to the level 1 satellites, a single level 1 satellite would be able to control a sector including $3.6E3$ level 2 satellites. For each sector, two level 1 satellites need to be put in place to fulfill **DSE14-RK-RSY-TT-TECH-2,3**. Knowing the number of satellites within the constellation from Chapter 4, the entire constellation will contain a total of 20 sectors which are being controlled by 40 level 1 satellites. One sector has a sphere of influence with an estimated radius of 500 km based on the satellite positions in the orbit determined in Chapter 10.

Table 11.4: Downlink budget from level 2 to level 1 satellite.[14]

Parameter	Symbol	Value
Frequency [GHz]	f	2.2
Transmission distance [km]	S	500
Transmitter power [W]	P	2
Effective Radiated Power [dBm]	$EIRP$	33
Transmitter antenna gain [dBi]	G_t	1
Line loss [dB] [16]	L_l	-0.97
Space loss [dB]	L_s	-153.3
Pointing loss [dB]	L_θ	0
Data rate [kbps]	R	33.63
Occupied Bandwidth [kHz]	B	33.63
Receiver antenna gain [dBi]	G_r	1
Receiver system temperature [K]	T_s	85
Received signal power [dBm]	C	-120.2
Signal to noise ratio [dB]	$\frac{E_b}{N_0}$	14.8
Required signal to noise ratio [dB]	$\frac{E_b}{N_0}$	13.3
Link margin [dB]	-	1.5

The downlink budget from the level 1 satellite to the relay satellite is shown in Table 11.5. For this budget it is assumed that the level 1 satellite receives the data from the level 2 satellite and instantaneously sends it to the relay without storing it. The technical parameters for the relay satellite were based on the TDRSS of the DSN [39]. It is assumed that the relay satellite cannot receive multiple signals at once with a single dish. Furthermore, as the level 1 satellites are assumed to send data continuously, it is concluded that each of the 20 sectors will need a separate relay satellite. These will not have to be redundant as each relay has emergency links to the ground to restore the pointing attitude.

Table 11.5: Downlink budget from level 1 to relay satellite.[14]

Parameter	Symbol	Value
Frequency [GHz]	f	8.5
Transmission distance [km]	S	7E5
Transmitter power [W]	P	12
Effective Radiated Power [dBm]	$EIRP$	71.79
Transmitter antenna gain [dBi]	G_t	31.97
Line loss [dB] [16]	L_l	-0.97
Space loss [dB]	L_s	-227.94
Pointing loss [dB]	L_θ	7.55
Data rate [kbps]	R	33.63
Occupied Bandwidth [kHz]	B	33.63
Receiver antenna gain [dBi]	G_r	50.21
Receiver system temperature [K]	T_s	253
Received signal power [dBm]	C	-163.71
Signal to noise ratio [dB]	$\frac{E_b}{N_0}$	15.8
Required signal to noise ratio [dB]	$\frac{E_b}{N_0}$	13.3
Link margin [dB]	-	2.5

11.2.3. TT&C Component Sizing

The TT&C subsystem generally consists of two components: antennas to receive or send the message and transceivers. The transceivers modulate to message that must be sent or demodulate the received message [34]. The selection of the antenna for the level 2 satellite was based on off-the-shelf components. The S-band patch antenna from ISISpace[23] was selected with a mass of 0.05 kg and volume of 0.025 L. Two of these antennas will be placed on the satellite to allow for omni-directional coverage. An antenna gain of 1 was assumed to simplify the budgeting and pointing requirements within the constellation. This assumption results in a more conservative budget. A compatible transceiver[24] was chosen with a mass of 0.217 kg and volume of 0.228 L operating at 13 W of input power. It was decided that four transceivers are needed to fulfill requirement **DSE14-RK-RSY-TT-TECH-1** as these instruments have a relatively low reliability.[34]

The sizing of the level 1 instruments is done through mass and volume estimations from [34]. For the level 1 satellite, a high gain parabolic reflector antenna will be used. From the required antenna diameter and an average antenna density of 6.5 kg/m^2 an antenna mass of 1.84 kg was obtained. The volume of the reflector antenna is estimated to be 0.11 L. The transceiver was sized based on the required power. For the level 1 satellites the output power is 12 W per transceiver resulting in a mass of 2.76 kg and volume of 3.68 L per instrument. The transmitter input power is estimated to be 60 W with a 20% transceiver efficiency [34]. Again four transceivers are implemented for redundancy. An additional gimbal antenna mount [25] for the reflector antenna is needed to keep pointing to the relay satellite. This gimbal mount has a mass of 0.17 kg a volume of 1 L and power consumption of 27 W.

[23]URL https://www.isispace.nl/product/s-band-patch-antenna [cited 19 June 2021]
[24]URL https://www.isispace.nl/product/s-band-transceiver/ [cited 19 June 2021]
[25]URL https://copterlab.com/2-axis-gimbal-system-for-satellite-antenna [cited 19 June 2021]

11.3. Attitude Determination and Control Subsystem (ADCS)

This section deals with all the components regarding the attitude determination and control subsystem. In Fig. 11.5 provides an overview of the different functions of the ADCS subsystem. The processes in the figure are later explained in more detail in Section 11.3.4. In Section 11.3.1, the disturbances encountered in the mission is modeled and analyzed. Then in Section 11.3.2, the required slew maneuvers to be performed are discussed. The configurations for the attitude control and attitude determination are discussed in Section 11.3.3 and Section 11.3.4, respectively. Finally, the final sizing for all the ADCS subsystem is performed in Section 11.3.5. During the process, all the components are designed with redundancy according to the DSE14-TECH-ADC-01 requirement.

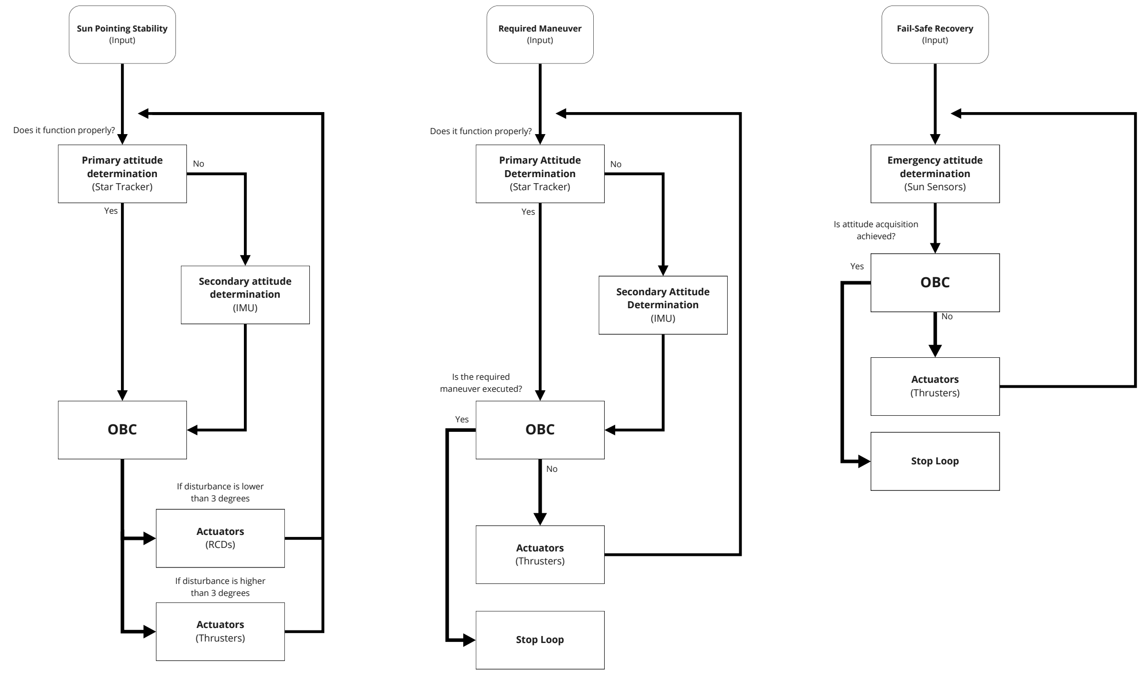

Figure 11.5: Control loops of three different operations inputs.

11.3.1. Modeling Disturbances

Modeling the disturbances to be counteracted is a crucial part of the mission and as previously established, DSE14-TECH-ADC-05 is the driving requirement that leads to the following analysis. During their transfer stage and once they reach the L_1 point, the spacecraft will encounter disturbances. The two most significant ones that are going to be further investigated are the solar radiation torque and the gravity gradient torque.

Firstly, a Gravity gradient torque will act on the spacecrafts. This type of torque forces a spacecraft to be aligned along the axis of the minimum mass moment of inertia. It is also an unstable effect as a small angle disturbance in the sun-pointing alignment of the spacecraft with respect to a large mass body, e.g. the Sun or the Earth, will lead to an even larger disturbance. Figure 11.6 shows how an angle change will cause some parts of the satellite's mass to experience a higher force which causes it to be closer to the large body mass and hence again experiencing an even higher force. Since this effect occurs in satellites with a long extended body, it will only be analyzed after deployment, which would happen once the satellites reach L_1.

In the design of the centripetal constellation, each spacecraft will have the following mass moments of inertia $(85\ 055, 85\ 055, 1.5E12)$ kg m^2, where the last value corresponds to the Axis perpendicular to the Sunshield's plane. The maximum value is significantly larger than the minimum value, which will result in an escalation of the gravity gradient effect. The torque can be estimated using the Zandbergen method shown in Eq. (11.8) and Eq. (11.9). Here I is the mass moment of inertia, ϕ and θ are small angle disturbances in radians, μ is the gravitational parameter of the body about which the motion takes place, and a is the semi-major axis [34].

$$\bar{T} \cong 3 \cdot n^2 \begin{bmatrix} (I_{zz} - I_{yy}) \cdot \phi \\ (I_{zz} - I_{xx}) \cdot \theta \\ 0 \end{bmatrix} \tag{11.8}$$

$$n = \sqrt{\frac{\mu}{a^3}} \tag{11.9}$$

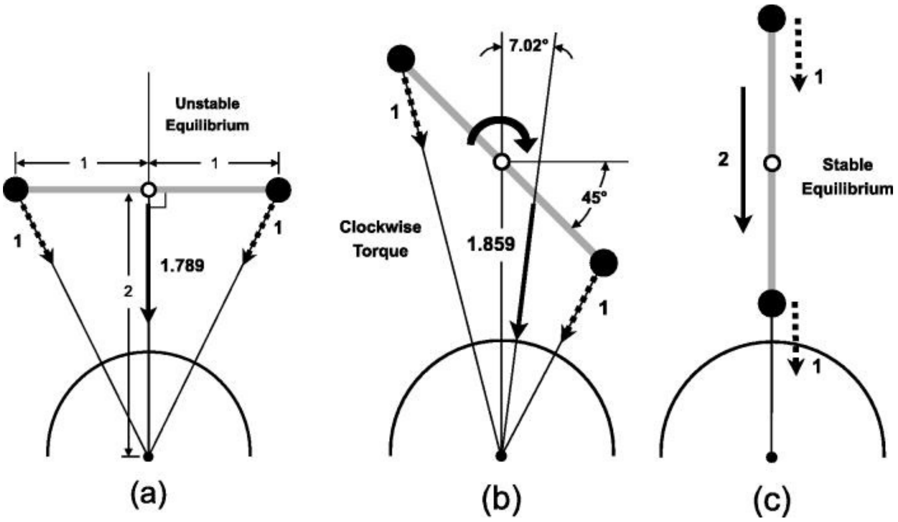

Figure 11.6: Depiction of gravity gradient torque on a satellite orbiting a body mass. [40]

Since the constellation is between the Sun and the Earth, the disturbances due to both bodies will be superimposed in the calculations.

The second significant disturbance acting on the spacecrafts, is the Solar radiation torque. This occurs by an imbalance in Solar radiation pressure between different sides of the spacecraft with respect to the center of mass. This effect will be used advantageously to establish attitude control of the spacecraft using the Reflective Control Devices discussed in [3]. These devices work by controlling their reflectivity inducing a change in solar pressure. By placing these devices on the outer edge of the Sunshield, a torque can be generated by turning them On and Off, depending on their position with respect to the torquing axis. This torque created by such imbalance can be calculated using Eq. (11.10), where F_s is the force due to Solar radiation and r is the distance between the satellite's center of mass and optical center of pressure of the RCDs.

$$T = r \times F_{\mathrm{s}} \tag{11.10}$$

The RCDs main function is to resist disturbances once a spacecraft reaches L_1. Those devices will be placed on the outer edge of the Sunshield to achieve high torques using the long-moment arms. The RCD thickness considered in the design is 6 μm, which is the thinnest configuration according to a research conducted to examine attitude control of solar sails [41]. In the study, the change of reflectance of the panel mentioned is 33%. The force values presented in the study are measured in a similar technology, yet has a different thickness of 125 μm and a change of reflectance of 60%. Moreover, these force values are measured through orientating several 6 m^2 RCDs in different configurations. In the current design, the Sunshield orientation should be perpendicular to the solar radiation once deployment takes place at the L_1 point, which leads to considering that the

RCDs will also be perpendicular to solar radiation. As a result, the maximum force value and RCD, size which is 6 m^2, in the study will be considered and scaled by the ratio between the two values of change of reflectance. The resultant estimated force is $23E-6$ N. This value will be used in sizing of the RCDs in Section 11.3.3. Finally, to compute the torque generated, a reflectance is 0% will be assumed when an RCD is off and no solar radiation pressure is exerted.

11.3.2. Correction Maneuvers

During the transfer phase of the mission, attitude corrections are required to adjust the propulsive acceleration vector. The chemical propulsion nozzle chosen will not be a gimballed thrust mechanism as explained in Section 11.4. This means the whole spacecraft has to turn during an attitude correction maneuver. Moreover, deployment of the shield will occur only once the spacecraft reaches L_1. This is advantageous as the undeployed mass moment of inertia around the axis perpendicular to the Sunshield is around $12E-6$% smaller than the deployed mass moment of inertia. This reduction means less torque is required in the case of using Reaction Wheels as shown in Eq. (11.11) or less force is required in the case of using Thrusters as shown in Eq. (11.12). In the equations, I is the mass moment of inertia, ω is the slew rate, L is the moment arm, t_{pulse} is the pulse duration, θ is the slew angle, and t is the maneuver duration. [34]

$$T = \frac{4I\theta}{t^2} \tag{11.11}$$

$$F_T = \frac{I\omega}{Lt_{pulse}} \tag{11.12}$$

As mentioned in Chapter 10, the trajectory of the spacecrafts to reach L_1 will consist of the insertion into the transfer orbit and performing a capture maneuver. From an attitude control perspective, two things matter. The first being the duration of the spacecraft from the point it separates from the launch vehicle until it reaches the capture point. And the second one is the required slewing angle. According to the optimization process of the trajectory, the spacecrafts will take 179.8 days to reach L_1. As for the slewing angle, it is unclear what the orientation of the spacecrafts will be once separation from the launch vehicle is performed. As a result, the worst-case scenario will be considered which is slewing the spacecrafts 180 degrees, around either the 2 axes which are non-parallel to the propulsive acceleration vector. It should be noted that the spacecraft has the same mass distribution in those 2 axes as such considering either axes is viable.

To perform the aforementioned maneuver, it would require either a reaction wheel with a mass of 1.38 kg or a propellant mass of $5.2E-6$ kg for the thrusters. The motivation for how the sizing was performed is explained in Section 11.3.3. It can be seen that thrusters are a much better option for slewing the spacecraft. This is due to the fact that the mission does not require many maneuvers to be performed: the spacecrafts have to be Sun-pointing at all times once L_1 point is reached. The usage of a reaction wheel is usually an advantageous option as it is fuel independent; however, it has the cost of it being a heavier option than thrusters. If this high mass is not compensated for by utilizing the reaction wheel in performing sufficient attitude control, using thrusters is the better option.

Once the spacecrafts reach L_1, and specifically, once they enter the Lissajous orbit, regular orbit maintenance will be required to keep the constellation from drifting away from L_1. The maintenance technique is performed by correcting the energy of the orbit by applying ΔV along the Spacecraft-to-Sun line in both directions. Thrust directed towards the sun adds energy to the orbit, preventing the decay of the orbit back towards Earth. On the other hand, thrust directed opposite to the sun removes energy from the orbit, preventing the spacecraft from escaping the Earth-Moon system into an independent orbit around the Sun [42].

Firing the thrust in two opposite directions through the main engine of a spacecraft requires frequent 180 degree slew maneuvers to correctly orient the thrust vector. However, the spacecrafts should be Sun pointing at all times once they enter the Lissajous orbit at L_1. In the past, a Lissajous orbit phase control was performed by the ACE mission. Orbit maintenance was done by two thrusters paired on the Sun-facing side to provide thrust in the direction opposite to the sun, and two other thrusters paired on the opposite side to provide thrust in the Sun's direction [42].

Using thrusters to provide ΔV is considered for the final design. The configuration of the thrusters around the spacecraft will be optimized for multi-usage in case of providing ΔV or controlling the pitch, yaw, or roll angles. It is estimated that the required ΔV is 0.5 m/s every 90 days [42]. Sizing the propellant mass for Lissajous orbit maintenance will be performed in Section 11.4. Similar to the SOHO mission [42], providing stability and control using thrusters for orbit maintenance will be considered in the final sizing in Section 11.3.3.

11.3.3. Attitude Control Configurations

RCDs are the main disturbances-resisting actuators. They should solely be capable of resisting gravity gradient torques up to a three degrees disturbance with respect to the plane perpendicular to the Sun based on the solar panels computation analyzed in Section 11.6.2. Using equation Eq. (11.8) and summing the gravity gradient disturbances due to both the Earth and the Sun, the disturbances in the non rotating axes are both 0.0248 N m due to the structures symmetry. In the final design, each spacecraft will have a Sunshield with a radius of 5.4 km. Assuming a minimal production design of RCD panels 6 m^2 each [41] and no solar radiation is exerted when the RCDs are off, and using the aforementioned force value of $23E-6$ N, the maximum torque obtained is 0.12 N m, given the RCDs are placed on the outer edge of the Sunshield.

With the torque value calculated, a pair of RCDs placed on opposite ends of the Sunsheild are able to resist disturbances up to 11.5 degrees. However, since the spacecraft has to be rotating for deployment and stiffness of the Sunshield, RCDs placed on the Sunshield will rotate changing the torque axis. This leads to the design idea of having multiple RCD panels placed around the outer edge of the Sunshield. Syncing the on and off switching of the devices with the rotation of the spacecraft, a controller could maintain the required torque. For 2 axis control, 4 RCDs placed 90 degrees apart from each other are sufficient to provide attitude control for any axis on the Sunshield's plane of rotation at any time. With the final Sunshield size, the distance between each RCD along the outer edge is 8.36 km. These large gaps could possibly induce disturbances on their own. In reality, more than 4 RCDs can turn on and off simultaneously to provide an efficient system. Yet, this solution requires an advanced dynamic model with time response simulations that will not be further investigated in this design.

To size the ACS thrusters, the pulse duration to perform a certain maneuver is firstly calculated by rearranging Eq. (11.12). Then a type of thruster-fuel combination is chosen with a specific impulse. For simplicity of the design, both the thrusters and the main propulsion engine will use the same fuel tank. The type of propulsion chosen in Section 11.4 is a chemical bi-propellant using MMH and MON-3, which have a specific impulse of 292 seconds. Of the compatible thrusters, the Ariane Bi-propellant S10-13 which has a thrust force of 10 N[26] and mass of 0.35 kg is chosen. The difference between the available options is not large, and therefore the S10-13 was chosen without a concrete trade-off. The final step is to calculate the required propellant mass using Eq. (11.13) [43], where I_{sp} is the specific impulse.

$$M_{prop} = \frac{F_T t_{pulse}}{I_{sp} g_0} \tag{11.13}$$

To size the reaction wheels for slew maneuvers, the torque needed to perform a maneuver is first calculated using Eq. (11.11). Then a type of reaction wheel is chosen. A common reaction wheel material used in space industries is Aluminum, therefore a density of $2.7E3$ kg/m^3 [44] is assumed.

[26]URL `https://www.space-propulsion.com/spacecraft-propulsion/bipropellant-thrusters/10-bipropellant-thrusters.html` [cited 22 June 2021]

Moreover, it can also be assumed that the wheel's radius is third of its height and has a maximum angular velocity of $3E3$ RPM [44]. The next step is to calculate the radius using Eq. (11.14), where ρ is the material density, ω is the angular velocity, and T is the required Torque. Once the radius is computed, the height can be obtained and the final total mass can be calculated.

$$r = \left(\frac{T}{\omega}\frac{t}{2}\frac{6}{\rho\pi}\right)^{\frac{1}{5}} \tag{11.14}$$

As means of redundancy for the RCDs to resist disturbances, a reaction wheel could be used as a momentum wheel by activating it at a constant speed [44]. Reaction wheels build momentum that needs occasional dumping using thrusters. For that Eq. (11.15) can be used to calculate the momentum, where T_D is the disturbance torque and P is the orbital period. In the current case, the orbital period of the Lissajous orbit will be used, which is around 178 days [42]. Then, Eq. (11.16) can be rearranged for solving time and inputting it in Eq. (11.13) to obtain the required propellant mass.

$$h = \frac{\sqrt{2}}{2} T_D \frac{P}{4} \tag{11.15}$$

$$F = \frac{h}{tL} \tag{11.16}$$

11.3.4. Attitude Determination Configurations

As previously established in [3], star trackers and IMUs are the final choices for the attitude determination devices. Star trackers will be used as the primary device. This choice goes in accordance with the requirement DSE14-TECH-ADC-02 to have a pointing knowledge accuracy of 18 arcsec [45].

However, if the spacecraft is spinning with a high angular velocity, the star tracker's camera might not function properly and this is when the IMUs will be used. Lastly, coarse sun sensors placed around each face of the spacecraft will be used for sun acquisition and emergency cases like fail-safe recovery.

To design attitude determination, the different phases of the mission, namely, the transfer phase and the orbiting phase at L_1 are inspected. During the transfer phase, attitude determination is crucial for 2 reasons: establishing communication and performing the capture maneuver. Both fall under the requirement of performing a certain slew maneuver. During the orbiting phase, the spacecrafts have to be Sun pointing at all times, which requires a certain control and stability. In Fig. 11.5, both the slewing maneuver and the control and stability operations are shown.

Starting with the left graph, which depicts the sun pointing stability. The first loop in the graph tests whether the star tracker functions properly or not. If not, the output from the IMU is used instead and flows directly to the onboard computer. Depending on whether the disturbance caused a deviation greater than 3 degrees or not, which is the same requirement discussed earlier in the section, either the RCDs or the thrusters will have to counteract it. Exceeding the 3 degrees limit is considered a critical case and therefore the use of the thrusters are called for to quickly counteract the disturbance. Then the whole process loops back again. It is notable to mention that this loop never ends as stability has to be always checked for.

The middle graph, which has the required maneuver as an Input, starts by checking the attitude through the star tracker. If for any reason the star tracker does not function properly, the IMU can be used. Again similar to the sun pointing graphs, the outputs feed into the OBC, Depending on whether the required maneuver was executed or not, the OBC either stops the loop or sends instructions to the actuators which happen to be the thrusters to perform the maneuver. Then the process loops again to ensure that the required attitude was achieved.

The right graph depicts the emergency case of Fail-Safe Recovery. In this operation, the coarse sun sensors try to detect the Sun and feeds the information to the OBC. If the attitude was not acquired, the OBC instructs the thrusters to perform recovery maneuvers to assist in determining the attitude. Then the process loops again to ensure that attitude acquisition is achieved.

11.3.5. Final Sizing

It was estimated, based on the information in the RCD study thesis [41], that the mass of a single 6 m^2 panel is approximately 0.75 kg and consumes around 0.5 W. For three-axis control, a total of 12 thrusters is needed. Yet, for a redundant system, 16 thrusters are required [34]. Each has a mass of 0.35 kg and consumes 7 W[26]. The reaction wheel on board will be used to resist disturbances. It was sized based on commercially available products with a margin to compensate for the huge unprecedented size of the spacecraft. A 50% margin was added to the sizing of the RDR 68 Momentum and Reaction Wheel[27], which results in a 13.5 kg wheel with a power consumption of 135 W. The sensors onboard were all sized based on commercially available options, as no further estimation is required; attitude determination is independent of the size of the spacecraft.

Finally, the fuel mass is calculated. The fuel onboard consists of fuel to perform the capture maneuver, ΔV for orbit maintenance, slew maneuver, desaturation, stability and control, and reserve. The first two will be discussed later in Section 11.4. The fuel mass required to perform the slew maneuver is calculated to be $5.2E-6$ kg. However, this value is not realistic as the pulse duration is around $100E-6$ s, which is too accurate for any thrust technology available. Moreover, as outlined in the requirement DSE14-TECH-ADC-05 a minimum slew rate of 0.03 deg/s is needed. Thus, a minimum pulse time of 2 s will be assumed, and a new fuel mass value will be calculated. This results in a fuel mass of 0.014 kg and an angular velocity of 1.8 deg/min, which means the capture maneuver can be started 100 min before reaching L_1 using minimum pulse duration. For the de-saturation, as mentioned before the torque build-up is 0.0248 N m, which builds up a momentum, that requires $846.6E-9$ kg of fuel, to dump. In 20 years lifetime of operation this adds up to $16.9E-6$ kg. For stability and control, it will be assumed that the spacecraft will need a $30°$ correction for every orbit maintenance performed, which occurs approximately every 90 days. This results in a total mass of 1.135 kg in the 20 years lifetime. The total fuel mass currently is equal to 1.15 kg. The final reserve fuel onboard will be calculated by assuming a margin of 50% on the total fuel mass, which results in a total fuel mass on-board of 1.725 kg.

The final results for the ADCS subsystem is a total mass of $28.8\ kg$ and power consumption of $289.4\ W$. It should be noted that the total power was calculated by considering the maximum consumption scenario with a 25% margin to take into account the estimation used in case of any component deviations or accessibility restrictions. Finally, all the mass and power values of the different actuators and sensors are summarized in Table 11.6

Table 11.6: ADCS Sensors and Actuators final sizing.

Actuators & Sensors	Mass [kg]	Power [W]	Quantity
Thrusters	0.35	7	16
RCD	0.75	0.5	4
Reaction Wheel	13.5	135	1
Star Trackers[28]	0.3	0.2	2
IMU [29]	1.9	12	2
Coarse Sun Sensor[30]	0.215	Passive	12
Total Mass	28.8 kg		
Total Power consumption	289.4 W		

[26]See page 78.
[27]URL `http://www.electronicnote.com/media/downloads/RDR%2068_A4.pdf` [cited 19 May 2021]

11.4. Propulsion Subsystem

The preliminary Midterm Report [3] trade-off was inconclusive, with slight advantage of chemical bipropellant propulsion over electric propulsion. Since then, a more detailed analysis has been performed, which includes the influence of different accelerations and the possibility of refueling the launcher in Low Earth Orbit as described in Section 10.4. This section first describes the considered thrusters and the choice of the propulsion method in Section 11.4.2. Next, the approach taken to determine the size of the tanks is outlined in Section 11.4.3. Section 11.4.4 talks about the chosen propellant pressurization method, and Section 11.4.5 talks about detailing said subsystem. The sizing of the feedlines is conducted in Section 11.4.6. Finally, recommendations for future analysis are given in Section 11.4.8.

11.4.1. Requirements Update

Some requirements required updating as the design progressed. Firstly, requirement **DSE14-TECH-PRP-02** has been reworded. The requirement stated that the propellants used shall be non-toxic and non-radioactive. After discussion with the client OHB System, it became clear that toxic propellants such as hydrazines are fine, since they have extensive use history, and safety precautions and risk mitigations for their use are well understood. Consequently, the requirement was updated to *The propellants shall be non-toxic and non-radioactive unless their risks are well understood and the propellants are actively used in industry with proper mitigation strategies.*, and the identifier updated to **DSE14-TECH-PRP-02-1**

Requirement **DSE14-TECH-PRP-05** stated that *The propulsion system shall be able to withstand a total number of <TBD> cycles.* This requirement assumed that the main engine would need to be restarted multiple times during the transfer. After further analysis, the optimum trajectory only requires a single maneuver as described in Section 10.4.

Several requirements for the propulsion system had yet-to-be-determined values. Some of them depend on the chosen transfer scheme, while some of them vary between different thrusters. Firstly, the requirement **DSE14-TECH-PRP-03** has been updated with the ΔV from Section 10.5.2, with a margin of 5% as recommended by ESA [46]. The resulting ΔV requirement for the main engine is 249.17 m/s and the requirement identifier has been updated to **DSE14-TECH-PRP-03-1** to indicate the change.

Additionally, the requirement **DSE14-TECH-PRP-04** has been reworded to remove the precise value of total impulse to be provided by the propulsion system. From [47], for constant thrust the total impulse can be proven to be $I_T = Ft$. With $F = \dot{m}v_e$ and $I_{sp} = \frac{v_e}{g_0}$, the total impulse is

$$I_T = (\dot{m}I_{sp}g_0)\left(\frac{m_p}{\dot{m}}\right) = I_{sp}g_0m_p$$

As can be seen, it is a direct function of the specific impulse and propellant mass, which is also a function of I_{sp} and spacecraft mass.

11.4.2. Propulsion System Selection

In order to create a good knowledge base on commercially available propulsion units, a list of 62 electric, chemical monopropellant and chemical bipropellant thrusters was compiled. This compiled a range of products from some of the industry leaders including Aerojet Rocketdyne[31], Arianes-

[28]URL `https://hyperiontechnologies.nl/wp-content/uploads/2015/07/HT_iADCS400_v2.1-flyer.pdf` [cited 19 May 2021]

[29]URL `https://satsearch.co/products/gnssmart-gs-imu3000ta-fiber-optic-gyroscopes-inertial-measurement-unit` [cited 19 May 2021]

[30]URL `https://static1.squarespace.com/static/603ed12be884730013401d7a/t/6054f5cb19b196477cd3f9cf/1616180685382/be_datasheet_css_2017jan.pdf` [cited 19 May 2021]

[31]URL `https://rocket.com/space/space-power-propulsion` [cited 27 May 2021]

pace[32], Northrop Grumman[33], IHI Aerospace[34], Busek[35], and Yuzhmash[36]. The thrusters that were left over to analyze were the NEXT, R-42, and R-40B from Aerojet Rocketdyne [48]. Their relevant specifications are compiled in Table 11.7. The NEXT is an ion propulsion system. It currently has a TRL of 8, with the first flight of the thruster delayed to late 2021[37]. The R-42 and R-40B are both MMH-MON3 storable liquid bipropellant thrusters. They are both flight-proven, although the R-40B is currently out of production and would require an obsolescence update.

Table 11.7: Thruster comparison (compiled from [48]

	NEXT	**R-42**	**R-40B**
Max. Thrust [N]	235E-3	890	4E3
I_{sp} **[s]**	4.1E3	305	293
Power Req. [W]	6.9E3 (continuous)	46 (valves)	70 (valves)
Total Impulse [Ns]	>10.6E6	24.3E6	92.1E6
TRL	8	9	9

Initially, after the analysis in Section 10.4, the R-42 was chosen. After further investigation, however, it turned out that it did not meet the resulting total impulse and cumulative firing time requirements. In order to simplify the attitude control and the propulsion feed system, the choice was made to not use more than one thruster. Doing so meant that a bigger thruster would be needed. Additionally, redundancy would be somewhat compromised. However, liquid bipropellant engines are a mature technology, with already high reliability. On the other hand, a single larger thruster is likely cheaper than two weaker ones. Additionally, asymmetric thrust is avoided, leading to simpler attitude control. In the end, the R-40B thruster was selected as the main engine of the spacecraft.

The orbit maintenance of the target orbit will require force adjustments in directions which significantly differ from the Sun-Earth line, so reaction control thrusters will still be required. For that reason, there is no need to employ thrust vectoring during the transfer phase, as RCS thrusters can be used to perform any necessary slew maneuvers. Thrust vectoring is usually performed via mechanical nozzle manipulation [49]. It would not only lead to increased complexity, but also increased mass and cost of the propulsion unit. In the end, the main engine will not be gimballed.

11.4.3. Propellant Tank Sizing

The propellant required was based on the ΔV requirements for the transfer and station-keeping, as described in Section 10.5.2 and Section 11.3.2 respectively. Margins of 5% and 100% were applied to those values as recommended by ESA [46]. The values are summarized in Table 11.8.

Table 11.8: Required ΔV values

Phase	Required ΔV[m/s]	Margin	Final ΔV value [m/s]
Transfer	188.9	5%	198.35
Station-keeping	40.56	100%	81.12
		Sum	279.46

Then, the propellant mass required was calculated using the ideal rocket equation [50] rearranged

[32]URL `https://www.space-propulsion.com/` [cited 27 May 2021]
[33]URL `https://www.northropgrumman.com/space/propulsion-products-and-services/` [cited 22 June 2021]
[34]URL `https://www.ihi.co.jp/ia/en/products/space/satprop/index.html` [cited 27 May 2021]
[35]URL `http://www.busek.com/` [cited 27 May 2021]
[36]URL `https://yuzhmash.com/en/product-category/liquid-rocket-engines/` [cited 27 May 2021]
[37]URL `https://www.nasa.gov/feature/dart-launch-moves-to-secondary-window` [cited 22 June 2021]

in the form of Eq. (11.17), with the launch mass from Section 10.1 and I_{sp} from Section 11.4.2.

$$m_p = m_{launch}\left(1 - e^{-\frac{\Delta V}{I_{sp} g_0}}\right) \tag{11.17}$$

The resulting propellant mass is $12\,048.15$ kg. A margin of around 4% should be taken into account for unused propellant [51]. With a mixture ratio of 1.65 [48], this means a total of $4\,546.47$ kg of fuel and $7\,501.68$ kg of oxidizer.

In order to keep all of the spacecraft at manageable temperatures, it was decided that the propellant would be stored at around 288.15 K - standard temperature. Additionally, it is well within the liquid range for both the fuel and ozidizer. Furthermore, both MMH and MON-3 can be considered incompressible fluids. Their densities at the considered temperature are approximately 879.63 kg/m^3 [52] and $1\,455.68$ kg/m^3 [53], and the corresponding propellant volumes can be calculated to be 5.17 m^3 and 5.15m^3 respectively.

The volume of gas above the propellant in a tank is called the ullage. Reference [54] says that a minimum ullage volume of 3% of the tank volume should be considered. Confirming this, [51] gives a range of 2.5% to 5%. With this margin, the required tank is calculated to be 5.32 m^3 for the fuel and 5.31 m^3 for the oxidizer tank volumes.

11.4.4. Pressurization Subsystem Selection

Each rocket engine has a design supply propellant pressure range. Additionally, the thrust level of a thruster can be sometimes throttled by decreasing the inlet propellant pressure. For those reasons, it is crucial to provide a subsystem that ensures that the pressure of the propellants is kept as desired.

By far the three most common pressurization concepts are blowdown, pressure regulated, and pump-fed. In a blowdown concept, the tanks are initially pressurized to the desired level, and as the propellant is expended, the tank pressure (and consequently the thrust produced) gradually decreases until it cannot sustain engine operation anymore. Optionally, repressurization can be used to refill the propellant tank with additional pressurant initially stored in a separate tank at a higher pressure, resulting in a pressure (thrust) increase as shown in Fig. 11.7.

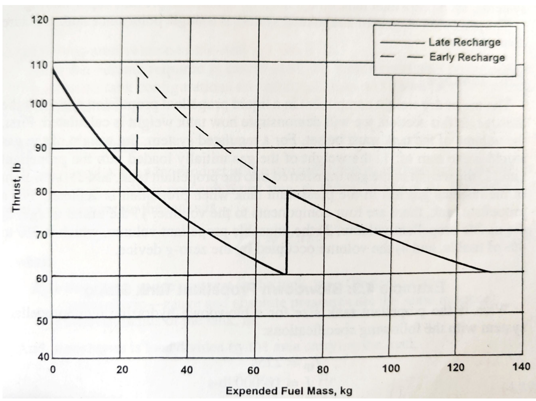

Figure 11.7: Blowdown operation mode with repressurization [54]

In a pressure-regulated mode, the pressurant gas (usually helium or nitrogen) is stored in a separate tank, and fed to the propellant tanks through a pressure regulator. This adds complexity but results in the ability to adjust the propellant pressure at will, allowing for optimal operation in all conditions.

Finally, in a pump-fed system, pumps are used to feed the propellant from the tanks into the engines by applying suction. This approach is the most efficient, at the cost of the highest complexity. It is generally used in large ΔV applications, which is why it is usually used in launch vehicles.

For the EOS mission, a pressure-regulated stored-gas system will be used. Since the mission has a relatively high propellant throughput requirement, pressure regulation will allow for much more optimal operation than blowdown. It is also deemed that the higher complexity of a pump-based design is not offset by added efficiency in this mission. Finally, although helium is the most common pressurant gas, it is quite a rare and non-renewable element. It is also heavily sought-after in for example medical applications [55]. For sustainability, a better choice is nitrogen. This element is incredibly abundant in Earth's atmosphere, meaning that unlike helium the mission will not cause a shortage of rare, important materials. Additionally, nitrogen's abundance results in a significantly lower price than helium.

11.4.5. Pressurization System Sizing

Initially, a propellant optimization tool was written. The tool optimized the tank geometry and pressurant pressure. In the end, it was decided to lock the tank length to a preset fraction of the spacecraft to act as a central structural element. Additionally, although the optimal pressurant pressure varied with the propellant volume, it usually remained in the vicinity of 250 bar. It was decided that for further analysis the pressurant pressure would be frozen at this value.

For the sizing of the pressurant tank, it was assumed that the gas undergoes isothermal expansion. Because of relatively small mass flows, a large thermal mass in the propellant, and additionally a heat source from the engine nearby the tank, this assumption should hold relatively well. Furthermore, the pressurization system was sized for a minimal pressure drop of $\Delta p = 5$ bar at the compressed gas regulator. The volume and pressure drop of the feedlines was neglected. Then, using the ideal gas law [56], the initial pressurant volume can be calculated from Eq. (11.18). Here, V_{press} is the volume of the pressurant required, p_{prop} is propellant supply pressure, V_{prop} is the total volume of the propellant tanks, and finally $p_{press,0}$ is the initial pressure of the pressurant gas.

$$V_{press} = \frac{p_{prop} V_{prop}}{p_{press,0} - p_{prop} - \Delta p} = 1.48 \text{ m}^3 \tag{11.18}$$

Additionally, assuming ideal gas theory, the density of nitrogen can be calculated to be 292.18 kg/m^3, resulting in the pressurant mass of 433.44 kg.

In order to size the compressed gas regulator, it is important to know the volumetric flow Q of the propellants. This can be related to the mass flow by $Q = \frac{\dot{m}}{\rho}$. The summative volumetric flow of the propellants is $1.20E-3$ m^3/s and it also has to be the volumetric flow of nitrogen past the gas regulator. An important property for choosing valves that describes the flow through them is the flow coefficient C_v. The critical condition for the lowest mass flow occurs when the flow is not choked at the valve, with the lowest pressure drop. From [57], the flow through a valve in those conditions can be described by Eq. (11.19), where q is the standard volumetric flow, Δp the pressure drop across the valve, p_1 the upstream pressure, N_2 is a constant equal to $6\ 950$ for q in [stdL/min] and pressures in [bar], G_g is the gas specific gravity equal to 0.967 for nitrogen[38], and T_1 the upstream temperature [K].

$$q = N_2 C_v p_1 \left(1 - \frac{2\Delta p}{3 p_1}\right) \sqrt{\frac{\Delta p}{p_1 G_g T_1}} \tag{11.19}$$

Because the temperature is assumed to already be at standard conditions, the conversion of volumetric flow to standard volumetric flow is only a function of pressure and can be calculated as $q = Q\frac{p_{prop}}{p_0}$, with $p_0 = 101\ 325$ Pa. The standard volumetric flow of the pressurant can then be calculated to be 2130.73 stdL/min. Finally using Eq. (11.19) to solve for C_v, a minimum value of 0.43 is obtained.

[38] URL `http://www.airproducts.net.br/products/Gases/gas-facts/physical-properties/physical-properties-nitrogen.aspx` [cited 18 June 2021]

11.4.6. Feedline sizing

For determining the size of the feedlines, the design flow velocity needs to be decided. According to Swagelok[39], the rule-of-thumb flow velocity should be at most 4.5 m/s for liquids above 7 bar and around 25 m/s for gases. Using the relation $Q = vA$, with v the flow velocity and A the cross-sectional area, and taking a circular cross-section, the inner diameters for the pipes can be computed. According to [58], a factor of 4 should be imposed on the maximum design pressure for the design burst pressure. Additionally, a safety factor of 1.4 should be imposed on the ultimate strength of the material. The material chosen was stainless steel, which is a common and relatively cheap material for pressure pipes. With a yield strength of 215 MPa and ultimate tensile strength of 505 MPa, the yield criterion was driving. Finally, in some cases, especially the low-diameter, high-pressure pipe, the thin-walled assumption cannot be used. Instead, Eq. (11.20) which is Lamé's equation for hoop stress in a thick-walled cylinder will be used. Rearranging to solve for r_o and substituting $\sigma_h = \sigma_y$, $p_o = 0$ bar (vacuum), $p_i = 4 \cdot MDP$, where MDP is the Maximum Design Pressure, and $r = r_i$ (highest stress location), results in Eq. (11.21).

$$\sigma_h = \frac{p_i r_i^2 - p_o r_o^2}{r_o^2 - r_i^2} + \frac{(p_i - p_o)\, r_o^2 r_i^2}{\left(r_o^2 - r_i^2\right) r^2} \tag{11.20}$$

$$r_o = r_i \sqrt{\frac{4 \cdot MDP + \sigma_y}{\sigma_y - 4 \cdot MDP}} \tag{11.21}$$

The results and used values are shown in Table 11.9, the feedline number codes are explained in Fig. 11.8.

Table 11.9: Results of feedline sizing

Line	MDP [bar]	Q [m^3/h]	v [m/s]	d_i [mm]	d_o [mm]
1	250	0.52	25	2.71	4.48
2	30	4.32	25	7.82	8.26
3	30	2.16	25	5.52	5.84
4	30	2.16	4.5	13.0	13.8

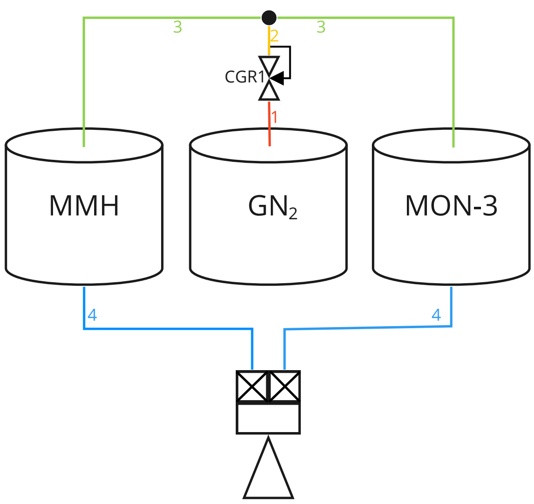

Figure 11.8: Feedline numbering

[39] URL `https://www.swagelok.com/downloads/webcatalogs/en/ms-02-369-e.pdf` [cited 18 May 2021]

11.4.7. Propulsion Layout

The final schematic diagram of the propulsion system is shown in Fig. 11.9.

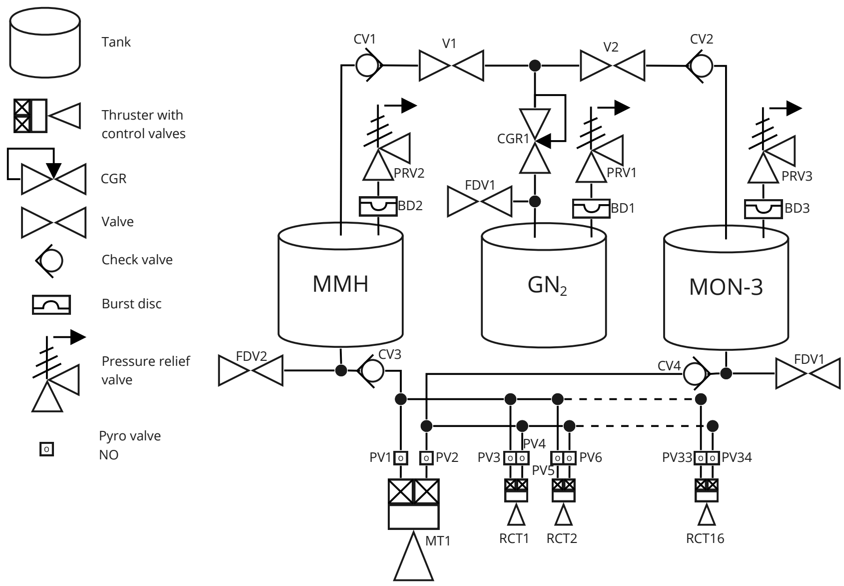

Figure 11.9: Schematic diagram of the propulsion system

An example CGR unit that fulfills the pressure and C_v requirements is a gas regulator from the TESCOM^{TM} 44-1300 Series[40]. For the latch valves, fill and drain valves, check valves, and filters, the Omnidea-RTG [59] components should be suitable. In order to satisfy requirement **DSE14-RK-RSY-TECH-2**, each of the tanks is equipped with a pressure relief valve. In order to prevent pressurant leakage during normal operation, there is a series burst disk installed before each pressure relief valve. For **DSE14-RK-RSY-TECH-3**, there is a latchvalve downstream of the CGR for both the fuel and oxidizer pressurant lines. In case of a faulty CGR, pressurant flow can be shut off there and the system possibly still operated in blowdown with repressurization mode. From **DSE14-RK-RSY-TECH-4**, there is normally-open pyro valves before all the thrusters. In case of thruster failure, the specific thruster can be shut off from the system.

11.4.8. Recommendations

A number of improvements could be made on the design of the propulsion subsystem with more research. First of all, pressure losses were neglected in this section. Additional analysis should be completed to determine the pressure drops in the system such as at the valves or from friction in the piping. Consequently, the propellants would likely need to be stored at a pressure slightly higher than the thruster inlet pressure in order to account for said losses. Additionally, flow velocity in the pipes and cross-sectional area can be optimized to limit said losses.

The pressurant gas was also assumed to be an ideal gas. In reality, especially at high pressures, more thorough analysis ought to be conducted. Similarly, the expansion was assumed to be isothermal. The real heat transfer and transient state between the structure and flowing gas should be simulated.

Furthermore, in this analysis, zero-g propellant control was largely ignored. It will be necessary for the spacecraft's propellant tanks, in order to guarantee satisfactory propellant outflow to the engines. Examples include a diaphragm, bladder, or capillary devices [54]. They would undoubtedly decrease the usable volume inside the tanks, as well as increase the mass of the tanks somewhat.

[40]URL `https://www.emerson.com/documents/automation/catalog-series-44-1300-pressure-regulator-valve-tescom-\en-5322214.pdf` [cited 18 May 2021]

Additionally, the thicknesses of the feedlines were sized purely based on hoop stress induced by the pressure differential. Whenever a change of momentum occurs in the flow through a pipe, a phenomenon known as hydraulic shock occurs. This puts additional stress on the pipes. Care should be taken that the lines are strong enough to withstand this load in addition to regular pressure-induced stress.

Moreover, the RCS thrusters are connected to the same feedsystem but do not necessarily accept the same pressure range. Possible means of reducing the pressure of the propellant before it flows toward the RCS thrusters should be investigated. A possible solution is employing a pressure-reducing orifice plate, which is a blockage in the flow with a small opening, which reduces the pressure of passing fluid by introducing an additional pressure drop.

Finally, solar sailing was in the end not chosen as a propulsion method for the EOS mission because of the complexity of analysis required, both in a structural and astrodynamics sense. However, it is believed that it is an appealing method of propulsion for a mission like ours, because of the Sunshield which effectively could be considered just one big solar sail. With more resources available for a more thorough study, this option should most certainly be reevaluated.

11.5. Thermal Control Subsystem

In this section, the thermal control subsystem design process is explained, together with a description of the equations behind the thermal model.

11.5.1. Thermal model

Originally, three different potential subsystem models were identified: the simple thermal balance model used in the midterm report (equating spacecraft thermal inputs and outputs to find a ”steady state” temperature), a Thermal Mathematical Model(TMM) as described through literature (each subsystem is a node, with different connections between them) and ESATAN, COMSOL, or other physical simulators.

Through talk with the tutor, it is determined that the simple thermal balance is too low-detail to suffice for the finalized DSE. In discussion with members of the aerospace faculty with knowledge and experience in the field of thermal control (and an early assumption from the students), it is determined that the time and effort required for ESATAN or similar approaches does not fit within the DSE timeline.

As such, development is begun in a simple nodal TMM to determine not only thermal balance and specific areas of interest, but additionally how the system responds to temporary stimuli.

A node is created for each subsystem and various nodes are made for the structure, depending on their position. The scheme for the nodes is found in Fig. 11.10. Thermal connections are made from node to node, where they physically connect within the satellite. The thermal connections are assumed to be purely conductive, ignoring radiative heat exchange.

In total, each node i has the potential of 3 distinct heat exchanges, depending on its location within the satellite and the location of the satellite itself:

- Heat acquired through solar influx, $\dot{Q}_s$
- Heat radiated to space from exposed area, $\dot{Q}_{irr}$
- Heat acquired/lost through conductivity with node j, $\dot{Q}_{\mathrm{c}_{ij}}$

As the spacecraft will be stowed inside Starship until deployment at L_1 as discussed in Chapter 10, the heat influx from Earth’s albedo and irradiance does not need consideration.

The heat acquired through solar influx is given by:

$$\dot{Q}_s = \alpha E A_{frontal}$$

Where $\dot{Q}_s$ [W] is power input due to the Sun, α is the absorptance of the spacecraft material facing

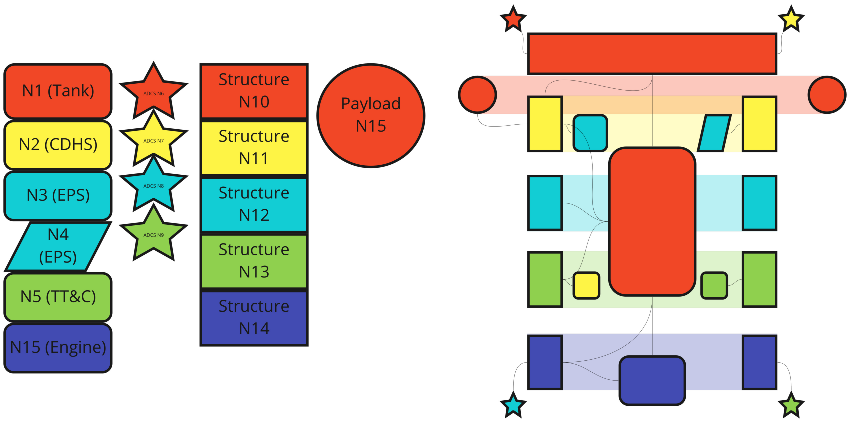

Figure 11.10: Nodes scheme

the Sun, E [W/m^2] is the solar irradiance (which varies depending on distance from the Sun), and $A_{frontal}$ is the area section normal to the Sun.

The heat radiated to space from the exposed area is given by:

$$\dot{Q}_{out} = \epsilon A_{exp_i} \sigma T_i^4$$

Where $\dot{Q}_{out}$ is the heat output, ϵ is the emittance of the node material facing space, A_{exp_i} is the total exposed area of the node, σ [K/m^2 K^4] is the Stefan-Boltzmann constant and T_i is the temperature of the node being investigated.

Finally, the conductive heat flow is given by:

$$\dot{Q}_{\mathrm{c}_{ij}} = \frac{\lambda A}{l}(T_j - T_i)$$

Where Q_c is the heat exchanged, λ W/(m K) is the thermal conductivity of the material between the nodes, A is the area through which the heat is exchanged, l is the length of the connection between the nodes, T_j is the temperature of node j, and T_i is the temperature of node i.

Assembling the equations above yields:

$$m_i c_i \frac{\Delta T}{dt} = \dot{Q}_s + \dot{Q}_e + \dot{Q}_\mathrm{c} - \dot{Q}_{out}$$

Where m_i is the mass of node i, c_i J/kg K is the specific heat capacity and ΔT is the difference in temperature from the previous timestep to the current one.

11.5.2. Design goal

With the model built, the range of operational temperatures for each subsystem is considered in Table 11.10.

As such, the final thermal margin will have to be between 270 K and 310 K for the general spacecraft and between 270 K and 300 K for the propulsion subsystem, specifically the propellant tank.

11.5.3. Thermal tool setup

For the tool's results to be significant, initial conditions must be set up to closely resemble actual conditions to be found. For these initial estimates, the same thermal balance tool used in the Midterm

[41] URL https://web.mscsoftware.com/support/library/conf/auc97/p01997.pdf#page=13&zoom=auto,-226,571 [cited 27 June 2021]

[42] URL https://www.azom.com/article.aspx?ArticleID=1933 [cited 27 June 2021]

Table 11.10: Range of operational temperatures per subsystem

Subsystem	Minimum Operational Temperature [K]	Maximum Operational Temperature [K]
Propulsion	270	300
TT&C	265	330
CDHS	270	310
ADCS	180	1250
Solar panels	172	371.15 [41]
Payload	-	428.15 [42]

Report is used [3], a simple thermal balance equation considering a point mass spacecraft. Using the most recent values of satellite sizing, exposed area and different material choices for satellite covering (Kapton, white paint and black paint) three different initial estimates are achieved, as shown in Table 11.11:

Table 11.11: Initial temperature estimate

Material	**Temperature estimate** [K]
Aluminized Kapton	278.95
White paint	225.32
Black paint	227.4

Two distinct simulation conditions are taken, each with their own initial conditions and settings. The first condition is standard operations: the satellite is in its design orbit, with all systems operational and with the solar panels and Sunshield facing the sun. For each material choice, the satellite temperature is taken from **??** as the initial temperature of each node, and the code is run until temperature stabilizes. The second condition is firing of the engine for orbit-keeping. Orbit and system operations are assumed to be identical, and as such the stabilized temperature of the first condition is taken as the starting conditions for the firing.

11.5.4. Thermal control design

Using the tool developed beforehand, analyzing different covering materials for the exterior of the spacecraft, and in diverse operational conditions, various worst case/standard operation values are achieved. These values are shown in Table 11.12:

From which it can be concluded that for Aluminized Kapton, the spacecraft bus subsystems are within their operational ranges both during normal functioning and engine firing.

Table 11.12: Range of operational temperatures per subsystem

Covering material	Scenario	Temperature Balance [K]	Worst-case temperature [K]
Aluminized Kapton	Standard operations (tank)	280.23	-
	Standard operations (SC)	280.42	-
	Engine firing (tank)	-	298.51
	Engine firing (SC)	-	295.43
White paint	Standard operations (tank)	231.20	-
	Standard operations (SC)	231.32	-
	Engine firing (tank)	-	278.16
	Engine firing (SC)	-	270.41
Black paint	Standard operations (tank)	233.15	-
	Standard operations (SC)	232.45	-
	Engine firing (tank)	-	278.50
	Engine firing (SC)	-	270.70

11.6. Power Subsystem

The power subsystem is responsible for the generation, storage, distribution, and transport of the electrical power amongst the entire spacecraft. Within this section of the report, the manner in which these tasks of the subsystem design will be completed will be denoted and clarified. This section provides complete oversight of the power subsystem design.

11.6.1. Power Budget

Before outlaying the design of the power subsystem, it is important to realize what said power is going to be employed for. Table 11.13 denotes the average power required per subsystem and the corresponding total average power usage.

Table 11.13: Constellation Average Power Usage

Average Power	Category 1
ADCS [W]	289.4
Comms [W]	13
C&DH [W]	44
Payload [W]	0
Thermal Control [W]	0
Thrust Valves [W]	0 - with impulses
Power Systems [W]	34.64
Total [W]	381.0
Margin [-]	0.15
Nominal + Margin [W]	437.75

11.6.2. Power Generation

As has been previously outlined [3], this design will employ solar panels to generate power. These solar panels will be located in front of the solar shield and will be directly attached to the structure. The calculations computing the required area, as well as the computation of the complete stringing scheme, can be found within this section.

The first step in computing the power generation design is to evaluate various commercially available solar cells, to evaluate which one would be most applicable to our design. It was selected to implement solar cells, rather than complete solar panels. This choice was made, because a custom panel made of implemented solar cells offers greater flexibility, which may be necessary considering the unique geometrical characteristics of this design. Additionally, implementing a custom solar cell design reduces costs.

An overview of the solar cells that were considered and some of their respective characteristics can be found in Table 11.14. Note, these are not all solar cell producers, however, considering the sheer amount of cells that need to be produced, the producer would require large production capabilities. These solar cell producers are the largest[43], and therefore, they were considered. Additionally, the costs of the solar cells have been graded relatively, these costs are not absolute.

The Analytical hierarchical process was applied to trade-off different solar cells, the attributes considered are described below, in addition to the reliability and production capabilities. The trade-off process presented the AzurSpace TJ Solar Cell Assembly 3G30A, visible in Fig. 11.11 as the best solar cell option, thus the EOS mission will employ this solar cell.

Table 11.14: Solar Cells Considered in AHP Trade-off

Product	Manufacturer	Efficiency [%]	Relative Cost
SpectroLab UTJ	SpectroLab	28.3 [60]	5 [60]
SpectroLab XTJ	SpectroLab	29.5 [61]	7 [61]
AzurSpace 3G30A	AzurSpace	32 [17]	6 [17]
CESI CTJ30	CESI	29.5 [62]	7 [62]
SolAero ITJ	SolAero	31 [63]	7 [63]
SolAero UTJ [W]	SolAero	28.5 [64]	5 [64]

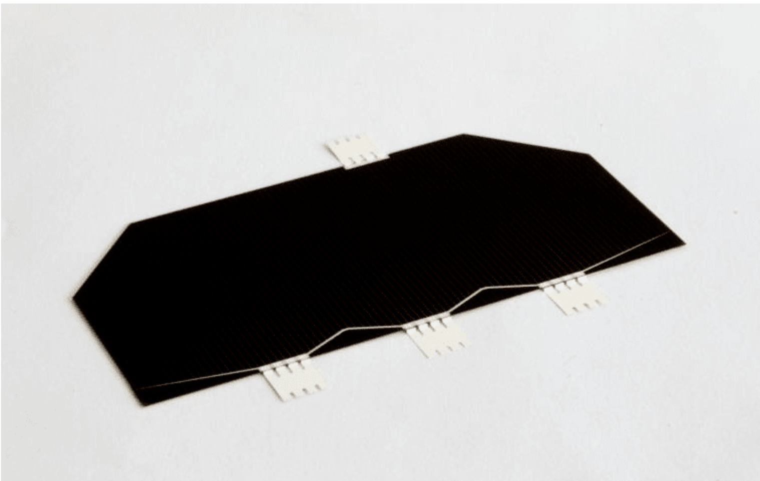

Figure 11.11: Solar Cell Azurspace 3G30A

Knowing the total required power, and the characteristics of a solar cell, the total required area and the number of solar cells may be calculated. This can be completed using Eq. (11.22) which calculates the solar panel area required.

Within this function, P_{sa} is equal to the average power required by a satellite, as documented in Table 11.13, the incoming solar power S_{in} was estimated to be equal to $1\,400$ W/m^2 [65].

The inherent degradation factor, which represents the amount of area of an array that is not directly exposed for power generation, I_d, is set to be equal to 1, as it is expected that during operation, the solar cells will always face the Sun with a maximum error margin of 3 deg, at a constant temperature, and there will be sufficient area to create an absolute efficiency packing factor. The margin of safety,

[43]URL `https://www.nasa.gov/smallsat-institute/sst-soa-2020/power` [cited 22 June 2021]

"m_s", was set to be equal to 1.2. This margin was based on the standard safety margins determined by the ESA Power Group[44].

Additionally, life degradation L_d can be calculated using Eq. (11.23), and a degradation factor δ of 0.005, obtained from the manual of the Azurspace TJ Solar Cell Assembly 3G30A Eq. (11.22). Similarly, a value for the efficiency of the solar cell η of 0.32 was found in the same manual. Note, that "x" is the lifetime of the mission, this will be taken as 20 years.

$$P_{sa} \cdot m_s = S_{in} \cdot A \cdot \eta \cdot I_d \cdot L_d \cdot cos(\Theta) \tag{11.22}$$

$$L_d = (1 - \delta)^x \tag{11.23}$$

Using these equations, the required solar panel area can be calculated to be equal to 1.35 m^2. As each respective solar cell has a total area of 30.18 cm^2, the total minimum amount of solar cells equals 448. The dimensions of each cell can be observed in Fig. 11.12. The total mass of these cells is equal to 1.12 kg. Within the following section, the manner in which these solar cells will be implemented in the design will be discussed.

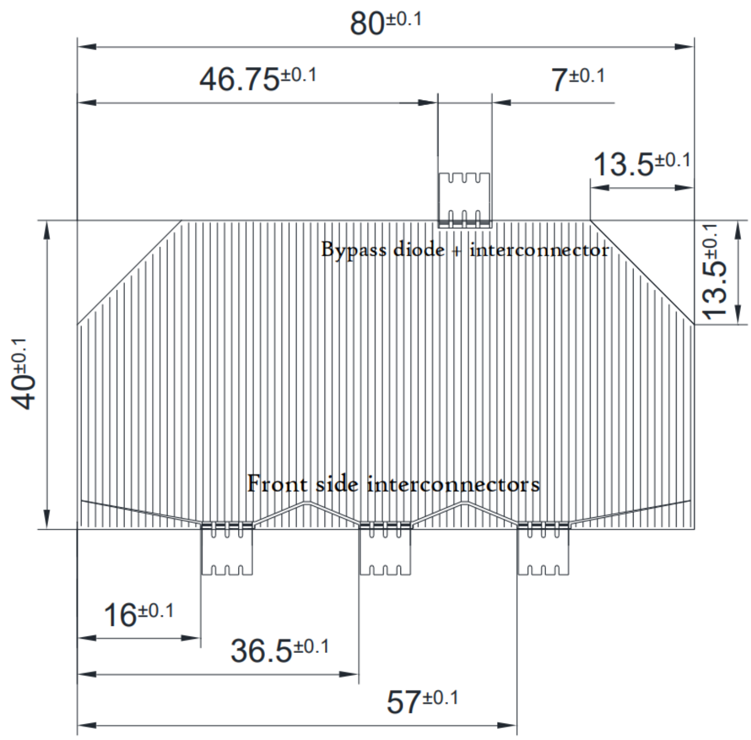

Figure 11.12: Dimensions Solar Cell Azurspace 3G30A [17]

Firstly, it is important to be aware of the internal systems that are included within the solar panel. Each solar cell contains, in addition to the solar cell, an integral bypass diode, interconnectors, and cover glass [17]. The cover glass is a protective cover over the cell and therefore has no active functioning, other than providing additional safety. The integral bypass diode offers a connection contingency in case of failure of the solar cell, and the interconnectors offer the ability to connect the solar cells to other systems. Overall, the electrical layout of one of the Azurspace TJ Solar Cell Assembly 3G30A can be seen in Fig. 11.13.

[44] Personal Communication with ESA System Engineer C. Pirat

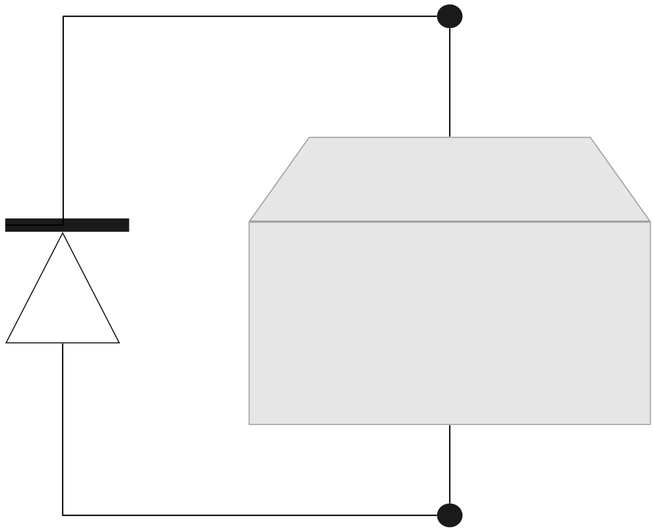

Figure 11.13: Electrical Layout Single Solar Cell

These solar cells need to be arranged in series in order to allow for the summation of their power generation. In order to create an even greater amount of contingencies, these solar cells will be grouped into ”blocks” of 12 solar cells. These blocks are created in order to add another level of contingency in case of the unlikely event of both a respective solar cell and diode failing. That is why each block has a bypass diode integrated into it. The electrical design of one of these blocks can be observed in Fig. 11.14.

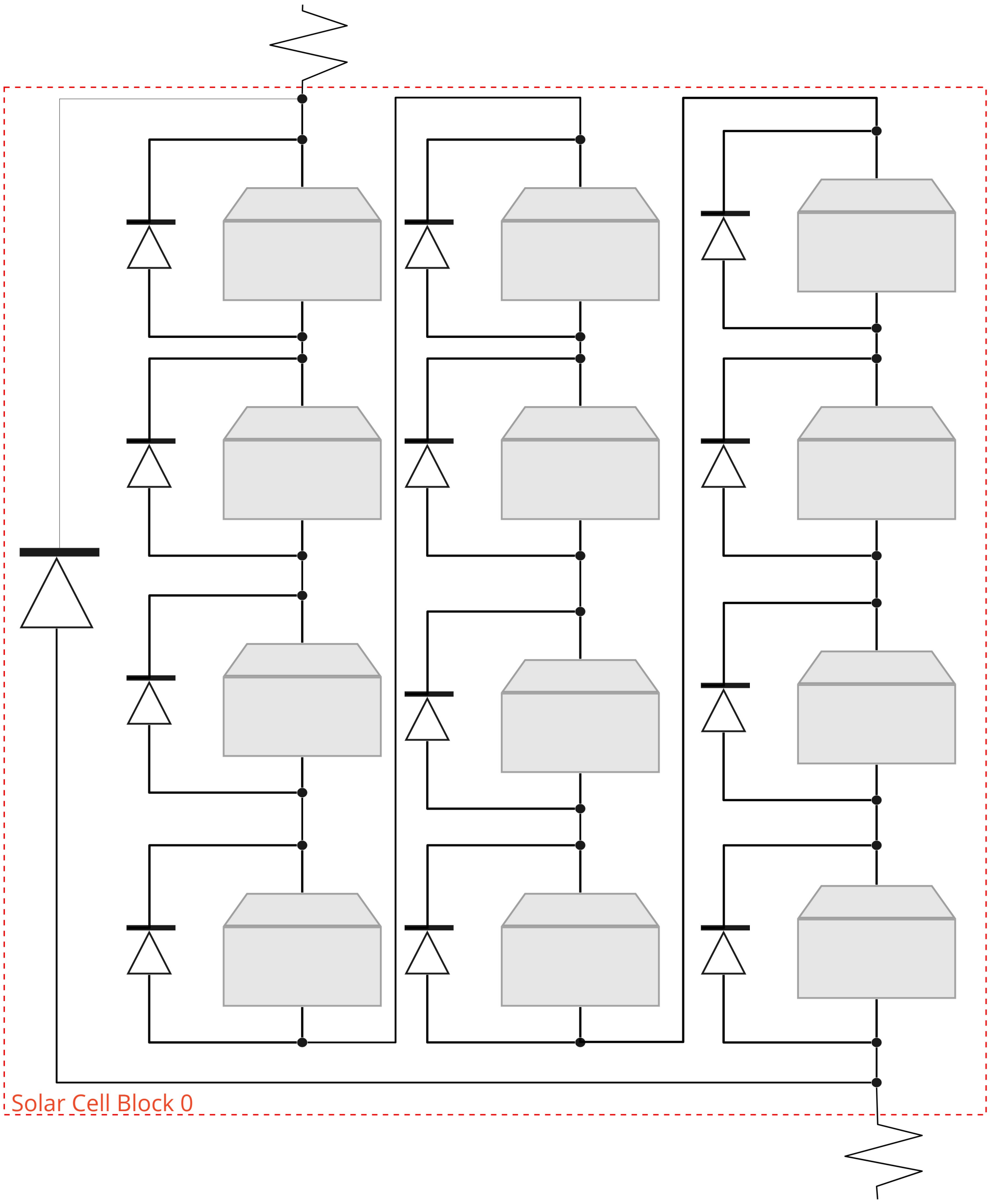

Figure 11.14: Electrical Layout Solar Cell Block

Then, as a final contingency towards possible failure within the power distribution system, the blocks will be divided into five sections, concurrent with the amount of contingency present. Each of these sections will contain eight blocks. Note, this results in 480 solar cells, which is more than the minimum 448. This discrepancy only creates additional power redundancy, increasing the reliability of the system. The section division is made to guarantee that failure of any part will not result in failure of the power generation system. The total solar cell array that follows from these design choices is depicted in Fig. 11.15.

Figure 11.15: Electrical Layout of complete Solar Panel

The power generated by the solar cells is subsequently distributed and stored. The manner in which this is sized and organised will be discussed in the subsequent subsections. The total cost of these solar cells is estimated based on the learner effect, as previously documented, as well as the base costs [17], and is set at $48E3$ \$.

11.6.3. Power Distribution

The power generated and stored by the power subsystem needs to be relayed and connected to the proper systems. In order to complete that task, the power distribution system is designed. The layout of said system is visible in Fig. 11.16. In the subsequent paragraphs, the functioning of individual sections of the power distribution system will be elaborated upon.

Thus, the first topic that will be discussed is the conditioning unit. This section of the power distribution unit employs multiple transformers, denoted ICT0 until ICT4, converting power to the corresponding voltage. Additionally, this unit includes five power sensors that may be employed in order to provide a diagnosis of the system while functioning.

Then, the distribution unit this unit controls the functioning of the entire power system, as well as relaying power to the external subsystems. The first element is the ”MCU” or microcontroller unit. This element controls the functions of every part, it is the brain of the power system. Then, the distribution unit employs several transformers converting power to the voltages required by the external subsystems, they are denoted as OCT0 - OCTX. At this stage of the design, the voltages of the respective subsystems are not known, therefore the amount of transformers is also unknown. In addition to these parts, the distribution unit houses a contingency in the form of a ”Hard Reset”, this function allows for the shutting on/off of the power system, to create a manual reset. Finally, the distribution unit has a number of power sensors to allow for functional diagnoses during flight.

The last unit that will be discussed is the battery unit. This system houses a transformer named BCT0, which converts the incoming power to the proper voltage for the battery and in the other direction as well. Then, it of course contains multiple batteries, with integrated fuses. It also encompasses an integrated heater system for the battery, with a temperature sensor, a heater, and internal heater control. Finally, it has a power sensor to allow for diagnoses during flight.

Finally, the power generation unit has already been depicted, thus that will not be discussed in detail. Two additional parts included are the umbilical connector as well as the external separation switch. These are standard parts for such a system, they are respectively critical during the testing phase and launching phase of the satellite. The umbilical connector allows for a connection to the software of the satellite during integrated testing, the external separation switch is a hardware indication for the satellite that the satellite has been deployed, and thus may start the countdown towards turning on.

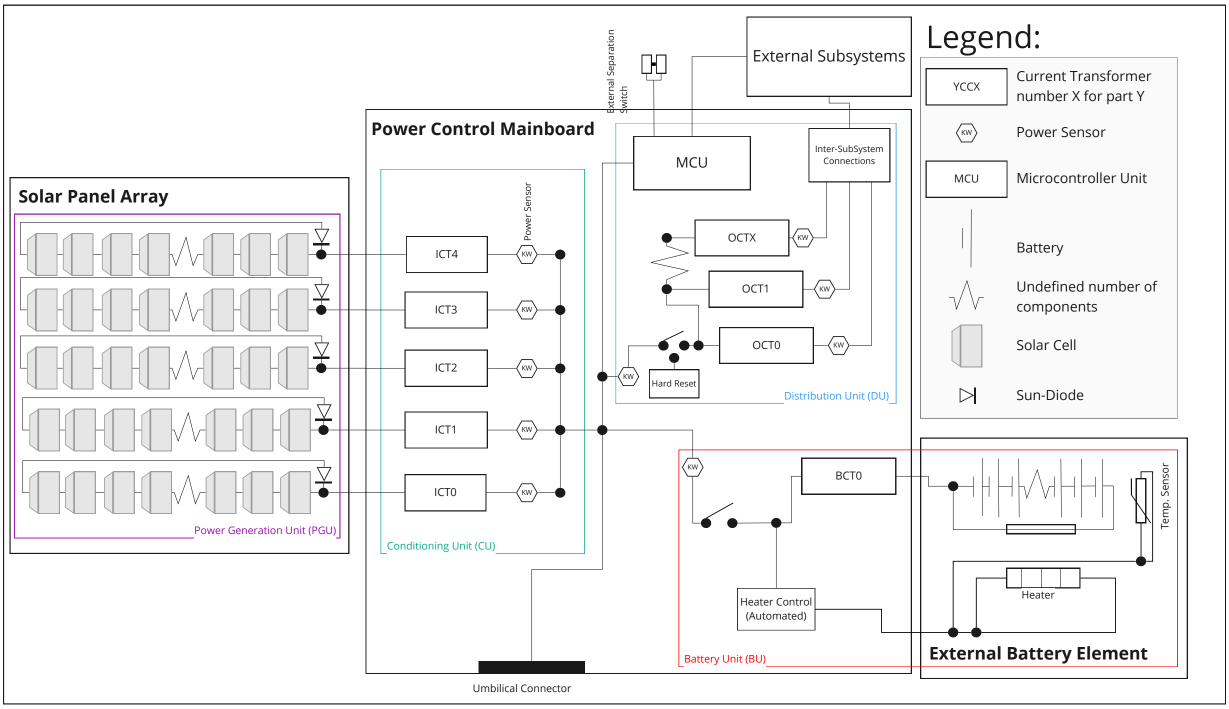

Figure 11.16: Power System Design

11.6.4. Power Storage

In order to be able to supply each system with power during operations, as well as during transfer to L_1, the satellite needs to have the ability to store power. Thus, the satellite requires batteries.

The first step in obtaining a sizing for the batteries is to create a trade-off of possible types of batteries. Table 11.15 depicts all the possible types of batteries that were evaluated in an analytical hierarchy process trade-off, considering specific energy, density, cost, and reliability. The trade-off revealed that the best option was the Lithium-Sulfur Dioxide battery due to its relatively high reliability and low cost relative to the other high specific energy options.

Table 11.15: Viable Types of Batteries Considered in AHP Trade-off [66]

Battery Type	Specific Energy $[Whr/kg]$
Hydrogen Fuel Cell	275
Lithium-Sulfur Dioxide	200
Lithium-thionyl chloride	200
Nickel-cadmium	30
Nickel-hydrogen	60
Silver-zinc	100

Thus, as the type of battery is known, said battery must now be sized appropriately. In order to do this, the maximum amount of power that needs to be stored will be computed. To compute the amount of power that needs to be stored, there are two causes that require power to be stored. Firstly, during an eclipse, as the solar panels cannot receive solar energy in this stage of orbit, the satellite will have sufficient energy to remain functional during the eclipse. Eq. (11.24) denotes the total energy necessary to maintain functionality during an eclipse. Additionally, Eq. (11.25) denotes the amount of battery necessary to maintain functionality for a time period $t_{response}$, a period which has been set at 24 hours based on external engineering judgment[44]. This period is the period in which possible

[44] See page 92

errors or reboots can be completed, in the case of an error of some form. Note, it was externally estimated that the detumbling period after launch would take less than 2 hrs, therefore, this may be neglected, as it cannot be the critical sizing.

As additional clarification, E_{bat} is the required energy in a battery. m_s is a standardized ESA safety margin[44], of 1.25. $t_{eclipse}$ is the largest eclipse period during transfer, this is equal to 0.0417 hr as per Chapter 10.

$$E_{bat} = m_s \cdot P_m \cdot t_{eclipse} \tag{11.24}$$

$$E_{bat} = m_s \cdot P_m \cdot t_{response} \tag{11.25}$$

For this system, Eq. (11.24) gives 18.27 Whr, Eq. (11.25) gives $10\ 516$ Whr. The response battery sizing is larger and thus critical. Applying the material properties of the Lithium-Sulfur Dioxide battery [66] gives a mass of 52.6 kg and a volume of 0.0414 m^3. These values show the estimated attributes of the custom battery system.

11.6.5. Power Mission Planning

Most satellite missions have eclipses and other varying functionalities included in their mission. However, within this mission, the transfer to the L_1 point is almost entirely completed within the launch vehicle. This means that at that stage the satellite is fully inactive.

Thus, the satellite is only turned on once it is stationed in an orbit where it has the ability to maintain a constant orientation towards the sun, and as it is at L_1, this is almost completely uninterrupted. Therefore, the plotting of the power mission planning is obsolete. The nature of the mission dictates that permanent exposure to the sun is present, from start of the mission until the end.

The single exception to this is during the capture maneuver, described Chapter 10. This maneuver turns the solar cells away from the sun for a little over 6 hrs. However, as the battery has the capability to sustain functioning of the satellite for up to 24 hrs, this is not a critical sizing, and a functionality that can be completed.

Overall, when the satellite is deployed, it orients its solar panel towards the sun. These solar cells will stay aimed towards the sun for the entirety of operation, with the exception of a single capture maneuver.

11.6.6. Subsystem Connections

Fig. 11.17 Provides an overview of the manners in which the hardware subsystem are connected electronically. Thus, it shows how power is transported to various subsystems, as well as the hardware data links.

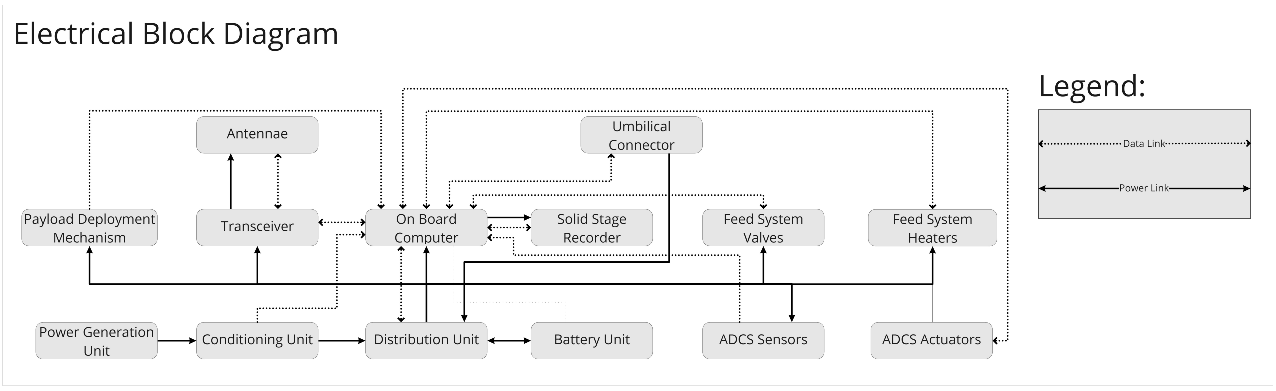

Figure 11.17: Electrical Block Diagram

[44]See page 92

11.7. Structures Subsystem

The main element of the structures subsystem is the primary structure. The purpose of the primary structure is to ensure the structural integrity of the vehicle, to transfer loads in the desired way, and to provide mounting to the individual subsystems. This section will present the design process for the primary structure of the spacecraft. Furthermore, the designs of the launcher interface, and the debris shielding will be presented in this section.

11.7.1. Requirements

In Chapter 6, the requirements on the structures subsystem can be found (the technical requirements on the structures subsystem use identifier **DSE14-TECH-STR-XX**). They were established in the baseline report [2] and revised in the midterm report [3]. These requirements provide the basis on which the structures subsystem will be defined.

11.7.2. Primary Structure Design Concept

In the midterm report, a preference for a structural design was expressed. The preferred option would have been to use a cylindrical primary structure. However, further consideration has shown that the truss/shelf option with a cylindrical core would offer a more flexible solution in case the designs of the other subsystems would change in dimensions. In this design, the tank will be a primary structural element. The remaining load-carrying structural elements will be comprised of struts used to carry compressive and tensile loads, and sandwich panels used to carry bending and torsional loads.

Sandwich panels will be used to form three platforms, on which subsystems can be mounted. These panels themselves will then be mounted to the truss structure and the tank. Furthermore, together with the tank, they give the spacecraft torsional/shear rigidity. Finally, sandwich panels will also be used to stiffen the launcher attachment section, since this can greatly increase the stiffness of the attachment and thus the natural frequency of the spacecraft with respect to the launcher.

The main purpose of the tank is to contain the propellants for both the ADCS and the propulsion subsystem. However, since the tank will most likely be very large and take up a large part of the internal volume of the spacecraft, it has been decided to make the tank a structural element as well. The tank will be sized in such a way, that it will be able to both carry the structural loads as well as the pressure loads from storing the propellant

The main purpose of the struts is to transfer loads from the sandwich panels and the tank into the launcher during launch. Each individual strut will be a thin-walled tube, whose thickness and diameter will be sized for the maximum load that each strut is expected to carry, in order to minimize the mass of the primary structure.

Furthermore, the structure will also include means of attachment to the payload adapter of Starship, and debris and radiation shielding. The designs for these two parts of the structure will be elaborated upon in Section 11.7.5 and Section 11.7.6 respectively. In Fig. 11.18, a schematic representation of this concept can be found.

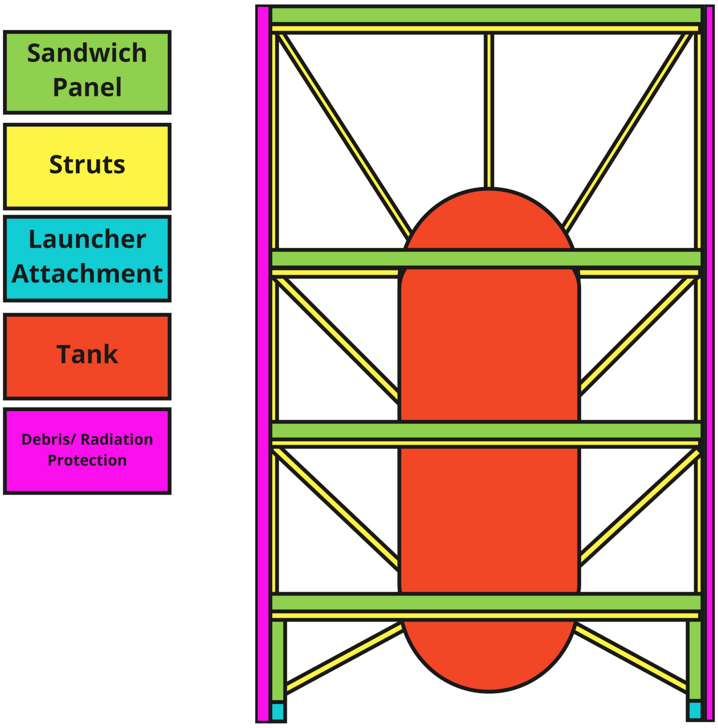

Figure 11.18: Overall structural concept

11.7.3. Simplified Truss Structure

To size the individual structural elements efficiently, the loads within each element have to be analyzed for the load that they carry. To accelerate and simplify this process, the structure will be simplified to a truss structure, which can then be more easily analyzed for its internal loading. The following assumptions/simplifications have been made [67]:

- The truss members only carry tensile or compressive loads.
- The tank will be considered as a sequence of vertical members in the middle of the structure
- The truss structure will be analyzed in 2D. There will be four sets of struts spaced equally around the tank. However in the worst case, only the two opposing sets of struts will carry all lateral loads, therefore it is valid to only consider the two-dimensional case.
- The shear forces carried by the sandwich panels will be introduced into the truss at the nodes where they are attached to.
- The sandwich panels only carry shear forces and bending moment, thus no tensile or compressive loads.
- The mass of the structure is neglected.
- Debris and radiation shielding do not carry any loads.
- The tank is assumed to be thin-walled

These simplifications produce the truss structure which can be found in Fig. 11.19. The load case shown in Fig. 11.19 emulates the loads during launch. In the analysis, loads will be introduced at all points except points **A** and **M**. These loads will simulate the loads induced by the sandwich panels and the subsystems mounted to them, as well as the tank, both due to longitudinal and lateral accelerations.

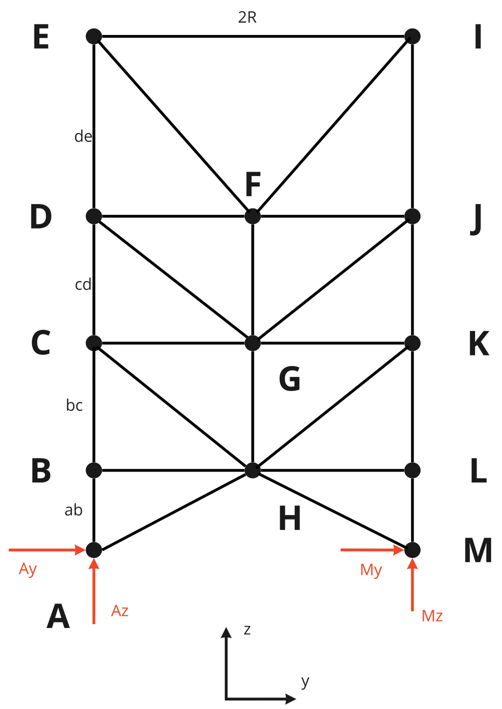

Figure 11.19: Simplified structure with the reaction forces during launch

11.7.4. Modeling

To be able to quickly and easily iterate through the structural design, a model has been created, which computes the internal loads on the main structural elements, sizes them according to the chosen material and ensures that the required natural frequency is sufficiently high. In this section, the composition and logic of the model will be explained. First, the inputs to the model will be defined. After this, the outer shape sizing of the primary structure will be performed. With this complete, the internal loads of the truss members will be determined, which will subsequently allow for their sizing. After this, the sandwich panels and tanks are sized. Finally, the natural frequency of the primary structure is estimated.

Inputs

The model uses several inputs to size the structure of the spacecraft. These inputs can be either fixed values, that are based on design choices, or parameters depending on the design of the other subsystems. Because of the latter, the design will have to be iterated multiple times, as the designs that influence the structural design often depend on the structural design. Table 11.16 shows the main inputs as a brief description for each, and where these inputs stem from.

Table 11.16: Input to the structures model

Parameter	Description	Source
Loading	Load distribution on the truss from different subsystems.	All other subsystems
Subsystem Area	The surface area required for each of the subsystems on one of the platforms.	ADCS, CDHS, TT&C, Power, and Propulsion
Tank Volume	Volume of the propellant tank, including oxidizer, fuel and pressurant.	Propulsion

Continued on next page

Table 11.16 – continued from previous page

Parameter	Description	Source
Tank Pressures	Pressure in the propellant tanks and maximum pressure in the pressurant tank.	Propulsion
ADCS Torque	Torque caused by the ADCS about the longitudinal axis of the spacecraft.	ADCS
Spacecraft dimensions	Dimensions R, ab, bc, cd and de from Fig. 11.19.	Design choice
Load factors	Maximum load factors (multiples of g) in lateral and longitudinal directions.	Launch vehicle
Truss geometry	Location of joints and the links between them	Design choice

These inputs will be then used to size all main structural elements and ultimately allow the design to converge to an efficient solution.

Initial Shape Sizing

With all the inputs defined, the spacecraft and tank diameters are the first sizes that are estimated. The optimal length for the spacecraft to maximize its internal volume has been determined to be 10 m [3]. Initially, the lengths ab, bc, de, and de have been all set to 2.5 m each, however, this might change at a later stage. Fortunately, the model is constructed in such a way that such a change will be easily applicable. The required tank volume is known as an input through the ΔV requirement. The length of the tank is defined by the length of the spacecraft, which is assumed to be 10 m. The tank is represented by vertical members FG and GH. The tank is assumed to be a cylinder with a spherical end cap on each end and is also assumed to be thin-walled. The volume of such a pressure vessel is given by Eq. (11.26), where V_t is the required tank volume, d_t is the tank diameter, and $bc + cd$ is the length of the cylindrical section of the tank.

$$V_t = \frac{\pi}{6}d_t^3 + \frac{\pi}{4}(bc + cd)d_t^2 \tag{11.26}$$

This equation is then solved for the required diameter of the tank. Next, the spacecraft diameter will be sized in such a way that the area of the three platforms within the structure will provide the surface area for all of the subsystems combined. This area-oriented approach was chosen over a volume-oriented approach since for a large tank diameter (3+ meter), the platform area might become unfeasibly small. Instead, the platform-area-oriented approach should result in a more feasible structural design in terms of subsystem integration. Based on this area, the spacecraft diameter can be determined using Eq. (11.27), where d_{sc} is the spacecraft diameter, d_t is once again the propellant tank diameter, and A_{sub} is the platform area required for all of the subsystems. Note that the latter value is divided by 3, as there are three platforms on which subsystems can be mounted.

$$d_{sc} = \sqrt{d_t^2 + \left(\frac{4}{\pi}\frac{A_{sub}}{3}\right)} \tag{11.27}$$

This completes the sizing of the outer dimensions of the spacecraft.

Truss Member Loading

To size the individual members of the simplified truss structure, the loads carried by them have to be computed. To allow the model to be iterated in the convergence process with changing input parameters, these loads have to be solved numerically within the model, rather than analytically. To achieve this while keeping the development time of the model to a minimum, it was decided to use the python package TrussPy[45]. This package can construct trusses and solve for their reaction forces based on a certain loading applied to the truss and the specified constraints. Furthermore, this package can compute truss deflections, if the material and geometry for each member are specified. This will be helpful for the natural frequency estimation. The results produced by the TrussPy package will also be verified and validated.

Initially, the truss is constructed using the geometries defined in the previous sub-subsection. Points **A** and **M** are defined as the points where the reaction forces act, both in y- and z-direction. The loads are distributed by considering three types of loading: the propellant mass, the sunshield mass, and the mass of the remaining subsystems. Table 11.17 shows the loads applied to the modeled structure. In the equations, m_{sub}, m_{prop}, and m_{ssh} represent the mass of the subsystems, the propellant, and the sunshield, respectively. Furthermore, g_0 is the standard acceleration due to gravity, and n_y and n_z are the load factors in y- and z-direction respectively. The mass is assumed to be equally distributed throughout the three platforms. The shield mass is assumed to be applied at the top of the spacecraft.

Table 11.17: Load Applied at each Member

Member	Load Applied in z-Dir.	Load Applied in y-Dir.
A	A_z	A_y
B	$-\frac{m_{sub}}{6} \cdot g_0 \cdot n_z$	$-\frac{m_{sub}}{6} \cdot g_0 \cdot n_y$
C	$-\frac{m_{sub}}{6} \cdot g_0 \cdot n_z$	$-\frac{m_{sub}}{6} \cdot g_0 \cdot n_y$
D	$-\frac{m_{sub}}{6} \cdot g_0 \cdot n_z$	$-\frac{m_{sub}}{6} \cdot g_0 \cdot n_y$
E	$-\frac{m_{ssh}}{6} \cdot g_0 \cdot n_z$	$-\frac{m_{ssh}}{6} \cdot g_0 \cdot n_y$
F	$-\frac{m_{prop}+m_{sub}}{3} \cdot g_0 \cdot n_z$	$-\frac{m_{prop}+m_{sub}}{3} \cdot g_0 \cdot n_y$
G	$-\frac{m_{prop}+m_{sub}}{3} \cdot g_0 \cdot n_z$	$-\frac{m_{prop}+m_{sub}}{3} \cdot g_0 \cdot n_y$
H	$-\frac{m_{prop}+m_{sub}}{3} \cdot g_0 \cdot n_z$	$-\frac{m_{prop}+m_{sub}}{3} \cdot g_0 \cdot n_y$
I	$-\frac{m_{ssh}}{6} \cdot g_0 \cdot n_z$	$-\frac{m_{ssh}}{6} \cdot g_0 \cdot n_y$
J	$-\frac{m_{sub}}{6} \cdot g_0 \cdot n_z$	$-\frac{m_{sub}}{6} \cdot g_0 \cdot n_y$
K	$-\frac{m_{sub}}{6} \cdot g_0 \cdot n_z$	$-\frac{m_{sub}}{6} \cdot g_0 \cdot n_y$
L	$-\frac{m_{sub}}{6} \cdot g_0 \cdot n_z$	$-\frac{m_{sub}}{6} \cdot g_0 \cdot n_y$
M	M_z	M_y

Using these loads and constraints, the model then can solve for compressive/tensile loads within each of the members. For the load factor, the maximum values of 6g in the longitudinal direction and 2g in the lateral direction have been used [3]. This load case is not likely to occur during launch, as within the envelope, these are the largest values, but they never occur at the same time. However, using this load case will ensure that the spacecraft will be able to sustain any loading within the load factor envelope specified by SpaceX [21].

Truss Member Sizing

The truss members will be designed as hollow cylindrical cross-sections. Since they will carry both compressive and tensile loads, the members will most likely be made from metal, since conventional composites are not as suited to carry compressive loads, due to their anisotropic nature. Since the

[45]URL: `https://adtzlr.github.io/trusspy/` [cited 14 June 2021]

struts will be loaded in either compression or tension, the two main failure modes of these truss members will be either tensile failure or buckling.

The model iterates through a certain range of thicknesses and diameters. For each thickness and diameter combination, Eqs. (11.28) and (11.29) [67] are used to determine the stress in the member and its buckling failure load, using the load in the strut P_t, the strut diameter d_s, the strut thickness t_s, the strut length L, and the strut's E-modulus E.

$$\sigma_t = \frac{P_t}{A} = \frac{P_t}{\pi(\frac{d_s^2}{4} - (\frac{d_s}{2} - t)^2)} \tag{11.28}$$

$$P_{cr} = \frac{\pi^2 EI}{L^2} = \frac{\pi^2 E \frac{\pi}{4}((\frac{d_s}{2})^2 - (\frac{d_s}{2} - t)^4)}{L^2} \tag{11.29}$$

For each strut and each combination of diameter and thickness, the model will compute both of these values. It will then compare the tensile stress to the maximum allowable stress defined by Eq. (11.28), and the load in the member to the critical buckling load defined by Eq. (11.29). If both of these values are within those limits, the design is added to a list of viable options for the design of this member. Furthermore, per requirement **DSE14-TECH-STR-05**, a safety factor of 1.4 is applied before the loadings are compared to the critical loads.

The results of this process are several different design options for each member, which will all be able to carry their respective loads. For each member, the optimum design is determined by finding the option with the minimum cross-sectional area. Since the members have constant cross-section over the length of the member, choosing the option with the minimal cross-sectional area will minimize the mass of each member. Finally, since the lateral loads can occur in equal magnitude in both directions, the members will be ”symmetrized”. This means that each member will be compared to its opposite across the z-axis. The stronger design of the two will be chosen for both sides of the spacecraft. This is to ensure that each member can sustain loads under acceleration in both lateral directions. This is not done in the z-direction, since the maximum load factor in the positive z-direction is 3 times larger than in the negative z-direction. It is therefore assumed that the positive z-direction load factors will be dominating in the design as compared to their negative counterpart.

Sandwich Panel Sizing

All the subsystems apart from the sunshield are mounted to sandwich panels, which form three platforms within the spacecraft. These sandwich panels will carry shear loads to the next vertical member (or the tank) where it can then be carried as a compressive or tensile load to either the launcher mounting or the engine of the spacecraft. There are multiple methods of sizing sandwich panels. They can be sized to be most resistant to buckling or face dimpling, or they can be sized for maximum stiffness, or maximum strength [18]. For this design, there are two driving constraints for these structural elements. They need to able to sustain the launch loads without failing (**DSE14-USR-SR-02, DSE14-TECH-STR-03, DSE14-TECH-STR-04**), and they need to make the structure stiff enough to fulfill the natural frequency requirement set out by the launcher (**DSE14-TECH-STR-01**). Finally, they also need to provide the mounting to the other subsystem (**DSE14-TECH-STR-08**). In this case, the bending strength is the more critical criterion to size for, since the sandwich panels do not contribute as much to the stiffness of the vehicle, especially not for z- and y-deflections.

Within the model, the load case for each of the sandwich panel platforms is defined as the platform carrying one-third of the subsystem mass, uniformly distributed over its surface. Note that in reality, the platform will be connected to both the outer vertical truss members and the tank in the center of the spacecraft. However, the difficulty in modeling this lies in the truss supports on the outer edge of the platforms being at four discrete locations, while the inner edge at the tank is supported continuously around the entire circumference. In order to be able to model this in such a way that the panel design will be able to carry the loads at any point of the panel, it will be sized assuming no supports at the outer edge. The design will be slightly over-designed due to this, however, this simplification will allow for a simple design iteration and convergence process. Finally, the load applied to each platform will be multiplied with a safety factor of 1.5 [68].

Fig. 11.20 shows the parameters that are used in the sizing of the sandwich panels. Furthermore, h_c will represent the thickness of the panel. Fig. 11.21 shows the load case as outlined previously used to model the loading of the platforms and subsequently sizing the panels.

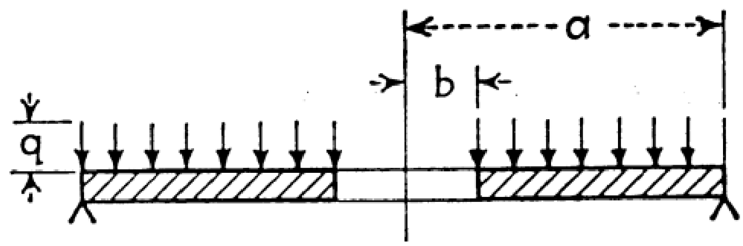

Figure 11.20: Parameters used in modeling a sandwich panel platform [69]

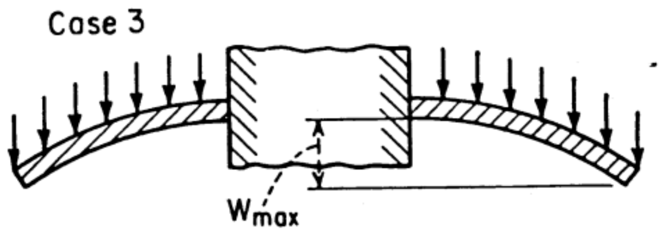

Figure 11.21: Load case used in modeling the panel [69]

The thickness h_c of the panel can then be sized using Eq. (11.30) [69], where q represents the distributed load per area, a is the outer diameter of the panel, σ_{ult} is the ultimate failure stress of the faceplate, and k is a dimensionless coefficient, which can be obtained from literature [69], where its value depends on the ratio of outer radius over the inner radius.

$$h_c = \sqrt{k\frac{qa^2}{\sigma_{ult}}} \tag{11.30}$$

For a sandwich panel, h_c will represent the core thickness. Since it was previously determined that the panels should be sized for bending strength, Eq. (11.31) [18] can be used to determine the ratio of core height h_c to the faceplate thickness t_f, based on the ratio of faceplate density ρ_f to core material density ρ_c. From this, the faceplate thickness can be sized using Eq. (11.32).

$$\frac{h_c}{t_f} = 2\frac{\rho_f}{\rho_c} \tag{11.31}$$

$$t_f = h_c\left(\frac{h_c}{t_f}\right)^{-1} \tag{11.32}$$

Since Eqs. (11.31) and (11.32) already size the panel face and core are already sized with minimum mass in mind [18], an additional mass optimization is not necessary anymore.

Finally, the model estimates the mass for the truss members and sandwich panels based on their individually determined geometry and the chosen materials. Furthermore, it also estimates the mass of the chosen debris shielding. The design of this part of the subsystem will be elaborated upon in Section 11.7.6.

Tank Sizing

As previously mentioned, the tank will be designed to be a load-carrying structural element. It will be especially useful in giving the spacecraft additional torsional rigidity. Since the tank will be a large part of the structure and additionally have to carry large pressure loads, it was decided to design this tank as a composite overwrap pressure vessel or COPV. This will help save mass as compared to a conventional pressure vessel made from aluminum, steel, titanium, etc. However, due to the anisotropic nature of composites, special attention needs to be paid to determining the correct material characteristics used in the design process.

COPVs are comprised of two main components: the liner and the overwrap. The liner is a metal bladder that contains the pressure and ensures the pressure vessel is leak-tight. This part is commonly made from metal, especially aluminum alloys such as aluminum 6061 [70]. The other main component is the overwrap. It is made from composite fibers, usually carbon fibers, which are wrapped over the pressure vessel. This is usually done under a certain angle, to ensure that both circumferential and longitudinal stresses are carried equally effectively. It is assumed that the overwrap solely carries the stress. The circumferential and longitudinal stress in a pressure vessel can be computed using Eqs. (11.33) and (11.34) [71] respectively, with the internal (feed) pressure P_f, tank diameter d_t and overwrap thickness t_t.

$$\sigma_{circ} = \frac{P_f d_t}{2t_t} \tag{11.33}$$

$$\sigma_{long} = \frac{P_f d_t}{4t_t} \tag{11.34}$$

Eqs. (11.33) and (11.34) can also be divided by each other to obtain Eq. (11.35) which determines the ratio of the circular stress to longitudinal stress. This value will be used in the calculation of the lay-up angle.

$$\frac{\sigma_{circ}}{\sigma_{long}} = \frac{\frac{P_f d_t}{2t_t}}{\frac{P_f d_t}{4t_t}} = \frac{\frac{1}{2}}{\frac{1}{4}} = 2 \tag{11.35}$$

To be able to size the overwrap, the angle of the overwrap with respect to the longitudinal axis α needs to be determined. From literature, [70], the relation between longitudinal or circumferential stress and the stress in the fibers σ_f can be obtained. These relations can be found in Eqs. (11.36) and (11.37).

$$\sigma_{circ} = \sigma_f sin^2(\alpha) \tag{11.36}$$

$$\sigma_{long} = \sigma_f cos^2(\alpha) \tag{11.37}$$

Combining Eqs. (11.35) to (11.37) will result in Eq. (11.38), which can then be solved for the lay-up angle α. This results in an optimal lay-up angle of 54.74° with respect to the longitudinal axis of the tank.

$$\frac{\sigma_{circ}}{\sigma_{long}} = \frac{\sigma_f sin^2(\alpha)}{\sigma_f cos^2(\alpha)} = tan^2(\alpha) = 2 \tag{11.38}$$

Hence the lay-up thickness will have to be sized for about 1.5 times the circumferential stress caused by the pressure.

When the sizing of the tank is performed in the model, four distinct failure modes are considered: pressure failure, buckling failure, pure compressive/tensile failure, and torsion. These modes stem from different loads applied throughout the mission. The model will compute the required thicknesses to prevent failure in each of these failure modes and will subsequently choose the largest resulting thickness since this thickness will then be able to also sustain all other lower loads. Finally, in each computation, a safety factor of 1.5 for non-metallic structures will be used [68]. The following paragraphs will elaborate on the sizing method for each of these modes.

The pressure design has already been elaborated upon. With the angle known, and thus the stress for which the overwrap has to be sized, Eq. (11.33) can be solved for the thickness of the overwrap.

In order to size for buckling loads, the compressive loads in the tank are considered. In Eq. (11.29), the moment of inertia can be replaced for the expression for the moment of inertia of a thin-walled circle. Furthermore, the column length L will not be the entire length of the tank, but only the distance between two platforms (the tank spans across the three lower platforms, meaning that this is half of the tank length, see Fig. 11.18). This equation can then be solved for the thickness, which can be found in Eq. (11.39) [67]. F_t represents the compressive load in the tank, L in this case will be the distance between two platforms, d_t is once again the tank diameter, and E represents the E-Modulus of the tank material.

$$t_t = \frac{8F_tL^2}{\pi^3 d_t^3 E} \tag{11.39}$$

Both this load case and the previous one are induced by the loads from the subsystems and the shield being transferred through the tank to the payload adapter of Starship. The approach to size the tank for compressive and/or tensile loads is a lot simpler. Eq. (11.40) [71] is simply the standard equation for normal stress, with the equation for a thin-walled ring substituted and once again solved for the thickness. This will yield minimum thickness for this load case.

$$t_t = \frac{F_t}{\pi d_t \sigma_f} \tag{11.40}$$

Finally, torsion is also considered. This load case mainly stems from the reaction control thrusters and reaction wheel of the ADCS. It will most likely be quite small compared to the other loads, however, for the sake of completeness, it shall still be considered here. Equation (11.41) determines the shear stress due to an applied torque, with torque T, tank diameter d_t, and polar moment of inertia J. If an expression for the polar moment of inertia for a thin-walled ring is substituted and Eq. (11.41) is solved for the thickness, Eq. (11.42) [67]. can be obtained. Note, that the shear stress τ has been replaced by the fiber stress $\frac{\sigma_f}{\sqrt{3}}$, by making use of the Von-Mises criterion.

$$\tau = \frac{Td_t}{2J} \tag{11.41}$$

$$t_t = \frac{2\sqrt{3}T}{\pi d_t^2 \sigma_f} \tag{11.42}$$

Finally, the pressurant tank is also sized as a spherical tank. Since it will not be carrying any loads apart from its own pressure loads, Eq. (11.34) can also be used to determine the thickness required for this tank, based on the material used and the maximum pressurant pressure.

Natural Frequency Estimation

The final step in modeling the structure is to analyze the primary structure for its natural frequency. It is important to ensure that the design is in accordance with requirement **DSE14-TECH-STR-01**. This is done by once again making use of the TrussPy package. Apart from being able to solve for the reaction forces in the members of a truss, it is also able to compute the deflection of a truss under a given loading and with the material and geometric properties specified. This functionality will be used to estimate the natural frequency. However, a few assumptions will have to be made to be able to perform this estimation:

- Loads are only carried by the truss members
- The system is assumed to be undamped
- The members behave the same way in compression and in tension
- The tank will not be included in the estimation

These assumptions will make the estimation less accurate, however the assumption should reduce the estimated natural frequency, hence the estimate should be conservative. In the model, identical loads in positive y-direction will be applied at nodes **I** and **E**. The sum of these two forces will be then divided by the resulting deflection in one of these points (deflection should be identical due to symmetry). The resulting value is the stiffness k_{eff} of the system. Since the system was assumed to be undamped, the natural frequency in Hertz can be computed using Eq. (11.43) [72], with previously determined stiffness k_{eff} and primary structure mass m_{ps}.

$$\omega_n = \frac{1}{2\pi}\sqrt{\frac{k_{eff}}{m_{ps}}} \tag{11.43}$$

As previously mentioned, this value is conservatively estimated, meaning that the real value for the natural frequency is likely to be much larger than the computed in this estimation.

11.7.5. Launcher Mounting

The payload will be launched onboard the SpaceX Starship launch vehicle. Requirement **DSE14-TECH-STR-09** defines the need for a payload attachment system, which can be released upon command. When designing the launcher mounting, two main aspects have to be considered. Firstly, a stiff (and ideally lightweight) attachment has to be provided, ensuring the payload will not interact with the launcher dynamics, while still being able to support the launch loads. Secondly, the payload needs to be able to separate from the launcher at the desired time in the mission, without inducing extreme shock loads into the payload, without ejecting large amounts of debris, and all while ensuring no re-contact occurs between the spacecraft [73].

Since the shock loads during ascent, staging, and payload bay opening will be negligibly low [21], the critical shock load case will occur during payload separation [3]. It is therefore advantageous to choose a separation system that induces very little shock loads into the payload. One of the best options is to use a clamp-band-system. This system is commonly used in many space missions [73].

The system uses a clamp-band like the one seen in Fig. 11.22 to firmly connect the payload to the launcher. The system is tensioned using springs, which push the payload away from the payload adapter in the launcher. However, the clamp-band prevents the two from separating by clamping so-called V-clamps to connect the payload and launcher. This can be seen in Fig. 11.23. Furthermore, in order to prevent the band from flying off and potentially causing damage to the launcher or the payload, a band catcher is installed in order to prevent this.

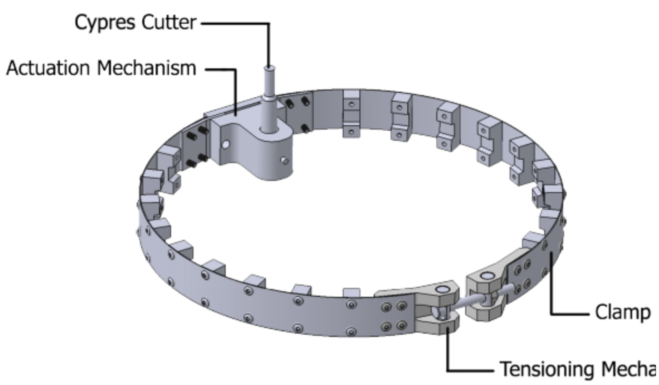

Figure 11.22: Simple version of clamp-band-system [74]

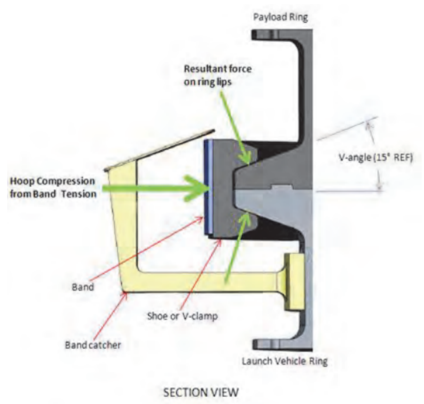

Figure 11.23: Cross-section of a more advanced clamp-band-system [73]

Should a requirement on minimum or maximum separation velocity ever arise, then the springs separating the two parts after clamp-band release can be sized accordingly.

11.7.6. Debris Shielding

Space debris can pose a rather large threat to a spacecraft. Requirement **DSE1-TECH-STR-07** stipulates, that the spacecraft's subsystems need to be adequately protected against impact from space debris. Therefore it has been decided to use so-called stuffed Whipple shields [75] for the debris protection of any exposed areas of the spacecraft. This mainly concerns the side of the spacecraft, since these areas would otherwise be directly exposed to the outside.

A stuffed Whipple shield is made from three main components. The outermost layer is called the bumper plate. It is the first layer that incoming debris will make contact with, and its main purpose is not to stop the incoming projectile but instead to disperse and vaporize the projectile [76]. This layer is usually a thin (<1mm) thick sheet of metal. The next layer of material is called the stuffing. This layer is tasked with actually stopping the cloud of vaporized and dispersed debris. It is commonly made from high-strength material like aramid fabric or basalt fabric [75]. Finally, the rear wall is tasked with stopping any remaining parts of the dispersed projectile, that the stuffing did not stop.

A shield like this one has been proven to be able to stop projectiles at a velocity of up to 8 km/s [75]. Finally, the top and bottom of the spacecraft do not need to be protected additionally, since the sandwich panels at the top and the bottom of the spacecraft will already act similarly to the Whipple shields used on the circumference of the spacecraft.

None of the spacecraft components require any special radiation protection, therefore **DSE14-TECH-STR-06** is fulfilled by default.

11.7.7. Material Choices

This subsection will outline the material choices made for the structures subsystem, and will present the processes that were used to obtain these material choices. This will be done for the three main structural elements, which have been considered here: The truss and its members, the sandwich panels (both core and face material), and the propellant tank. Table 11.18 shows the materials which have been considered for each of these elements, which were collected from literature [18] as commonly used materials in spacecraft structures.

Structural Element	Material Family	Type/Alloy
Truss Structure	Aluminum	2014-T6
		2024-T36
		6061-T6
		7075-T6
	Steel	RH1050
		D6AC
	Titanium	Ti6Al-4V
	Magnesium	AZ31B
		AZ31B-H24
Tank overwrap	Carbon Fiber	HM Fibers
		HT Fibers
Sandwich Panel Face Material	Carbon Fiber	HM Fibers
		HT Fibers
	Glass Fiber	E-Glass Fibers
		S-Glass Fibers
Sandwich Panel Core Material	Aluminum	Various 5056 honeycomb geometries

Table 11.18: Materials considered in the structures design process [18]

The structural model was initially run to iterate the design through each permutation of the materials listed in 11.18. Afterward, the most lightweight permutation was chosen. In this process, it was observed that the truss structure has by far the largest impact on the mass of the entire primary structure. Hence, mass savings in the tank or the sandwich panels have a relatively small impact on the mass of the entire structure. These materials can therefore be optimized for cost savings instead of mass savings. Furthermore, for the truss structure material, availability will also be considered. Since this is by far the largest component of the structure mass, it will be assumed that the other materials chosen will be at least equally available, since far less material will be required.

Truss Structure Material

The ideal material for the truss structure, in terms of mass, was determined to be Titanium, more specifically the Ti6Al-4V alloy. This comes as no surprise since titanium is a strong yet lightweight material. The mass for the truss structure with this material would be $4\ 040$ kg. However, while this material has extremely high specific strength, it is relatively expensive at 26.8 $\$/$kg [77]. This would mean that a titanium structure would cost almost $113E3$ $\$$ per spacecraft. The next lightest material was determined to be Aluminum 7075-T6. With this material, the structure would have a mass of $5\ 476$ kg. While this is heavier, with a cost of 5.62 $\$/$kg [77], the structure made from this aluminum alloy would only cost $31E3$ $\$$. However, the reduced mass from using the Titanium alloy will reduce the cost per launch, as less propellant will required both onboard the spacecraft and on the launcher. This saving will be roughly $30E3\$$ larger than the saving from choosing aluminum and accepting the higher mass.

With these metal alloys, it also important to consider their supply risk and economic importance. The European Commission published an assessment of the criticality of resources in 2020 [78]. In this report, the supply risk and economic, among others, were assessed for a variety of raw materials, including aluminum and titanium. They were given a relative score for both of these criteria, the derivation of which is outlined in the same document. A higher value in the score means a higher risk in the supply and a higher economic importance respectively. The supply risk for aluminum is rated at 0.6 and titanium is rated at 1.3. The fact that the supply of titanium is at a higher risk than aluminum stems mostly from aluminum being partially produced in the EU (41% [78]) and partially outside of the EU (59% [78]). Titanium on the other hand is exclusively sourced from outside of the EU. However this should have a lesser impact on the availability, since the EOS mission has to be performed with a maximum amount of international cooperation either way, both because of the large budget and the scale of the project. In terms of economic importance, aluminum scores at 5.4 and titanium scores at 4.7. This means that a large scale demand in titanium will affect the general economy less than a large scale demand in titanium.

Finally, the annual worldwide titanium production in 2020 was $210E3$ tons, with a potential maxiumum of $341E3$ tons[46]. With a primary structure mass of 4040kg and $71E3$ spacecraft, and a safety factor of 1.5 to account for manufacturing losses, the total required mass of titanium would be 4040 kg $\cdot$ 71000 kg $\cdot$ $1.5 = 430E3$ tons. With a deployment time of 10 years, this would require roughly 13% of the potential annual titanium production of 2020. With EOS aiming to solve a problem on such a large and international scale, this is a realistic prospect. Therefore, Titanium Ti6Al-4V will be used for the material of the truss members.

Propellant Tank Material

For the tank, the choice was between HM (high elastic modulus) and HT (high tensile strength) fibers. In this case, the choice between those two options becomes quite clear, when considering tank mass and material cost for both materials. If the tank was to be made from HM fibers, it would have a mass of 661.8 kg and HM fibers have a specific cost of 105 $\$/$kg. If instead, the tank were to be produced using HT fibers, the tank would mass 442.2 kg and these fibers have a specific cost of 33.6 $\$/$kg [77]. From this, it becomes clear that HT fibers pose the best option, both in terms of mass and in terms of cost. Therefore, they shall be used for the overwrap of the tank.

Sandwich Panel

For the face material of the sandwich panels, E-Glass, S-Glass, HM carbon, and HT carbon fibers were considered, each as quasi-isotropic lay-up in epoxy. Since the masses of these four options

[46]URL: `https://www.usgs.gov/centers/nmic/titanium-statistics-and-information` [cited 29 June 2021]

do not differ by more than 1%, the main decision point here will be the specific cost. Out of these options, E-Glass fibers in epoxy have the lowest specific cost with 31.1 $/kg. Therefore, this material will be chosen for the sandwich panel face material.

Finally, the core materials of sandwich panels in space application are commonly constructed using aluminum 5056 alloys. Once again, the different honeycomb geometries result in very similar masses for the panels used in the spacecraft. This also means that cost will be extremely similar between the options. Therefore, the choice of which exact type of geometry to use will depend on the ease of manufacturing of each of the options.

Material Summary
Table 11.19 summarizes the materials chosen for the primary structure of the spacecraft.

Material	Use	Yield Strength [MPa]	Ultimate Strength [MPa]	Young's Modulus [GPa]	Density [kg/m³]	Specific Cost [$/kg]
Titanium Ti6Al-4V	Truss Structure	910	980	119	4450	26.8
HT Carbon fibers	Tank over-wrap	N/A	4400	225	1840	33.6
E-Glass fibers in epoxy	Sandwich panel face	N/A	304	21.8	1970	37.1
Aluminum 5056 hon-eycomb	Sandwich panel core	0.222	0.253	0.017	150	36.5
Aluminum 6061-T6	Tank liner, debris shield	241	289	67	2710	2.79
Basalt Fiber	Debris shield	N/A	2800	85	2800	37.1 (similar to E-Glass)
Polyethylene Naphtha-late [47]	Sunshield	N/A	175	5.5	1360	5

Table 11.19: Characteristics of the materials used in the primary structure [77, 18, 76]

11.8. Payload

The payload is among the most important subsystems of the EOS mission. Its role is to accomplish the mission objective. In order to ensure that the price is minimized and the effectiveness maximized, the payload of each spacecraft should be as large as possible. Having decided on the Centripetal motion shield concept discussed in [3], the actual detailed design of the payload itself must be created. There are a few assumptions which will be used to this end based on information available related to the potential options of the near future. The main assumptions for the sizing is that the use of a currently non-existent material with a 1 g/m^2 mass per area value as given by [22] will be

[47]URL: `https://www.steinerfilm.de/en/our-products/steinerfilmr-e/` [cited 14 June 2021]

possible in the future, and the assumption that the sheet can be created without large changes to property, mass or shape due to adhesives.

This assumption for the areal density is used because, as of current technology in solar sails, the most commonly referenced areal density is approximately 20 g/m^2 [48] with the IKAROS mission using a polymide shield of 10 g/m^2. The ACS3 mission, using metallized polyethylene napthalate (PEN), and missions using newer Mylar sheets have both reached approximately 2 g/m^2 as well [79], [80]. Research is being actively done into using, for example, graphene in the future which is capable of vastly reducing this value. The theoretical smallest areal density possible with graphene is using a single layer of atoms. This gives a mass per area value of 0.77 mg/m^2 [49]. Unfortunately, a single layer of graphene would not be realistic for use due to both structural and effectiveness concerns. But these values do suggest that the OHB Systems estimation of a potential near future areal density is viable and may perhaps even be large for what may, in fact, be possible within the near future. This being the case, it is deemed that the 1.15 g/m^2 value for the areal density found from Chapter 10 calculations is viable in the near future and will be assumed as the shield material value. For the sake of this project it will be assumed that the material is PEN as it is the least dense of the options explored and therefore is most likely to be able to sustain this theoretical improvement as the material will remain slightly thicker than other options and more structurally sound.

As a further note on the use of PEN, the material will not be coated with an aluminum layer, but rather with a material allowing for the necessary 3% reflectivity. Such materials are currently under development such as using coatings of silica nanotubes [50] which can reduce reflectivity to even below 1%. The viability of using the currently existing materials must, however, be investigated further at a later date. Furthermore, the coating would only be within the nanometer range and the areal density includes coatings within its assumption, therefore this coating changes little to nothing for the future calculations.

The second assumption, the assumption that the adhesives will not cause a large difference in the values and final design, is used due to the sheer scale and the lack of information on how the adhesives will affect the overall shield in terms of volume and mass. It can be presumed that the shield will be heavier but the extent to which this occurs is unknown at this stage. It will therefore not be considered due to the fact that the goal of this section is to design the payload as accurately as possible to give an upper bound on both the size and the stowing of the material itself based on theoretical and potential technological advancements.

There are three distinct limiting factors to the shield sizing which have been identified. The first of the three is the mass of the payload itself. The payload cannot have a mass that would surpass the total mass allowed for launch after the necessary subsystems are also considered. The second limiting factor is the material resistance to the spinning motion and the centripetal forces induced by it. Tearing of the shield must be avoided as it could be catastrophic. Depending on the size of the shield there is a possibility that it could tear although reference [3] suggests this is not the case through initial preliminary calculation. Even so, it will be investigated with actual design options and materials to ensure this fact is taken into account. The third limiting factor is the stowed volume of the shield itself. Due to the scale of the shield, the stowing and deployment must be properly handled such that the material fits within the confines of the launcher without severely reducing the deployed sizing. This means the folding and stowing methods must be carefully selected.

11.8.1. Mass based Sizing

The mass based sizing of the shield is the easiest to determine. Given the masses of each of the other subsystems and the structure as a whole as well as knowing the maximum launch mass, the

[48]URL`https://www.techbriefs.com/component/content/article/tb/pub/techbriefs/mechanics-and-machinery/25346` [cited 16 June 2021]

[49]URL:`https://www.acsmaterial.com/graphene-facts` [cited 16 June 2021]

[50]URL:`https://www.newscientist.com/article/dn11302-nanorod-coating-makes-least-reflective-material-ever/#:~:text=A%20type%20of%20material%20known,create%20thin%20coatings%20from%20this.` [cited 27 June 2021]

mass of the sheet itself is determined using Eq. (11.44):

$$m_{Total} = m_{Structural} + m_{Propulsion} + m_{Power} + m_{CDHS} + m_{ADCS} + m_{Thermal} + m_{TTC} + m_{Payload} + m_{margin} \quad (11.44)$$

Where the mass values are as given in the other subsystem sections. The margin is an additional mass that remains after the design was iterated. It is there to account for errors the iterations may cause and is 1% of the total mass used.

This formula results in an allowed mass of 107079 kg for the payload. Using the assumed 1.15 g/m^2 and by applying a margin of an additional 1% for the deployment mechanism, an area of approximately $93E6$ m^2 is found which results in a maximum radius of the shield of 5.4 km.

11.8.2. Material Resistance Sizing

The second limiting factor is the material itself. In order to determine the maximum size of the shield, the potential materials must be considered and the stresses calculated. By using the maximum stress the material can handle, the maximum tension forces can be found. Additionally, the rotational velocity and the dimensions can be computed such that the material does not tear which gives the sizing based on this criterion. The method is as follows: firstly, the maximum radial and tangential stress formulas, Eq. (11.45) and Eq. (11.46)[51], are used, where w is the rotational velocity, v is the Poisson ratio of the material, σ_t and σ_r are the tangential and radial maximum stresses, R_0 is the inner radius, and R is the outer radius.

$$(\sigma_r)_{\text{max}} = \frac{3+v}{8}\rho w^2 \left(R - R_0\right)^2 \quad (11.45)$$

$$(\sigma_t)_{\text{max}} = \frac{\rho\omega^2}{4}\left[(3+v)R^2 + (1-v)R_0^2\right] \quad (11.46)$$

These can be restructured to have the outer radius as the variable to be calculated. The smaller radius must be selected once the values are computed as this is the critical case. However, in the formulas, there remain two unknowns: the angular velocity and the radius. This, unfortunately, means that there is no limit as, for any size, there is a corresponding velocity at which the sheet does not tear. As a result of this fact, and due to the ADCS subsystem being flexible to the requirements of the sheet, this method is instead used later in order to find the angular velocity for the sizes given by the alternative two methods.

11.8.3. Volume Sizing

Finally, the volume sizing requires knowledge of the size of the bus and the folding technique applied. The main stowing method considered is the use of origami designs to compactly fold and store the shield. For an initial estimate of the total surface area that the sheet could potentially cover, the case where the sheet is simply rolled around the spacecraft is used. This model, if unrolled, would produce on extremely long and narrow rectangular sheet rather than a circular shield. By taking this case, a simple calculation can be applied to find the total surface area by using the following method:

$$A = \pi \cdot \left(R_{Launcher}^2 - R_{Bus}^2\right) \quad (11.47)$$

$$L = \frac{A}{t} \quad (11.48)$$

$$SA = L \cdot h \quad (11.49)$$

Where A is the cross-sectional area seen from above, L is the length of the material, SA is the surface Area and h is the height. Here, t is the thickness of the sheet and is found to be $84.56E-6$ m. This is computed based on the density of the material and the volume density as the volume density multiplied by the thickness should give the areal density.

[51] URL: `http://homepages.engineering.auckland.ac.nz/~pkel015/SolidMechanicsBooks/Part_II/index.html` [cited 27 June 2021]

This calculation gives an indication of the total material which can fit within the volume without considering the final shape which is required. The total surface area of the shield using this method is computed as $396E6$ m^2.

Next, the actual folding which will be used must be selected. There are certain distinct methods by which the folding problem can be simplified. Generally, each of these changes the shape of the shield in some way. A regular solid circle of material is not necessarily the optimal shield shape, especially when considering that folding up a circle is far more difficult than shapes with clear sides and edges. In order to simplify this, the shape could be changed, or gaps could be implemented in the shield for the fold simplicity.

The first method to consider is a method similar to the Znamya satellite [81] where instead of a solid shield, large slits are introduced thereby creating multiple sheets rather than just one single one. This allows for each individual sheet to be rolled independently and makes folding easier as the sheet folding will produce fewer creases and unwanted overlaps. Unfortunately, this would also result in a smaller shield surface area for an equal diameter which means either the diameter must be increased and therefore the folding required per sheet, or the overall number of satellites is increased. Additionally, the various independent sheets are more susceptible to changes in orientation and this could lead to tangling.

The second method being considered is using Origami folding. The Flasher model as can be found in Fig. 11.24, is one such origami design that has been investigated for solar panels by NASA.

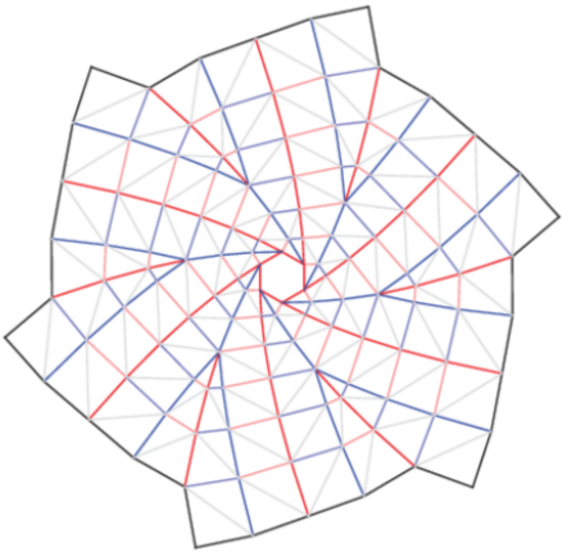

Figure 11.24: Flasher model for Origami folding [82]

This form of folding requires a change in the shape of the shield as well, however, the folding can be used for a shield formed out of a single piece. Origami folding can be used to stow a large shield into a relatively small volume while maintaining a full solid structure and therefore not requiring more satellites due to open holes in the shield. After researching various other missions as well as corresponding with NASA, it was unfortunately found that a more detailed model than the previous calculation is not possible with the current understanding of Origami folding. According to Olive R. Stohlman from NASA, it appears as though the determining factor of how well packed the material can be is the skill of the people involved in the folding process. As such, it will be assumed that the origami folding can be used such that the material is stored just as compactly as in the case the material was rolled as in the previous calculation. Considering the surface area which can be stored in the volume remaining within the launcher, this results in a radius of the shield of 11.2 km. The flasher model is not a perfect method of storing the sheet, however, as the folding does not result in as compact of a structure as needed nor does it fill up the entire space within the launcher perfectly.

A method of mitigating the empty space is by making the material thinner. Unfortunately, the material thickness is set based on the assumed areal density mentioned before which is based on the material not being able to be thinned further. The second option is by changing the number of sides the final shape will have. Once folded, the Flasher model does not perfectly follow the circular spacecraft shape. The difference can be reduced by adding more sides thereby resulting in an increasingly circular shape. One final method of reducing the wasted space is through the mechanism which holds the shield in place. From [83], the restraining method can be tightened such that the material is as closely shaped along the outside of the bus as possible, thereby becoming as close to the role model as possible. This is shown in Fig. 11.25.

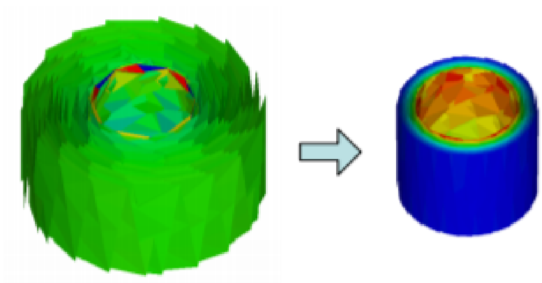

Figure 11.25: Reduction in radius due to restraints [83]

Alternative folding patterns are also available such as the Tree Leave fold (Fig. 11.26) and the Frog Leg fold (Fig. 11.27), both of which are not applicable to this specific concept as they do not work with circular sails effectively, and the spiral fold which is simpler in terms of folds than the flasher but offers a similar solution [84]. The Spiral model in Fig. 11.28 is a better model for the Sunshield due to its slightly simpler structure than the Flasher model, however, the Flasher model may be the better option to use in real production due to less material needing to be moved per every fold during production.

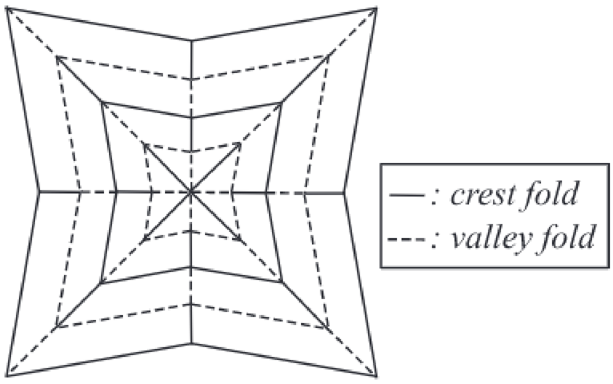

Figure 11.26: Tree Leave fold [84]

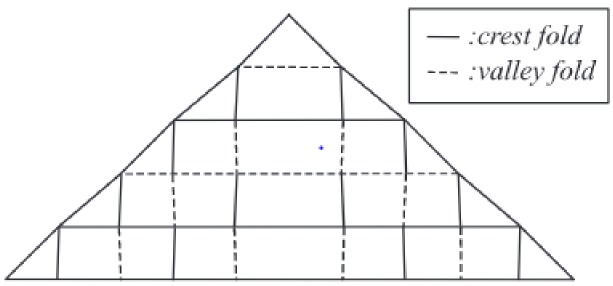

Figure 11.27: Frog Leg fold [84]

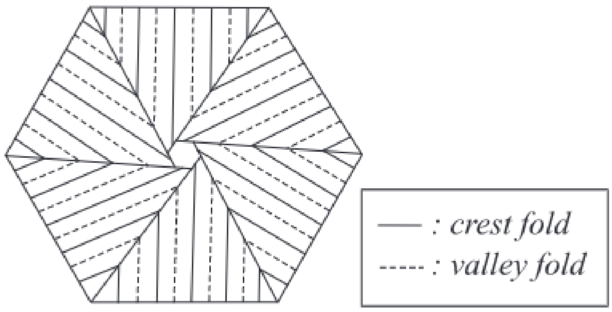

Figure 11.28: Spiral fold [84]

11.8.4. Final Sizing

Having completed the three sizing calculations, of which only 2 imposed actual limits, the final sizing must be decided. Of the 2 sizes found, the smaller radius is the most critical as adding more shield results in one of the conditions not being met. The final limit to the size is therefore determined by the mass of the shield rather than the volume. The shield radius is approximately 5.4 km which results in a total area of $93.1E6$ m^2. From this, the final stowed radius can be determined and the boundaries of the rotational velocity. By reversing the calculations for the other methods above, the final result of the stowed radius is found to be 2.20 m. The maximum angular velocity allowed before the stress becomes too high when deployed is determined from the stress computations as 0.102 rpm where the smaller angular velocity of the transverse and radial calculations is picked due to it being the critical condition. The radial is deemed to be the limiting stress.

Another calculation can be done in order to determine the minimum angular velocity which should be allowed. This is required due to the solar radiation pressure which is constantly pushing against the sheet. At the very ends of the shield, the effect is most noticeable and if the shield begins to deflect due to the pressure, both the effectiveness and satellite are put at risk. The more the shield deflects towards the rear, the less overall surface which is blocking sunlight. Furthermore, eventually, it would end up wrapping around the other side of the satellite effectively blocking the propulsion system and potentially compromising the satellite as a whole.

The calculation to find this minimum angular velocity is accomplished using the formulas related to circular motion. First of all, the deflection which will be allowed is chosen. A value of 5 degrees is selected for θ, the deflection angle, as the overall effectiveness of the shield after a 5-degree deflection is still above 99%. The value is still somewhat arbitrary and more investigation would be required to determine the precise effects on the sheet, however, this was deemed sufficient for a preliminary estimate of the deflection. With the deflection angle established, the angular velocity to maintain this angle can be found. The formula used is as in Eq. (11.51) after finding the tension in Eq. (11.50).

$$Tension = \frac{TSPF}{sin(\theta)} \tag{11.50}$$

$$\omega_{min} = \sqrt{\frac{\sqrt{Tension^2 - TSPF^2}}{\rho R}} \tag{11.51}$$

Where TSPF is the total solar pressure force acting on the entire surface of the shield. The final value is a rotational velocity of 0.0263 rpm.

11.8.5. Restraining Mechanism

Another important part of the payload to consider is the method through which the sheet is kept in place until it is to be deployed. An early deployment of the shield can cause damage to the sheet itself and also cause a failure to reach the necessary final orbit. There are two main criteria the mechanism must adhere to. The first criterion is that the shield is deployed only when needed and not any sooner, the second is that it does not pose a risk to the satellites. Because there is no need to stow the shield after deployment, a one time use method can be considered. A disposable system would be ideal as mass is then reduced after deployment, but the free floating masses create significant quantities of debris. Since the debris is only released at L_1, this could cause severe issues for the other constellation satellites. Another option would be to use non-detachable methods which simply unlatch the sheet and fold away. Alternatively, some form of pyrotechnics could be used in order to distance the components and send them towards the sun.

Many potential deployment system options were considered like, for example, the use of a form of fairing that would fold outwards, the use of wires to keep the ends of the shield in place, or the use of a net pulled tightly across the shield to hold it.

The fairing design would effectively be a case which keeps the payload in position during the launch. It would encompass the entire payload, and therefore the majority of the bus. This would add a large amount of mass as well as a complicated opening system in order to release the payload.

The use of wires at the ends of the shield was also explored. This would involve using holes with metal reinforcement through which wires would be pulled. These wires would attach the ends of the shield to the main bus and could be wrapped around the bus in order to compact the shield more tightly against the bus itself. The wires could be disconnected from the bus through means of a pyrotechnic device which would allow the shield to then deploy leaving the wires attached at the very ends of the shield. The issue posed by this design is the reinforcement required on the shield which adds mass to the very edges of the shield which could cause damage at lower angular velocities as the force becomes greater. Another issue is the lack of support for the vertical direction which is critical in the launch phase.

Finally, of these examples, the net design would use a cable or rope net which would hold the shield tightly against the bus. The net would provide support both laterally and vertically during launch and transfer. The net would allow for deployment by having a detachment mechanism along the wires themselves such that the net splits into an upper and lower section. During deployment, as the spacecraft spins, the centripetal motion would extend the nets outwards similarly to the shield itself, thereby removing them as an obstruction to the shield while still keeping them attached to the spacecraft to prevent problems with debris.

In the end, after deliberation, the net appeared to be the most reasonable choice. It adds the more mass than, for example, the wires but has an overall higher effectiveness due to the improve support in both vertical and horizontal directions. The net can be used to compactly hold the sail. Additionally, due to the nature of such a design, by having the net formed out of two parts it is possible to deploy the sail effectively while the net moves out of the way due to centripetal motion much like the shield.

In order to distribute the launch loads on the net caused by having the net hold the shield up and in place, the connection points must be carefully considered in order to have the most efficient net design. As the main load case is during launch where the force on the net is downwards, the ideal connection points are in locations where the net is held in tension at both sides (top and bottom). This results in the best design being as is seen in Fig. 11.29.

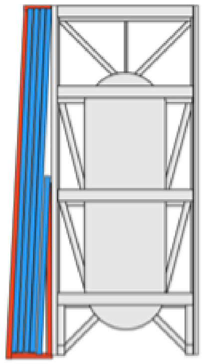

Figure 11.29: Simplified example of the net (red) around the shield (blue).

This design allows both connection points to support the payload together. The net is cut through some form of pyrotechnic or UV susceptible material at the green marked location and then, due to the rotation of the satellite, the result which is obtained once the full deployment is complete is shown in Fig. 11.30. By doing this, the net moves out of the way of the shield allowing full deployment. Additionally, the net does not block sunlight and does not act as a redundant additional shield as it is both far smaller and simply a net.

Figure 11.30: Deployed shield with net also stiffened outwards similarly to the shield

12 Risk

For this mission, the initial risk analysis and the corresponding mitigation strategies were presented in the baseline [2] and midterm report [3]. However, new risks arose as the payload and subsystems have been developed further during the current design stage. Thus, an updated risk analysis and mitigation strategy is required. Additionally, risk is an important factor to account for in the detailed system design of the EOS satellites. First, a new risk assessment will be performed in Section 12.1. Next, mitigation strategies for the analyzed risks will be established in the form of requirements in Section 12.2.

12.1. Risk Assessment

The first step in the risk analysis process is to identify and update the risks with respect to the mission. Risks were identified and classified on a high mission level and on a detailed technical level. Each type of risk is presented with a unique code. Next, the risks were scored on probability of occurrence and severity of consequence, the higher the combination of the latter properties, the higher the total risk for the mission. The meaning of each of the scores can be seen in Table 12.1. The impact is explained on a mission and system level. For other impacts an engineering decision was made on when a risk is catastrophic, critical, moderate, low or negligible. Based on this scoring, the risks are placed in the risk map shown in Fig. 12.1. Risks in the red zone pose the largest threat to the mission while risks in the green zone are acceptable. Requirements derived from mitigation strategies need to be established to bring the risks from the right to the left side of the diagonal. The risk map after mitigation is shown in Fig. 12.2.[3]

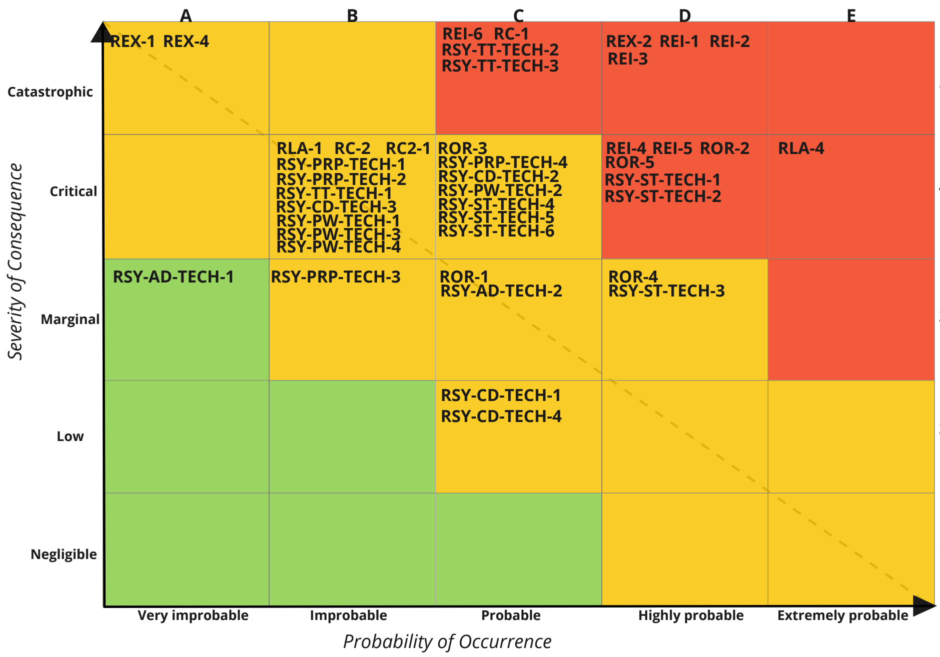

Figure 12.1: Risk map before mitigation (RBM)

Table 12.1: Probability and impact scoring in risk maps.

Probability		**Impact**	
A Very improbable	<0.1%	**1** Negligible	Negligible influence on performance
B Improbable	0.1%-1%	**2** Low	One system requirement is not met
C Probable	1-5%	**3** Moderate	Multiple system requirements are not met
D Highly probable	5-25%	**4** Critical	Loss of spacecraft (LOS)
E Extremely probable	>25%	**5** Catastrophic	Loss of mission (LOM)

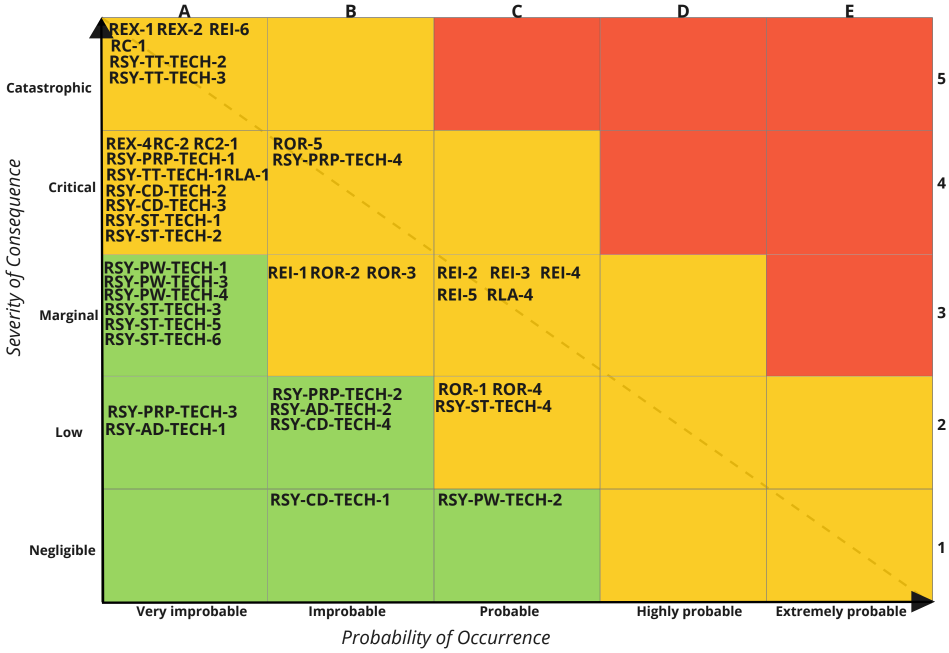

Figure 12.2: Risk map after mitigation (RAM)

12.1.1. Mission Level Risk Assessment

The mission level risk assessment considers all risks in the context of the mission rather than the risks related to the design of the spacecraft itself. The risks were split into four categories: Launch Risks, External Risks, Earth Impact Risks and Organizational Risks. In respective order, these have been labeled RLA-X, REX-X, REI-X and ROR-X. Table 12.2 displays each identified risk with its label, description, cause, impact, Risk Before Mitigation (RBM) and Risk After Mitigation (RAM). These risks were first identified in a baseline report [2] and were update to fit the current design stage.

Table 12.2: Mission level risk assessment [2] .

Risk	Cause	Impact	RBM	RAM
RLA-1 Loss of Launch Vehicle.	Premature flight termination of the launch vehicle before final orbit delivery.	Loss of spacecraft and launcher.	B4	A4
RLA-4 Launch delays	Adverse weather, technical problems with the launcher, delays in production and so on.	Missing launch window and potentially the operational deadline of the constellation.	E4	C3
REX-1 Climate Change Mitigated Before Start of Mission.	Climate change being slowed enough for the mission to be obsolete.	Mission becomes obsolete.	A5	A5
REX-2 Shift in Political Agenda.	Shifted political agenda towards other initiatives or less initiative to stop climate change.	Potential loss of support and/or funding for the mission.	D5	A5

Continued on next page

Table 12.2 – continued from previous page

Risk	Cause	Impact	RBM	RAM
REX-4 Intended destruction of the Sunshield.	Attack from terrorism or external opposition on the Sunshield.	Loss of the mission and severe reaction of the climate on Earth [85].	A5	A4
REI-1 Unknown impact on marine biosphere.	Lack of knowledge about marine biospheres.	Impact could potentially be catastrophic or irreversible, loss of fishing haul.	D5	B3
REI-2 Inconsistent reduction in rainfall.	Lack of knowledge on the impact of the climate on the rain cycles.	Extended droughts, excessive rainfall.	D5	C3
REI-3 Uneven climate temperature decrease.	Sunshield not equally reducing solar radiation across the entire planet.	Unforeseeable effects on local and global weather systems and climate behavior.	D5	C3
REI-4 Decline in net primary productivity in tropical evergreens and taiga.	Increase in carbon sequestering [86].	Harm to certain ecosystems on Earth.	D4	C3
REI-5 Possible harming of unknown processes.	Some processes on Earth might not be known, thus their reaction to the change in solar radiation cannot be estimated.	Unforeseen consequences for some ecosystems or for the system Earth as whole.	D4	C3
REI-6 Increase in global warming rate after abrupt mission failure.	Abrupt disappearance of the Sunshield like destruction of shield or other failure.	Temperature on Earth may rise more strongly then before the shield was introduced [85].	C5	A5
ROR-1 Insufficient funds.	Improper project planning or financial management, withdrawal of funds.	Project not able to be completed due to lack of funds.	C3	C2
ROR-2 Shortage of materials/resources.	Insufficient resource availability, inability to obtain necessary resources.	Inability to manufacture the spacecraft and/or other systems related to the mission.	D4	B3
ROR-3 Production Mistakes.	Lack of adequate quality control, inexperienced manufacturers.	Low-quality product, increased risk of component, subsystem or system failure.	C4	B3
ROR-4 Timeline Delay.	Improper project planning, shipping delays, production delays, delays from external parties.	Missing launch windows, project running over budget, climate change goals not met.	D3	C2
ROR-5 Over budget.	Improper project planning or financial management.	Mission cannot be continued without extra budget.	D4	B4

12.1.2. Technical Risk Assessment

A similar risk assessment was performed in Table 12.3 but now on the technical risks that EOS constellation of satellites could face. The risk were identified for the payload, propulsion, ADCS, TT&C, CDHS, power and structures subsystems. In respective order these have been labeled RC-X, RSY-PP-TECH-X, RSY-AD-TECH-X, RSY-TT-TECH-X, RSY-CD-TECH-X, RSY-PW-TECH-X and RSY-ST-TECH-X.

Table 12.3: Technical risk assessment [3] .

Risk	Cause	Impact	RBM	RAM
RC-1 Collision of spacecraft within constellation.	Faulty or inaccurate positioning of the spacecraft with respect to the others.	Loss of multiple spacecraft in the constellation and creation of space debris.	C5	A5
RC-2 Jammed deployment system.	Mechanical failure of the deployment system.	Spacecraft is rendered useless as no shield is deployed.	B4	A4
RC2-1 Foil tangles/wraps around the satellite.	Deployment error or reduced spin of satellite.	No deployment and potential loss of entire spacecraft.	B4	A4
RSY-PRP-TECH-1 Early main engine failure.	Faulty unit.	Spacecraft cannot reach its L_1 destination.	B4	A4
RSY-PRP-TECH-2 Propellant tank overpressure.	Faulty CGR.	Burst tank.	B4	B2
RSY-PRP-TECH-3 Loss of pressurant.	Faulty CGR.	Insufficient pressurant to sustain propellant pressure.	B3	A3
RSY-PRP-TECH-4 Loss of propellant.	Any thruster's valve stuck open.	Insufficient propellant for orbit maintenance towards the end of the mission.	C4	B4
RSY-AD-TECH-1 ADCS sensors failure.	Internal failure of the sensors.	Spacecraft is not able to determine attitude.	A3	A2
RSY-AD-TECH-2 ADCS actuators failure.	Internal failure of the actuators.	Spacecraft is not able to perform attitude control.	C3	A2
RSY-TT-TECH-1 Transceiver component failure.	Failure due to low reliability.	Signal cannot be modulated/demodulated, no communication possible.	B4	A4
RSY-TT-TECH-2 Level 1 gimbal antenna mount failure.	Mechanical failure of the gimbal instrument.	Loss of communications for entire sector within the constellation.	C5	A5
RSY-TT-TECH-3 Communication failure of relay satellite.	Uncontrollable attitude of the relay satellite.	Loss of communications for an entire sector of satellites.	C5	A5
RSY-CD-TECH-1 Software failure due to bugs.	Mistakes or bugs in the code used on board the spacecraft.	Generation of false commands and readings from the spacecraft.	C2	B1

Continued on next page

Table 12.3 – continued from previous page

Risk	Cause	Impact	RBM	RAM
RSY-CD-TECH-2 On board computer failure due to radiation.	Improper radiation hardening of the OBC.	Loss of a single satellite.	C4	A4
RSY-CD-TECH-3 Failure of data routers.	Improper radiation hardening, connection failures.	Loss of all instruments connected to the router.	B4	A4
RSY-CD-TECH-4 Failure of the SSR.	Improper radiation hardening, connection failures.	Data cannot be stored and must be transmitted directly.	C2	B2
RSY-PW-TECH-1 Unexpected Power Consumption	Unknown source of power consumption or incorrect power consumption for subsystems determined.	Loss of subsystem functionality.	B4	A3
RSY-PW-TECH-2 Solar Cell Failure.	Hardware failure within the Solar Cells of the Power Generation Subsystem.	Power Loss.	C4	C1
RSY-PW-TECH-3 Power Connection Failure.	Improper connection during integration.	Loss of subsystem functionality.	B4	A3
RSY-PW-TECH-4 MCU Software Failure.	Incorrect software implementation or unaccounted for situation.	Hardware Reset or Software Breakdown.	B4	A3
RSY-ST-TECH-1 Truss element failure.	Failure modes incorrectly considered, production errors.	Truss elements are underdesigned and prone to failure.	D4	A4
RSY-ST-TECH-2 Tank failure.	Failure modes incorrectly considered, production errors.	Tank is under-designed and prone to failure.	D4	A4
RSY-ST-TECH-3 Sandwich panel failure.	Failure modes incorrectly considered, production errors.	Sandwich panels are under-designed and prone to failure.	D3	A3
RSY-ST-TECH-4 Debris strike.	Space debris and micrometeorites.	Damage to individual subsystems.	C4	C2
RSY-ST-TECH-5 Insufficient natural frequency.	Low stiffness of the entire structure.	Interaction with vehicle dynamics, leading to structural failure.	C4	A3
RSY-ST-TECH-6 Separation system failure.	Failure of mechanisms and/or pyrotechnics.	Failure to separate from the launch vehicle.	C4	A3

12.2. Risk Mitigation Requirements

The identified risks located to the right or on the diagonal of Fig. 12.1 were mitigated to reduce the overall risk to the mission to an acceptable level. The mitigation strategies can be translated into specific design requirements. These are additional requirements that were taken into account throughout the design process or are requirements that will have to be considered for future design stages. The risk from which the requirement originates is mentioned in the identifier as DSE14-RK-”risk code”. In Table 12.4 the requirements from the mission level risks are shown. Table 12.5

contains the payload and subsystem requirements from the technical risk assessment.

Table 12.4: High level mission requirements from mitigation strategies determined in baseline report [2]

Identifier	Requirement
DSE14-RK-RLA-1	A launch provider with a reliable track record according to set launch standards shall be employed.
DSE14-RK-RLA-4	A set time buffer shall be created to allow for launch delays, as well as contractual incentives to comply with the established schedule.
DSE14-RK-REX-2	A detailed agreement on the continuation of the mission shall be established with governments and clients before the start of the next mission phase.
DSE14-RK-REX-4	Protective measures to prevent attacks on the Sunshield shall be investigated and created before the start of the operational phase of the mission.
DSE14-RK-REI-1	A marine biosphere analysis and consequence prediction shall be performed before the start of the next mission phase.
DSE14-RK-REI-2	An analysis and consequence prediction of the ramifications on global rainfall shall be performed before the start of the next mission phase.
DSE14-RK-REI-3	The orbit selection for the Sunshield shall be done in order to optimize the shading pattern in light of an even climate temperature decrease on Earth.
DSE14-RK-REI-4	Research and development of methods to support ecosystems during the operational phase of the mission shall be performed before the next mission phase.
DSE14-RK-REI-5	An analysis of the mission's synergies with other supplementary bioengineering and geoengineering strategies shall be performed before the next mission phase to reduce the total environmental impact.
DSE14-RK-REI-6	An end-of-life strategy shall be established in order to minimize global warming effects created by the removal of the Sunshield.
DSE14-RK-ROR-1	A closed budget shall be established before the initial launch of the project.
DSE14-RK-ROR-2	Materials for spacecraft construction shall be analyzed and selected based on a RAMS analysis.
DSE14-RK-ROR-3	Verification and validation procedures shall be integrated in the production plan.
DSE14-RK-ROR-4	Buffers shall be implemented taking into account delays throughout the entire production process to maintain target timelines up until launch.
DSE14-RK-ROR-5	A cost analysis with implemented contingencies shall be performed and frequently updated along the design process.

Table 12.5: High level mission requirements derived from the mitigation strategies presented in the baseline report [2]

Identifier	Requirement
DSE14-RK-RSY-PRP-TECH-1	Flight proven and reliable engines shall be used.
DSE14-RK-RSY-PRP-TECH-2	The tanks shall have protection against overpressure.
DSE14-RK-RSY-PRP-TECH-3	There shall be means of shutting on/off the flow of pressurant.
DSE14-RK-RSY-PRP-TECH-4	The thrusters shall be able to be cut off.

Continued on next page

Table 12.5 – continued from previous page

Identifier	Requirement
DSE14-RK-RSY-TT-TECH-1	The transceiver system shall be redundant to achieve a minimum reliability of 0.95 over the mission operational lifetime
DSE14-RK-RSY-TT-TECH-2,3	There shall be no single points of failure in the sectoral control of the level 1 satellites.
DSE14-RK-RSY-CD-TECH-1	The OBC shall be able to receive software uploads.
DSE14-RK-RSY-CD-TECH-2,3,4	The CDHS instruments shall be able to handle a total radiation dose of 7E5 rad [19].
DSE14-RK-RSY-ST-TECH-1,2,3	Sufficient safety factors shall be used in the design of the structural elements.
DSE14-RK-RSY-ST-TECH-1,2,3,5	Design reviews with experts shall be held regularly in the design process.
DSE14-RK-RSY-ST-TECH-4	Sufficient debris shielding shall be implemented on the spacecraft.
DSE14-RK-RSY-ST-TECH-5	Vibration tests shall be part of the acceptance/qualification tests.
DSE14-RK-RSY-ST-TECH-6	The separation mechanism shall be thoroughly tested before launch.
DSE14-RK-RSY-PW-TECH-1	A minimum power generation margin of 20% shall be employed in the sizing of the power system.
DSE14-RK-RSY-PW-TECH-2	Failure of any solar cell shall not reduce the functionality of any other solar cell.
DSE14-RK-RSY-PW-TECH-3	Each Hardware Connection shall be tested.
DSE14-RK-RSY-PW-TECH-4	The functionalities of the software shall be verified and validated.
DSE14-RK-RSY-AD-TECH-1,2	All the ADCS components shall be implemented with redundancies.

13 Reliability, Availability, Maintainability & Safety

The RAMS analysis assesses the reliability, availability, maintainability, and safety of the system. The main target is to analyze any causes of drawbacks occurring throughout the lifetime of the mission and limit those points of failure. In this chapter, the aforementioned aspects will be discussed.

13.1. Reliability & Redundancy

Reliability is the probability measure that a system performs its functions during the mission's lifetime. The value is very closely related to the failure rates of each component and the number of anomalies estimated. The design presented in this conceptual design phase maximizes reliability and redundancy within the feasible limit of the mission.

Several redundancies have been implemented in design in several subsystems. Firstly, in the ADCS subsystem, all configurations are redundant. As an example, all the required sensors onboard are doubled and the thrusters system is configured in a way to allow for full redundancies in three axes. Moreover, the RCDs system has a reaction wheel as a back-up.

In the CDHS every instrument is implemented twice, each with separate connections to avoid single points of failure. Several internal redundancies are integrated with the components themselves as well. For the TT&C, four transponders are included because of the low reliability of these instruments. The antennas have high reliability and will therefore not be redundant. However, two-level 1 satellites will be put in charge of one sector because of the high pointing requirements and possible gimbal failures.

In the power subsystem, redundancy is created within the power generation system by introducing three layers of bypass diodes, as well as separating the system into three sections with independent transformers. Additionally, by the implementation of multiple connections to the various system, with the added introduction of fuses, the connections to the power availability for subsystems is guaranteed to the highest extent viably possible. In this manner, the reliability of the power subsystem is increased.

Redundancies in the other subsystem were not implemented as it was either too costly or not feasible. As an alternative, safety margins were applied.

Assessing the reliability of each component requires further and deeper analysis. Especially since the mission investigates components that are not thoroughly used nor their full details are accessible. The concept of having a massive Sunshield with the current size is unprecedented, and the design phase involved several other concepts that are not fully tested. Moreover, the dependability between each subsystem also requires further investigation. Even though a great effort was put to ensure high reliability through investigating redundancy methods, the reliability of the entire mission cannot be accurately calculated at this stage and further study is required.

13.2. Availability

For the availability of the system, assuming the constellation made it to space, will mainly depend on the transmission windows with the ground station. The strategy designed is to automate all the mission processes as means of limiting the need for communications with the constellation.

13.3. Maintainability

Maintainability is generally done for both the software and the hardware. Maintenance of the hardware components is not considered in the current design stage as it generally complicates the conceptual design aspect. However, as mentioned earlier a redundancy strategy was implemented instead. Moreover, several system maintainabilities will be autonomously performed throughout the mission.

As discussed in Chapter 10, the constellation will enter an unstable Lissajous orbit where several orbit maintenances are required and as such was designed for by allocating a certain amount of fuel mass. Another example is that the sun-pointing of the Sunshield is maintained and worst-case scenarios of tilt above a certain angle are also accounted for. Maintainability is also accounted for in establishing a connection with the ground station. In the TT&C subsystem, a gimballed system is installed to control and maintain the antenna's connection with the relay satellites.

Software maintenance of the components on board has to be scheduled throughout the lifetime of the mission. Great care has to be considered in that aspect as transmission can not occur at all times. According to Section 11.2, the transmission window per day is 8 hours distributed throughout the day with a maximum of 2 hours of transmission time. However, since the mission does not involve gathering scientific data through instruments and specific slew maneuvers to be performed, few anomalies are expected with respect to a common space mission. One more issue to be considered is that software maintenance will be performed outside orbit maintenance phases to reduce the risk of having a downtime that might be detrimental to the entire mission.

13.4. Safety

The safety aspect is involved during the production phase and during the mission lifetime. In the production phase, the most critical safety regulation has to do with involving the crew in storing and transporting the toxic bipropellant MMH and MON-3 fuel. To overcome that aspect, experienced professional workers will be hired. This type of fuel was used many times in several past missions and as such shall not be problematic.

During the mission, safety in the launch phase will be handled by the launch providers (SpaecX). Once the spacecrafts are in orbit, they shall not be a cause of hazard anymore as the constellation will stay in L_1 and will not cross pass by earth. Moreover, the end-of-life strategy ensures that the spacecraft enters a grave yard orbit as explained in Section 8.4.

14

Logistics and Operations

The purpose of this chapter is to outline the logistics of the mission. The mission is divided into phases which have different logistical needs. A preliminary analysis is made to determine which of the logistical phases poses the greatest challenge for the mission. To put the overall mission logistics in context; With the design presented in this report, it would be necessary to build and launch around 20 spacecraft per day for the next 10 years to meet the timeline requirement.

In the following chapters, it is elaborated why having the mission operational by 2031 with the design presented in this report is unrealistic. Nevertheless, it is believed that the design could be revised and taken in a direction that would make it more likely for the mission to be successful by 2031. The group recommendations for further investigations for the mission logistics will also be included in this chapter.

14.1. Logistics (Mission Phases)

For a mission of this magnitude, the logistics of the operation become the main challenge. The enormous amount of shields needed requires a parallel process between manufacturing, launching, and deployment. The final design will have a number of shields in the order of $71\,000$. Therefore in order to comply with the timeliness of the mission, $7\,100$ shields would have to be manufactured, launched, and transferred every year on average from now until 2031 in order to meet the requirement.

For this logistical analysis the worst case scenario for logistics was used. The worst case scenario was defined as the one that has the highest total cost. Other cases were presented in Chapter 15, but the one with the highest cost was deemed the most realistic.

Manufacturing

Currently, there are around 5 thousand satellites orbiting the earth, with an average increase of 3 % per year [52]. Therefore, it is clear that currently there are no manufactures capable of manufacturing around $7\,100$ satellites per year. Additionally, the mass of the shield (100 tons), would make it necessary to have large quantities of the primary materials readily available near the construction site

[52]URL `http://www.unoosa.org/oosa/en/spaceobjectregister/index.html` [cited 27 May 2021]

and specialized treatment facilities. The assumed material of the shield is Polyethylene naphthalate (poly(ethylene 2,6-naphthalate) or PEN). It is unknown whether the market can supply with the high demand on such short notice. Nevertheless, it is very likely that such high demand will be a major logistical challenge for the mission. Finally, the dimensions of the shields would require special facilities. Additionally, the time it would take to design and build all the facilities needed would be in the order of years, which would decrease the time to manufacture and therefore even more facilities would be needed. At this stage of the analysis, the manufacturing issues seem to be the biggest concern in terms of the timeliness of the mission.

According to Chapter 15, the cost of building the facilities is estimated to be 177.36 billion USD. Additionally, the cost of building the spacecraft including manufacturing will be 213.4 billion USD. Therefore, the manufacturing-related cost required the largest portion of the budget.

It was assumed that building the most efficient shield in terms of mass would also automatically optimize the logistical needs. Nevertheless, the relationship between shield efficiency in terms of total mass and logistical challenges is a more complicated relationship than expected. It is possible that optimizing the mission in terms of the total mass is not a viable option. Having smaller, less efficient, easier to manufacture shields might be the only way to have the mission operational by 2031, even though many more launches will be required. A more detailed analysis is required to determine if building smaller, less efficient shields would make manufacturing logistics easier while keeping launching cost balanced.

Launch

The number of launches needed will be 3.8 times more than the amount of spacecraft due to re fulling. Therefore, around $26\ 000$ launches will have to be done every year to meet the timeline requirement. To illustrate the current launch capabilities, in 2020 Space X launch 25 times only [53]. The launch capabilities are also a major issue for the timeliness of the mission. Nevertheless, the recent fast-paced development of aerospace companies such as Space X, seem to suggest that the main constrain of the mission will still be the manufacturing of the shields. The reasoning behind launch capabilities not being the biggest logistical problem is that the technology readiness of the launch providers is much higher than for manufacturing. Many of the technology miles stones needed for launching at such high volume have already been tested and proven market-ready. For example, the re-usability capabilities of Space X launchers have already been operational for a few years.

Additionally, the cost estimations of the launch are 646.1 billion USD. This cost is far below the price of manufacturing the spacecraft and creating the facilities. If the relative cost is equated to the relative logistical challenges, then it can be inferred that manufacturing will be more challenging logistically.

Time of flight

The time of flight for the shields will be around 180 days. This will not be a major challenge in terms of logistics since it will only represent a shift in the schedule in the order of months. For a timeline of 10 years, a few months is important but not critical for the mission.

Ground support: Deployment, Orbit maintenance

According to the internal cost estimations in Chapter 15, the ground support will cost around 410 million USD for 20 years of operations. This cost does not include the R&D for ground support. If it is assumed that the cost is proportional to the logistical complexity, then it can be assumed that the logistics of ground support will be relatively small compare to other mission phases.

The high complexity of the constellation will make it necessary to make use of AI algorithms to maintain the constellation. Therefore, it is very likely that a substantial amount of money and time

[53] URL `https://spaceflightnow.com/2021/01/05/u-s-companies-led-by-spacex-launched-more-than-any-other-country-in` [cited 27 May 2021]

will have to be invested in developing this constellation maintenance algorithm. At this stage of the analysis, it is unclear how much time and money it would take to develop the technology necessary. Nevertheless, the novelty of the mission allows predicting that a significant amount resources would be needed for research, development, and testing.

14.1.1. Recommendations

As demonstrated in the sections above, the logistical needs for manufacturing are the major constraint for the mission timeline. It will be beneficial to design a constellation of shields that does not aim to optimize for the smallest launch mass, but rather for the total cost of the mission. The design presented in the report was made with the assumption that the lowest total mass would yield the most cost-effective mission and therefore fastest to implement. Nevertheless, it can be inferred from the results that designing a sub-optimal shield that is easy to manufacture could be the most cost-effective option that meets the timeline.

15 Cost Breakdown

In this chapter, a breakdown of the different cost sources from the EOS mission will be performed. The goal of this process is to gain insight in the expected magnitude of the required budget and to check if the budget requirement of a total mission cost within 1 trillion USD is complied with. First, the non-recurring costs will be discussed in Section 15.1. Secondly, in Section 15.2, the recurring costs will be presented. Lastly, a summary of the complete budget breakdown will be shown in Section 15.3.

15.1. Non-Recurring Cost

The non-recurring costs are one time costs that occur in the first phases of the mission life cycle. These costs include the development of the final design, verification/validation of the design, software development and the facilities needed for the production.

15.1.1. Research, Development, Testing and Evaluation (RDT&E)

Additional research, development , testing and evaluation must be done in order to complete the final design of the satellites. This design phase will be another source of cost that must be taken into account. From [14] this non-recurring cost can be roughly estimated by multiplying the first unit cost of one satellite with a factor of 1.5. From the first unit cost determined in Section 15.2.1, a total design cost of 61 million USD was calculated.

The software development costs can also accumulate quite drastically as the software must be thoroughly tested and verified before it can be implemented. This is a time consuming and costly process. From [14], the software development cost equals 664 USD per SLOC taking in to account that there will be moderate modifications from existing flight software. The total number of SLOC's was estimated in Section 11.1.3 which results in a total software cost of 42.5 million USD.

15.1.2. Facilities

The facilities required for a project of this scale are a challenge of their own. Such a large scale building has never been built in the past as the overall dimensions lead to a building twice the radius of the large Hadron Collider. The cost of such a building and the time it would take to construct cannot easily be estimated as it verges on an impossible construction project. The facility will be unable to have support pillars and additionally must be one entire clean room with a radius of 5.94km and many countries would be required to build one or more of them in order for this global project to be completed.

In order to determine the costs, it will instead be assumed that the building can be constructed in time. Furthermore, it will be noted both what the maximum price can be before the budget requirement fails, and, alternatively, what the price is realistically based on current technology.

The first estimate uses the price per area of satellite construction clean rooms. This ignores the difficulties of the structure and scale and simply linearly extrapolating the price. Modular clean rooms from Mecart [54] have a price per ft^2 of 100 USD. After converting to square meters, the price of the building such that it can encompass the entire satellite and shield results in a price per building of 909.5 million USD. Assuming each country has, on average, one facility, results in 195 facilities being built. It is further assumed that, despite the need for 20 satellites on average per day, that this would be sufficient as the production becomes increasingly efficient, this will result in a total price for just facilities of 177.36 billion USD.

The second estimate will take into consideration the budget of 1 trillion USD and the price of all technical aspects of the mission. The remaining budget after the satellite prices and costs of all technical components are taken into account is the maximum cost for which all facilities must be constructed in as large a number as possible. If this is achieved, the mission can be completed under the required 1 trillion USD as specified in the requirements. The final price the facilities must adhere to is 139.95 billion USD

Finally, the third estimate assumes an approximate value which could be deemed realistic for the construction of the facilities. By looking at the largest projects ever accomplished thus far such as the Burj Khalifa, the Hadron Collider and the Three Gorges Dam an approximate range can be estimated. The likely price of such a building, along with its challenges, will most likely cost more than the Burj Khalifa, and is around double the size of the large Hadron Collider with the full center hollowed out. The most comparable building in the world to date is the New Century Global Center in China with a floor area of almost 2km^2. This took 3 years to build at a price of approximately 8 billion USD[55].

The price of the facility intended for this mission will be possibly many times this value with a reasonable estimate for the lower price of at least 15 billion based purely on assumption. As more such facilities are built it can also be assumed that the price may decrease with increased skill of the construction teams. Throughout the entire mission, and for the sake of comparison, a value of an average of 10 billion will be taken. The likely time it will take to construct such buildings will be over 5 years and every country would have to be building as many as can be afforded to attempt to finish the mission in the given timeline. The number being built at one time will be taken as an average of 2 per country for the pure sake of this calculation. Within 5 years, around 400 facilities would be completed. To meet the production schedule from Section 14.1, a conservative number of 600 spacecraft must be produced per month.

If both timeline and budget are removed from consideration, a sufficient number of facilities, with these estimations, would be possible to be achieved in over 10 years time such that enough facilities exist to produce the satellites by 2041. This is computed as in 10 years there would be 800 facilities approximately, thereby allowing the entire construction to be completed in the following 10 years once all building is completed. As such the mission, in the worst case, would commence with a delay of 10 years and be completed 10 years late. Alternatively, the number of facilities can be decreased and production would be done until 2041 therefore only requiring 300 satellites a month on average. Starting within 5 years time, sufficient facilities would exist thereby reducing cost of

[54]URL: `https://www.mecart-cleanrooms.com/learning-center/cost-cleanroom-per-square-foot/` [cited 22 June 2021]

[55]URL: `https://www.iofficecorp.com/blog/amazing-facts-about-the-worlds-largest-buildings` [cited 22 June 2021]

facilities overall. In this situation, the final price of all facilities would still amount to around 3 trillion USD.

One other option should be investigated. This is the creation of the shield in the folded state. By doing so, the size of the facility could be greatly reduced as the material is attached to the bus itself and the stowed material. It could be possible to use already existing and relatively inexpensive to build clean rooms and add automation to the process. The method by which this would occur would have to be researched or developed past the scope of this report, however, this would benefit the price of the facilities greatly. This would completely nullify the price of developing or building facilities and reduce it to rental, equipment and materials.

Due to the scale of the project, a single clean room is unlikely to be sufficient for an entire satellite to be built within a month. The sheet would have to be built by parts and hence the process would end up relatively bottle-necked if only a single production line is used for each sheet. As such it is most likely that multiple rooms would be needed. It is assumed that 10 clean rooms are sufficient to build one spacecraft per month, taking into account the improvement of both personnel and the automation. The number of clean rooms needed to produce 600 spacecraft per month would be approximately 6000 neglecting construction time. If the design is also assumed to be standardized, the clean rooms should be able to hold the entire spacecraft in the undeployed state. This gives the height of such a building as above 8 m tall. An example of a large existing clean room is the SSDIF High Bay Cleanroom at NASA's Goddard Space Flight Center with an area of $1\ 161$ m^2 [87]. This results in a single empty facility cost of 175.27 thousand USD assuming the same area and clean room class[56]. The combined facility cost equals 1.05 billion USD.

15.2. Recurring costs

The recurring costs are costs that occur at regular intervals throughout the mission life cycle. This includes: manufacturing and assembly costs, launch costs and costs during the operational phase of EOS.

15.2.1. Space Segment Cost

The cost breakdown of the EOS satellites is given in Table 15.1. All costs are expressed in US Dollars in the fiscal year 2020 (FY2020) with K=thousands, M=millions, B=billions. First the unit costs are estimated for the payload and each subsystem. Similar cost estimates were used for the payload, structure and thermal control subsystems based on material cost and the labor required to finish the product. For the labor costs the average monthly salary of a Dutch Citizen was taken which equals 4 880 euros[57]. For the payload, an engineering estimate was made for a production time of 30 labor days with 100 employees working simultaneously on the shield. This estimate assumes some type of automation for the folding process as the labor costs would otherwise be extremely high for a sheet of this scale. Similarly, the production of the structure would take 10 working days with 10 employees. Determining the exact amount of time it would take to manufacture the shield and the structure is practically impossible at this point in the design stage.Therefore, a large margin is put on these rough cost estimates. Most of the other subsystem costs were based on off-the-shelf components. Detailed information on these instruments was given in the respective sections of Chapter 11. Combined, these give a closer indication of the expected subsystem costs which results in lower error margins. However, a different approach was taken for the ADCS as no accurate instrument costs could be found. The cost of the ADCS was estimated from the IKAROS mission as the technology used is very similar to the configuration considered[58]. According to [34], the ADCS takes around 13% of the total cost of a mission [34]. IKAROS cost 16 million dollars in 2010[59], which is 19.3 million with the current inflation rate. This means the ADCS costs around 2.5 million dollars

[56]URL: `https://compassinternational.net/2019-pharmaceutical-biological-facility-cleanroom-cost-data-benchmarks/` [cited 28 June 2021]

[57]URL: `http://www.salaryexplorer.com/salary-survey.php?loc=152&loctype=1` [cited 22 June 2021]

[58]URL `https://www.nasa.gov/smallsat-institute/sst-soa-2020/power` [cited 22 June 2021]

[59]URL `https://phys.org/news/2010-04-japan-space-yacht-propelled-solar.html` [cited 23 June 2021]

for each spacecraft.

The integration, assembly and test category includes material and labor costs for the integration of the different subsystems and payload into the complete spacecraft body. It also take into account the costs for performing and scheduling testing/analysis procedures. The program level costs arise from contractor costs for systems engineering, program management, reliability, scheduling, quality assurance, project control and other costs. These costs were obtained through cost estimation relationships from SMAD [14]. Summing up the aforementioned costs results in a total first unit cost of 40.63 million USD which is the cost of one fully finished satellite. This price is slightly lower compared to other missions. For example, geostationary communication satellites usually cost around 70 million USD to produce [34]. Yet, it can be concluded that this satellite production cost is a fair first estimate as the order of magnitude of the costs are similar. From Chapter 4, a total number of 71E3 satellites need to be included to complete the constellation. The total number of spacecraft that need to be produced will be slightly higher to take production, launch and other failures into account. A failure margin of 2% was established as a preliminary estimate resulting in an additional $1\ 420$ satellites that need to be produced.

Next, an important aspect to consider is the learning curve (LC). The LC compares the effort needed for the creation of a product with the number of products made. As more of the same products are produced, workers will have to put less effort in the production because of repetition and learning. This means that for example, the production cost of a single sheet will decrease as the number of units produced increases. The total lot production cost of N units can be estimated with Eq. (15.1). $T1$ represents to production cost of the first product, N the number of produced products and S the slope of the learning curve [14] [2].

$$\text{Total lot Cost } = T1 \times N^{\left(1+\frac{\ln(S)}{\ln(2)}\right)} \tag{15.1}$$

In the aerospace industry an average learning curve slope of 85 %[60] can be assumed as a guideline. The learning curve is applied to all the aforementioned costs. This would not directly apply to ordering quantities of materials for example. However, it is assumed that the reduced cost from ordering large batches is equals to the cost reduction of the LC. Looking at the total constellation production cost, the cost changes drastically with the implementation of the LC because of the large number of satellites that are produced. With the LC, the last satellite will only cost 2.3 million USD to produce. The total constellation production cost including the LC equals 213.42 billion USD.

[60]URL: `https://web.archive.org/web/20120830021941/http://cost.jsc.nasa.gov/learn.html` [cited 22 June 2021]

Table 15.1: EOS satellite cost breakdown.

Cost component	quantity	Unit Cost [K]	Combined Cost [K]	Margin [%]
Payload[77]				
Material [kg]	105 058.69	0.005	512.5	40
labor [days]	30	472.26	14 167.74	1000
Structures [77]				
Material [kg]	4040	0.027	108.27	20
labor [days]	10	15.74	157.42	1000
Thermal control				
Kapton foil[61] [m^2]	125.37	0.24	30.23	1000
Power				
Solar Cell	480	0.1	48	10
Battery	1	120.1	120.2	25
PDU	1	10	10	25
TT&C				
Patch antenna	2	2.15	4.3	0
Transceiver	4	8.5	34	10
CDHS				
SSR	2	15	30	20
Databus	4	10	40	20
OBC	2	250	500	10
ADCS	1	2500	2500	100
Propulsion[88][89]				
Thruster	1	316.71	316.71	40
Propellant [kg]	14115.99	0.21	2992.45	10
Total Component Cost [M]			23.47	
Integration, Assembly & Tests [M]			4.97	
Program Level [M]			12.19	
Total First Unit Production Cost [M]			**40.63**	
Total Constellation Cost No LC [B]			**2942.57**	
Total Constellation Cost with LC [B]			**213.43**	

15.2.2. Launch Segment Cost

The total costs for the launch segment can be found by multiplying the cost of one launcher by the total amount of launchers required. From Table 10.6, it can be seen that 2.64 refuelings are necessary for each spacecraft. Therefore 3.64 launchers are required for each spacecraft. The complete constellation consists approximately of $71E3$ spacecraft (Chapter 4) , resulting in a total of $258\ 440$ launches required. The cost of one launch was determined to be 2.5 Million USD, resulting in a total cost for the launch segment of 646.1 Billion USD.

15.2.3. Operations and Maintenance Cost

Another recurring cost is the operation cost for the ground station. A service cost estimation relationship as seen in Eq. (15.2) was provided for the Deep Space Network [90]. Here, AF is the weighted aperature fee per hour of use and equals $1\ 279$ USD, R_B is the contact dependent hourly rate, A_W is the aperature weighting which equals to 1 for the 34m BMW antenna and F_C is the number of contacts per week. It is assumed that there will be four contacts of 2 hours each every day. This would results in a total DSN operation cost of 413.4 million USD taking to account the operational lifetime of 20 years.

$$\mathrm{AF} = \mathrm{R_B}\left[\mathrm{A_W}\left(0.9 + \frac{\mathrm{F_C}}{10}\right)\right] \tag{15.2}$$

15.3. Cost summary

The complete cost breakdown for the EOS mission is given in Fig. 15.1. Three cases from Section 15.1.2 were considered. In case a, a first facility cost estimate was made based on the deployed shield size and current clean room prices. In case b, the facility cost was estimated based on the left-over budget. Case c assumed additive assembly of the shield where the facility area was based on existing clean rooms. For the first case the budget requirement of 1 trillion USD is not met by 3.74%. The second case is inherently designed to meet the budget requirement. It shows the advancements in construction which must be made given that the budget for the facility construction is determined. Lastly, a margin of 14% of the budget is left for case c, making it the cheapest option. Therefore, it is recommended to investigate similar production and assembly possibilities in the future. Overall, the preliminary cost estimation of a mission of this scale has questionable accuracy as many assumptions and simplifications were made throughout the budgeting process. As the budget may vary and all estimates are in close proximity to the required budget, it can be concluded that this requirement is met.

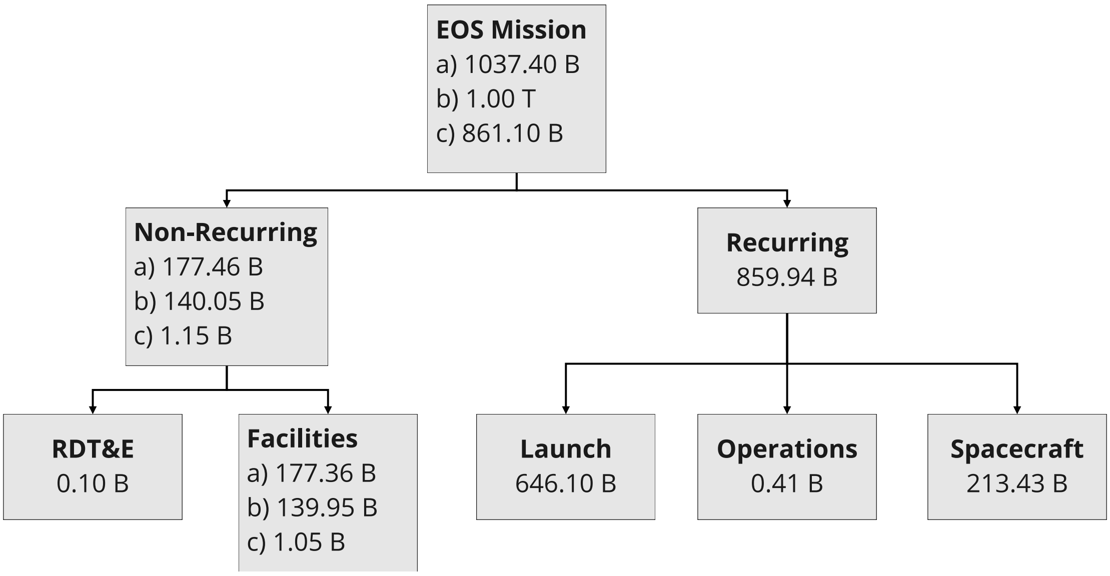

Figure 15.1: EOS mission cost breakdown structure.

16 Verification and Validation Procedures

In this chapter, a review of the verification and validation procedures used throughout the design is done, for models, calculations and requirements. Section 16.1 will show the verification and validation methods for the models. Section 16.2 will discuss how the requirements imposed on the product will be verified and validated. Various verification and validation procedures are extracted from [91].

16.1. Model Verification

The verification and validation procedures ensure that models and calculations work as intended. The (general) main difficulty in verification is defining criteria that make different models fit for comparison and creating tests that compare both models in a fair manner. For the design of a spaceshield, there is the additional difficulty of little to no models existing for specific components/models created by the group.

Despite these difficulties, the models were verified and validated using methods described in the following paragraphs.

Code verification Before the models can be verified, first the code needs to be verified. This step ensures that the code developed and used by the team is bug-free. Python IDEs aid in debugging and discovering syntax errors.

Model verification To verify the model, unit and system tests must be performed. Testing was done comparing code outputs with the expected results from the inspected segments, reviewing consistency and stability of the model for different inputs, and comparing the model output with the output of a simplified model [91]. If a model for a subsystem was verified, then the specifics about that process can be found in that subsystem's section.

Model validation For validation, the usual procedure is comparing models to experiments. As this is strictly a conceptual design project, no experimentation from the group was possible to validate the results. Again, reviewing the reference [91] various procedures for validation can be determined: using already validated models to check the outputs of the developed models, peer review all model components and theoretical bases by team members not involved in the development, and using test data in code segments to compare the output.

16.2. Product Verification

Additionally, the design product needs to be verified with regards to the requirements. There are various verification methods available, as shown from the previous reference [91]: inspection of the product's physical characteristics, technical analysis of the product (such as computer simulations), demonstration of compliance by the product, or testing the product through physical tests. These different methods will be applied after the design process shown in this report is completed, as these methods are too complicated or complex to perform in the current design stage.

References

[1] F. Aleksandrowicz et al. *Space-based Geoengineering to Mitigate Climate Change Project Plan*. Tech. rep. 2021, p. 23.

[2] F. Aleksandrowicz et al. *Space-based Geoengineering to Mitigate Climate Change Baseline Report*. Tech. rep. 2021, p. 46.

[3] F. Aleksandrowicz et al. *Space-based Geoengineering to Mitigate Climate Change Midterm Report*. Tech. rep. 2021, p. 73.

[4] N. Vaughan and T. Lenton. “A review of climate geoengineering proposals”. In: *Climatic Change* 109.1 (2011), pp. 745–790.

[5] R. Angel. “Feasibility of cooling the Earth with a cloud of small spacecraft near the inner Lagrange point (L1)”. In: *Proceedings of the National Academy of Sciences of the United States of America* 103.46 (2006), pp. 17184–17189.

[6] J. McClellan, D. Keith, and J. Apt. “Cost analysis of stratospheric albedo modification delivery systems”. In: *Environmental Research Letters* 7.3 (2012).

[7] S. Salter, G. Sortino, and J. Latham. “Sea-going hardware for the cloud albedo method of reversing global warming”. In: *Philosophical Transactions of the Royal Society A* 366.1882 (2008), pp. 3989–4006.

[8] T. Barker et al. “Contribution of Working Group III to the Fourth Assessment Report of the Intergovernmental Panel on Climate Change”. In: *(Geneva: IPCC) Table SPM4* ().

[9] IRENA. “Global energy transformation: A roadmap to 2050”. In: *International Renewable Energy Agency* (2019).

[10] Report Linker. *Green Technology and Sustainability Market by Technology, Application, Component And Region - Global Forecast to 2025*. 2020. (Visited on 04/28/2021).

[11] L. M. F. S. Space and T. B. Development. *RAD6000 Radiation Hardened 32-Bit Processor*. 2021.

[12] S. Parkes. *SpaceWire User's Guide*. STAR-Dundee Limited. 2012.

[13] A. D. S. Corporation. *miniRv2® Solid-State Recorder*. 2020.

[14] J. Wertz, D. Everett, and J. Puschell. *Space Mission Engineering: The New SMAD*. Vol. Vol. 28. Hawthorne, CA: Microcosm Press, 2015.

[15] C. T. *205 34-m and 70-m Command*. Jet Propulsion Laboratory California Institute of Technology. Dec. 2014.

[16] C. C. J. R. "Protocol of Communications for VORSat Satellite". In: *FACULDADE DE ENGENHARIA DA UNIVERSIDADE DO PORTO* (Sept. 2012).

[17] AZUR SPACE Solar Power GmbH. *30% Triple Junction GaAs Solar Cell Assembly Type: TJ Solar Cell Assembly 3G30A*. 2020.

[18] J. Wijker. *Spacecraft structures*. Springer Science & Business Media, 2008.

[19] F. T. "Estimates of radiation doses in space on the basis of current data". In: *Life Sci Space Res.* (1963).

[20] J. Werner et al. *Cost Comparison in 2015 Dollars for Radioisotope Power Systems – Cassini and Mars Science Laboratory*. USDOE, 2016.

[21] SpaceX. *Starship Users Guide*. Mar. 2020.

[22] OHB System AG. "Mission Concept Assessment Report". Bremen, Jan. 2021.

[23] J. Heiligers. *AE4889 Special Topics in Astrodynamics*. University Lecture. 2021.

[24] J. Heiligers, G. Mingotti, and C. McInnes. "Optimisation of solar sail interplanetary heteroclinic connections". In: *Strathprints Institutional Repository* (2014).

[25] L. van der Ham. "Interplanetary Trajectory Design using Dynamical Systems Theory". In: *TU Delft* (2012).

[26] J. Parker and R. Anderson. *Low-Energy Lunar Trajectory Design*. 1st ed. Pasadena, California: Jet Propulsion Laboratory, 2013.

[27] K. Howell. "Three Dimensional, Periodic, Halo Orbits". In: *Celestial Mechanics* 32 (1984), pp. 53–71.

[28] J.-P. Sanchez and C. R. McInnes. "Optimal Sunshade Configurations for SpaceBased Geoengineering near the Sun-Earth L1 Point". In: (2006).

[29] A. Roger. "Feasibility of cooling the Earth with a cloud of small spacecraft near the inner Lagrange point (L1)". In: (2006).

[30] J. Liu. *Intelligent Control Design and MATLAB Simulation*. Springer Singapore, 2017. ISBN: 9789811052637.

[31] M. Mudde. *Chebyshev Approximation*. Rijksuniversiteit Groningen, 2017.

[32] M. Reddy. "Space solar cells—tradeoff analysis". In: *Solar Energy Materials and Solar Cells* 77.2 (2003), pp. 175–208. ISSN: 0927-0248. DOI: `https://doi.org/10.1016/S0927-0248(02)00320-3`.

[33] K. A. Horowitz et al. "A Techno-Economic Analysis and Cost Reduction Roadmap for III-V Solar Cells". In: (Nov. 2018). DOI: `10.2172/1484349`.

[34] B. T. C. Zandbergen. *AE1222-II: Aerospace Design & Systems Engineering Elements I, Part: Spacecraft (bus) design and sizing*. Delft University of Technology. 2018.

[35] B. Aerospace. *HIGH ACCURACY STAR TRACKER*. 2021.

[36] Star-Dundee. *SpW-10X Router ASIC Evaluation Kit*. 2021.

[37] V. Domingo, B. Fleck, and A. Poland. "The SOHO mission: An overview." In: *Sol Phys 162* (Dec. 1995), pp. 1–37.

[38] K. Howell and H. Pernicka. "Sun-earth libration point trajectories that avoid the solar exclusion zone". In: *Journal of the Astronautical Sciences* 38 (Oct. 1990).

[39] T. J. PHUNG P. B. GUEDENEY V. S. "TRACKING AND DATA RELAY SATELLITE SYSTEM (TDRSS) RANGE AND DOPPLER TRACKING SYSTEM OBSERVATION MEASUREMENT AND MODELING". In: *GODDARD SPACE FLIGHT CENTER* (Sept. 1980).

[40] C. Rorres. "Archimedes' floating bodies on a spherical Earth". In: *American Journal of Physics* 84 (2016).

[41] T. Theodorou. "Three-Axis Attitude Control of Solar Sails Utilising Reflectivity Control Devices". In: *Surrey Space Centre* (2016).

[42] C. Roberts. "Long term missions at the Sun-Earth libration point L1: Ace, SOHO, and WIND". In: *Advances in the Astronautical Sciences* 142 (Jan. 2012), pp. 1263–1282.

[43] J. R. Wertz and W. Larson. *Space Mission Analysis and Design*. Springer, 1991.

[44] A. Cervone. *Attitude Determination & Control System*. TU Delft. 2021.

[45] Son-Goo Kim and Jang-Soo Chae. "Attitude Control System Performance Estimation for Next Generation Small Satellite 1". In: *The 2015 world congress on Aeronautics, Nano, Bio, Robotic, and Energy* 1 (2015).

[46] SRE-PA & D-TEC staff. *Margin philosophy for science assessment studies*. June 2012.

[47] G. P. Sutton and O. Biblarz. *Rocket Propulsion Elements*. Ninth edition. Hoboken, New Jersey: John Wiley & Sons Inc, 2017. ISBN: 9781118753651.

[48] Aerojet Rocketdyne. *In-Space Propulsion Data Sheets*. Tech. rep. 4.8.20. Redmond, WA: Aerojet Rocketdyne, Apr. 2020.

[49] M. R. Schaefermeyer. "AERODYNAMIC THRUST VECTORING FOR ATTITUDE CONTROL OF A VERTICALLY THRUSTING JET ENGINE". In: *UTAH STATE UNIVERSITY* (2011).

[50] J. Barkley Rosser, R. R. Newton, and G. L. Gross. *Mathematical Theory of Rocket Flight*. New York and London: McGraw-Hill Book Company, Inc., 1947.

[51] E. Ring. *Rocket Propellant and Pressurization Systems*. Prentice-Hall International Series in Space Technology. Eaglewood Cliffs, NJ: Prentice-Hall, 1964.

[52] W. R. Marsh and B. P. Knox. *Hydrazine Fuels*. Vol. 1. USAF Propellant Handbooks. Buffalo, NY: Air Force Rocket Propulsion Laboratory, Research and Technology Division, Air Force Systems Command, Mar. 1970.

[53] A. C. Wright. *Nitric Acid/Nitrogen Tetroxide Oxidizers*. Vol. 2. USAF Propellant Handbooks. Denver, CO: Air Force Rocket Propulsion Laboratory, Research and Technology Division, Air Force Systems Command, Feb. 1977.

[54] C. D. Brown. *Spacecraft propulsion*. AIAA education series. Washington, DC: American Institute of Aeronautics and Astronautics, 1996. ISBN: 9781563471285.

[55] I. Vishik. "Why We Are Running Out of Helium And What We Can Do About It". In: *Forbes* (Jan. 2016).

[56] É. Clapeyron. "Mémoire sur la puissance motrice de la chaleur". French. In: *Journal de l'École Polytechnique* XIV (Jan. 1834), pp. 153–190.

[57] Swagelok. *Valve Sizing Technical Bulletin*. Dec. 2007.

[58] K. S. Bernstein. *Structural Design Requirements and Factors of Safety for Spacecraft Hardware For Human Spaceflight*. Tech. rep. JSC 65828. Houston, TX: Lyndon B. Johnson Space Center, Oct. 2011.

[59] Omnidea-RTG. *Space Propulsion Components Product Catalogue*. Feb. 2016.

[60] Spectrolab Staff. *DataSheet UTJ*. 2021.

[61] Spectrolab Staff. *DataSheet XTJ*. 2021.

[62] CESI S.p.A. *Triple-Junction Solar Cell for Space Applications (CTJ30)*. 2021.

[63] SolAero Technologies Staff. *DataSheet ITJ*. 2021.

[64] SolAero Technologies. *DataSheet UTJ*. 2021.

[65] "Solar Energy for Space Exploration". In: *National Aeronatuics and Space Administration Teacher's Guide* (2018).

[66] J. B. et al. *PLANETARY LANDERS AND ENTRY PROBES*. 2007.

[67] T. Megson. *Materials: engineering, science, processing and designs*. 6th ed. Oxford, United Kingdom: Butterworth-Heinemann, 2017.

[68] D. Oh et al. "Analysis of System Margins on Deep Space Missions Using Solar Electric Propulsion". In: *44th AIAA/ASME/SAE/ASEE Joint Propulsion Conference and Exhibit* (July 2008). DOI: 10.2514/6.2008-5286.

[69] S. Timoshenko and S. Woinowsky-Krieger. *Theory of plates and shells*. 1959.

[70] J. Slugg. *Preliminary Design of Composite Overwrapped Pressure Vessels for a Suborbital Pressure Fed Liquid Rocket*. North Carolina State University, 2020.

[71] M. Ashby, H. Shercliff, and D. Cebon. *Materials: engineering, science, processing and designs*. 3rd ed. Oxford, United Kingdom: Butterworth-Heinemann, 2014.

[72] D. J. Inman and R. C. Singh. *Engineering vibration*. Vol. 3. Prentice Hall Englewood Cliffs, NJ, 1994.

[73] C. Lazansky. *Refinement of a Low-Shock Separation System*. 2012.

[74] L. Pepermans et al. "Flight testing of parachute recovery systems aboard REXUS". In: *3rd Symposium on Space Educational Activities* (Sept. 2019).

[75] R. Putzar et al. "A stuffed Whipple shield for the Chinese space station". In: *International Journal of Impact Engineering* 132 (2019), p. 103304.

[76] F. L. Whipple. "Meteorites and space travel." In: 52 (Jan. 1947), p. 131. DOI: 10.1086/106009.

[77] ANSYS. *CES EduPack*. Version 2020. June 20, 2020. URL: https://www.ansys.com/products/materials/granta-edupack.

[78] G. Blengini et al. "Study on the EU's list of Critical Raw Materials (2020) Final Report". In: (Sept. 2020). DOI: 10.2873/11619.

[79] W. K. Wilkie et al. "An Overview of the NASA Advanced Composite Solar Sail (ACS3) Technology Demonstration Project". In: *AIAA SciTech Forum*. VIRTUAL, 2021. DOI: 10.2514/6.2021-1260.

[80] L. Herbeck et al. “Solar Sail Hardware Developments”. In: *European Conference on Spacecraft Structures, Materials and Mechanical Testing* (2002), p. 2.

[81] C. Garner, B. Diedrich, and M. Leipold. “A Summary of Solar Sail Technology Developments and Proposed Demonstration Missions”. In: *35th Joint Propulsion Conference and Exhibit Los Angeles, California, USA* (1999).

[82] S. Magleby et al. “Accommodating Thickness in Origami-Based Deployable Arrays”. In: *Journal of Mechanical Design* 135 (Nov. 2013). DOI: 10.1115/1.4025372.

[83] N. Okuizumi and T. Yamamoto. “Centrifugal Deployment of Membrane with Spiral Folding: Experiment and Simulation”. In: *Journal of Space Engineering* 2.1 (2009), pp. 1–10.

[84] B. Fu, E. Sperber, and F. Eke. “Solar sail technology—A state of the art review”. In: *Progress in Aerospace Sciences* 86 (2016), pp. 1–19. ISSN: 0376-0421. DOI: https://doi.org/10.1016/j.paerosci.2016.07.001.

[85] H. D. Matthews and K. Caldeira. “Transient climate–carbon simulations of planetary geoengineering”. In: *Proceedings of the National Academy of Sciences* 104.24 (2007), pp. 9949–9954. ISSN: 0027-8424. DOI: 10.1073/pnas.0700419104.

[86] N. E.Vaughan and T. M. Lenton. “A review of climate geoengineering proposals”. In: *Climatic change* 109.3 (2011), pp. 745–790.

[87] G. S. F. Center. *ENVIRONMENTAL TEST AND INTEGRATION FACILITIES HANDBOOK*. National Aeronautics and Space Administration. Greenbelt, Maryland 20771, 2012.

[88] R. Sninsky. *DOD Standard Prices for Aerospace Energy Category Items*. Tech. rep. Defense Logistics Agency, Sept. 2019.

[89] J. S. Nieroski and E. I. Friedland. “Liquid Rocket Engine Cost Estimating Relationships”. In: *AIAA Second Annual Meeting*. San Francisco, CA, July 1965.

[90] NASA. *NASA’s Mission Operations and Communications Services*. Oct. 2014.

[91] W. Larson. *Applied Space Systems Engineering*. 2nd ed. Space Technology Series, 2014.